Controlled FES-assisted gait training for hemiplegic stroke patients based on inertial sensors

vorgelegt von
Sivilingeniør Nils-Otto Negård

Von der Fakultät IV - Elektrotechnik und Informatik
der Technischen Universität Berlin
zur Erlangung des akademischen Grades
Doktor der Ingenieurwissenschaften
– Dr. Ing. –

genehmigte Dissertation

Promotionsausschuss:

Vorsitzender:	Prof. Dr.-Ing Reinhold Orglmeister
Berichter:	Prof. Dr.-Ing. Jörg Raisch
Berichter	Prof. Dr. Fabio Previdi

Tag der wissenschaftlichen Aussprache: 18. November 2009

Berlin 2009
D 83

Abstract

Stroke is one of the leading causes to disability in the western world. The effects of stroke are many and in many cases include impairment of motor, sensory input, emotion, language, perception and cognitive functions. Impairment of motor functions usually involves paralysis or paresis on one side of the body. One crucial component in rehabilitation following a stroke is the restoration of mobility of which walking is an essential part. For almost 50 years Functional Electrical Stimulation (FES) has been applied to restore motor function and to improve gait. In 1961 Liberson used functional electrical stimulation to elicit the withdrawal reflex during the swing phase.

This work is concerned with the technological development of a new system for FES-assisted gait training for stroke patients. The system is based on an inertial sensor system consisting of 2 inertial sensor units mounted to each foot. Algorithms for estimation of foot orientation, detection of gait phases and estimation of movement parameters as well as strategies for multichannel FES-assisted gait training have been developed. The algorithm for gait phase detection uses all possible information from one inertial sensor to detect four distinct gait phases. The gait phases are represented as states in a state machine and the transitions are governed by logical functions. The detection system was validated by use of an insole foot pressure measurement system. In experiments involving five hemiplegic subjects, it was found that the detection system worked robustly, meaning that all gait phases were detected and no critical failure in the phase detection occurred.

Based on the gait phase detection algorithm and the estimation of foot orientation, an algorithm for estimation of movement parameters like step length and foot clearance was developed. The method takes into account known constraints of the movement, like initial and end conditions in order to improve the accuracy. The estimated movement parameters were compared with measurement from an optical motion analysis system for 5 stroke patients walking on a treadmill. The results showed that the movement parameters could be estimated from inertial sensor data with a high accuracy.

Furthermore, on basis of the gait phase detection algorithm, a multichannel stimulation strategy for stroke patients walking on a treadmill was developed and implemented in a laboratory set-up. Gait analysis measurements with an optical motion analysis system for two stroke patients showed that the electrical stimulation had an immediate positive effect on the gait pattern. Furthermore, a closed-loop strategy was derived in order to control movement parameters the estimated by the inertial sensor system. By evaluating the movement parameters after a completed stride the stimulation intensity was found for the next stride. The closed-loop strategy was successfully tested in simulation. In experiments with one stroke patient having a drop foot, the strategy was successfully applied to control the maximum sagittal angle of the foot by stimulation of tibialis.

In summary, inertial sensors have proven to be suitable for the exact control of FES-assisted gait training in a clinical environment. The developed system is reliable, robust, easy to mount on a patient and does not require re-calibration before use.

Zusammenfassung in deutscher Sprache

Ein Schlaganfall führt in der Regel zu massiven Störungen des zentralen Nervensystems und oftmals zur Invalidität des Betroffenen. Als Folge der Hirnschädigungen kommt es häufig zur Beeinträchtigung motorischer und sensorischer Funktionen, zu Ausfällen in der Sprache sowie zu einer gestörten Wahrnehmung. Ein einseitiger Schlaganfall bezüglich des Gehirns führt in der Regel zu einer halbseitigen Lähmung der gegenüberliegenden Körperseite. Die Lähmung kann dabei vollständig oder teilweise (paretisch) sein. Ein wichtiger Bestandteil in der Rehabilitation nach Schlaganfall stellt die Mobilisierung der Patienten dar. Die Unterstützung des Gehens mittels Funktioneller Elektrischer Stimulation (FES) der paretischen Muskeln wurde erstmals von Liberson et al. 1961 bei Schlaganfallpatienten mit Fußheberschwäche praktiziert. Die Stimulation wurde dabei mittels eines einfachen Fußkontaktschalters getriggert. Der Elektrostimulation lassen sich sowohl prothetische als auch ein therapeutische Effekte nachweisen.

Die Dissertation beschäftigt sich mit der technologischen Entwicklung und Erforschung eines neuartigen Therapiesystems für das FES-unterstützte Gangtraining bei Schlaganfallpatienten. Das Training findet auf einem Laufband mit teilweiser Gewichtsentlastung des Patienten statt. Grundlage der Entwicklung ist ein Inertialsensorsystem bestehend aus zwei Miniaturinertialsensoren, die an beiden Schuhen des Patienten angebracht sind. Jeder Sensor besteht aus 3 Beschleunigungs- und 3 Winkelratensensoren mit orthogonaler Anordnung. Im Rahmen dieser Arbeit wurden Algorithmen entwickelt zur Gangphasenerkennung und zur Schätzung der Orientierung sowie der Raumtrajektorie des Fußes basierend auf den Inertialsensordaten. Unter Ausnutzung der gewonnenen Informationen wurde eine geregelte mehrkanalige funktionelle Elektrostimulation realisiert, bei der die Stimulation mit dem Gang exakt synchronisiert ist und ausgewählte Gangparameter, wie z.B. der Grad der Fußhebung, gezielt beeinflusst werden können.

Das Gangphasenerkennung mit Intertialsensoren erlaubt die Unterscheidung von 4 Gangphasen (Belastungsantwort, Standphase (Fußflachphase), Vorschwungphase und Schwungphase) sowie die Registrierung von 3 Gangereignissen (initialer Bodenkontakt, Ablösung von Ferse und Zehen vom Boden). Der entwickelte Algorithmus funktioniert robust für verschiedene Patienten ohne individuelle Anpassungen. Die Sensoren müssen lediglich in Zeitabständen von mehreren Monaten kalibriert werden. Am Patienten ist keine Kalibrierung der Sensoren notwendig, so dass das System nach einer einfachen Montage der Sensoren an den Außenseiten der Schuhe sofort einsatzbereit ist. Die Gangphasenerkennung mittels Interialsensoren wurde in einer klinischen Studie mit 5 Schlaganfallpatienten erfolgreich getestet und die Ergebnisse mit einem kommerziellen Gangphasenerkennungssystem mit Drucksensoren unter der Fußsohle verglichen.

Für die Schätzung der Orientierung des Fußes wurde ein Kalman-Filter verwendet. Als Vergleichsmessungen für die aus den Winkelraten berechneten Sensorlagen wurden die statischen Beschleunigungsmessungen in den Standphasen des Ganges herangezogen. Zur Bestimmung der Raumkurve des Fußes wurde eine Doppelintegration der gemessenen Beschleunigungen durchgeführt. Um den Einfluss von Offsetfehlern der Beschleunigungsmessungen auf die Berechnung der Raumkurve zu reduzieren, wurde die Raumkurve offline nach jedem Schritt ermittelt unter Berücksichtigung bekannter Randbedingungen, wie z.B. der Geschwindigkeit des Fußes in den Standphasen. In einer klinischen Studie mit 5 Schlaganfallpatienten konnte die hohe Genauigkeit der Raumkurvenschätzung nachgewiesen werden. Konkret betrachtet wurden die aus der Raumkurve abgeleiteten Kenngrößen Schritthöhe und Schrittweite. Als Referenzmesssystem wurde ein optisches Messsystem verwendet.

Neben der exakten zeitlichen Synchronisation der Elektrostimulation mit dem Gang erlaubt das entwickelte System auch eine gezielte Anpassung der Stimulationintensität, um gewünschte Sollwerte für ausgewählte Gangparameter zu realisieren. Bei dem vorgestellten Regelungskonzept werden nach jedem Schritt die gemessenen Kenngrößen des Ganges mit den Sollvorgaben verglichen. Anschließend werden die Stimulationsintensitäten für den nächsten Schritt angepasst. Während eines Schrittes werden die Stimulationsintensitäten konstant gehalten. Um die Machbarkeit einer solchen Regelung zu demonstrieren, wurden experimentelle Untersuchungen mit einem Schlaganfallpatienten mit ausgeprägter Fußheberschwäche durchgeführt.

Zusammenfassend lässt sich feststellen, dass ein hochgenaues und zuverlässiges System zur Gangphasenerkennung und Bewegungsschätzung mittels Inertialsensoren realisiert werden konnte. Für den späteren klinischen Einsatz spricht ferner die einfache und schnelle Anbringung der Sensoren am Patienten. Das System eignet sich sehr gut für die Regelung der Elektrostimulation beim Gangtraining von Schlaganfallpatienten.

Acknowledgement

The work in this thesis was done during my time as research assistant at the Max Planck Institute for Dynamics of Complex technical Systems from April 2002 till September 2006.

I wish to acknowledge and thank those people who contributed to this thesis. First and foremost, I would like to thank my supervisor Dr. Thomas Schauer, who convinced me to start this research in the field of functional electrical stimulation, for contributing with ideas, for the numerous hours of discussion and for proofreading this thesis.

I would also thank Prof. Dr.-Ing. Jörg Raisch for giving me the opportunity to perform this research at the Max Planck Institute and for refereeing this thesis. Thanks goes also to Prof. Dr. Fabio Previdi for refereeing this thesis.

Moreover, I would like to thank the whole staff of the Max Planck Institute as there are the secretary staff, the computing staff as well as the workshop people. My thanks go also to the project students Sabine Haumann, Steffi Geist, Stephan Schmidt and Robert C. Salbert and the exchange students Jaques de Gersigny and Simona Ferrante for their collaboration and contribution to the development of this thesis.

Furthermore, I want to acknowledge the fruitful cooperation with the company Hasomed GmbH and thank the CEO, Dr. Peter Weber for financial support of this project, and I would especially thank Dr. Ralf Kauert for fruitful discussions and comments on the thesis.

My thank goes also to the Prof. Dr. med. Volker Hömberg at St. Mauritius Therapiklinik in Meerbusch for giving me the opportunity to work in his klinik and to Silke Schumacher and Helmut Krause for supporting me at the time there. Thanks goes also to all the physiotherapist who worked with me there and the subjects who participated in the study.

Contents

List of Figures

List of Tables

Nomenclature

Abbreviation

ISU	Inertial Sensor Unit
INS	Inertial Navigation System
EKF	Extended Kalman Filter
FES	Functional Electrical Stimulation
FSR	Force Sensitive Resistors
CFT	Constant Frequency Train
ENG	Electroneurogram
EMG	Electromyogram
DFS	Drop Foot Stimulator
UMN-DF	Upper Motor Neurone Drop Foot
UMNL	Upper Motor Neurone Lesion
GPS	Global Positioning System
GPD	Gait Phase Detection
GPD-IS	Gait Phase Detection system based on Inertial Sensor
ALN	Adaptive Logic Network
PBWS	Partial Body Weight Support
RMS	Root Mean Squares

1. Introduction

1.1. Stroke

Stroke is one of the leading causes to disability in the western world. The effects of stroke are many and often include impairment of motor and sensory input, emotions, language, perceptions and cognitive functions. Impairment of motor functions involves paralysis or paresis on the contralateral body side of the lesion. Damage to the neural pathways results in abnormal regulation of spinal motorneurons and causes a degradation of the voluntary movements. Typically the muscles extending the leg, the calf and the quadriceps, are spastic and the muscles of flexion, the anterior tibialis and the hamstrings are weak or inactive.

One crucial component in the rehabilitation of stroke is the restoration of mobility in which walking is an important component. The time and degree of recovery of walking function after stroke were studied prospectively in a population of 804 consecutive acute stroke patients in Copenhagen [39]. In this study it was reported that at the time of admission to rehabilitation 51 % of the subjects had no walking functions and 12 % needed assistance in ambulation. After rehabilitation, only 18 % of the participants still had no walking function and 11 % required assistance. A persistent, long-term disability remaining in approximately 10 to 20% of stroke survivors is Upper Motor Neuron-Drop Foot (UMN-DF). UMN-DF typically involves an inability to dorsiflex the foot during the swing phase of gait (drop foot) as well as a loss of normal knee flexion, inability to push-off, and spasticity of the calf muscle group in the stance phase [89].

1.1.1. Neuropathological Changes

Stroke is defined through rapidly developing clinical signs of focal disturbance of cerebral function lasting more than 24 hours with no other apparent cause than a vascular origin [81].

Stroke is either occlusive (due to closure of a blood vessel) or haemorrhagic (due to bleeding from a vessel). Insufficiency of blood supply is termed ischaemia; if it is temporary, symptoms and signs may be found with little or no pathological evidence of tissue damage. Ischaemia does reduce the blood

supply and is thereby deprives tissue of oxygen, glucose and prevents the removal of potentially toxic metabolites such as lactic acid. When ischaemia is sufficiently severe and prolonged, neurons and other cellular elements die. Haemorrhage may occur at the brain surface. Alternatively, hemorrhage may be intraparenchymal causing a blood clot or haematoma within the cerebral hemispheres, in the brainstem, or in the cerebellum. An infarction in the middle cerebral artery causes the most frequently stroke syndrome with contralateral weakness, sensory loss and visual field defect. Weakness and sensory loss affect the face and the arms more than the legs because these are controlled by both hemispheres.

1.1.2. Epidemiology and Risk Factors

The WHO MONICA project of 12 224 registered stroke patients in eleven countries [84] identified the highest attack rates in men in Finland and Russia. The attack rates were three times higher in those countries compared to those found in Italy and Germany. In women, the highest attack rates were also seen in Russia, where stroke events were more than three times higher than in Italy. It was also shown that stroke incidence rate was higher in men compaired to women, and in half of the countries twice as many men suffered of stroke compaired with women. In the same study smoking and elevated blood pressure explained 21 % of the variation in stroke incidence in men and 42 % in women [84].

A meta-analysis of 22 studies indicated that smoking can double the risk of an ischaemic stroke [81]. Subjects who stop smoking reduced this risk by 50 %. For middle-aged women who smoke, the relative risk for stroke may be as 2.6 times higher as for aged-matched non-smokers. Lowering high blood pressure can substantially reduce the risk to vascular complications and overall mortality, depending on the magnitude by which blood pressure is lowered. In addition to decreasing blood pressure and smoking cessation, lifestyle modification includes additional factors to reduce the risk of stroke e.g. regular physical activity and use of a low salt, low saturated fat, high fruit and vegetable diet rich in fibre [27].

1.2. Functional Electrical Stimulation

An important feature of Upper Motor Neurone Lesions (UMNL) is that electrical excitability of the associated peripheral nerves is still intact, thus facilitating the use of Functional Electrical Stimulation (FES) to restore or enhance motor functions. Electrical stimulation for the correction of spastic drop foot in hemiplegia was first applied by Liberson et al. [43] in 1961. When the patient lifted the heel to take a step, the stimulator was activated. Stimulation was stopped when the heel contacted the ground. This was the first ever use of stimulation, and the terminology Functional Electrical Stimulation (FES) was born. Later many applications of FES have followed both for stroke and in paraplegia. FES can either be used as an orthotic device as in a foot drop stimulator, which the patient has to use permanently or as a part of a rehabilitation program. Studies have shown that a statistical improvement of the gait speed

can be achieved through the use of FES in gait rehabilitation [72, 92]. Other effects of FES are increased muscle strength and a reduction of spasticity [16]. As stroke patients normally still have their sensory nerves intact, they can feel a pain when the muscles are electrically stimulated. The pain threshold is individual to each patients and for some patients who have a low pain threshold, FES cannot be applied.

Apart from provoking contraction of skeletal muscles, FES is used in other neuroprosthetic devices, e.g. the cochlea implant, the phrenic pacemaker, and the sacral anterior root stimulator for bladder control (see Rushton [73] or Stein et al. [85] for an overview). Applications of FES in paraplegia with the aim of motor function restoration include cycling [76, 86], walking [22], rowing [15, 35], standing-up and sitting-down [68, 69] and standing [37].

The underlying neurophysiological principle of FES is the generation of action potentials in the uninjured peripheral lower neurons by application of low levels of pulsed electrical current to the nerves. Muscle contractions can be artificially released by electrical stimulation of efferent (motor) nerves innervating the paralysed muscles or by electrical stimulation of afferent (sensory) nerves provoking reflexes via intact reflex arcs. An example of the latter is the stimulation of the peroneal nerve to elicit the withdrawal reflex. Stimulation can follow either through percutaneous stimulation of peripheral nerves by needle electrodes through the skin, or as in this work through transcutaneous stimulation with surface electrodes. Charge-balancing can be realised either by means of a capacitor or using biphasic stimulation pulses. The stimulator used in this work is current controlled and therefore delivers constant biphasic current pulses. The current pulses usually have a duration between 10 and 500 μs and an amplitude between 0 and 125 mA.

The muscle force produced by FES depends on the number of recruited motor units and the activation rate. A motor unit is a single motor neuron and the group of muscle fibres (of the same type) innervated by it. When the pulse charge (pulsewidth $\times$ pulse amplitude) is sufficiently high and the neuron is close to the electrode, the motor neuron will be polarised above threshold and an electric action potential will be released. The muscle force increases with the number of recruited motor units (spatial summation), and therefore modulation of pulsewidth or pulse amplitude can be used to control muscle force. The muscle force can also be controlled by modulation of the stimulation frequency (temporal summation). The traditional method for neuromuscular stimulation employs a train of brief rectangular stimulating current pulses, at frequencies typically between 10 and 100 Hz.

Although FES can elicit strong and effective muscle contractions, there are significant limitations. Normally, muscles contain a mixed population of slow fatigue-resistant (type 1), fast fatigue-resistant (type 2A) and fast fatiguable (type 2B) motor unit types. The terms *fast* and *slow* refer to the contractile speed of the muscle fibres. Compared with the physiological recruitment order (the Hennemann *size principle* [30]), recruitment with FES is thought to be inverted [24]. When low muscle forces are desired, and thus low intensity electrical stimulation pulses are applied, mainly rapidly fatiguing large motor units which are close to the electrodes are activated. This is because the fast fatiguable fibres of type 2B motor unit are associated with large-diameter nerve axons, which have a lower firing threshold to externally applied

stimulation. With increasing intensity of the pulses, also small neurons (related to slow fatigue-resistant (type 1) and fast fatigue-resistant (type 2A) motor units) with higher firing threshold and neurons which are located further away from the electrodes are recruited. In addition to this, at a constant stimulation intensity and for the same electrode position, the same motor units are activated all the time. With FES, the action potentials of different motor units are triggered simultaneously. This is different from the CNS which activates motor units asynchronously.

1.3. Outline of the Thesis

The work in this thesis is concerned with the development of a system for contolled FES-assisted gait training for stroke patients by means of inertial sensors.

- In Chapter 2, the state of the art in FES-assisted gait training and Foot Drop stimulation is reviewed.
- In Chapter 3, an introduction and descriptions of the sensor systems and the stimulator used within this thesis are given. The physical principles of an inertial sensor unit are explained as well as how an inertial sensor unit is calibrated. Furthermore, technical features of the stimulator RehaStim are discussed and its different operation modi are explained. Moreover, a brief description and technical details are given for the Lukotronic optical motion analysis system and for the Parotec foot insole pressure measurement system.
- In Chapter 4, an algorithm for obtaining the orientation of an inertial sensor unit is derived based on an Extended Kalman Filter (EKF). The EKF is an indirect filter in which the error between the estimated orientation based on an integration of the angular velocity and the real orientation is estimated in the filter. The acceleration measurement is used in the stance phase of the gait to give the real orientation of the sensor under the assumption that the sensor is not accelerated.
- In Chapter 5, a novel algorithm for online detection of gait phases is presented. The algorithm exploits all possible information derived from an inertial sensor unit. Four distinct gait phases are represented as states in a state machine. The transitions between the states are governed by logical functions based on the angular velocity, orientation and acceleration of the sensor. The robustness of the algorithm was tested in a clinical study involving 12 hemiplegic stroke patients. During the tests all parameters of the gait detection algorithm were held constant. Furthermore, for five hemiplegic patients out of the total twelve, reference data were recorded with a foot insole pressure measurement system and gait phases detected by means of this system were compared with those detected with the inertial sensor unit.
- In Chapter 6, a method for estimating the three dimensional trajectory of the foot during gait is described using data from an inertial sensor unit. Based on this trajectory, gait movement parameters of gait like step length and foot clearance are computed. The accuracy of these calculations

is improved by the introduction of start and stop constraints on the movement. For validation purposes, measurements with an optical motion analysis system were performed with five patients and the estimated movement parameters were validated. The advantage of using a full inertial sensor unit (3 accelerometers and 3 gyroscopes) instead of a reduced sensor (2 accelerometers and 1 gyroscope) was demonstrated.

- In Chapter 7, a prototype system for FES-assisted gait training is described. The system consists of an inertial sensor system with two inertial sensor units, a standard laptop and an 8-channel stimulator unit. The gait phase detection system described in Chapter 5 was implemented and runs online on a laptop using the Linux operating system. The detected gait phases form a basis for the stimulation pattern generator i.e. the synchronisation of the stimulation with the gait cycle. Strategies for stimulation of muscles as well as for closed-loop stimulation are presented in this chapter. The proposed FES-assisted gait training system based on inertial sensor was successfully tested on 12 hemiplegic subjects and the feedback control strategy was successfully applied to one patient.

Conclusions and recommendations for future work are given in Chapter 8.

1.4. Contributions of the Thesis

The main contribution of the thesis consists of the development of algorithms by means of an inertial sensor unit in the application of FES-assisted gait training. The different algorithms developed throughout the thesis are connected together and depend upon each other, but the contributions can be divided into the following parts:

On-line Gait phase detection: A new algorithm for online gait phase detection has been developed. The algorithm requires that the sensor is mounted to the outside of the foot. Beside an initial calibration of the inertial sensor to estimate biases on the gyroscopes and accelerometers, no extra calibration or adaption of the sensor is required for each patient individually. The algorithm takes advantage of the information derived from the inertial sensor such as the angle between foot and ground and velocity of the foot as well as the acceleration and angular velocity directly measured by the sensor. This algorithm represents a novelty as it is the first algorithm using a full inertial sensor unit. The feasibility and robustness of the algorithm has been verified in experiments with stroke patients.

Calculation of movement parameters by means of a full and reduced inertial sensors. A new algorithm for calculation of gait movement parameters based on the 3D-movement trajectory of the foot during gait has been developed. The algorithm uses the already detected gait phases for start and stop

times. The acceleration is integrated two times in order to obtain the foot position. The accuracy of the estimation is improved by using constraints on the integration i.e. that the velocity is zero at the start and at the end of the integration. The estimation of movement parameters was investigated for a full inertial sensor and for a reduced inertial sensor unit with only 3 sensors (1 gyroscope and 2 accelerometers). The novelty of this work lies in the experimental validation of the proposed methods and comparison of the different algorithms. The algorithms were experimentally tested on 5 patients who were walking on a treadmill and the movement parameter estimations were compared with measurements from an optical 3D motion analysis system.

Developement of a closed-loop FES-assisted gait training system: A new strategy for FES-assisted gait training was developed. The developed stimulation strategy depends on the gait phase detection algorithm. The gait cycle is divided into 11 subparts, and each stimulation channel can be uniquely programmed to be active in selected parts. The gait cadence is observed and the stimulation pattern is scaled to the gait cadence. A new closed-loop control strategy was derived in order to control the stimulation intensity with the aim to achieve desired movement parameter. The open loop control strategy was successfully tested on 12 hemiplegic patients, whereas the feasibility of the closed-loop control strategy was demonstrated on one stroke patient. This was the first time that an inertial sensor unit was used in the application to closed-loop FES-assisted gait.

1.5. Publications

The results presented in this thesis have previously been partly published in the following articles:

1. Negård, N.-O., Kauert, R., Andres, S., Schauer, T. and Raisch, J. Gait phase detection and step length estimation of gait by means of inertial sensors, In *Proc. of the 3rd European Medical & Biological Engineering Conference*, Prague, Czech Republic. Oct. 2005.

2. Negård, N.-O., Schauer, T. and Raisch, J. Robust Nonlinear Control of Knee-Joint Angle: A Simulation Study, In *Proc. of the 3rd Wismar Symposium on Automatic Control*, Hansestadt Wismar, Germany. Sep. 2003.

3. Negård, N.-O., Schauer, T.,Kauert, R. and Raisch, J. An FES-assisted gait training system for hemiplegic stroke patients based on inertial sensors, In *Proc. of the 6th IFAC Symposium on Modelling and Control in Biomedical Systems*, Reims, France. Sep. 2006.

4. Negård, N.-O., Schauer, T., Gersigny, J., Hesse, S. and Raisch, J. Application Programming Interface and PC control for the 8 channel stimulator MOTIONSTIM8, In *Proc. of the 10th Annual Conference of the International Functional Electrical Stimulation Society (IFESS 2005)*, IFESS, Montreal, Canada. Aug. 2005.

5. Negård, N.-O., Schauer, T.,Raisch, J.,Schumacher, S. and Hömberg, V. Control of FES-assisted gait training after stroke using inertial sensors., In *Proc. of the 11th Annual Conference of the International Functional Electrical Stimulation Society (IFESS 2006)*, IFESS, Zao, Japan. Sep. 2006.

6. Schauer, T., Negård, N.-O., Nahrstaedt, H. and Raisch, J. Regelung von Peroneus-Stimulatoren zur Kompensation von Fußheberschwäche nach Schlaganfall. *ORTHOPÄDIETECHNIK*, 60(2):78-83, 2009

2. State of the Art in FES-Assisted Gait Training

2.1. Summary

This chapter gives an overview of Functional Electrical Stimulation (FES)-assisted gait training and mainly represents a literature review with discussions. Section 2.2 outlines the advantages of FES-assisted gait training in comparison to other types or gait training e.g. treadmill training with partial bodyweight support. In Section 2.3, a description of normal gait and terminology of this are given. In Section 2.4 existing sensors, methods and algorithms for gait phase detection are presented. An introduction to FES-assisted gait training as well as the muscle selection, stimulation parameters and timing of the electrical stimulation is given in Section 2.5. Furthermore, different approaches and strategies for closed-loop control the stimulation intensity during gait are outlined in Section 2.6. The application of inertial sensors for motion estimation and the accuracy of such sensors are reviewed in Section 2.7. Finally, a discussion of open research issues in FES-assisted gait training are given in Section 2.8

2.2. Gait Rehabilitation after Stroke

Following stroke, it is necessary to start rehabilitation as soon as possible. In Europe, the Bobath training approach is the most used training concept applied for stroke rehabilitation. This method is based upon repetitive exercises of single movements in preparation for gait, while gait itself is not so much practised.

In the last decade, a new form of gait training with use of a treadmill and Partial Body Weight Support (PBWS) has been brought into clinical practice for patients with neurological impairment caused by stroke [32, 98], spinal cord injury [5] or other neurological diseases e.g. cerebral palsy [77]. In this novel approach patients use an overhead suspension system which supports a percentage of the body weight while the patients walk on a treadmill. The reduction of weight makes it possible for the patients to carry their remaining weight adequately, i.e. without knee collapse and excessive hip flexion during the single stance period of the affected limb. The body weight support is reduced as the walking ability increases, allowing more and more realistic gait training. This training regime allow the practice of a complete gait cycle with many repetitions in an early stage of the gait rehabilitation. Use of harness support minimises the delay before the patients can start the walking training. In addition, PBWS gait training is providing

Table 2.1.: Walking mobility criteria for levels of ambulation

Criterion	Description
1. Physiologic ambulator	Endurance, strength of level of assistance required make the ambulation not functional. May require assistance to stand. (Walks for exercise only)
2. Limited household ambulator	Walks in the home but limited by endurance, strength or safety (Walks rarely in the home/never in community.)
3. Independent household ambulator	Walks continuously for distances that are considered reasonable for inside the home. May require assistance with stairs inside and curbs, ramps outside the home. A wheelchair may be used outdoors. (Walks occasionally in home/ rarely in community)
4. Limited community ambulator	Walks outside the home and can manage doors, low curbs and ramps. A wheelchair may be used for long distances. (Walks regularly in the home/ occasionally in community)
5. Independent community ambulator	Walks for distances of approximately 400 meters at a speed at least 50 % of normal. Can manage all aspects of walking safely including curbs, stairs and doors. (rarely/never uses wheelchair)

an environment that discourages the development of compensatory strategies compared to gait training with walking aids which favours an asymmetrical gait pattern. In a study by Hesse et al. [32] it was shown that patients could practise a more favourable gait on the treadmill with a higher rate of symmetry and a prolonged stance phase on the affected side.

Repetitions of gait movements are assumed to lead to an activation of central gait pattern generators. The background for this theory is based upon experiments in adult spinalized cats and incompletely lesioned primates, showing an entrainment of presumed spinal and supra-spinal pattern generators by locomotor therapy [36]. The central pattern generator activation has not been shown for human beings but the plasticity of the brain allows relearning. Recently a large study [31] compared the Bobath program and a task-specific motor re-learning program in 61 acute stroke patients. Their results showed that patients who were trained with PBWS treadmill training stayed fewer days in hospital and their general improvements in motor functions and walking mobility criteria (see Table 2.1) were significant better as for the patients in the Bobath group.

PBWS treadmill training can also be enhanced by functional electrical stimulation. In a study by Hesse et al. [33] the effects of the combined use of functional electrical stimulation and treadmill training in hemiparetic patients were studied. Threadmill training with functional electrical stimulation was shown to be superior to traditional physiotherapy with regard to restoration to gait function. On the other hand, it has never been proven that functional electrical stimulation itself has positive effects. But clearly the use of functional electrical stimulation has several advantages in treadmill training as the stimulation can improve and support the movement and ease the manual labour for the physiotherapists.

The first usage of electrical stimulation to improve gait was done by Liberson et al. [43]. Peroneal nerve stimulation was used to elicit the withdrawal reflex in order to achieve dorsiflexion throughout the swing

phase. About 10% - 20% of chronic stroke patients develop a Upper Motor Neurone Drop Foot (UMN-DF). This means an inability to dorsiflex the foot during the swing phase of gait. For these patients a permanent drop foot orthosis can be a useful alternative to mechanical braces.

2.3. Description of Normal Gait

As this thesis is concerned in a broad way with gait and rehabilitation of gait, a short introduction to the gait and its definition is given in this section. There are several definitions and descriptions of gait as well as its phases in the literature. The most common definitions have been derived by Perry [65] and are therefore used within this thesis.

Walking is the most convenient way for human beings to travel short distances. As the body moves forward, one limb typically provides support while the other limb is advanced and prepares for the role to be the supporting limb. The Gait Cycle (GC) in its simplest form comprises swing and stance phase. The stance can furthermore be divided into 3 parts, initial double-limb support, single-limb support and terminal double-limb support. Each double-limb support period lasts for 10 % of the GC, while the swing phase typically endures 40 % of the GC and single double-limb period typically represents 40% of the gait cycle. Slight variations occur normally in the percentage of stance and swing related to gait velocity. The duration of stance decreases normally as walking velocity increases. As velocity increases, double-limb support time decreases. Running constitutes forward movement with no periods of double-limb support. The term ipsilateral is used to describe the same side of the body, and the term contralateral is used to describe the opposite side of the body or the opposite limb. The direction of walking is referred to as the line of progression.

A stride is the equivalent of a GC. The duration of a stride is the time between sequential initial floor contacts by the same limb. A step is recognised as the interval between sequential floor contacts by ipsilateral and contralateral limbs. Two steps make up each GC, which is roughly symmetric in normal individuals.

2.3.1. Functional Tasks of Gait

The gait can be divided into eight functional parts, these are sub phases. Each of the eight sub gait phases has a functional objective and a critical pattern of selective synergistic motion to accomplish this goal. The sequential combination of the gait phases enables three basic tasks, which are Weight Acceptance (WA), Single-Limb Support(SLS) and Limb Advancement(LA).

Task A: Weight Acceptance

The first functional task is Weight Acceptance. In this functional task two phases are involved, Initial Contact and Loading Response. The demand for immediate transfer of body weight onto the limb as

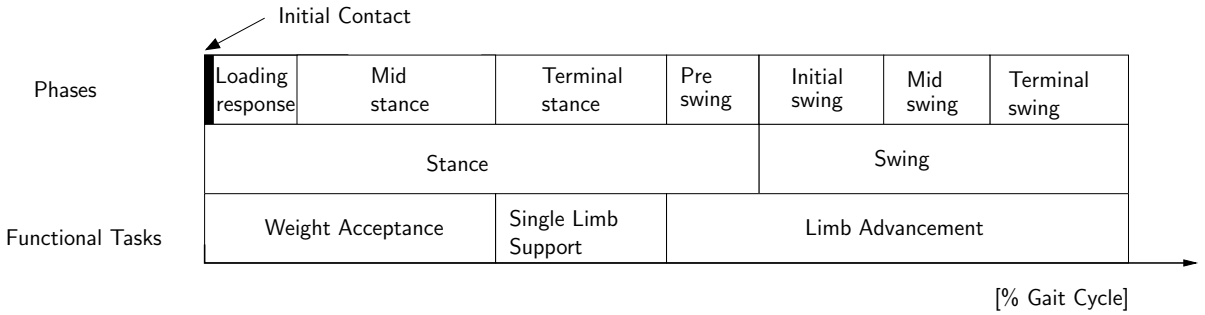

Figure 2.1.: Gait phases and functional tasks during gait according to Perry [65].

soon as it contacts the ground requires initial limb stability and shock absorption while simultaneously preserving the momentum of progression.

Task B: Single-Limb Support

The second functional task is the single-limb support. Primarily two phases are associated with the single-limb support, midstance and terminal stance. When the contralateral foot starts the swing phase, the single-limb support intervals begins for the stance limb. Midstance is the first half of the single- limb support phase, begins as the other foot is lifted and continues until the body weight is aligned over the forefoot. Terminal stance completes the single-limb support until the other foot strikes the ground.

Task C: Limb advancement

This task can be divided into four phases: Pre-swing, initial swing, midswing and terminal swing. Pre-Swing is the final phase of stance and the second double stance interval in the gait cycle. The weight is transferred from one side to the another, but this leg is not actively contributing to this, instead it is preparing for the swing. Initial swing begins with the foot lift from the floor and ends with the swinging leg opposite of the stance leg. Midswing begins when the swinging leg is opposite of the stance leg and ends when the swinging leg is in a vertical position. Terminal-swing concludes the swing when the foot strikes the floor.

2.3.2. Gait Phases

The gait cycle can be described in the phasic terms of initial contact, loading response, midstance, terminal stance, pre-swing, initial swing, midswing and terminal swing (see Figure 2.1). The stance period consists of the first five phases: initial contact, loading response, midstance, terminal stance and preswing. The swing period is primarily divided into three phases: initial swing, midswing and terminal swing. Pre-swing, however, prepares the limb for swing advancement and could in that sense be considered as a component of the swing phase.

Initial Contact is an instantaneous point in time which occurs in the moment as the foot touches the ground. Most of the motor functions of the leg which occur during initial contact are for the preparation

of the loading response that follows the initial contact.

The *Loading Response* phase takes up about 10 % of the gait cycle and constitutes the period of initial double-limb support. During this phase the whole foot becomes in touch with the ground. While this is done all the body weight is transferred onto the stance limb. This phase ends at the time as the contralateral leg is lifted off the ground.

Midstance represents the first half of single-limb support. This phase occurs in the range from 10 % to 30 % of the gait cycle. It begins when the contralateral foot leaves the ground and continues as the body weight travels along the length of the foot until it is aligned over the forefoot.

Terminal Stance constitutes the second half of single-limb support. This phase begins with the heel rise and continues until the contralateral foot touches the ground. Terminal stance happens in the range 30 % to 50 % of the gait cycle. During terminal stance the body weight is moving ahead of the forefoot.

Pre-swing is the terminal double-limb support period and this phase takes place during the last 12 % of the stance phase in the range between 50 % and 62 %. This phase begins as the contralateral foot comes in contact with the ground and ends as the toe looses contact with ground. During this period, the body weight is transferred onto the contralateral side.

The *Initial Swing* phase takes place in the range from the 62 % to 75 % of the gait cycle. This phase starts as the toe lifts of the ground and continues until the maximum flexion of the knee is achieved.

Midswing occurs in the second third of the swing period in the range from 75 % to 85 % of the gait cycle. This phase begins at the moment as the knee is maximal flexed and ends in the moment as the tibia is in a vertical position.

Terminal Swing takes place in the range from 85 % to 100 % of the gait cycle. The phase starts at the tibia passes beyond perpendicular sagittal orientation and continues until the knee fully extends in preparation for heel contact.

2.4. Gait Phase Detection

The task of a Gait Phase Detection (GPD) system is to identify the phases of gait based on some sensory input mostly for the purpose to trigger electrical stimulation in a drop foot stimulator or in FES-assisted gait training. GPD is especially important for drop foot orthoses, as there is a need to detect the gait phases robustly for all possible situations in daily life. For FES-assisted treadmill training, where the patients are consequently either walking forward or standing, the requirements on a gait phase detection system are weaker. A gait phase detection system for foot drop has to detect the intention to take a step and at the same time it has to exclude other daily life non-walking tasks e.g. sitting down and standing up. In gait phase detection systems developed so far, the gait cycle is divided into two or more phases.

The number and definition of these phases varies. As already described in Section 2.3, normal gait is usually divided into as much as eight gait phases for each leg. This division is hard to fulfill and to detect with a sensory system. Normally, in a gait phase detection system, four or less gait phases are detected depending on the sensors used.

2.4.1. Gait Phase Detection: Sensors and Robustness

The first sensor taken into use, and still the most frequently used sensor in gait phase detection systems, is the foot switch. The fact that foot switches are mounted beneath the foot imply that mechanical wear will degrade the performance after a while, and as reported by Willemsen et al. [100], they are quite unreliable and susceptible to mechanical failure. The inadequacy of footswitches in detecting foot contact events was shown in [50]. On average, the foot switches detected heel contact falsely 1.3-7.6% of the time. In a paper by Taylor et al. [88] a questionnaire were done among the users of the Odstock Dropped Foot Stimulator (ODFS) and nearly 40 % of the patients reported problems related to the stimulator's foot switches.

These facts lead to the desire to use more reliable sensors in gait phase detection. Another goal is to improve the robustness and accuracy of detection. But the concept of accuracy can be somewhat difficult to define as transitions between phases occur gradually, and might be interpreted differently by different investigators who are manually detecting gait events e.g. by evaluating a video. Therefore, no sensor can be considered completely accurate in the detection of gait events, and comparison between different sensor systems and detection algorithms can only show relative differences.

So far, besides the simple foot switch, combinations of manual switches, foot switches, force sensitive resistors, inclinometers, goniometers, gyroscopes, accelerometers and ENG (electroneurography) have been proposed as sensory systems to detect gait phases, and consequently to control the timing of the stimulation sequences in FES-assisted training systems. The usage of 2 or 3 foot-switches has been reported by Chen et al. [11] and insole force measurement was applied in [23]. A switch sensor at the heel of the affected side can be used to trigger quadriceps stimulation on the disabled foot during the stance phase [11]. More extensively equipped with sensors were the subjects in the study described in [20]. In addition to foot switches and angle measurement by use of goniometers, acceleration was also measured at the hip joint. All this information was used in a machine learning regime. In [100], four accelerometers were used to measure the radial and tangential acceleration of the shank segment. A rule based algorithm was developed to detect four distinct gait phases with the emphasis on detecting heel-off as this is essential in a peroneal nerve stimulator. This algorithm worked well for three out of four patients, but for the forth patient the heel-strike was constantly detected too early due to disturbances. An approach using accelerometer sensors was described in Williamson and Andrews [101]. Three accelerometers were attached in the tibial crest region. Two of the accelerometers were oriented in the horizontal direction and the last one in the vertical direction. Force-sensitive resistors were used

to generate reference signals of gait phases from the foot-floor contact pattern. In this paper an Adaptive Logic Network (ALN) was applied in order to detect gait phases from the accelerometer measurements. A remarkable high accuracy of the proposed sensor system was achieved by comparing the detection based on accelerometers mounted on the shank with a traditional FSR sensor system. The heel strike and the toe off detections were reported to have an accuracy of 99 % and 96 % respectively. As the data were sampled with a frequency of 33 Hz, this accuracy means that only 1 out of 10 samples missed with one sample at 99% accuracy.

Other alternatives for triggering stimulation like goniometers measuring hip, knee and ankle angles have also been proposed [60]. Recently, the interest in using a combination of gyroscopes and accelerometers by use of Inertial Sensor Units (ISU) and reduced ISUs has grown for the purpose of detecting gait phases. Kotiadis et al. [40] used an inertial sensor system. Although using a complete ISU with 3 gyroscopes and 3 accelerometers, only the 2 accelerometers in the sagittal plane and the gyroscope measuring angular velocity in the sagittal plane were considered in that work. Contrary to the work in this thesis, the sensor was fixated on the shank segment just below the knee. A similar placement of tilt sensors in [14] showed that this sensor configuration leads to a bad differentiation between gait movement and standing up/sitting down. A similar study was done by Sabatini et al. [75] where spatial gait parameters were estimated in addition to the temporal parameters. In a reduced ISU two accelerometers and one gyroscope collect the most valuable information, the additional sensors in a complete ISU might improve the robustness and accuracy. Furthermore, a complete ISU would provide a more accurate estimation of foot velocity and position which could possibly be used for transitions rules between states in a gait phases detection system. To the author best knowledge, no GPD system utilising all gyroscopes and accelerometers in an inertial sensor unit has been developed until now.

Another method is described in Strange and Hoffer [87] to detect the transition between swing and stance phase by exploiting an afferent nerve input. By implanting nerve-cuff electrodes in cats they were able to detect the transitions between stance and swing with a relability of 99%. Later, similar detection systems have been applied in human beings [29]. By attaching the nerve-cuff to the peroneal nerve and using a switching circuit, stimulation followed through the same electrode. Such systems are invasive and only detect two phases. A major disadvantage of these sensors is that force sensitive resistors have to be used in a calibration procedure in order to train an adaptive logic network. In [10] a system using EMG signals was used for triggering stimulation. Electrodes at the tibialis anterior are used to sense voluntary motion. This signal is rectified and integrated. When the processed signal exceeds a threshold the stimulation is initiated on two other electrodes, and continuing for as long as the patient maintains the EMG signal.

Closely related to real-time gait phase detection systems are offline gait analysis systems measuring temporal and spatial gait parameters. Such a system was developed by Aminian et al. [2] who attached gyroscopes to the shank. A method applying wavelets was designed to detect heel-strike and toe off events. In similarity to [101], the detected events were compaired with data recorded from FSR attached to the heel and to the toe. In the study, the participants were divided into two groups; one consisting of young and one of elderly people. Heel strike detection based upon gyroscopes was found to have a

systematic delay of 10 ms with regard to FSRs with a confidence interval between 7 and 13 ms. A similar study was performed by Jasiewicz et al. [38]. An algorithm searches in windows to find peaks in either acceleration data or in gyroscope. The sensor, a reduced ISU with one gyroscope and two accelerometers, was mounted to the foot and shank segments, and the detected gait phases were compared with gait phases gained from foot switches. The results were similar to those found in [2] for subjects with normal walking pattern. For patients with abnormal gait pattern, a larger deviation in the detection of the two events was observed for events detected with the data from the shank segment.

2.4.2. Methods of Gait Phase Detection

In methodology there are mainly two approaches to detect the gait phases. The first is a rule based approach in which the gait phases are defined as states of a finite state machine and the transitions between the states are functions of the sensory input [14, 40, 64, 75, 100]. An example of a rule based gait phase detection system can be found in Papas et al. [64]. In this approach one gyroscope and three FSRs were applied. One FSR was placed underneath the heel while the two others were placed underneath the metatarsal heads since the foot is not always symmetrically loaded. The gyroscope was attached to the heel and was applied to calculate the tilt angle relative to the ground. This was done by filtering and integrating the gyroscope signal. Drift was avoided by resetting to zero when all force resistive sensors were loaded. The gait detection algorithm divided the gait cycle in four different gait phases: stance, heel-off, swing and heel-strike. These phases were represented as states in a state machine, and the transitions were governed by a knowledge-based algorithm. The algorithm allowed 7 transitions between states (See Figure 2.2). The gait phase detection system was validated by use of a 3D motion analysis system. It was reported that the GPD system had a systematic delay compared with motion analysis system in the worst case of 90 ms. The correlation was reported to be good but no numbers were given indicating the variance of the detection.

The second approach is from the methodology completely different compared to the first. Instead of having clearly defined rules for transitions, the detection system is represented as a black box where the gait phases are the outputs and sensory information are inputs [60, 83, 101]. Such black-box systems are usually related to machine learning techniques, fuzzy logic systems or neural networks. Normally, such systems have to be trained in advance by using a known reference. Such reference can be transitions which are found by manually evaluating video data. The advantage of such systems is that they can be trained to accurately and robustly detect gait phases for one subject. On the other hand, the disadvantage of those systems is that they have to be trained for each subject separately with some sort of reference detection system, possibly by foot switches or manually by a hand switch. This is a time-consuming procedure that has to be redone as the gait rehabilitation progresses and consequently the gait changes. That makes this approach difficult to implement in a clinical setting.

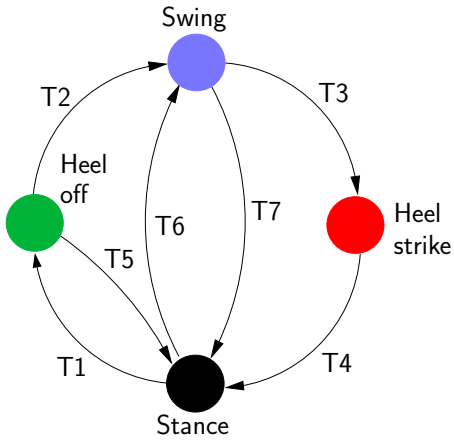

Figure 2.2.: Gait phase detection system represented as a state machine. The gait phases are represented as 4 states and 7 transitions [64].

2.5. FES-Assisted Gait Training Systems

In this section, a review of FES-assisted gait training is outlined. The focus will be on surface stimulation approaches applied to stroke patients. A summary of studies is given in Table 2.2.

FES-assisted gait systems can be used for rehabilitation purposes for acute hemiplegic stroke patients or as a permanent orthosis called Drop Foot Stimulator (DFS) for chronic drop foot patients. The technological aspects for both DFS and FES-assisted gait training systems are similar e.g. the stimulation is synchronised to the gait phases. FES-assisted gait training systems are usually applied in the rehabilitation a short time after stroke, and are usually applied to patients who can ambulate independently on a treadmill with partial body weight support. The general idea of FES-assisted gait training is that the gait movement should be repeated many times in order to relearn walking. In a metastudy by Robbins et al. [72] all relevant articles on the usage of FES to relearn gait were investigated in order to conclude on the effects of FES on gait. The results of the study showed that the usage of FES gives a statistical improvement on the gait speed. Furthermore, an increased muscle strength was shown to be significant. On the other side, the overall functional ability was not significantly improved. A further metastudy by van Peppen et al. [92] confirms this saying that while there is moderate evidence that FES has a positive effect on gait speed and muscle strength, it could not be proved that FES increases the scores on Activity of Daily Living (ADL).

As already mentioned in Chapter 1, 20 % of stroke survivors develop a long term disability to dorsiflex the foot during the swing phase of gait. In 1961 Liberson et al. [43] developed the first orthosis based on electrical stimulation for patients with drop foot. In their innovation the withdrawal reflex was employed to achieve dorsiflexion throughout the swing phase. A heel switch was mounted in the sole of the shoe to synchronise the stimulation to the peroneal nerve during the swing phase. When the pressure released

Table 2.2.: Stimulated muscle groups or nerves using surface electrodes in FES-assisted gait training: Q - quadriceps, H - hamstrings, G - gluteus maximus, TA - tibialis anterior, S - Soleus, P - peroneal nerve. The last column indicates the number of patients participating in the study. If the study is of pure technical nature it is marked with (T).

Source	Q	H	G	TA	S	P	Patient type	N / Study type
Liberson et al. [43]						×	Hemiplegic	7
Vodovnik et al. [99]							Hemiplegic	T
Kralj et al. [41]	×		×			×	Paraplegic	3
Bogataj et al. [7]							Paraplegic	T
Malezic et al. [48]	×	×	×	×		×	Stroke and Brain damaged	18
Hesse et al. [33]	×	×	×	×		×	Hemiparetic	11
Bogataj et al. [6]	×	×	×		×	×	Stroke	1
Chen et al. [11]	×			×			Hemiplegic	1
Taylor et al. [89]/ODFS						×	Hemiplegic	151
O'Keeffe and Lyons [62]						×	Hemiplegic	-
Granat et al. [25]						×	Hemiplegic	19
Quintern et al. [67]						×	Hemiplegic	38
Hansen et al. [28]						×	Hemiplegic	1
Lyons et al. [47]						×	Hemiplegic	1
Sepulveda et al. [80]						×	Hemiplegic	1

off the heel-switch at heel off the delivery of stimulation started and continued until the the heel-switch closed at heel strike. Clearly, the system lacked sophistication and delivered stimuli in a crude fashion compared to the natural activation of the neuromuscular system. In this case study, seven hemiplegic patients participated, and in all subjects a considerable improvement of the gait was shown when they used the foot drop orthosis. A good survey paper by Lyons et al. [46] describes the technological developments in neural protheses for the correction of upper motor neurone drop foot since 1961.

After the first development of Liberson, many hard-wired single channel system followed in the seventies and eighties [99]. One problem that was frequently reported was the occurrence of a reflex spasm provoked by electrical stimulation. Vodovnik et al. [99] described a DFS system where they proposed to solve this problem by filtering the onset activation signal by a low-pass filter in order to enable a soft onset and a soft stop of the stimulation current. Other innovations described by Vodovnik et al. [99] were:

- use of both manual and conventional foot switch triggering.
- use of electromyography (EMG) for triggering ES rather than using foot switches.

The paper of Vodovnik et al. from 1978 was of pure technical character and no experiments with patients were described.

In 1983, the first use of multichannel FES was proposed by a group at the University of Ljubljana in Slovenia [41]. In this paper, they demonstrated the usage of a three channel portable stimulator. The stimulator incorporated a radio link between the heel-switch and the stimulator. The three stimulation channels enabled different muscle groups to be controlled independently, such as ankle dorsiflexors, knee flexors and knee extensors. A drawback of the system was that the clinician was required to make multiple adjustments to optimise the delay settings for each of the three stimulation channels following detection of the heel-off event. The stimulator system described in the paper was experimentally tested on 3 SCI patients.

In the paper by [7] from 1984, the first use of microcontroller/microprocessor technology in a FES-assisted gait training system was reported. Bogataj's system consisted of a 6-channel stimulator and a control unit with an embedded stride analyser. On the control unit there was an array of 16 switches which were used to refine the stimulation pattern. By using 8 switches for the swing phase and 8 switches for the stance phase for every stimulation channel, a refinement of the stimulation pattern was possible. The increments were scaled in time to the duration of the swing and stance phases by the stride analyser. The stride analyser was also used to display vital parameters of the gait like the number of steps, the mean stride time and the swing/stance duration. As for many multichannel stimulation devices this was only suitable for clinical use.

In the early nineties the Ljubliana group developed a new 2-channel microprocessor based DFS [48]. This stimulator had in addition to the stimulation part, a programmable stride analyser. The clinicians could independently program all the stimulation parameters for each channel via the programmer unit. The subjects could only adjust the current amplitudes. As for the earlier 6-channel stimulator unit by [7], the duration of the stimulation sequence was adapted to the subject's cadence. Two foot-switches could be connected to the stimulator unit and if additional stimulation channels were required a cascade arrangement of the stimulators was possible. In addition, the programmer unit gathered parameters of gait like the number of strides recorded in a session, the duration of left and right stride as well as the duration of swing and stance phase. Recording of gait parameters is useful because it allows the clinician to assess how the DFS is performing in a home environment. In this study 11 stroke and 10 Traumatic Brain Injured (TBI) patients were stimulated during gait. Different stimulation combinations of peroneal nerve, hamstring, quadriceps, triceps brachii, and gluteus maximus were applied. The purpose of the clinical evaluation was to determine the stimulators performance in therapeutic and orthotic use. The main efforts was directed to the evaluation of the flexibility of the program to different stimulation approached. It was concluded that the stimulator proved to be adequate for the restitution of gait in stroke and TBI patients because the nature of the stimulator units a large variety of stimulation sequences and parameters could be adapted to a large patient group.

In a study by Hesse et al. [33] from 1995 the effects of the combined use of functional electrical stimulation and treadmill training in hemiparetic patients was described. Muscle stimulation to the affected lower limb muscles were applied using surface electrodes. The stimulator provided a selection of the stimulation within eight stance phases and eight swing phase increments for every channel (See Figure

2.5). The durations of the phase increments were updated corresponding to the cadence. The peroneal nerve was stimulated by use of surface electrodes for the dorsal flexion and moderate eversion during the swing and initial stance phase in ten subjects. The quadriceps muscle was stimulated for the knee extention in the terminal swing and the first part of the stance phase. The hamstring was stimulated for the knee flexion in the pre and initial swing phase. Finally, the gluteus maximus was stimulated for hip extention throughout the stance phase. In total 11 patients participated in this study, divided into two groups, where the first group consisted of 4 patients who received treadmill training besides conventional physiotherapy. In the second group, a single case A-B-A study was applied, where phase A was 15 treadmill/stimulation treatments, phase B conventional physiotherapy for 15 days and last phase A was consisting of another 15 treadmill/stimulation treatments. The first four patients improved their gait ability considerably during the additional treadmill training. After the study one patient was completely independent, two patients needed verbal support and one patient was still dependent on intermittent support. In the seven patients assessed in the A-B-A study the functional ambulation category improved during the two A phases, and remained fairly constant in the B phase. The Rivermead score and the Ashworth score indicated no differences between the two therapy treatments in muscle strength and spasticity in the A-B-A study.

In 1999, Taylor et al. [89] described the use of a single-channel hard wired stimulator, the Odstock Drop Foot Stimulator (ODFS). This stimulator had incorporated a few new innovative solutions. Stimulation of the hemiplegic leg could be controlled by a heel-switch worn on either the hemiplegic or nonhemiplegic side. When the switch was on the nonhemiplegic side, stimulation was initiated by heel strike and terminated by heel rise. Furthermore, miniature potentiometers were introduced in order to allow adjustment of both the rate at which the stimulation was ramped up at toe-off and the rate at which stimulation was ramped down at heel-strike. In this study 151 patients divided into 3 groups of stroke, MS and ISC. After the patients had got their drop foot stimulator fitted, they used it on a daily basis. An assessment of Physiological Cost Index (PCI) and speed of walking was made initially and after four and a half months. The stroke patients showed a statistically significant improvement in both measurement parameters. The immediate effect of using the stimulator was also shown to be statistically significant, with an increase in walking speed of 12 % and a decrease in effort of 18 %. For the stroke patients a short term “carry-over” effect when not using the stimulator was shown after four and a half months.

The tibialis anterior is the major muscle controlling dorsiflexion of the ankle joint. During the swing phase of gait the typical EMG activity pattern of tibialis anterior has two peaks; at the initial swing and the loading response. In [61] an optimisation scheme was introduced in order to find the optimal stimulation pulse width of the tibialis anterior. This was done by comparing the value of the natural EMG profile with the EMG profile developed from electrical stimulation. A stimulation pulse width trajectory which produced an EMG pattern similar to a natural pattern was found by optimisation. It was shown that this optimised stimulation pattern resulted in a significantly higher dorsiflexion range than the normal trapezoidal stimulation. Additionally, only half of the stimulation charge had to be applied which led to reduced muscle fatigue. The experiment described in this paper was performed on one 23 year old

healthy subject who was seated in a CON-TREX MJ isokinetic dynamometer. As the experiment was not performed during walking no conclusions can be drawn on whether the improvements could also be expected in walking.

In 2000, Lyons et al. [47] implemented a similar "natural" activation envelope to the one described in [61] in form of a look-up table in a stimulator. By observing the duration of the swing phase, the stimulation envelope was scaled in time whereas the shape and amplitude stayed constant. The stimulation envelope was applied to a 52 year old hemiplegic patients. The results showed that using the "natural" stimulation envelope, a 76 % increase in dorsiflexion range was obtained for this specific patient.

A study by Quintern et al. [67] showed that the stimulation of flexor reflex afferents during gait retraining of non-ambulant hemiplegic stroke patients improved the rehabilitation of gait. The inclusion criterion of the study was that the patients should be able to stand without the help of a therapist but they should not be able to walk more than 10 metres. Patients who did not have a positive flexion reflex response on electrical stimulation were excluded. The study followed two groups both receiving gait training; one with electrical stimulation, and one without. The main result of the study showed that the walking speed in the FES group was significantly higher than in the other group.

An alternative to treadmill training is the application of robot-like walking machines. Examples of these are the Gait Trainer GT I developed by Hesse et al. [34] and distributed by the company Reha-Stim GmbH[1] and the Lokomat developed by Colombo et al. [13] and distributed by the company Hocoma AG Medical Engineering[2]. These are machines that in principle are moving the disabled limbs on a predefined path. They are expensive and take up a lot of space but represent a real alternative to treadmill training for severe hemiplegic patients who are not able to walk independently even with partial body weight support. A multicentre study (DEGAS) was recently performed in Germany [66] in order to evaluate the effects of repetitive locomotor training on the GT I in subacute stroke patients. The patients were divided into two groups. Group A received 20 minutes of locomotor training and 25 minutes of physiotherapy whereas Group B received 45 minutes of physiotherapy. Primary outcome measures were gait ability and Activity of Daily Living (ADL). The results showed that significantly more patients in Group A compared to Group B could walk independently (at least 75 on the Barthel index) after four weeks of training. Recently, the GT I has also been enhanced with functional electrical stimulation [57, 90]. The latter study involved training with two patients for a period of 4 weeks. By the end of the training period, both patients showed improvements in the scores on the Barthels index, and improvement of balance and in functional ambulance. In a 6-month follow up assessment further improvements on ambulation and balance were found. Further randomised studies are needed to evaluate whether combined training with FES on an electromechanical trainer is superior to training on an electromechanical trainer alone.

[1] http://www.reha-stim.de
[2] http://www.hocoma.ch/

2.5.1. Stimulation Sites and Stimulation Parameters

In DFS and in the FES-assisted gait relearning with the use of PBWS and treadmill training, the choice of which muscles to stimulate is an important question. The following list shows the most common stimulation sites during FES-assisted gait training:

- Stimulation of the peroneal nerve during the swing phase in order to elicit the withdrawal reflex. The withdrawal reflex is causing ankle dorsiflexion, knee flexion and hip flexion. The stimulation is usually prolonged to the end of the swing phase. [6, 33].
- Stimulation of the soleus muscle in order to provide or correct the push-off in the terminal stance and in the pre-swing phase.
- Stimulation of the quadriceps muscle for correction of knee extension in the terminal swing, initial, and midstance phases [11, 42].
- Stimulation of the hamstring muscles in order to establish or correct knee flexion in the pre-swing and initial swing phases.
- Stimulation the gluteus maximus muscle throughout the stance phase to enable weight shift to the affected lower limb.

Care has to be taken to find the best placement of electrodes. Especially the placement of the surface electrodes for peroneal nerve stimulation has been reported in the literature to cause some problems [9]. In Figure 2.3 the electrode positions of the major muscle groups as well as the peroneal nerve are depicted. The placement of the electrodes has to be done with a trial and error approach in order to find the optimal response to obtain balanced dorsiflexion and eversion of the foot. This time consuming task has to be performed before each session. To achieve a more precise stimulation, usually smaller electrodes are used compared to muscle stimulation. For the peroneal nerve stimulation is the active electrode placed over the common peroneal nerve, just below the head of fibula. The other electrode is located approximately 5 cm below, slightly forward of the active electrode over the motor point of tibialis anterior [9]. Quintern et al. [67] used other stimulation sites in order to elicit the withdrawal reflex. They stimulated either the sole of the foot, dorsum of the foot or lateral to medial aspect of the knee joint. The placement of the electrodes for muscle stimulation is easier than the placement of electrodes for eliciting the withdrawal reflex. The active quadriceps electrode is placed above the knee and slightly medially in order to recruit the vastus medialis. The active electrode is placed midway up the thigh and 3 cm to the lateral side. The active electrode for gluteus maximus is placed below the dimples at the top of the sacrum. The other electrode is placed approximately one hand's breath below the active electrode. The active hamstring electrode is placed over the centre of the muscle. The other electrode is placed at the bottom of the hamstring, just above the back of the knee. The active calf muscle electrode is placed above the widest part of the calf muscle and the indifferent electrode is placed towards the bottom of the calf muscle.

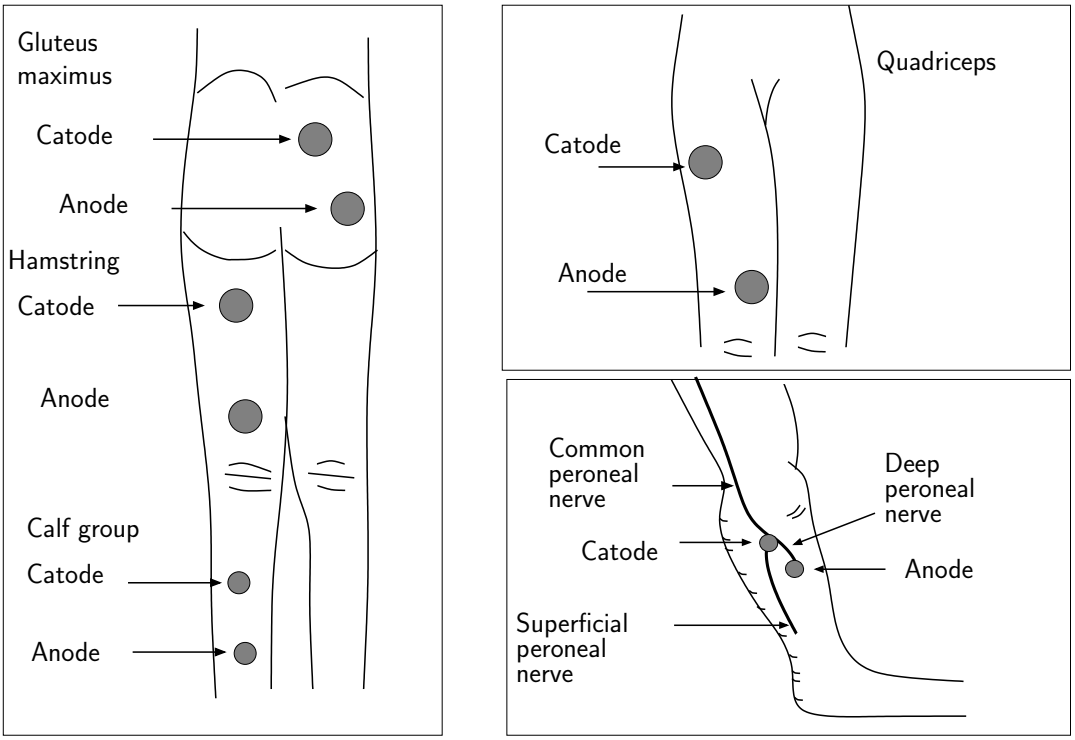

Figure 2.3.: The figure shows the most common stimulation sites: The left figure shows the stimulation of gluteus maximus, hamstrings and to the calf group. The upper right figures shows the stimulation sites of the quadriceps. The lower left figure shows the most common position of the electrodes of the peroneal nerve stimulation [9].

The type of stimulation pattern is dependent of how the gait phases are detected. When using a single foot switch at the heel as Liberson et al. did, the stimulation is ramped up at the toe off event and ramped down after the heel strike event as illustrated in Figure 2.4. When more advanced gait phase detection system are used, the possibility to refine the stimulation pattern can be achieved as well. In Figure 2.5 an example of a stimulation pattern used for hemiplegic patients is shown where both the swing and the stance phases were each divided into 8 time periods which also were scaled in time according to the cadence. This stimulation pattern was applied by Bogataj et al. [6]. In addition to the timing and duration of the stimulation there are a few other parameters that can be set e.g. the current amplitude, the frequency and the pulse width. The pulses are normally biphasic and typical values for the current amplitude are between 10 mA to 50-60 mA. The pulse width lies between 10 and 500 μs. Normally either the current amplitude or the pulse width is kept constant and the other one is varied to achieve the desired movement. For the stimulation to be effective, it must produce a strong muscle contraction without discomfort and muscle fatigue. Regarding the frequency, there is a difference whether the peroneal nerve or a muscle is stimulated. The applied stimulation frequency of the peroneal nerve has an impact on the withdrawal reflex response with regard to habituation. An increasing habituation was found in the studies of Hesse et al. [33] and Malezic and Hesse [49] when a stimulation frequency of 20 Hz was applied. This meant

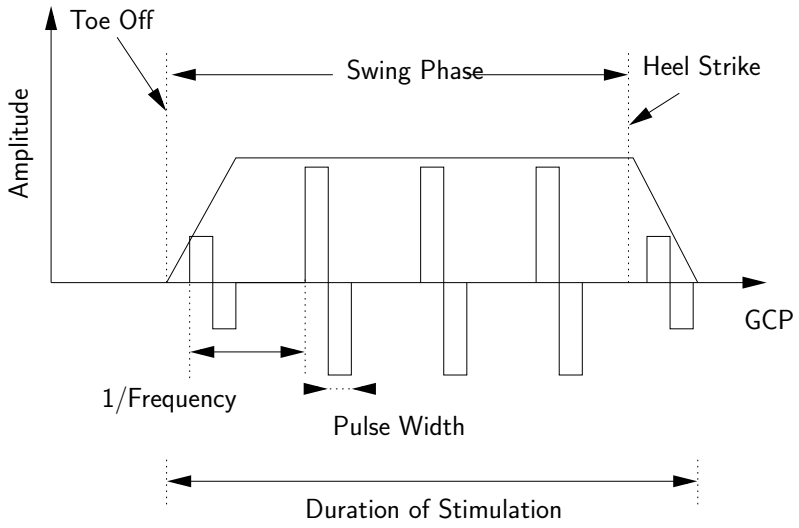

Figure 2.4.: An example of a stimulation pattern when a heel and a toe switch is applied. The stimulation is ramped up at toe off and continued until heel strike when the stimulation is ramped down.

that an increased stimulation intensity had to be applied, subsequently until the highest allowed level was reached. The stimulation frequency was then shifted to 60 Hz which was shown to provide a sustained activation with less habituation [49]. In the same study, the EMG signals of the tibialis anterior, soleus, biceps femoris and rectus femoris were recorded in several tests where frequencies of 20, 50 and 100 Hz were applied. The EMG measurements showed an increased ratio of peak amplitudes between the tibialis anterior and the soleus in favour of dorsiflexion with increased stimulation from 20 to 50 Hz, but decreased at 100 Hz. For the biceps femoris and rectus femoris there was no big differences between the different stimulation frequencies. At the end, a frequency of 60 Hz was chosen which gave a better dorsiflexion for all patients. With this frequency the dorsiflexion remained stable without too much habituation. In the article of Field-Fote [19], the stimulation of the peroneal nerve was in the range 50-80 Hz, but no special attention was payed to investigate the effects of different frequencies. In both these studies the investigations were done with paraplegic patients.

In a study of stroke patients by Quintern et al. [67] a frequency of 40 Hz was used to elicit the withdrawal flexor reflex. In muscle stimulation, usually a lower frequency (20Hz) is used. Fatigue poses less of a problem for intermittent stimulation burst, like stimulation during the swing phase of walking, compared to other applications were continuous stimulation are applied e.g. standing up or sitting down. In [17] it was shown that an increase of stimulation frequency from 50 Hz to 60 Hz had no influence on the fatigue for FES-cycling but even though the power output increased with 25 %. As stimulation pattern for FES-cycling is similar to pattern for FES-assisted gait, this result should be valid for FES-assisted gait as well.

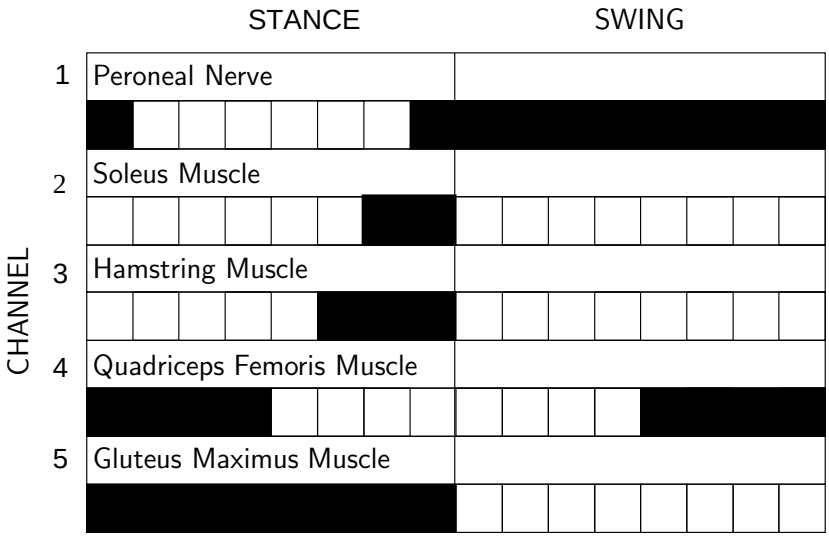

Figure 2.5.: Stimulation pattern for FES-assisted gait training used by Bogataj et al. [6]. Both swing and stance phases are divided into 8 time intervals which are scaled to the cadence. Selected time intervals are used to refine the stimulation pattern.

2.6. Control Approaches for Drop Foot Stimulators and FES-Assisted Gait Training

One aspect of DFS and FES-assisted gait training systems that has received little attention in the literature is closed-loop control of the stimulation intensity. In all the approaches described in the previous sections the intensity of the stimulation was either pre-programmed before the session started and then kept constant throughout the session, or a fixed pattern was programmed and adapted to the gait cadence. These approaches with a preprogrammed stimulation intensity represent a disadvantage that the stimulation intensity usually is chosen to large in order to achieve the desired movement. By using sensors and by giving feedback (closed-loop control) from the motion, a more desired movement can be achieved with use of less stimulation which will in turn reduce the fatigue and prolong the time the stimulation can be applied. In this section, closed-loop control of stimulation will be reviewed. When using the term “control” in the application of DFS and FES-assisted gait training, the adaptation of either the stimulation intensity (pulse width or current amplitude) or the length of the stimulation burst is meant.

Control systems for adaption of stimulation intensity in FES-assisted gait training can be classified in two methods: Classical feedback and adaptive feed forward control. Feedback control is based upon continuous measurements of joint angles which are used to readjust the stimulation intensity in order to follow a predefined angle trajectory. Due to non-linearities between stimulation intensity and angle trajectories such as time delay which is causing a limited bandwidth, this method is not very useful in FES-assisted gait training. Feed forward control means that a stimulation pattern is chosen beforehand.

The stimulation pattern can be changed after a completed step based upon measurements of the movement. A cycle to cycle controller of the gait is a special case of adaptive feed forward control. By using this strategy, information from the last stride is used to adapt the stimulation intensity in the next stride. Common to both strategies is that some sort of sensory information such as that from goniometers, force sensitive resistors, accelerometers or inertial sensors has to be present.

Feedback Control of Angle Trajectories

In this section, different strategies found in the literature which are dealing with the control of hip, knee and ankle joint are reviewed. An FES-system for preventing drop foot and for compensation of the quadriceps weakness in hemiplegic patients was developed by a group in Taiwan [11]. The system consists of three Force Sensitive Resistors (FSR), two attached to the affected foot as well as one attached to the healthy foot. Additionally, three magneto-resistive angular position sensors were applied to measure knee and ankle joint angles. The stimulation of the quadriceps was related to the FSRs on the affected side. The tibialis anterior stimulation was triggered by the FSR on the unaffected side. If a drop foot was detected, meaning that the toe-strike event happend before the heel-strike event, the pulse duration of the tibialis anterior was increased. This work was later extended by a fuzzy logic controller [12].

Another closed-loop control approach to drop foot was reported in [55]. The ankle joint angle was measured with a goniometer and a force sensitive resistor was used to detect the heel contact with ground. The intensity of the stimulation was adjusted according to an embedded control law which was not closer described in the paper.

In the neuroprothesis system “WALK!” developed by Fuhr and Schmidt [23] an Integral (I)-controller with a dead zone was applied in the late swing phase and throughout the stance phase to control the knee extension in paraplegic subjects. The knee angle was measured with a goniometer. If the knee angle was lying between two threshold values the stimulation intensity was kept constant. Furthermore, if it was detected that the knee was hyper-extended the intensity was lowered through an I-controller. When the knee joint was more flexed than the lower threshold, the intensity was increased through an I-controller similar to the first one but with a lower gain.

Adaptive Feed Forward control

As already mentioned, the second approach to control the intensity of stimulation during gait is on a stride to stride basis i.e. the stimulation intensity for the next step is based on information from the previous strides. Related to this is cyclical control of lower limbs. Such control can be performed in a set-up where the patients are sitting on a bench where the shank can be freely moved or the patients are sitting on a bicycle seat restricting the movement of hip and knee angle to the sagittal plane. The first attempt described in the literature to control a single limb movement in a cycle to cycle manner

by use of functional electrical stimulation applied to the quadriceps group was done by Veltink [93]. In his experiments the patients were sitting on a bench such that the lower limb could swing freely and the knee angle was measured with a goniometer. By applying cyclical stimulation with the same time period as the free swinging leg, a cyclical movement could be produced. A PID-controller was designed to achieve a constant maximum knee angle. The time-discrete PID controller adapted the burst time whereas the pulse width and current amplitude were kept constant. The experiments showed that the controller compensated for the influence of fatigue for at least 150 cycles. After 150 cycles, the controller was saturated and the maximum knee angle decreased.

An extention of the single limb movement has been done in [95] where a two degree of freedom movement was considered in simulation. Later the same concept were experimentally validated [21]. The SCI injured patients were standing in a stand device with arm support. In the stand frame, the movement of the free swinging limb was fixed to the sagittal plane. The ankle, knee and hip joint of the other leg were locked. Additional support was provided from a bicycle saddle. Stimulation were applied to the hip flexor, hamstring and quadriceps in order to generate a cyclical movement. The optimal stimulation onsets and burst durations of the three muscle groups were identified experimentally. First the stimulation of the hip flexor was found by gradually increasing the burst duration until a desired hip range movement was achieved. Hamstring stimulation was added in order to achieve sufficient foot clearance in the forward swing. Quadriceps was then added to achieve knee extention. The hamstring and quadriceps stimulation were kept constant, while the hip flexor stimulation was adapted using a discrete PID controller working on a cycle to cycle level. The authors concluded that stimulation patterns for the major swing phase objectives during gait can be achieved in paraplegic subjects. Furthermore, slowly time-varying system characteristics such as fatigue were compensated by using a slowly varying cycle to cycle PID controller, and a desired swing of leg for a prolonged period of time was successfully maintained. A neuro-fuzzy control strategy for the same set-up was studied in van der Spek et al. [91]. No large differences between the PID and neuro-fuzzy controller were observed.

Another method to cyclically control one or two segments of the leg is with use of a two stage neural network control system was persuaded by Abbas and Triolo [1], Riess and Abbas [71]. An extention of this work to two limb cyclical control were done by stimulating the peroneal nerve, hamstring quadriceps and gluteus [63]. They used a set-up similar to Veltink et al. [95]. Cyclical control of one and two segments of the leg by use of a two stage neural network was demonstrated. A first layer of the neural network, the Pattern Generator (PG) generated a periodic signal, typically consisting of over-layered sinusoidal functions. Usually this parts is kept constant during experiments, which means this part is only producing a periodic signal. The next layer of the neural network the Pattern Shaper (PS) shaped this periodic signal by using angle measurement from knee joint compared with pre-defined angle trajectory. In this approach the peroneal nerve, hamstring quadriceps and gluteus were stimulated. The peroneal nerve stimulation and the gluteus stimulation were kept to a constant value, while the hamstring and quadriceps stimulation were set by the neural PG/PS controller. The objective of the controller was to track predefined knee and hip joint angle trajectories.

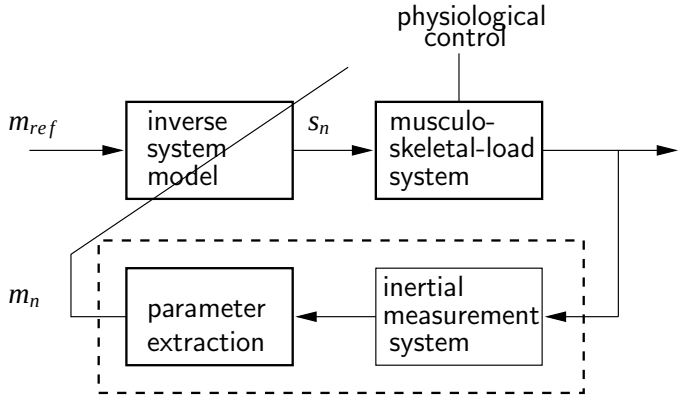

Figure 2.6.: Conceptual scheme for adaptive tuning of a two channel drop-foot stimulator using movement parameters derived from inertial sensor movement sensor Veltink et al. [96]. s_n represents a stimulation channel whereas m_n represents a movement parameter. m_{ref} is the reference movement parameter.

All the approaches for cyclic control of lower limb movement described so far have been for free swinging leg in a static position. Veltink et al. [96] proposed a new adaptive tuning strategy for cycle to cycle adaption of stimulation during gait. The scheme is depicted in Figure 2.6. Movement criteria were defined on the level of walking cycle. Two channels were stimulated: the deep peroneal nerve and the superficial peroneal nerve. Movement criteria for both the stimulation channels were defined on the level of walking cycle, e.g. sagittal and coronal foot orientation before foot landing. For each new step, stimulation parameters were determined in advance from the movement criteria using an inverse model of the relation between stimulation and movement parameters. This relation was assumed to be static and nonlinear. The parameters of this relation are recursively identified and updated, using the applied stimulation parameters and resulting movement parameters in every walking cycle. The proposed strategy was implemented and tested in simulations. In the simulations it was shown that a static linear model with only one parameter yielded the best model adaption and control performance. No experiments have been undertaken to prove this concept in real life.

2.7. Application of Inertial Sensors for Motion Estimation

Recently, the usage of inertial sensors in biomedical systems has become popular. One reason for the popularity is that a complete ISU with three accelerometers and three gyroscopes is not sensitive in regard to how the sensor is mounted to the body. An example for the usage of combination of accelerometers and gyroscopes is given in [52]. By the use of four uniaxial accelerometer and one gyroscope mounted to both the thigh and shank segment the kinematics in the sagittal plain were obtained. Later, an extention to this work were done by [82] who used a sensor pack consisting of 5 ISUs in order to estimate knee

and hip joints. For both studies Root Mean Square (RMS) errors between Vicon and the body-mounted sensors were reported to be 5.2 % (fast walking) and 1.9 %(slow walking) in percentage of the maximal angle. Application of body-mounted sensors have several advantages to other measurement systems. Such systems can obtain the same data as optical and ultrasound 3D motion analysis systems, but are easier to take into use. Another example of angle joint estimation is demonstrated by Moreno et al. [54] who used two ISUs connected to the shank and to the foot respectively. In addition were gait events like heel strike and heel-off detected. In [45] it was demonstrated that inclination angle of human body segments in activities of daily living can be accurately estimated by use of an ISU.

2.7.1. Stride Length and Stride Velocity Estimation

Miyazaki [53] proposed an ambulatory monitoring system using a piezoelectric gyroscope strapped just above the knee. Based on a model of gait and with the assumption that the gait is symmetric, the approximate stride length was estimated using simple trigonometry as well as the lengths of the body segments. A calibration over a known distance was performed to determine the coefficients of a linear regression in order to improve the accuracy. Tests were performed with multiple subjects on a 40 meter long test track. The maximum error for normal subjects was ±15 % whereas for patients with abnormal walking pattern the maximum error was ±25 %. By using a double segment gait model taking both the thigh and shank movements into consideration and by measuring both the angular velocity of the thigh and shank Aminian et al. [2] reported an error of ±7 %.

A slightly different approach was pursued by Sabatini et al. [75]. They used a simplified ISU with two uniaxial accelerometer and one gyroscope measuring in the sagittal plane. The ISU was attached to the instep of the foot. The angle was estimated by integration of the angular velocity and the gravity component was subtracted in order to find the unbiased acceleration which was integrated twice to obtain the position. As with some of the stride modelling techniques [2, 53] this concept does also assume that the foot motion is primarily in the sagittal plane. This assumption will work properly for people with normal walking pattern, but for patients with abnormal walking pattern the accuracy will decline. However, these methods have an advantage because they measure step length directly and do not make further assumptions about the user's height, gait, or walking environment. An enhancement of the method proposed by Sabatini et al. [75] was done by Veltink et al. [97]. They proposed to use a complete ISU measuring acceleration and angular velocity to reconstruct 3D movement of a foot during gait. In that paper, the sensory signals were recorded using a data-logger and the data were later processed offline for analysis purposes of the gait.

2.8. Summary and Conclusions

Treadmill training is a task-specific approach in walking rehabilitation for a range of neurological diseases. Several studies shows that this training regime decreases the time for improvement of walking abilities compared to traditional physiotherapy. It cannot be concluded that PBWS treadmill training is superior to traditional training, but it can be seen as a complimentary treatment to the traditional training. Several studies have shown that by the use of treadmill training the scores are better in ambulatory skills. On the other hand, the general motor functions are equal compared to the patients who went through traditional training.

Since the sixties many studies on FES-assisted treadmill training have been conducted, yet this is still not standard practise. For drop foot the situation is slightly different and a few commercial systems are on the market. But most of the closed-loop strategies for adapting stimulation intensity during gait have never found a way into clinical use. One reason for this is that mounting of sensory systems like goniometers is very time consuming and not realistic in a clinical setting. Furthermore, calibration of sensors takes time making it difficult to take such systems into clinical use. For a system to be taken into clinical use, the applied stimulation must be easy tunable or automatically tuned, not too many sensors should be necessary and they should be easily mountable such that physiotherapists are able to take it into use without help from engineers or scientists.

In Chapter 5, a new gait phase detection system is described. In this approach an inertial sensor mounted to the foot is used to detect gait phases. This gait phase system offers an advantage over the foot switches as more than two phases are detected. In addition the problem of mechanical wear is eliminated as the sensor is mounted with braces to the outer side of the foot. No calibration of the sensor is needed as the implemented algorithm detects the sensor's orientation and the parameters of the algorithm are tuned to fit a variety of patients. In Chapter 7 the gait phase detection system is used to trigger the stimulation in an FES-assisted gait training system. The use of inertial sensors in FES-assisted gait training has several advantages compared with traditional foot switches. There is no need to calibrate the sensors before use like finding appropriate thresholds and at the same time they can be used to monitor the progress of the training by examining the temporal and spatial information given by the inertial sensors.

Regarding a feedback strategy on a stride to stride basis by controlling objective like hip range, stride length and foot clearance, the disadvantage of the cycle objectives is that there are no possibilities to apply feedback within a stride and to react to disturbances occurring within a stride as a result of the slow adaptation. This is also the case for the adaptive feed forward controller by [63]. On the other hand it is actually more important in FES-assisted treadmill training that these variables are kept constant than that a predefined trajectory is followed i.e. that fatigue is compensated. A controller on a stride to stride basis has the ability to do that. In Chapter 7, a new control scheme is described where information from an inertial sensor is used in a feed forward manner. The sagittal foot angle before heel strike is used as a measurement for how well the step is performed. In the next step the stimulation of the tibialis anterior is changed in order to reach a preferred reference value.

3. Experimental Setup

3.1. Summary

This chapter gives an introduction to the stimulator and the measurement systems used within this thesis. In Section 3.2 the Inertial Sensor is explained in detail. The operation modes of the stimulator RehaStim are explained in Section 3.3. Section 3.4 contains technical specification and working principle of the LUKOtronic motion analysis system are given. At last, in Section 3.5 the technical specifications and a description of the Parotec foot insole pressure measurement system are given.

3.2. Inertial Sensor System

If one tri-axial accelerometer and one tri-axial gyroscope are mounted approximately in the same point they form an inertial sensor, also called Inertial Motion Unit (IMU) or an Inertial Sensor Unit (ISU). If the sensor is correctly calibrated, the acceleration in three orthogonal directions and the angular velocity around these axes are measured. By using a calibrated ISU and if the initial position and orientation are known, it is theoretically possible to derive the orientation of the sensor. Orientation can be found by integration of angular velocity. The gravity can be extracted from the acceleration measurement using the known orientation, and the sensor position can be found by integrating the acceleration twice. In the following sections the physical principles behind accelerometers and gyroscopes are explained.

3.2.1. Accelerometers

There are in principle two types of accelerometers, mechanical and solid-state. In this section the mechanical accelerometer is explained. This is the original accelerometer and has been developed over decades. A mechanical accelerometer is exploiting the inertia of a mass. When a force is acting on a mass it will accelerate. This is also known as Newton's second law of motion which states that to accelerate a mass m a force F is needed. In equation form this becomes

$$F = ma. \tag{3.1}$$

A single accelerometer works as a damped spring system (see Figure 3.1). The spring is connected to a housing and a mass. When the mass is displaced the distance Δx the spring will restore a force proportional to the displacement

$$F = k\Delta x. \tag{3.2}$$

An acceleration of the housing will cause the mass to be displaced by

$$\Delta x = \frac{ma}{k}. \tag{3.3}$$

In this way the problem of measuring acceleration has been turned into measuring the displacement of the mass connected to the spring. Typically an electrical signal u_a is measured which is related to the

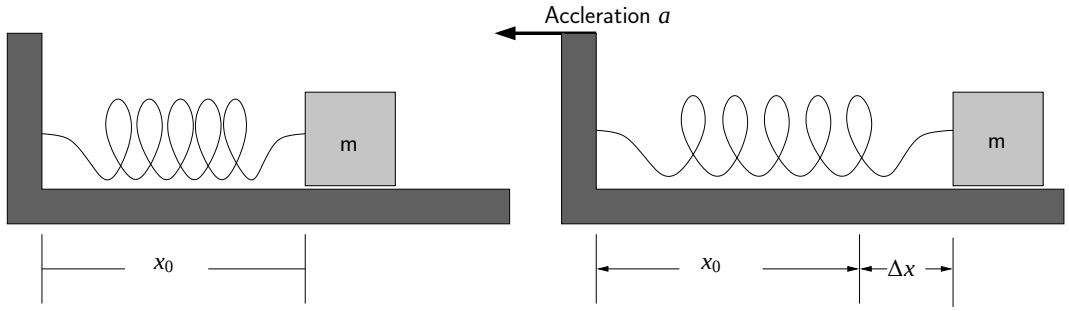

Figure 3.1.: A single axis accelerometer.

physical quantities

$$u_a = k_a(a - g) + b_a \tag{3.4}$$

where k_a is representing the scaling factor, b_a is the offset, g is the gravity constant whereas a is the sensor acceleration. By mounting three single accelerometers together all in orthogonal directions, a tri-axial accelerometer can be constructed. The gains and offsets as well as the orientation of the sensitive axis with respect to the housing can be found by the calibration algorithm described by Ferraris et al. [18].

3.2.2. Gyroscopes

Gyroscopes or angular rate sensors can be constructed in different ways. Most common are spinning rotor gyroscopes, laser gyroscopes and vibrating mass gyroscopes. For navigation purposes the most common used gyroscopes are conventional spinning rotor and laser gyroscopes. The vibrating mass gyroscopes are small, inexpensive and have a low power consumption.

A schematic view of a typical vibrating mass gyroscope is depicted in Figure 3.2. The vibrating mass gyroscope has a vibrating element, and when the gyroscope is rotated it is influenced by the Coriolis acceleration. This is causing a secondary vibration orthogonal to the original vibrating direction. By

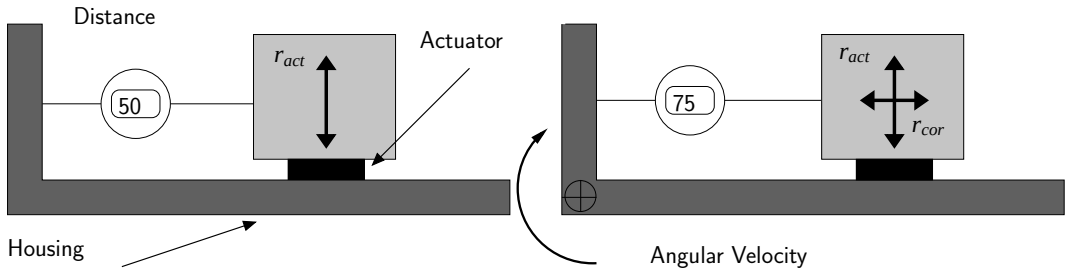

Figure 3.2.: A gyroscope consists of a mass that is vibrating due to an actuator r_{act}. When the gyroscope is rotated around the axis perpendicular to the plane shown in the figure, the mass is displaced in the direction perpendicular to the rotation and to the direction of vibration.

sensing the secondary force f_{cor} in the direction r_{cor}, the rate of turn can be detected. This is done by sensing the displacement of the mass perpendicular to the vibration direction. The force sensed is only apparent in the sensor coordinate system, not in the inertial coordinate system. The magnitude of the Coriolis force f_{cor} is given by:

$$f_{cor} = 2 \cdot m \cdot v \cdot \omega \tag{3.5}$$

where m is the mass, v the momentary mass speed and ω the angular velocity. Thus the displacement caused by the Coriolis force is proportional to the angular velocity and is used therefore as a measure of angular velocity. In order to induce and detect the vibration of the test mass, a piezo-electric actuator is often used. Therefore vibrating gyroscopes are often called “piezo”, “ceramic”, or “quartz” gyroscopes, although in fact vibration and detection do not necessarily use the piezo effect.

A tri-axial gyroscope can be assembled using three single axis gyroscopes. As for the tri-axial accelerometer, a method for obtaining the gain, offset and the sensitivity axis is once again described in Ferraris et al. [18].

3.2.3. The RehaWatch™ Inertial Sensor System

The portable inertial sensor system RehaWatch™ produced by the German company HASOMED GmbH[1] was applied in this work. Figure 3.3 shows the inertial sensor system. The RehaWatch inertial system consists of one Digital Signal Prosessing (DSP) unit, two inertial sensor units and two foot braces. The braces can be easily mounted outside the shoes. The technical specifications of the inertial system are listed in the Table 3.1. The inertial sensor system is intended for offline use, and is equipped with an USB interface for exchanging data with an external PC. A protocol for online reading of the sensor data was specially provided by the producer of the sensor.

[1] www.hasomed.de

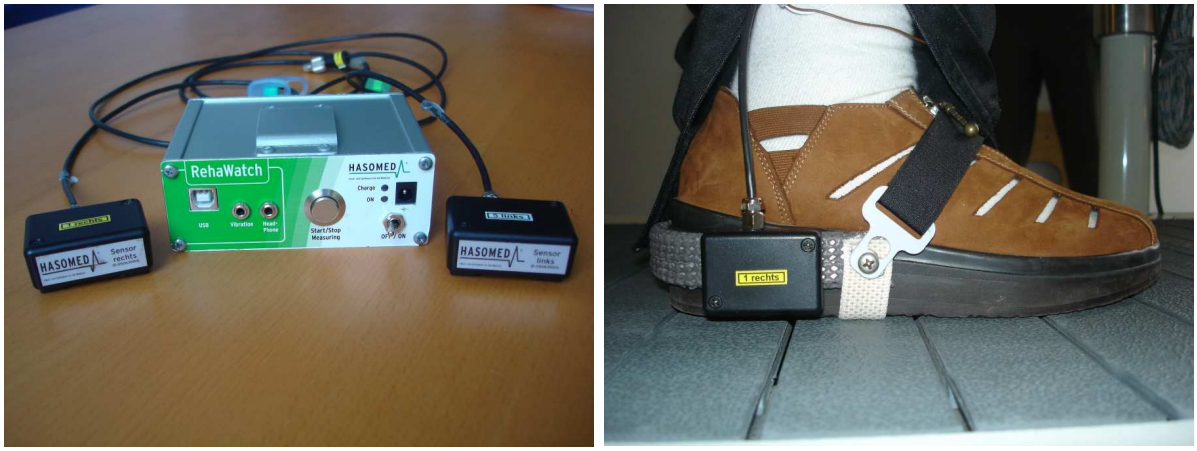

Figure 3.3.: Inertial sensor system: On the left the RehaWatch inertial sensor system is shown. On the right a brace and an ISU mounted on a foot are shown.

Table 3.1.: Technical specifications of the RehaWatch inertial sensor system.

	Gyroscopes	Accelerometers
Degrees of freedom	3	3
Operating range (OR)	± 900 [deg/s]	± 50 [m^2/s]
Linearity	0.1 [% of OR]	0.2 [% of OR]
Bias stability	5 [deg/s]	0.02 [m^2/s]
Scale factor stability	0.5 [deg/s]	0.02 [m^2/s]
Noise	0.7[deg/s]	0.01 [m^2/s]
Alignment error	0.1 [deg]	0.1 [deg]
Bandwidth	50 [Hz]	30 [Hz]
Sampling rate	500 [Hz]	500 [Hz]

3.3. Stimulation Device and Pattern Generator

The portable stimulation device RehaStim pro^{TM} employed in this work is produced by the German company HASOMED GmbH. The current-controlled 8 channel stimulator is a certified medical product and possesses two independent current sources which are multiplexed to 4 outputs each. The main processor of the stimulator is an ultra-low-power 16-bit RISC mixed-signal processor from Texas Instruments (MSP430F169). There are two independent stimulation modules hosting each one of the current sources. Each stimulation module owns another microprocessor (MSP430F149) which is responsible for the pulse generation timing. The stimulation module A has the stimulation channels 1 to 4, stimulation module B has the stimulation channels 5 to 8. Since both modules function independently simultaneous pulse generation on module A and B is possible.

Figure 3.4 shows the stimulator device. The device is operated by a touch panel with illumination. The technical specifications are listed in the Table 3.2. Notice that the RS232 and USB interfaces share the same UART interface of the MSP430 so that multiplexing must be applied when using both interfaces at the same time. In the PC-controlled configuration the USB interface is employed for communication with the PC and the RS232 is free. The stimulator possesses additional inputs and outputs which are not used here. Galvanic isolation between high voltage generation/electrodes and the rest of the stimulator electronics has been realised for safety reasons.

Figure 3.4.: Portable 8 channel stimulator

Table 3.2.: Technical details of the stimulation device.

Current	0 . . . 126 mA in 2 mA steps
Pulsewidth	$0, 20 \ldots 500\,\mu$s in $1\,\mu s$ steps
Frequency	see Section 3.3.1
Pulse form	biphasic
Channels	8 (2 times 4 on two modules)
Serial ports	RS232 and USB with galvanic isolation
Digital and analogue I/O	8 pins which can be assigned individually as 12-bit analogue inputs (8 available), 12-bit analogue outputs (2 available) or digital inputs/outputs (8 available)
Sensor supply	5 V / 100 mA

Figure 3.5 shows the form of a delivered bi-phasic pulse on an ideal resistive load. Current amplitude and pulsewidth are defined in the figure. Notice that there is a fixed pause of $100\,\mu$s between the two phases of the pulse. At the end of the pulse the remaining charge on the electrodes and skin is removed by an active shortcut (change of electrode polarity for $1\,\mu$s).

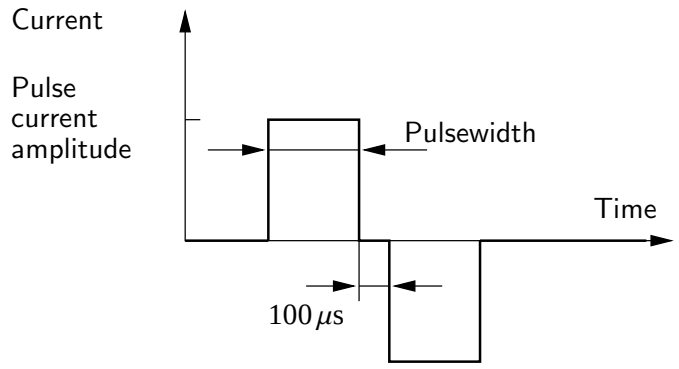

Figure 3.5.: Definition of pulsewidth and current amplitude for a biphasic pulse.

3.3.1. Pulse Generation Modes

The stimulator offers different modes of stimulation pulse generation. An Application Programming Interface (API) is provided which enables the development of customised stimulator applications using the different modes of pulse generation. Moreover, a serial communication protocol is available so that the pulse generation can also be controlled by sending commands with 115200 Bauds from an external device, preferably a PC.

The following modes of pulse generation are available:

- **Single Pulse Mode:** On an external command or an API function call the stimulator generates a single pulse on a specified channel with desired current amplitude and pulsewidth. The stimulator will generate the pulse immediately after processing the command. Complex stimulation patterns may be generated by sending more than one command. The application program inside the stimulator or the external device (PC) are responsible for controlling the stimulation timing, i.e. the stimulation pulse interval. Therefore, the API of the stimulator provides a 16-bit timer with a resolution of 1 ms.
- **Continuous Channel List (CCL) Mode:** Using this mode, the generation of complex patterns is greatly simplified. The main processor and the processors of the stimulation modules control the pulse generation by means of timer-interrupts. A list of stimulation channels has to be specified, on which pulses or even pulse groups (doublets or triplets) will repeatedly be generated. Figure 3.6 defines the main stimulation period t_1 and the inter-pulse time t_2 of doublets and triplets with the help of an example. The channel list is repeatedly processed with time period t_1. Pulse generation takes place on the selected channels, ordered by the channel numbers. For each selected channel a time slot of 1.5 ms is reserved, even if current or/and pulsewidth are zero for the channel or if the pulsewidth is smaller than 1.5 ms. At least 1.5 ms pass between the stimulation of different

channels of one module. The stimulation modules A and B process the channel list in parallel with a time offset of 0.6 ms. Module A generates pulses on the channels 1 to 4 if applicable, and module B generates pulses on the channels 5 to 8 if applicable. The inter-pulse time t_2 of doublets and triplets is fixed for all channels and is set during an initialisation step. When doublets or triplets have to be generated the channel list will be processed two or three times more with period t_2. Stimulation takes place only on the channels on which doublets or triplets have to be generated.

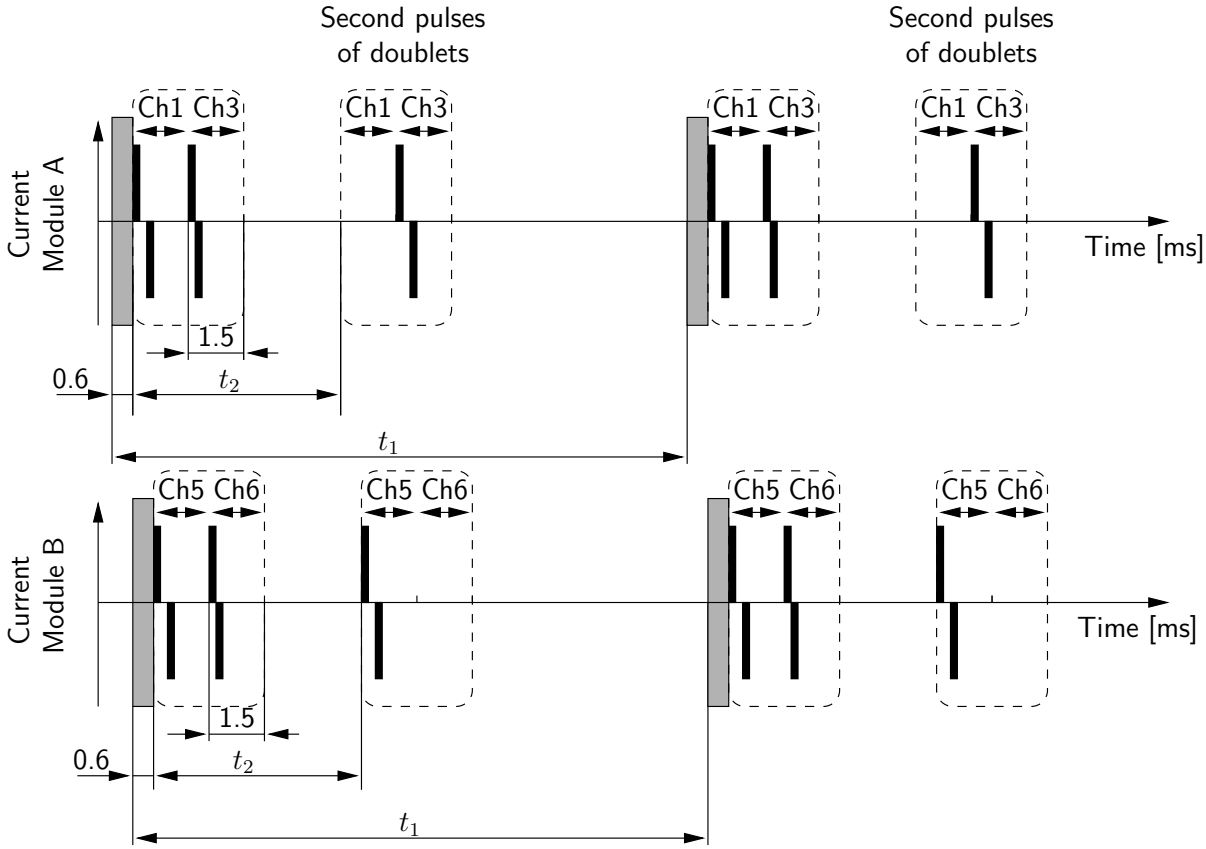

Figure 3.6.: Example for the Continuous Channel List Mode of the stimulator. The channel list encloses the channels 1, 3, 5 and 6. The main stimulation frequency is $1/t_1$. Doublets are generated on the channels 3 and 5 with a frequency $1/t_2$. The grey bars indicate some communication periods in which the actual stimulation settings are transferred from the main controller to the stimulation modules. Stimulation pulses are represented by black bars where the same width and amplitude have been assumed for simplicity.

The main stimulation frequency is specified by the period t_1. Some channels of the channel list can be assigned to a lower frequency which has the period nt_1 where n is a positive integer.

The CCL mode must be initialised by an API function call or a command (external control). Used channels, main time t_1, inter-pulse time t_2 and the maximal size of pulse groups must be chosen at this stage. The minimal possible inter-pulse time t_2 depends on the maximal number of channels

assigned to the individual stimulation modules as follows

$$t_2 \geq 1.5\,\text{ms} \cdot \max(n_{ch_A}, n_{ch_B}) \tag{3.6}$$

where n_{ch_A} and n_{ch_B} are the number of selected channels of stimulation modules A and B respectively. The minimal possible period t_1 depends on t_2 and the maximal size n_{pg} of pulse groups used ($n_{pg} = 1$ for single pulses, $n_{pg} = 2$ for doublets, $n_{pg} = 3$ for triplets). The constraint for t_1 is then

$$t_1 \geq n_{pg} \cdot t_2 + 1.5\,\text{ms} \tag{3.7}$$

where the 1.5 ms above results from a communication between the main processor and the stimulation modules as indicated in Figure 3.6. The period t_1 can be changed in the range $3 \ldots 1023.5$ ms in 0.5 ms steps subject to the constraint (3.7), and t_2 can be altered in the range $3 \ldots 16$ ms in 0.5 ms steps subject to the constraint (3.6). Using all 8 channels, a minimal group time t_2 of 6 ms can be achieved, i.e. a doublet or triplet frequency of 180 Hz. When only doublets and single pulses with a frequency of 180 Hz are applied ($n_{pg} = 2$), a minimal value of 13.5 ms for period t_1 is obtained, i.e. a maximal possible main frequency of 74.1 Hz.

Another API function call or external command deactivates the CCL mode. When the CCL mode is active, the pulse parameters (pulsewidth, current amplitude and group mode (single pulse, doublet or triplet) of the selected channels can be altered by a corresponding API function call or an external command. The new parameters will be used from the next processing of the channel list onwards.

The main processor controls the frequency $1/t_1$ by which the channel list is processed. Each time the stimulation cycle repeats, the main processor sends the actual stimulation settings to the two stimulation modules which then generates the individual pulses on the selected channels. The processors on the stimulation modules guarantee that specified pulsewidths and inter-pulse times of the doubles and triples are realised.

- **One Shot Channel List (OSCL) Mode:** Just as in the Continuous Channel List Mode a channel list is defined by an initialisation step. However, processing of the channel list is not automatically repeated so that the time period t_1 is no longer relevant. Instead, the channel list will be processed once and pulses and/or pulse groups are generated only if a special API function call or an external command are issued. Pulse parameters (pulsewidth, current amplitude and group mode of the selected channels) are specified by the API function call or the external command.

  The OSCL mode offers the possibility to control the main stimulation frequency from an application program running in the stimulator or from an external device while the inter-pulse time of the doublets and triplets is realised by the stimulation modules.

The (OSCL) Mode was applied in the work described in Chapter 7.

3.4. Optical Motion Analysis System

The LUKOtronic AS 202 measurement system from the company LUKOtronic Lutz-Kovacs-Electronics OEG[2] was used as a reference measurement system in Chapter 6 and for motion analysis purposes in Chapter 7. In this section the technical specifications and the functionality of the system are summarised. The AS 202 is a portable measurement system for capturing 3D-movements in real time. The system can be deployed everywhere and is not fixed to one room. The measurement unit consists of one measurement beam which is connected to a laptop (see Figure 3.7). Two marker chains with active markers are connected to the body. The markers are activated through an RF-link. During the measurement,

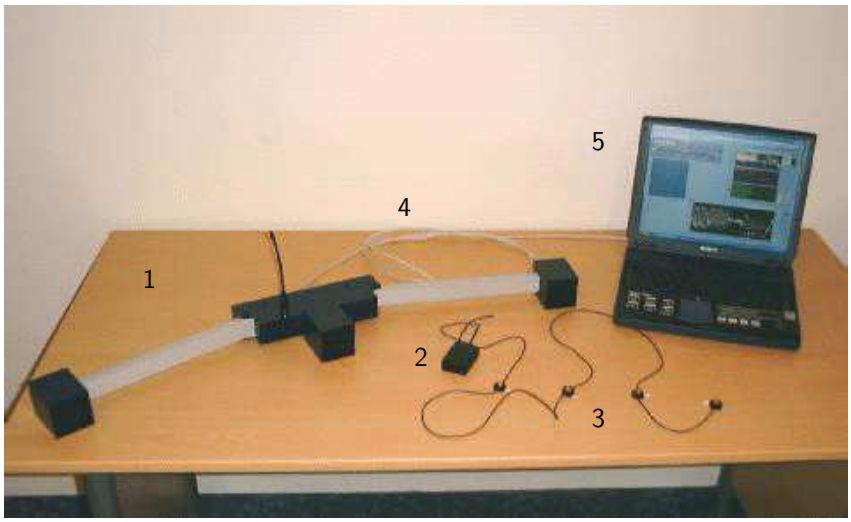

Figure 3.7.: LUKOtronic AS 202 measurement system: (1) The measuring beam with three cameras. (2) The transmitter control box. (3) Active infrared markers connected in a chain. (4) USB cable between laptop and measurement beam. (5) Standard laptop with driver software

the active markers are transmitting light impulses in the infrared spectrum. One marker at the time is active such that each marker can unambiguously be identified. The measurement beam with the three cameras is powered up by the USB connection whereas the transmission control unit is powered up by a rechargeable battery. The cameras are sensing the 3D positions of the active markers. From the marker positions, the movement of the patients can be calculated and graphically displayed within the PC software. The position data can also be stored and exported to ASCII such that they can be read by some external software e.g. MATLAB/SIMULINK . The technical specifications of the LUKOtronic AS 202 are listed in Table 3.3.

[2] www.lukoctronic.com

Table 3.3.: Technical data of the LUKOtronic AS 202 system.

Sum Sample Rate	1200 Hz
Number of Markers	48
Measurement Range	5-7 Meter
Resolution	0.1 mm
Opening Angle	20 degrees
Transmission Frequency	433 MHz
Opening Angle Marker	± 90 degrees
Weight	2.4 Kg

3.5. Insole Pressure Measurement System

The in-shoe pressure measurement system Parotec (see Figure 3.8) from the company Paromed Medizintechnik GmbH[3] was used in the validation of the gait phase detection in Chapter 5 as well as for analysis in Chapter 7. The measurement system Parotec consists of two insole foot sensors and a control unit box. Each of the foot insole sensors has 24 piezoresistive microsensors embedded in hydrocells measuring the sum of the horizontal and shearing forces acting on the cell. Each hydrocell consists of an incompressible fluid preserved in a constrained polyurethane pack that can only be deflected at the top and bottom. The design allows a pressure measurement that unifies the normal and tangential components of the force applied. The microsensor consists of a Wheatstone bridge circuit fixed onto a silicone membrane that deflects under pressure into an evacuated chamber. This allows for the measurement of loads between the foot and the supporting material and is considered to be selfcompensating against changes in temperature. Different insole sizes are available with the sensors placed in the correct relative position for each foot size. For the online measurement mode the sampling rate is 60 Hz, whereas for offline measurement sampling rates up to 250 Hz are possible. The pressure sensors work with a resolution of 2.5 kPa in a range of 600 kPa.

[3] www.paromed.de

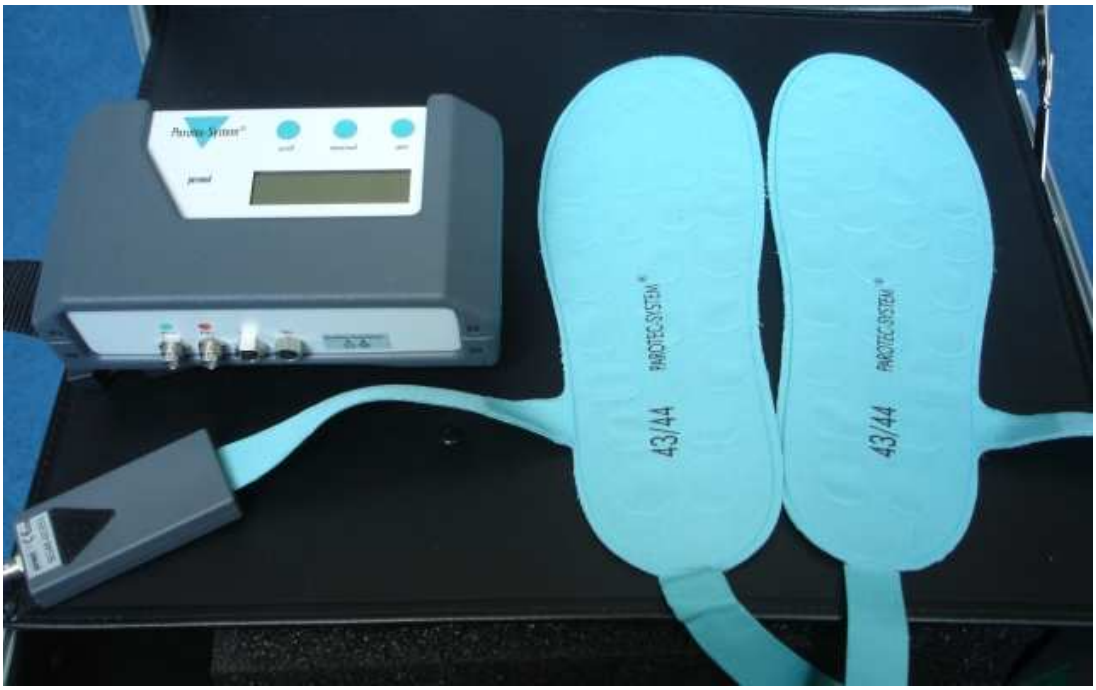

Figure 3.8.: Parotec insole pressure measurement system.

4. Estimation of Sensor Orientation

4.1. Summary

Aim: The aim of the work presented in this chapter was to develop an algorithm for obtaining the orientation of an inertial sensor mounted to the foot during gait. The orientation of the foot is of high importance in later chapters as it is employed in gait phases detection and for the estimation of movement parameters.

Methods: An Inertial Motion Unit (IMU) measures angular velocity and acceleration in three orthogonal directions. In principle, the orientation can be obtained directly by integration of the angular velocity measured with the gyroscopes. However, an integration will unavoidably drift off after a short time due to timevarying biases in the gyroscope measurements. Fortunately, the accelerometers can under the assumption that the sensor is not accelerated, measure the earth's gravity vector, which serves as a fixed orientation reference and enables the determination of two independent angles.

To fuse the information from the gyroscopes and the accelerometers a Kalman filter is used. Kalman filters are frequently applied to estimate not directly measureable states of a linear dynamic system, by using measurements linearly related to the state but corrupted by white noise. The Kalman filter is stochastic optimal with respect to a quadratic function of the estimation error. An Extended Kalman Filter (EKF) is a Kalman filter in which states of a nonlinear dynamic system can be estimated. A model of the error between the estimated orientation from the direct integration of the measured angular velocity and the measured orientation from the accelerometer was developed. The measured error based on the accelerometers was used as a reference measurement in the Kalman filter update only during the foot flat phase in order to correct the estimate based on the integration of the angular velocity.

By use of the orientation between the sensor and a global coordinate system, the angle between the sensor and the ground in the walking direction can be easily calculated. This is done under the assumption that the sensor is mounted such that the sensors x-axis lies in the sagittal plane. Especially in the gait phase detection algorithm described later, the accurate angle between foot and ground is of high importance. A linear filter was used to estimate the angle offset between the sensor and the foot during the foot flat

phase.

Results: The Kalman filter was successfully applied. Even though the heading was drifting off, the orientation could be estimated for a very long time. No specific evaluation was performed to validate the accuracy of the obtained orientation, but the results presented in the following chapters give the supposition that an accurate orientation estimate can be achieved by the developed approach.

Conclusions: An indirect Kalman filter for obtaining the orientation of the foot using an inertial sensor has been developed and is suitable.

Contribution: The author developed the methods, and implemented the experimental software. Furthermore, the author planned and ran the experiments. Parts of this work are published in [56].

4.2. Introduction

The determination of position and orientation of moving objects is of interest in a variety of fields. Typically, in navigation systems, the Global Positioning System (GPS) is used in combination with an Inertial Navigation System (INS), consisting of an Inertial Motion Unit (IMU) mounted on the vehicle, to estimate the position and if required the orientation. In the application considering human motion the usage of GPS is not beneficial as the resolution of the GPS measurement is not good enough for this purpose and usually only one single IMU or more IMUs are used. An inertial measurement unit is composed of one tri-axial accelerometer and one tri-axial gyroscope. Integration of angular velocity measured by the gyroscope will lead to an increasing error in the estimated orientation. Even a small offset on the gyroscope signal will lead to large integration errors over short time. Moreover, if an absolute orientation is required instead of a change in orientation, a reference orientation has to be obtained at least once during a recording. Algorithms for integration of the angular velocity can be found in [8].

Orientation can also be estimated by combining the measurements from gyroscopes and accelerometers. This approach is applied in the automotive field and for the assessment of human balancing [4]. A tri-axial accelerometer measures the earth's gravity vector if the sensor is not exposed to acceleration. The gravity vector is a measure for the orientation of the sensor in relation to an earth fixed coordinate system. The accelerometers do not contain any information about the rotation around the gravity vector and do not give a complete description of the orientation. Typically, a state estimator, i.e. a Kalman filter is used to fuse the information from both gyroscopes and accelerometers by using the acceleration as measurement update. The accelerometers inevitably measure both the body acceleration as well as the gravity component, but general assumptions on the human movement is made such that the body acceleration can be filtered out. When only accelerometers and gyroscopes are used, no information about the rotation around the vertical axis (the sensor heading) is known, and this state will unavoidably drift off. To avoid this drifting, a measurement of the earth magnetic field by magnetometers can be used

[51, 74].

A Kalman filter using an IMU for orientation estimation can be designed in a several ways. The states in a Kalman filter can be chosen to be any representation of the orientation. In [44] they used rotation matrices and vectors to represent the orientation while as in [51] and [74] the orientation is represented by quaternions. The filter can be designed in an indirect or a direct filter. When the states in the Kalman filter are the orientation then it is called a direct filter. When the error between estimated orientation obtained by a pure integration and the the measured orientation from the accelerometers are the states in the Kalman filter it is called an indirect filter.

In this chapter an Extended Kalman Filter (EKF) is designed that fuses the information from a tri-axial accelerometer system with a tri-axial gyroscope system in order to measure orientation of the foot during gait. In Section 4.3 the theoretical background and the EKF algorithms are presented. Furthermore, in Section 4.4 the main filter structure is presented and the error model is deduced. In Section 4.5 the angle between foot and ground is found based on the estimated orientation and a slow filter estimating the angle between the sensor and the foot. At last an experimental evaluation of the extended Kalman filter is given in Section 4.6.

4.3. Extended Kalman Filter (EKF) Equations

A Kalman filter is an optimal way to estimate states for linear systems based on measurements and knowledge of stochastic parameters of the system and measurement noise. The Kalman filter is optimal in the sense that the expectation value of the estimate is not biased and that the variance of the estimate is minimal. The use of a Kalman filter for nonlinear system is called Extended Kalman Filter (EKF). This filter is no longer optimal, but has been applied successfully in many applications. The algorithm can be found in many books e.g. [26], and is shortly outlined here.
Given the continuous stochastic system

$$\dot{\mathbf{x}}(t) = \mathbf{f}(\mathbf{x}(t), \mathbf{u}(t), \mathbf{v}(t)) \tag{4.1}$$

where $\mathbf{f}(\mathbf{x}(t), \mathbf{u}(t), \mathbf{v}(t))$ is a nonlinear vector function of the state vector $\mathbf{x}(t)$, the input vector $\mathbf{u}(t)$ and the white noise vector $\mathbf{v}(t)$ which is the plant noise with the covariance matrix $\mathbf{Q}$. The measurements $\mathbf{z}(k)$ are done at discrete time instants $t = t_s \cdot k$ with the sample time t_s

$$\mathbf{z}(k) = \mathbf{h}(\mathbf{x}(k)) + \mathbf{w}(k) \tag{4.2}$$

where $\mathbf{h}(\mathbf{x}(k))$ is a function of the states and $\mathbf{w}(k)$ is the white measurement noise described with the covariance matrix $\mathbf{R}$.

This system can be made time-discrete by help of the forward Euler method

$$\mathbf{x}(k+1) = \mathbf{f}_k(\mathbf{x}(k), \mathbf{u}(k), \mathbf{v}(k)) \tag{4.3}$$

$$\tag{4.4}$$

where

$$\mathbf{f}_k(\mathbf{x}(k), \mathbf{u}(k)) = \mathbf{x}(k) + t_s \mathbf{f}(\mathbf{x}(k), \mathbf{u}(k), \mathbf{v}(k)) \tag{4.5}$$

The Extended Kalman Filter algorithm can be summarised like this: .

1. Initialisation of the error covariance matrix $\bar{\mathbf{P}}(0)$ and the initial state $\bar{\mathbf{x}}(\mathbf{0})$:

$$\begin{aligned} \bar{\mathbf{x}}(\mathbf{0}) &= \mathbf{E}\{\mathbf{x}(\mathbf{0})\} \\ \bar{\mathbf{P}}(0) &= \mathbf{E}\{(\mathbf{x}(0) - \bar{\mathbf{x}}(0))(\mathbf{x}(0) - \bar{\mathbf{x}}(0))^T\} \end{aligned} \tag{4.6}$$

   Here, $\mathbf{E}\{*\}$ is the expectation operator

2. Compute the Kalman filter gain

$$\mathbf{K}(k) = \bar{\mathbf{P}}(k)\mathbf{H}(k)^T \left(\mathbf{H}(k)\bar{\mathbf{P}}(k)\mathbf{H}(k)^T + \mathbf{R}\right)^{-1} \tag{4.7}$$

3. Compute the posteriori state estimate

$$\hat{\mathbf{x}}(k) = \bar{\mathbf{x}}(k) + \mathbf{K}(k)\left(\mathbf{y}(k) - \mathbf{H}(k)\bar{\mathbf{x}}(k)\right) \tag{4.8}$$

4. Update the posteriori error covariance matrix after new measurement:

$$\hat{\mathbf{P}}(k) = \left(\mathbf{I} - \mathbf{K}(k)\mathbf{H}(k)\right)\bar{\mathbf{P}}(k) \tag{4.9}$$

5. Update the a priori estimate

$$\bar{\mathbf{x}}(k+1) = \hat{\mathbf{x}}(k) + t_s \mathbf{f}(\hat{\mathbf{x}}(k), \mathbf{u}(k), \mathbf{0}) \tag{4.10}$$

6. Update the a priori error covariance matrix

$$\bar{\mathbf{P}}(k+1) = \mathbf{\Phi}(k)\hat{\mathbf{P}}(k)\mathbf{\Phi}(k)^T + \mathbf{V}(k)\mathbf{Q}\mathbf{V}(k)^T \tag{4.11}$$

In the algorithm the following notation is used:

$$\mathbf{\Phi}(k) = \left.\frac{\partial \mathbf{f}_k(\mathbf{x}(k), \mathbf{u}(k), \mathbf{0})}{\partial \mathbf{x}(k)}\right|_{\mathbf{x}(k)=\hat{\mathbf{x}}(k)}, \quad \mathbf{V}(k) = \left.\frac{\partial \mathbf{f}_k(\mathbf{x}(k), \mathbf{u}(k), \mathbf{w}(k))}{\partial \mathbf{w}(k)}\right|_{\mathbf{x}(k)=\hat{\mathbf{x}}(k)} \tag{4.12}$$

and

$$\mathbf{H}(k) = \left.\frac{\partial \mathbf{h}(\mathbf{x}(k))}{\partial \mathbf{x}(k)}\right|_{\mathbf{x}(k)=\bar{\mathbf{x}}(k)} \tag{4.13}$$

In the case no measurement is available, $\mathbf{H}(k)$ is set to zero. It will then follow that the Kalman filter gain $\mathbf{K}(k)$ becomes zero and that $\hat{\mathbf{x}}(k) = \bar{\mathbf{x}}(k)$ and $\hat{\mathbf{P}}(k) = \bar{\mathbf{P}}(k)$. It will then follow that the EKF becomes a state predictor.

4.4. Design of a Filter for Orientation Estimation

An indirect Kalman filter was designed to estimate the orientation of the IMU by combining the tri-axial accelerometer and a three-axial gyroscope by using a model of the IMU. The structure of the algorithm is depicted in Figure 4.4. The state of the Kalman filter is the error in the orientation. The orientation is in first place calculated by an independent strap down integration, where basically the angular speed is integrated in 3 dimension. The correction state update is done by the acceleration measurement. The indirect filter has the advantages that:

- The error state model is not that non-linear as the real state model.
- The parameters of the model can be treated as stochastic processes.

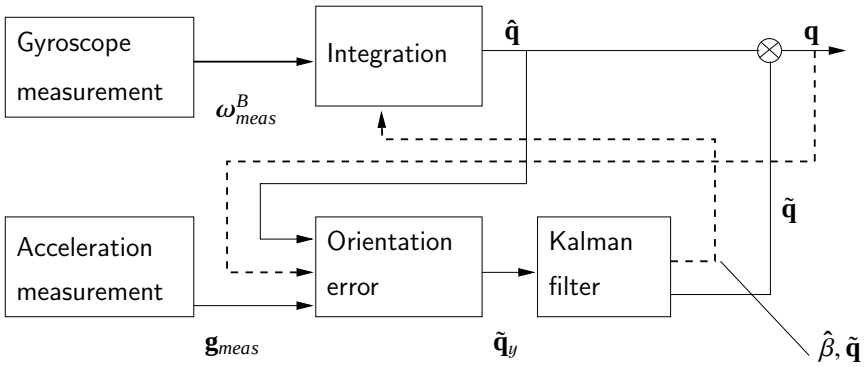

Figure 4.1.: Block structure of the orientation estimation

In the following, a model which describes the sensor output is presented which considers the output of the sensor system affected of uncertain states driven by white noise. By considering the model of the sensor output of both the gyroscopes and accelerometers the error model is derived.

4.4.1. Sensor Signal Model

The sensor is assumed to be attached to a human body segment i.e. the foot that rotates and translates with respect to a global coordinate frame. The measured gyroscope signals, represented as the vector $\boldsymbol{\omega}^B_{meas} = [\omega^B_{meas,x}\ \omega^B_{meas,y}\ \omega^B_{meas,z}]^T$ are assumed to be the sum of angular velocity $\boldsymbol{\omega}^B$, a slowly varying bias $\boldsymbol{\beta}$ and random white noise $\boldsymbol{\xi}_\varepsilon$.

$$\boldsymbol{\omega}^B_{meas} = \boldsymbol{\omega}^B + \boldsymbol{\beta} + \boldsymbol{\xi}_\varepsilon. \tag{4.14}$$

The spectrum of the gyroscope offset has a low cut-off frequency in comparison with the bandwidth of the kinematic signals that are to be measured. The slowly varying bias in the gyroscope measurements is modelled as a first order Markov process driven by a white noise vector $\boldsymbol{\xi}_\beta$

$$\dot{\boldsymbol{\beta}} = -\mathbf{T}_\beta{}^{-1}\boldsymbol{\beta} + \boldsymbol{\xi}_\beta. \tag{4.15}$$

$\mathbf{T}_\beta$ is the diagonal matrix with the time constants of the Markov processes on the diagonal axis. A tri-axial accelerometer measures acceleration, the gravity plus a white noise component, all in the sensor coordinate frame. The accelerometer signals are modelled as the sum of the linear acceleration vector $\mathbf{a}^B$, the gravity vector $\mathbf{g}^B$ and white noise $\boldsymbol{\xi}_a$

$$\mathbf{a}^B_{meas} = \mathbf{a}^B + \mathbf{g}^B + \boldsymbol{\xi}_a. \tag{4.16}$$

The superscript B is used to indicate that the signals are expressed in the sensor coordinate system.

4.4.2. Representation of Orientation

Rotation of a body in 3D space is fully described with three parameters. Rotation is always defined between two coordinate frames. We define two coordinate systems, one system fixed to the sensor or body-fixed B and one global coordinate system I. The latter is always fixed once defined and the $\mathbf{z}^I$-axis is always pointing in vertical direction. Rotation can be represented in several ways; the most important representations are [79]:

- Rotationmatrix: 9 parameters, 6 constraints
- Euler angles: 3 parameters
- Angle axis parametrisation: 4 parameters
- Euler parameters (Quaternions): 4 parameters, 1 constraint
- Euler Rodriguez parameters: 3 parameters

Minimal representations with only three parameters always contain a singularity. The most common Euler angles definitions, also called the roll-pitch-yaw is not defined for a pitch angle of ±90 degrees. However in many practical application, e.g. marine vehicles, this parameter region is not likely to be entered. An advantage of the Euler parameters is their computational efficiency, in opposite to Euler angles. The Euler angles are computed by numerical integration of a set of nonlinear differential equations. This involves computation of a large number of trigonometric functions.

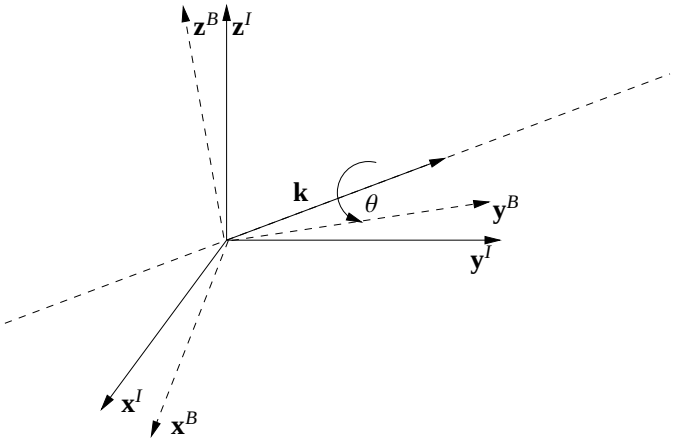

Figure 4.2.: Orientation systems: Illustration of the rotation between two coordinate systems represented as one axis and one angle.

In this work we use the Euler parameter representation or unit quaternion. In the following an introduction to quaternions is given and the connection with spatial rotation is explained.

The Euler parameters (unit quaternion) are defined as

$$\mathbf{q} = \begin{bmatrix} \eta \\ \boldsymbol{\varepsilon} \end{bmatrix} \in \mathbb{R}^4 \tag{4.17}$$

where η is called the scalar part of the quaternion while $\boldsymbol{\varepsilon}$ is the vector part. Quaternions form a group whose underlying set is the four dimensional vector space $\mathbb{R}^4$ with a multiplication operator $\otimes$ that contains both the dot and cross product. The quaternion product between two quaternions $\mathbf{q}_1$ and $\mathbf{q}_2$ is defined by:

$$\begin{bmatrix} \eta \\ \boldsymbol{\varepsilon} \end{bmatrix} = \begin{bmatrix} \eta_1 \\ \boldsymbol{\varepsilon}_1 \end{bmatrix} \otimes \begin{bmatrix} \eta_2 \\ \boldsymbol{\varepsilon}_2 \end{bmatrix} = \begin{bmatrix} \eta_1\eta_2 - \boldsymbol{\varepsilon}_1^T\boldsymbol{\varepsilon}_2 \\ \eta_1\boldsymbol{\varepsilon}_2 + \eta_2\boldsymbol{\varepsilon}_1 + \mathbf{S}(\boldsymbol{\varepsilon}_1)\boldsymbol{\varepsilon}_2 \end{bmatrix} \tag{4.18}$$

where

$$\mathbf{q}_1 = \begin{bmatrix} \eta_1 \\ \boldsymbol{\varepsilon}_1 \end{bmatrix}, \ \mathbf{q}_2 = \begin{bmatrix} \eta_2 \\ \boldsymbol{\varepsilon}_2 \end{bmatrix}. \tag{4.19}$$

The product can be written as:

$$\begin{bmatrix} \eta \\ \boldsymbol{\varepsilon} \end{bmatrix} = \begin{bmatrix} \eta_1 & -\boldsymbol{\varepsilon}_1^T \\ \boldsymbol{\varepsilon}_1 & \eta_1\mathbf{I} + \mathbf{S}(\boldsymbol{\varepsilon}_1) \end{bmatrix} \begin{bmatrix} \eta_2 \\ \boldsymbol{\varepsilon}_2 \end{bmatrix} \tag{4.20}$$

$$= \mathbf{F}(\mathbf{q}_1)\mathbf{q}_2 \tag{4.21}$$

or as

$$\begin{bmatrix} \eta \\ \boldsymbol{\varepsilon} \end{bmatrix} = \begin{bmatrix} \eta_2 & -\boldsymbol{\varepsilon}_2^T \\ \boldsymbol{\varepsilon}_2 & \eta_1\mathbf{I} - \mathbf{S}(\boldsymbol{\varepsilon}_2) \end{bmatrix} \begin{bmatrix} \eta_1 \\ \boldsymbol{\varepsilon}_1 \end{bmatrix} \tag{4.22}$$

$$= \mathbf{E}(\mathbf{q}_2)\mathbf{q}_1 \tag{4.23}$$

The quaternion product between $\mathbf{q}$ and $\mathbf{q}^*$ results in the identity quaternion $\mathbf{q}_{id}$

$$\mathbf{q}_{id} = \mathbf{q}^* \otimes \mathbf{q} = \mathbf{q} \otimes \mathbf{q}^* = \begin{bmatrix} 1 \\ 0_{3x3} \end{bmatrix} \tag{4.24}$$

The time derivative of the identity quaternion gives

$$\dot{\mathbf{q}}_{id} = \dot{\mathbf{q}}^* \otimes \mathbf{q} + \mathbf{q}^* \otimes \dot{\mathbf{q}} = 0 \tag{4.25}$$

from which this useful relation is obtained by postmultiplication by $\mathbf{q}$

$$\dot{\mathbf{q}}^* = -\mathbf{q}^* \otimes \dot{\mathbf{q}} \otimes \mathbf{q}^*. \tag{4.26}$$

To rotate a vector $\mathbf{x}^B$ by the rotation encoded in $\mathbf{q}$, the following quaternion multiplication can be carried out

$$\tilde{\mathbf{x}}^I = \mathbf{q} \otimes \tilde{\mathbf{x}}^B \otimes \mathbf{q}^*, \quad \tilde{\mathbf{x}}^B = \begin{bmatrix} 0 \\ \mathbf{x}^B \end{bmatrix}, \quad \tilde{\mathbf{x}}^I = \begin{bmatrix} 0 \\ \mathbf{x}^I \end{bmatrix} \tag{4.27}$$

Furthermore, a very usefull feature of quaternions is that in similarity to rotation matrices, a series of sequential rotations can be simplified to one rotation by multiplication i.e. if $\mathbf{q}_1$ and $\mathbf{q}_2$ are unit quaternion then the combined rotation that is resulting from the rotation $\mathbf{q}_1$ followed by the rotation $\mathbf{q}_2$ correspond to the rotation $\mathbf{q}_3 = \mathbf{q}_2 \otimes \mathbf{q}_1$.

Their relation to the angle-axis parametrisation is:

$$\eta \equiv \cos\left(\frac{\theta}{2}\right) \tag{4.28}$$

$$\boldsymbol{\varepsilon} \equiv \begin{bmatrix} \varepsilon_1 \\ \varepsilon_2 \\ \varepsilon_3 \end{bmatrix} = \mathbf{k}\sin\left(\frac{\theta}{2}\right) \tag{4.29}$$

They are constrained by the condition

$$\mathbf{q^T q} = \eta^2 + \boldsymbol{\varepsilon}^T \boldsymbol{\varepsilon} \equiv 1 \tag{4.30}$$

hence the name unit quaternion. The relation between the quaternion and the rotation matrix is

$$\mathbf{R}(\eta, \boldsymbol{\varepsilon}) = \mathbf{I}_{3x3} + 2\eta\mathbf{S}(\boldsymbol{\varepsilon}) + 2\mathbf{S}^2(\boldsymbol{\varepsilon}). \tag{4.31}$$

The quaternion extracted from $\mathbf{R}^{-1} = \mathbf{R}^T$ is denoted $\mathbf{q}^*$ and is defined as

$$\mathbf{q}^* \equiv \begin{bmatrix} \eta \\ -\boldsymbol{\varepsilon} \end{bmatrix}. \tag{4.32}$$

The quaternion representation of a rotation is related to angle-axis parametrisation. Euler's displacement theorem tells that any rotation can be expressed as a simple rotation by the angle θ around one axis $\mathbf{k}$. A rotation matrix $\mathbf{R}_B^I$ between a global coordinate system I and the body system B can be obtained by the following equation from the axis $\mathbf{k}$ and the angle θ

$$\mathbf{R}_B^I = \cos(\theta)\mathbf{I} + \mathbf{S}(\mathbf{k})\sin(\theta) + (1 - \cos(\theta))\mathbf{k}\mathbf{k}^T \tag{4.33}$$

$$= \mathbf{I} + \mathbf{S}(\mathbf{k})\sin(\theta) + \mathbf{S}^2(\mathbf{k})(1 - \cos(\theta)) \tag{4.34}$$

where $\mathbf{I}$ is the identity matrix and $\mathbf{S}$ is the skew symmetric matrix defined as:

$$\mathbf{S}(\mathbf{k}) = \begin{bmatrix} 0 & -k_3 & k_2 \\ k_3 & 0 & -k_1 \\ -k_2 & k_1 & 0 \end{bmatrix} \quad \mathbf{k} = \begin{bmatrix} k_1 \\ k_2 \\ k_3 \end{bmatrix}. \tag{4.35}$$

4.4.3. Kinematics

To continuously derive the orientation we need an expression for the time derivative of the rotation matrix. Given two coordinate systems I and B where the rotation between them is represented by the rotation matrix $\mathbf{R}_B^I$, the time derivative of the rotation matrix is given as

$$\dot{\mathbf{R}}_B^I = \mathbf{S}(\boldsymbol{\omega}_{IB}^I)\mathbf{R}_B^I = \mathbf{R}_B^I\mathbf{S}(\boldsymbol{\omega}_{IB}^B) \tag{4.36}$$

where $\boldsymbol{\omega}_{IB}^I$ is the angular velocity between system I and B. The same relation can be found using the quaternion representation. If the quaternion $\mathbf{q}_{IB} = [\eta \ \ \boldsymbol{\varepsilon}^T]^T$ represents the rotation between the system I and B, and ω_{IB} is the angular velocity of system B relative to system I, the time derivative of $\mathbf{q}_{IB}$ for

system I becomes:

$$\dot{\mathbf{q}}_{IB} = \frac{1}{2}\begin{bmatrix} 0 \\ \boldsymbol{\omega}_{IB}^{I} \end{bmatrix} \otimes \mathbf{q}_{IB} \tag{4.37}$$

$$= \frac{1}{2}\begin{bmatrix} -\boldsymbol{\varepsilon}^{T} \\ \eta\mathbf{I} - \mathbf{S}(\boldsymbol{\varepsilon}) \end{bmatrix} \boldsymbol{\omega}_{IB}^{I}. \tag{4.38}$$

The same kinematics can be described in system B:

$$\dot{\mathbf{q}}_{IB} = \frac{1}{2}\mathbf{q}_{IB} \otimes \begin{bmatrix} 0 \\ \boldsymbol{\omega}_{IB}^{B} \end{bmatrix} \tag{4.39}$$

$$= \frac{1}{2}\begin{bmatrix} -\boldsymbol{\varepsilon}^{T} \\ \eta\mathbf{I} + \mathbf{S}(\boldsymbol{\varepsilon}) \end{bmatrix} \boldsymbol{\omega}_{IB}^{B}. \tag{4.40}$$

4.4.4. The Error Model of the Orientation

Even though quaternions have many advantages as representation of orientation, there is a weakness in connection with the Kalman filter. The constraint on the four parameters makes the four parameters linearly dependent upon each other. By an implementation of all four parameters as states in a Kalman filter a singularity in the covariance matrix would occur because of this linear dependency. A possible solution (out of others) to avoid this singularity is to use a truncated representation of the quaternion. This is accomplished by using the error of the orientation instead of the direct orientation.

We now proceed to find the dynamic equation of the error in orientation will be deduced as well as the equation for the inertial navigation system. The goal of this section is to deduce the dynamics of the error caused by the bias on the gyroscope measurement. In the following the quaternion $\mathbf{q}_{IB}$ which is representing the rotation from the inertial system I to the sensor coordinate system B is $\mathbf{q}$, and the estimated orientation from the direct integration of the gyroscope signal is represented by $\hat{\mathbf{q}}$ and which is found by using Equation (4.39)

$$\dot{\hat{\mathbf{q}}} = \frac{1}{2}\hat{\mathbf{q}} \otimes \begin{bmatrix} 0 \\ \boldsymbol{\omega}_{meas}^{B} \end{bmatrix}. \tag{4.41}$$

Here, $\boldsymbol{\omega}_{meas}^{B}$ is the angular velocity measured directly from the gyroscopes. Given that the integration is not perfect, the obtained orientation $\hat{\mathbf{q}}$ can be assumed to be the rotation from system I to an unknown system $\hat{B}$. The rotation error between the sensor system B and $\hat{B}$ is denoted $\tilde{\mathbf{q}}$ as illustrated in Figure 4.3. Since this rotation error also represents a rotation, we may relate $\tilde{\mathbf{q}}$, $\mathbf{q}$ and $\hat{\mathbf{q}}$ by

$$\tilde{\mathbf{q}} = \mathbf{q}^{*} \otimes \hat{\mathbf{q}} \tag{4.42}$$

where $\tilde{\mathbf{q}}$ is the orientation error of which the dynamics is to be derived. The time derivative of Equation

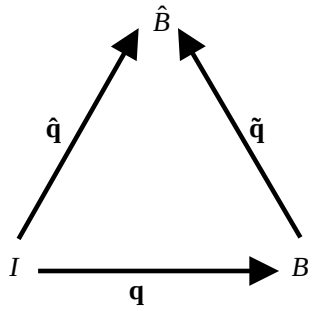

Figure 4.3.: Relation between the global coordinate system and the sensor fixed coordinate system when there is and error in the orientation.

(4.42) is found by using the chain rule:

$$\dot{\tilde{\mathbf{q}}} = \mathbf{q}^* \otimes \dot{\hat{\mathbf{q}}} + \dot{\mathbf{q}}^* \otimes \hat{\mathbf{q}} \tag{4.43}$$

which by using Equation (4.26) can be written as

$$\dot{\tilde{\mathbf{q}}} = \mathbf{q}^* \otimes \dot{\hat{\mathbf{q}}} - \mathbf{q}^* \otimes \dot{\mathbf{q}} \otimes \mathbf{q}^* \otimes \hat{\mathbf{q}}. \tag{4.44}$$

From Equation (4.37) the kinematics for $\hat{\mathbf{q}}$ and $\mathbf{q}$ is given through

$$\dot{\hat{\mathbf{q}}} = \frac{1}{2}\begin{bmatrix} 0 \\ \boldsymbol{\omega}^I_{meas} \end{bmatrix} \otimes \hat{\mathbf{q}} = \frac{1}{2}\hat{\mathbf{q}} \otimes \begin{bmatrix} 0 \\ \boldsymbol{\omega}^B_{meas} \end{bmatrix} \tag{4.45}$$

$$\dot{\mathbf{q}} = \frac{1}{2}\begin{bmatrix} 0 \\ \boldsymbol{\omega}^I \end{bmatrix} \otimes \mathbf{q} = \frac{1}{2}\mathbf{q} \otimes \begin{bmatrix} 0 \\ \boldsymbol{\omega}^B \end{bmatrix} \tag{4.46}$$

Using these relations the error state becomes:

$$\dot{\tilde{\mathbf{q}}} = \mathbf{q}^* \otimes \frac{1}{2}\begin{bmatrix} 0 \\ \boldsymbol{\omega}^I_{meas} \end{bmatrix} \otimes \hat{\mathbf{q}} - \mathbf{q}^* \otimes \begin{bmatrix} 0 \\ \boldsymbol{\omega}^I \end{bmatrix} \otimes \mathbf{q} \otimes \tilde{\mathbf{q}} \tag{4.47}$$

$$= \frac{1}{2}\begin{bmatrix} 0 \\ \boldsymbol{\omega}^B_{meas} \end{bmatrix} \otimes \mathbf{q}^* \otimes \hat{\mathbf{q}} - \begin{bmatrix} 0 \\ \boldsymbol{\omega}^B \end{bmatrix} \otimes \mathbf{q}^* \otimes \mathbf{q} \otimes \tilde{\mathbf{q}} \tag{4.48}$$

$$= \frac{1}{2}\begin{bmatrix} 0 \\ \boldsymbol{\delta}_\omega \end{bmatrix} \otimes \tilde{\mathbf{q}} \tag{4.49}$$

where $\boldsymbol{\delta}_\omega$ is defined from

$$\boldsymbol{\omega}^B_{meas} = \boldsymbol{\omega}^B + \boldsymbol{\delta}_\omega \tag{4.50}$$

The error model is in component form

$$\begin{bmatrix} \dot{\tilde{\eta}} \\ \dot{\tilde{\varepsilon}} \end{bmatrix} = \frac{1}{2}\begin{bmatrix} 0 & -\boldsymbol{\delta}_\omega{}^T \\ \boldsymbol{\delta}_\omega & \mathbf{S}(\boldsymbol{\delta}_\omega) \end{bmatrix}\begin{bmatrix} \tilde{\eta} \\ \tilde{\varepsilon} \end{bmatrix} \tag{4.51}$$

Since $\tilde{\eta} = \cos(\tilde{\theta}/2)$, and assumed that the error is small, the following approximation that $\tilde{\eta} \approx 1$ can be used. This results in:

$$\dot{\tilde{\varepsilon}} = \frac{1}{2}\boldsymbol{\delta}_\omega + \frac{1}{2}\mathbf{S}(\boldsymbol{\delta}_\omega)\tilde{\varepsilon} \tag{4.52}$$

By substituting $\boldsymbol{\delta}_\omega = \boldsymbol{\beta} + \boldsymbol{\xi}_\varepsilon$ the dynamics of the error becomes

$$\dot{\tilde{\varepsilon}} = \frac{1}{2}\boldsymbol{\beta} + \frac{1}{2}\mathbf{S}(\boldsymbol{\beta})\tilde{\varepsilon} + (\mathbf{I} - \mathbf{S}(\tilde{\boldsymbol{\varepsilon}}))\boldsymbol{\xi}_\varepsilon \tag{4.53}$$

4.4.5. Total Model Used in Kalman filter

The states which are estimated by the Kalman filter are the vector part of the quaternion error and the bias vector on the gyroscope:

$$\mathbf{x} = \begin{bmatrix} \tilde{\boldsymbol{\varepsilon}} \\ \boldsymbol{\beta} \end{bmatrix} \tag{4.54}$$

By putting together the model equation for the bias and the dynamical model of the quaternion error, the following continuous differential equation for the states in the Kalman filter can be written as

$$\begin{aligned} \dot{\mathbf{x}} &= \begin{bmatrix} \frac{1}{2}\boldsymbol{\beta} + \frac{1}{2}\mathbf{S}(\boldsymbol{\beta})\tilde{\boldsymbol{\varepsilon}} \\ -\mathbf{T}_\beta^{-1}\boldsymbol{\beta} \end{bmatrix} + \begin{bmatrix} \frac{1}{2}(\mathbf{I} - \mathbf{S}(\tilde{\boldsymbol{\varepsilon}}))\boldsymbol{\xi}_\varepsilon \\ \boldsymbol{\xi}_\beta \end{bmatrix} && (4.55) \\ &= \mathbf{f}(\mathbf{x}(t), \mathbf{v}(t)) && (4.56) \end{aligned}$$

with

$$\mathbf{T}_\beta = \begin{bmatrix} T_\beta & 0 & 0 \\ 0 & T_\beta & 0 \\ 0 & 0 & T_\beta \end{bmatrix} \tag{4.57}$$

To use this model in a Kalman filter, it has to be in a time-discrete form. By using the forward Euler method with the sampling time t_s, the following difference equation is derived

$$\begin{aligned} \mathbf{x}(k+1) &= \mathbf{x}(k) + t_s\mathbf{f}(\mathbf{x}(k), \mathbf{v}(k)) && (4.58) \\ \mathbf{x}(k+1) &= \begin{bmatrix} \tilde{\boldsymbol{\varepsilon}} + t_s\frac{1}{2}\boldsymbol{\beta} + t_s\frac{1}{2}\mathbf{S}(\boldsymbol{\beta})\tilde{\boldsymbol{\varepsilon}} \\ \boldsymbol{\beta} - t_s\mathbf{T}_\beta^{-1}\boldsymbol{\beta} \end{bmatrix} + \begin{bmatrix} t_s(\mathbf{I} - \mathbf{S}(\tilde{\boldsymbol{\varepsilon}}))\boldsymbol{\xi}_\varepsilon \\ t_s\boldsymbol{\xi}_\beta \end{bmatrix}. && (4.59) \end{aligned}$$

The linearised error matrix $\mathbf{V}(k)$ and the error covariance matrix of the process noise $\mathbf{v}(k)$ become:

$$\mathbf{V}(k) = \begin{bmatrix} t_s\frac{1}{2}(\mathbf{I}_{3x3} - \mathbf{S}(\hat{\tilde{\boldsymbol{\varepsilon}}}(k))) & \mathbf{0}_{3x3} \\ \mathbf{0}_{3x3} & t_s\mathbf{I}_{3x3} \end{bmatrix}, \mathbf{Q}(k) = \begin{bmatrix} \mathbf{I}_{3x3} \cdot \sigma_\varepsilon^2 & \mathbf{0}_{3x3} \\ \mathbf{0}_{3x3} & \mathbf{I}_{3x3} \cdot \sigma_\beta^2 \end{bmatrix} \tag{4.60}$$

The linearised transition matrix becomes:

$$\mathbf{\Phi}(k) = \begin{bmatrix} \mathbf{I}_{3x3} + t_s\frac{1}{2}\mathbf{S}(\hat{\boldsymbol{\beta}}(k)) & t_s\frac{1}{2}\mathbf{I}_{3x3} - t_s\frac{1}{2}\mathbf{S}(\hat{\tilde{\boldsymbol{\varepsilon}}}(k)) \\ \mathbf{0}_{3x3} & \mathbf{I}_{3x3} - t_s\mathbf{T}_\beta^{-1} \end{bmatrix} \tag{4.61}$$

4.4.6. The Initial Orientation

When an integration of the angular velocity is started, the initial orientation of the sensor in relation to a global system must be found. As only the tri-axial accelerometer gives a direct measurement of the orientation, this is applied for this purpose. Under the assumption that the sensor is not accelerated meaning that the patients have to stand still as the integration starts, this can be done. As already mentioned, the acceleration measurements only give partial information about the orientation; the angle about the vertical axis (heading) is not contained in the acceleration measurement. From that it follows that the global coordinate system has to be chosen at the moment when the integration starts.

The acceleration measurement of the unaccelerated sensor gives the gravitation vector in the sensor coordinate system. This vector is here denoted as $\mathbf{g}_{meas}$. The global system is defined such that the $\mathbf{z}^I$-axis is pointing in opposite direction of the gravity vector. The $\mathbf{x}^I$-axis and $\mathbf{y}^I$-axis have to be orthogonal in respect to each other as well as to the $\mathbf{z}^I$ constructing a right handed coordinate system. The $\mathbf{x}^I$ axis is chosen to be the projection of the sensors $\mathbf{x}^B$ on the global horizontal plane. This means that at the beginning of the integration the yaw angle (heading) in a roll-pitch-yaw representation would be zero.

To find the initial orientation of the sensor, the axis of which the body system is rotated in relation to the global system is found as well as the corresponding angle. With this knowledge the initial rotation formulated as a quaternion can be easily found. The rotation from the body system to the global system is along the axis orthogonal to the global $\mathbf{z}^I$ axis and orthogonal to the normalised gravity vector $\mathbf{g}_{meas}$. By using the cross product, the axis $\mathbf{k}_{init}$ can be found

$$\mathbf{k}_{init} = \frac{\mathbf{g}_{meas} \times \mathbf{z}^I}{\|\mathbf{g}_{meas} \times \mathbf{z}^I\|} \tag{4.62}$$

with $\mathbf{z}^I = [0 \;\; 0 \;\; 1]^T$. Now, as the axis of rotation is found, the next step is to find the angle to rotate. This is the angle between the vector $\mathbf{z}^I$ and $\mathbf{g}_{meas}$. This angle is found by the cosine relation

$$\cos(\theta_{init}) = \frac{{\mathbf{z}^I}^T \mathbf{g}_{meas}}{|\mathbf{z}^I| \cdot |\mathbf{g}_{meas}|} \tag{4.63}$$

The initial orientation can now be represented by a quaternion

$$\hat{\mathbf{q}}_{init} = \begin{bmatrix} \cos(\frac{\theta_{init}}{2}) \\ \mathbf{k}_{init} \sin(\frac{\theta_{init}}{2}) \end{bmatrix} \tag{4.64}$$

Note that by the calculation of $\hat{\mathbf{q}}_{init}$, both the initial orientation i.e. the sensor's orientation in relation to

the global system, as well as a definition of the global system I, are simultaneously found.

4.4.7. Measurement Equation

The measurements from the accelerometers are used to make an estimate of the orientation error and are included in the Kalman filter through the measurement equation. The gravitation vector $\mathbf{g}_{meas}$ is the measured acceleration in the sensor system B. This vector is pointing in the opposite direction of the $\mathbf{z}^I$-axis. The corresponding gravitation vector $\hat{\mathbf{g}}$ by the pure integration is found by this equation.

$$\hat{\mathbf{g}} = \hat{\mathbf{R}}^T \mathbf{z}^I \tag{4.65}$$

where $\hat{\mathbf{R}}$ is the orientation found by the pure integration of the measured angular velocity $\boldsymbol{\omega}^B_{meas}$ and $\mathbf{z}^I = [0\ 0\ 1]^T$. The axis of the error rotation goes through the axis orthogonal to the measured gravitation vector as well as the axis orthogonal to the gravitation vector $\hat{\mathbf{g}}$. This axis can now be found by applying the cross product between the respecting vectors:

$$\tilde{\mathbf{k}} = \frac{\mathbf{g}_{meas} \times \hat{\mathbf{g}}}{|\mathbf{g}_{meas} \times \hat{\mathbf{g}}|}. \tag{4.66}$$

Now as the axis of rotation is found, the next step is to find the angle to rotate. This is simply the angle between the vectors $\hat{\mathbf{g}}$ and $\mathbf{g}_{meas}$, found by this equation:

$$\cos(\tilde{\theta}) = \frac{\hat{\mathbf{g}}^T \cdot \mathbf{g}_{meas}}{|\hat{\mathbf{g}}||\mathbf{g}_{meas}|} \tag{4.67}$$

Now the error orientation can be described by a quaternion:

$$\tilde{\mathbf{q}}_\mathbf{y} = \begin{bmatrix} \cos\left(\frac{\tilde{\theta}}{2}\right) \\ \tilde{\mathbf{k}} \sin\left(\frac{\tilde{\theta}}{2}\right) \end{bmatrix}, \ \tilde{\varepsilon}_\mathbf{y} = \left[\tilde{\mathbf{k}} \sin\left(\frac{\tilde{\theta}}{2}\right)\right] \tag{4.68}$$

with the corresponding measurement matrix $\mathbf{H}(k)$

$$\mathbf{H}(k) = \begin{bmatrix} \mathbf{I}_{3x3}\chi_{g,rest} & \mathbf{0}_{3x3} \end{bmatrix}. \tag{4.69}$$

As the measurement based on the accelerometers is only valid when the sensor is not accelerated, the measurement in the Kalman-filter is only updated during the foot flat phase or more precisely during the gyroscope rest $\chi_{g,rest}$ which is defined and explained in Chapter 5. The measurement equation is given by

$$\mathbf{y}_k = \mathbf{H}(k)\mathbf{x}_k + \mathbf{w}(k) \tag{4.70}$$

where $\mathbf{w}(k)$ is the measurement noise vector related to the measurement of the error orientation.

Table 4.1.: Parameters of the Kalman filter.

σ_β [s]	σ_ε[rad/s]	T_β[s]	σ_r
0.01	0.01	100	0.05

4.4.8. Implementation Issues

The model of the orientation error is based on the assumption that the error remains small. Because of the unknown bias in the gyroscope measurement, the estimated error will after a while drift off. To avoid this the estimated error and bias from the Kalman filter are fed back to the integration of $\boldsymbol{\omega}^B_{meas}$. This is done at fixed time interval of 10 seconds.

Filter Parameters

Parameters of the extended Kalman filter are the initial error covariance matrix $\bar{\mathbf{P}}(0)$, the initial a priori state vector $\bar{\mathbf{x}}(0)$, as well as the covariance matrices $\mathbf{Q}$ of the process error $\mathbf{v}(k)$ and the covariance matrix to the measurement error $\mathbf{w}(k)$, namely $\mathbf{R}$. The initial error covariance matrix is chosen to be a diagonal matrix. Larger values indicate that there is a larger discrepancy between initial state estimates and real values. For increasing measurement noise variances, the EKF will trust the internal model predictions more than the measurements. Smaller corrections of the a priori state estimate are generated by discrepancies between the measurement and the predicted output. The noise covariance matrix $\mathbf{Q}$ is set according to Equation (4.60) whereas values of the standard deviation σ_ε and σ_β to the white noise processes $\boldsymbol{\xi}_\varepsilon$ and $\boldsymbol{\xi}_\beta$ are listed in Table 4.1. The noise covariance matrix $\mathbf{Q}$ is very much a tuning parameter, when small values are chosen will this result in a low bandwith filter which is good for slow moving signals. High values will result in a high bandwidth filter that can track fast moving signals but with a high noise. The initial error covariance matrix $\bar{\mathbf{P}}(0)$ and the initial state vector $\bar{\mathbf{x}}(0)$ were chosen to be:

$$\bar{\mathbf{P}}(0) = \begin{bmatrix} 1\,\mathrm{s}^2 & 0 & 0 & 0 & 0 & 0 \\ 0 & 1\,\mathrm{s}^2 & 0 & 0 & 0 & 0 \\ 0 & 0 & 1\,\mathrm{s}^2 & 0 & 0 & 0 \\ 0 & 0 & 0 & 1\,\mathrm{rad}^2/\mathrm{s}^2 & 0 & 0 \\ 0 & 0 & 0 & 0 & 1\,\mathrm{rad}^2/\mathrm{s}^2 & 0 \\ 0 & 0 & 0 & 0 & 0 & 1\,\mathrm{rad}^2/\mathrm{s}^2 \end{bmatrix}, \quad \bar{\mathbf{x}}(0) = \begin{bmatrix} 0 \\ 0 \\ 0 \\ 0 \\ 0 \\ 0 \end{bmatrix} \tag{4.71}$$

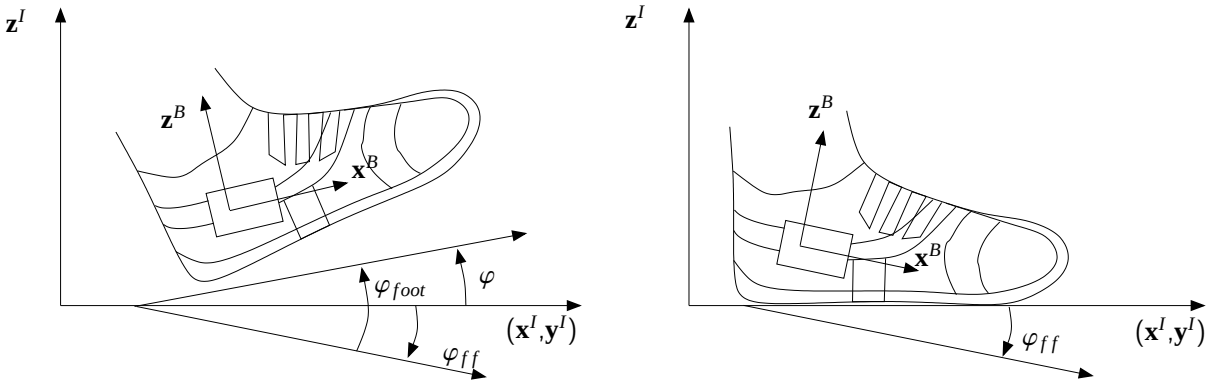

Figure 4.4.: In the gait phase detection algorithm the angle between the sensors $\mathbf{x}^B$ axis and the global coordinate systems $\mathbf{x}^I$ and $\mathbf{y}^I$ is denoted φ. The angle between foot and the horizontal ground is denoted φ_{foot}.

4.5. The Angle between Foot and Ground

In the gait phase detection algorithm explained in Chapter 5, the angle between the sensor's $\mathbf{x}^B$-axis and the ground is denoted as φ as shown in Figure 4.4. The angle is defined as positive in anticlockwise direction seen from the right side. More precisely φ is the angle between the sensor's $\mathbf{x}^B$ axis and the plane constructed by the $\mathbf{x}^I$ and $\mathbf{y}^I$ axes of the global coordinate system. In the foot flat phase the angle φ is nearly constant but the angle is depending on how the sensor is mounted. The angle φ_{ff} is introduced as the offset such that the angle φ_{foot} between the foot and ground is zero during the foot flat phase. The φ_{foot} can be calculated as

$$\varphi_{foot} = \varphi - \varphi_{ff}. \tag{4.72}$$

The angle φ_{ff} is only depending on how the sensor is mounted, and once the sensor is fixated, the angle remains constant. In order to allow a variation of the mounting, the angle φ_{ff} is estimated during the foot flat phase through the following filter

$$\varphi_{ff}[k] = (\varphi_{ff}[k-1] + \alpha * \varphi[k])/(1+\alpha) \tag{4.73}$$

calculating recursively the mean of the angle. The forgetting factor α was chosen to be very small ($\leq$0.005).

4.6. Evaluation of the Extended Kalman Filter

As no experimental validation of the EKF has been performed, some experimental results will briefly be shown in this section. In Figure 4.5 the elements of the estimated orientation are plotted in the upper

graph. In the middle graph is the c rest is plotted. The period in which the Kalman filer update is active $\chi_{g,rest}$ is one. In the lower graph the bias states are plotted. From the figure it can be seen that during the period in which the Kalman filter update are performed, the biases are changing, when $\chi_{g,rest}$ is zero and no measurement update are performed the biases stay constant. In Figure 4.6 the same plot is shown with a smaller time scale.

In Figure 4.7 the bias φ_{ff} between the sensor and foot is shown in the upper graph whereas the sagittal angle between the foot and ground φ_{foot} is shown in the lower graph. It can be observed that the bias φ_{ff} converges after ca. 2.5 seconds.

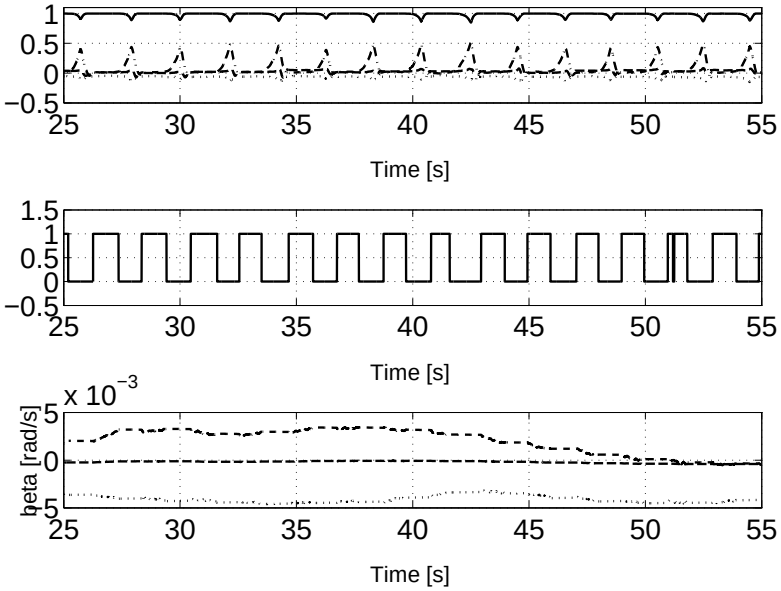

Figure 4.5.: Upper graph shows the elements in the quaternion, η (solid line), first vector component (dotted), second vector component (dashdotted) and the third vector component (dashed). The lower graph shows the corresponding bias elements: first element (dotted), second (dashdotted) and third element (dashed).

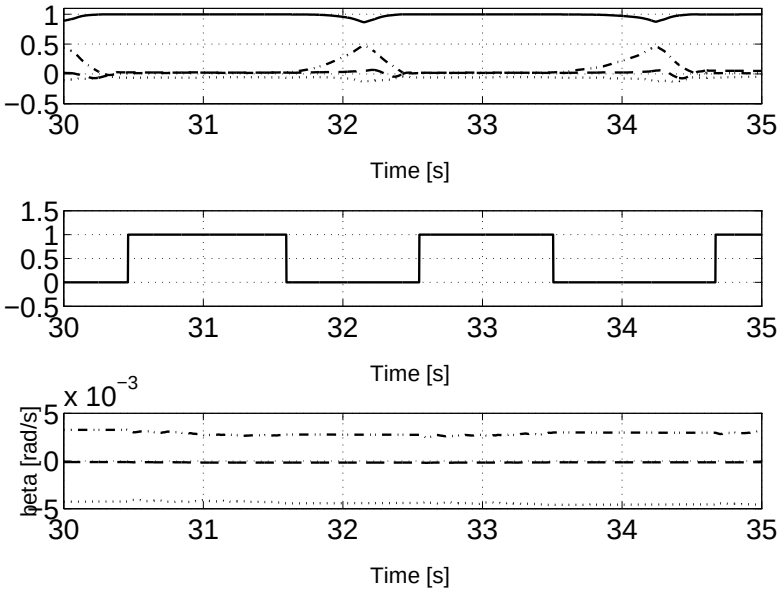

Figure 4.6.: Upper graph shows the elements in the quaternion, η (solid line), first vector component (dotted), second vector component (dashdotted) and the third vector component (dashed). The lower graph shows the corresponding bias elements: first element (dotted), second (dashdotted) and third element (dashed).

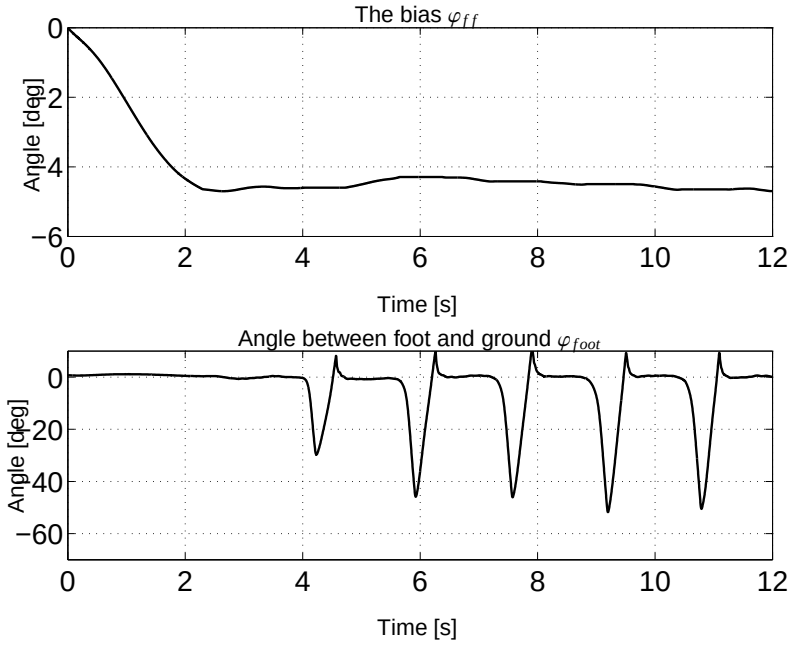

Figure 4.7.: Results of the bias angle estimation during gait. Upper graph shows the bias on the angle φ_{ff}. In the lower graph the sagittal angle between foot and ground φ_{foot} is shown.

4.7. Discussion and Conclusions

In this chapter an indirect extended Kalman filter was developed to estimate the orientation of an inertial sensor. The extended Kalman filter was developed for the usage in an FES-assisted gait training system with the sensor mounted to the foot. Information from the gait phase detection system developed in Chapter 5 was used to decide whether the sensor was at rest. When the sensor was at rest, the accelerometer measurement was used as orientation measurement in the Kalman filter. No experiments has been conducted in order to directly validate the accuracy of the Kalman filter in this chapter, but the EKF is used extensively in the following chapters of this thesis. In Chapter 5, the angle between foot and ground plays an important role in the gait phase detection algorithm. In Chapter 6, a method for finding the 3D movement of the foot is developed and experimentally verified with an optical measurement system. Furthermore, in Chapter 7 an FES-assisted gait training system based on the gait phase detection system is developed. In that chapter a closed-loop control loop is developed, where electrical stimulation applied to the tibialis anterior is used as the plant input and the maximum angle between the foot and the ground is used as feedback variable.

5. Gait Phase Detection

5.1. Summary

Aim: The work presented in this chapter aims to develop a robust gait phase detection system for use in FES-assisted gait rehabilitation by means of inertial sensors. The target is to show that one robust algorithm can work for a variety of subjects without the need to tune the parameters individually for each patient.

Methods: By help of braces inertial sensors can be easily mounted on the feet in short time. A new Gait Phase Detection algorithm based on an Inertial Sensor Unit was developed (GPD-IS). From all the information one inertial sensor delivers, four distinct gait phases were detected: foot flat, pre-swing, swing and loading response. The inertial sensor system applied in this chapter consists of 2 sensor units making it possible to detect the gait phases on both sides. Five stroke patients with different pathological gait patterns were chosen to validate the algorithm. To validate the detection algorithm the insole pressure measurement system Parotec manufactured by the company Paromed GmbH[1] was used. This system consists of a foot insole with 24 hydro-cells making it possible to measure the distributed pressure underneath the foot. All patients walked with a parachute harness support on a treadmill for at least 3 min, and the detected phases from the GPD-IS were compared with the obtained gait phases from the Parotec system.

Results: In five hemiplegic subjects, all strides were detected by the GPD-IS in walking tests on a motorised treadmill. In the comparison with the insole pressure measurement system, which is similar to the traditional force resistive sensors used for triggering electrical stimulation during gait, no large time differences in the detection of the events were found, but a systematic delay of the toe off event was found. The heel strike event was systematically detected earlier than that of the reference system. For the two other events no systematic bias of the event detection could be found. For one patient the detection of the loading response phase failed for more than 20% of the steps on the affected body side using the GPD-IS algorithm. The variations of the event detection for each individual patient were small indicating a high

[1] www.paromed.de

repeatability of the detection.

Conclusions: The developed gait phase detection system has been shown to work robustly for five hemiplegic patients. The errors in the event detection compared to the reference system are limited and it can be concluded that in an FES-assisted gait training system the obtained gait phases from the inertial sensor can be used to trigger the stimulation.

Contribution: The author developed the methods and implemented the experimental software. Furthermore, the author planned and ran the experiments. Parts of this work are published in [56].

5.2. Motivation

There are several reasons for using an inertial sensor for gait phase detection. The sensor can with the help of a special made brace be attached on the foot outside the patient's shoe in a short time (half a minute for a trained person). This makes it more attractive for therapists to take it into use compared to traditional foot switches which have to be attached underneath the foot. This had the consequence that the patients had to take off the shoes in order to attach the sensor. In addition, a full inertial sensor possesses an advantage over similar sensors also containing gyroscopes and accelerometers; not only the raw signals angular velocity and acceleration can be used in an algorithm for detecting gait phases but also values derived from the orientation of the sensor such as the angle between foot and the ground as well as the acceleration without the gravity component expressed in the global coordinate system. The goal here was to develop an algorithm which will work for a wide variety of patients without having the need to tune the parameters of the algorithm for each patient individually.

Within this chapter methods for obtaining gait phases based on the inertial sensor and the validation of those methods with a foot insole pressure reference measurement system are presented. A robust algorithm for estimating four distinct gait phases by using all available information from the inertial sensor is explained in Section 5.4. Furthermore, in Section 5.5 an experimental validation of the obtained phases from GPD-IS is described. In this section a reference algorithm for detection of gait phases based on the insole foot pressure measurements, the experimental setup and the experimental procedure are described. Experimental results from the comparison of the gait phases from GPD-IS with the obtained phases from the reference measurement system are given in Section 5.6. Finally, the results are discussed in Section 5.7.

5.3. Introduction

There are many different definitions and description of gait. The most commonly used reference on gait has become the book by Perry [65]. She defines the gait phases based on its functional tasks. Since a measurement of the gait with foot switches or gyroscopes and accelerometers can only detect events that are caused by some repetitive patterns in the movement and in the measured signals, the phases detected from sensors differ from those based on functional tasks. Perry describes five stance phase periods and three swing phase periods. The stance phase periods are as follows: initial contact, loading response, mid-stance, terminal-stance, and pre-swing. The swing phase periods are initial-swing, mid-swing, and terminal-swing. Initial contact is defined as the moment when the foot touches the floor. The loading response is the reaction of the limb as it absorbs the impact. The period of single limb support during which the body progresses over a stationary foot is mid-stance. Terminal-stance is the period in the gait cycle in which the body moves ahead of the supporting foot and weight begins to fall on the contralateral limb. The final stance phase period, pre-swing, is the transitional period of double support, during which the limb is rapidly unloaded in preparation for swing. Initial swing is the point in which the limb is lifted from the floor and initial advancement of the thigh is assumed to achieve toe clearance and forward propulsion. During mid-swing, the limb is advanced further in order to achieve a vertical tibial position. Continued tibial advancement toward full knee extension, deceleration of the thigh, and maintenance of the foot position are included in the terminal swing. These completes the full cycle from initial contact to terminal swing.

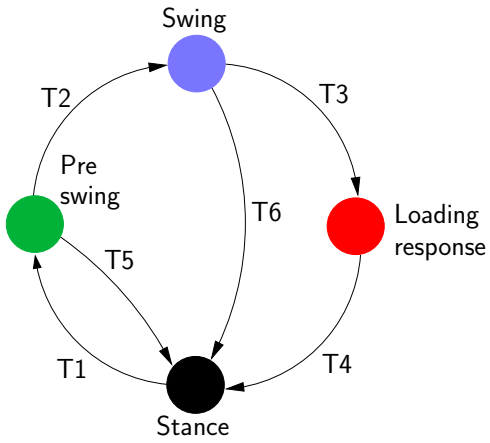

Figure 5.1.: Gait phase detection system represented as a state machine. The gait phases are represented as four states where six transitions between the states are possible.

Four distinct gait phases are detected in the algorithm described here (GPD-IS) (cf. Figure 5.1). These four phases are the foot flat, pre-swing, swing and loading response phases. The phase transitions can be seen as gait events; the transition from foot flat to pre-swing is the heel off event, the transition between pre-swing and swing is the toe off event. Furthermore, the transition from swing to loading response

is the initial contact/heel strike whereas the transition between loading response and foot flat is the full contact event. The transitions between the phases will in this work be based upon characteristics in the sensor signals and not on functional tasks. Shortly described, the heel strike event is detected by a peak in acceleration, full contact is detected by a low amplitude in both gyroscope signals and in the accelerometer signals. The heel off event is detected by increasing amplitude in the signals and the toe off event is detected by a change in the rotational movement of the foot.

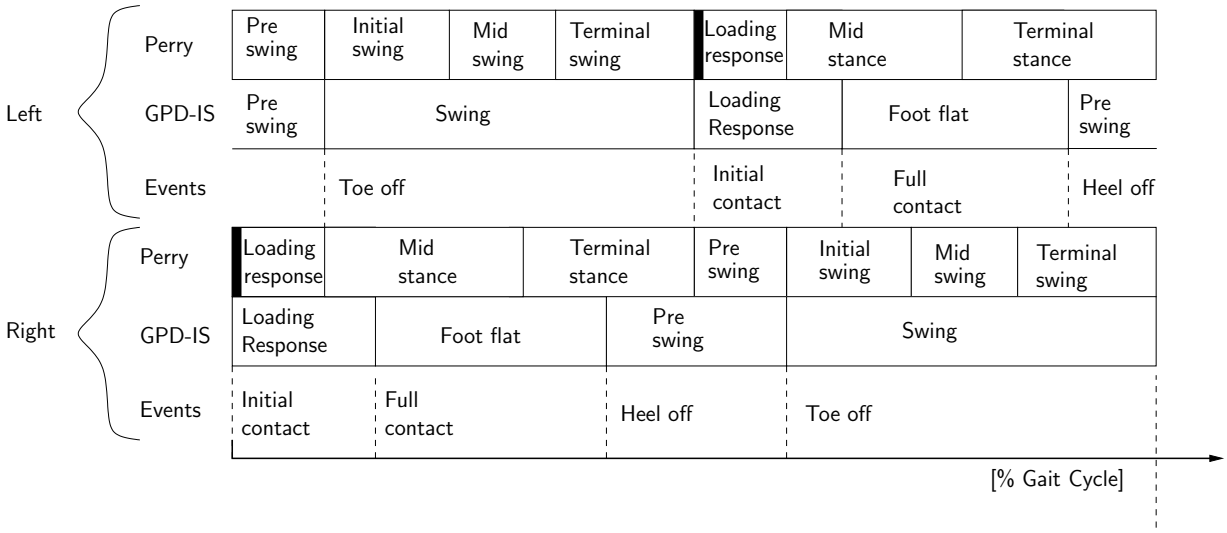

Figure 5.2.: The first row shows the gait phases as defined by Perry [65], the second shows the gait phase definition used in this work (GPD-IS) whereas the last row indicates the corresponding gait events.

In Figure 5.2 a comparison of the phases gait phases by Perry and the phases used within this work is shown. The initial contact event initiates the loading response phase in both definitions. In the definition by Perry, the loading response lasts until the contralateral side toe lifts off. In GPD-IS, the next event detected is the full contact which also ends the loading response phase and starts the foot flat phases. Perry uses the notation stance which is divided into middle stance and terminal stance, and in the middle stance the weight is shifted from heel to toe, and the contralateral foot is progressing beyond the stationary foot. The next phase that is detected by GPD-IS is the heel off event. This event initiates the pre-swing phase. This is occurring at the same moment as the terminal stance phase starts according to Perry. The phase between heel off and toe off is within this work called the pre-swing phase, whereas Perry divides this phase in terminal stance and pre-swing. In the terminal stance the weight moves ahead of the foot, and in the pre-swing phase the contralateral side has its initial contact, and the weight is shifted to the other side.

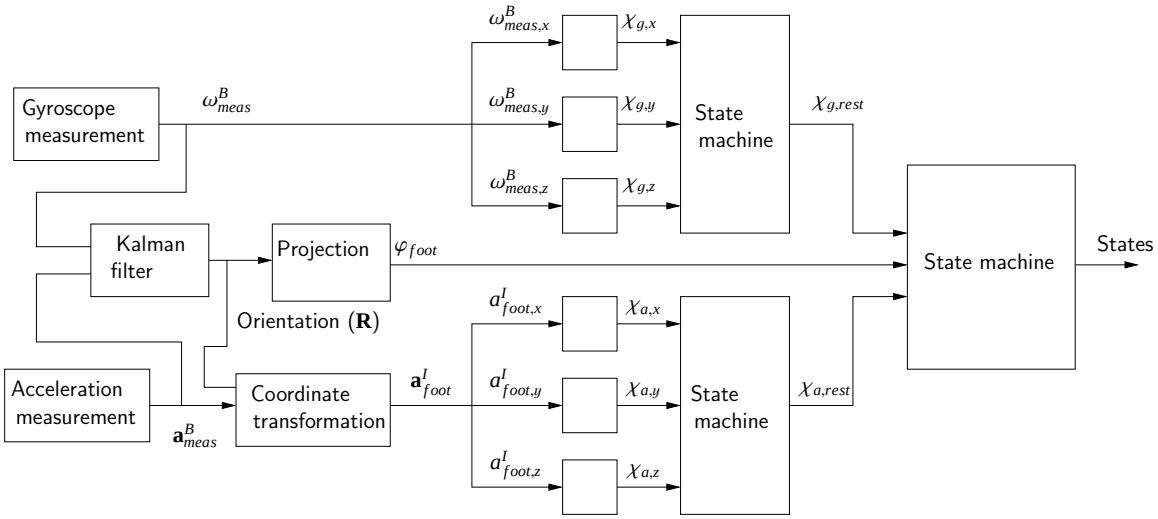

Figure 5.3.: Block structure of the algorithm used in the gait phase detection based on inertial sensors (GPD-IS).

5.4. Methods

5.4.1. Detection Algorithm

The algorithm developed in this chapter detects the gait phases for one side under the assumption that the sensor is mounted on the side of the foot with braces in such a way that the sensor's x^B axis is pointing in forward walking direction, and the sensor z^B axis is pointing towards the direction of gravity when the subject is standing. The y^B axis is pointing in the orthogonal direction of the two other axes, forming a right handed coordinate system.

In Figure 5.3 the structural scheme of the developed gait phase detection system based on inertial sensors (GPD-IS) is depicted. The block "Kalman filter" is referring to the Kalman filter developed in Chapter 4 where a method for orientation estimation of the sensor with respect to a global coordinate system was proposed. In the gait phase detection algorithm, the orientation of the sensor is applied to transform the measured acceleration into the global coordinate system. The measured acceleration $\mathbf{a}^B_{meas}$ is the sum of the real acceleration of the sensor $\mathbf{a}^B$, the gravity component $\mathbf{g}^B$ and an unknown bias $\boldsymbol{\gamma}$

$$\mathbf{a}^B_{meas} = \mathbf{a}^B + \mathbf{g}^B + \boldsymbol{\gamma}. \tag{5.1}$$

The unknown bias is in this section taken to be as zero in contrary to Chapter 6 where this bias is calculated offline. The sensor's acceleration $\mathbf{a}^I_{foot}$ in the global coordinate system without the gravity

component can be calculated by this equation

$$\mathbf{a}^I_{foot} = \mathbf{R}\mathbf{a}^B_{meas} - \mathbf{g}^I. \tag{5.2}$$

Here $\mathbf{R}$ is the rotation matrix representing the orientation of the sensor in relation to the global coordinate system and $\mathbf{g}^I$ is the gravity component.

Based on the angular velocity and the acceleration measurement a coarse detection is performed whether the sensor is at rest or if it is moving. This is done independently for the angular velocity measurement and the acceleration measurement. These coarse detections are denoted as $\chi_{a,rest}$ for the accelerometers and $\chi_{g,rest}$ for the gyroscopes, where the logical value 1 means that the sensor is at rest and the logical value 0 means that the sensor is indicating a movement. The algorithms are both for the gyroscopes and the accelerometers similar in the structure but the parameters are different and only the detection of $\chi_{g,rest}$ is outlined here.

The detection of gyroscope rest $\chi_{g,rest}$ and acceleration rest $\chi_{a,rest}$

To each of the gyroscope sensors $\omega^B = \left[\omega^B_x, \omega^B_y, \omega^B_z\right]^T$ a logical variable $\chi_{g,x}, \chi_{g,y}$ and $\chi_{g,z}$ is associated. Each variable describes if this gyroscope is indicating rest or not. $\chi_{g,x}$ is the state in a state machine containing 2 states; rest and not rest. Similar to the gyroscope for each accelerometer sensor the logical variables $\chi_{a,x}$,$\chi_{a,y}$ and $\chi_{a,z}$ are associated.

For both states there is a condition for transition to the other one. Let the following function $g(i, x, \delta, N)$ is defined

$$f(x,\delta) = \left\{ \begin{array}{l} 1 \textbf{ if } x \geqslant \delta \\ 0 \textbf{ if } x < \delta \end{array} \right\}, \quad g(i, \mathbf{x}, \delta, N) = \sum_{j=i-N}^{i} f(\mathbf{x}[j], \delta). \tag{5.3}$$

The function $g(i, \mathbf{x}, \delta, N)$ is merely counting the number of samples for which the vector $\mathbf{x}$ is exceeding a limit within the last N samples.

Transitions for single sensor detection of rest/movement

All the logical values $\chi_{g,x}$, $\chi_{g,y}$, $\chi_{g,z}$, $\chi_{a,x}$, $\chi_{a,y}$, $\chi_{a,z}$ have the same conditions for transitions but with different parameters. The transition from rest to movement for $\chi_{g,x}$ is as follows:

$T_{single,r\rightarrow m} : rest \rightarrow movement$

The condition for the transition from rest to movement for the individual sensors is depending on the angular velocity. When the angular velocity of the last N=25 samples exceeds a limit 6 times a transition to movement occurs:
$g(i, \omega^B_x, \delta_{w,x}, N) > 6$

$T_{single,m\rightarrow r}$: *movement* $\rightarrow$ *rest*

The condition for the transition from movement to rest for the individual sensors is depending on the angular velocity and its derivative. When the angular velocity of the last N=25 samples does not exceed a limit more than 2 times and the derivative of the angular velocity does not exceed a certain limit the last 25 samples the transition to rest occurs $\left(g(i, \omega_x^B, \delta_{w,x}, N) \leqslant 2\right) \wedge \left(g(i, \dot{\omega}_x^B, \delta_{w,x}, N) = 0\right)$.

Transitions for detection of rest/movement based on all sensors

The transition of $\chi_{g,rest}$ from rest to movement and vice versa can be described by using the logical variables of the separate sensors.

$T_{r\rightarrow m}$: *rest* $\rightarrow$ *movement*

$\overline{\chi}_{g,y}[i]$

$T_{m\rightarrow r}$: *movement* $\rightarrow$ *rest*

$\chi_{g,x}[i] \wedge \chi_{g,y}[i] \wedge \chi_{g,z}[i]$

The conditions for the transitions of the GPD-IS

The main state machine consists of four states. The transitions between the states in the gait detection system are dependent on the coarse detection represented by the logical variables $\chi_{g,rest}$ and $\chi_{a,rest}$.

The transitions between the states have the following conditions:

T1: foot flat $\rightarrow$ *pre-swing*

In the foot flat phase, the only transition which can occur is the one to the pre-swing state. This is done when both $\chi_{a,rest}$ and $\chi_{g,rest}$ are indicating a movement and when the angle of the foot in the sagittal plane is exceeding a certain limit in negative direction: $(\overline{\chi_{a,rest}}) \wedge \left(\overline{\chi_{g,rest}}\right) \wedge \left(\varphi_{foot} < \delta_{\varphi,T1}\right)$.

T2: pre-swing $\rightarrow$ *swing*

In the pre-swing state the algorithm anticipates the transition to the swing state. The condition for the transition to the swing phase is that at least one of the sensors is indicating movement. The second condition for swing phase is that the rotational movement of the foot in the sagittal plane is changing from clock wise to anticlockwise direction when seen from the right side. To make this detection more robust, a change of sign from positive to

negative for both the angular velocity as well as the derivative of the angular velocity is used. The condition for the transition becomes:
$\left(\overline{\chi_{a,rest}} \vee \overline{\chi_{g,rest}}\right) \wedge \left(\text{csign}(\dot{\omega}_y^B, \delta_{\dot{\omega},y}) \vee \text{csign}(\omega_y^B, \delta_{\omega,y}\right)$, where

$$\text{csign}(x, \delta) = \left\{ \begin{array}{c} 1 \textbf{ if } g(i-22, x, \delta, 3) > 2 \wedge g(i, x, \delta, 3) > 2 \\ \textbf{else } 0 \end{array} \right\}. \tag{5.4}$$

T3: swing → loading response

In the swing phase the algorithm awaits the transition to the loading response phase that begins with the first contact of the foot with the ground. Thus, the algorithm is awaiting for a peak in the accelerometer signals. This is detected evaluating the derivative of the acceleration, the jerk. Furthermore, for several patients the foot might touch the ground during the swing phase. This leads to a peak in the acceleration signal which can trigger the transition to the loading response. In order to avoid such false transitions, the angle of the foot in the sagittal plane has to exceed a certain threshold and in addition the velocity in the horizontal level has to be limited:
$\left(|\dot{\mathbf{a}}_{foot}^I| > \delta_{\dot{a},T3}\right) \wedge \left(\varphi_{foot} > \delta_{\varphi,T3}\right) \wedge \left(|\mathbf{v}_{foot,(x,y)}^I| < \delta_{v,T3}\right)$.

T4: loading response → foot flat

After the loading response the next phase is foot flat which begins when both front and rear part of the foot touch the ground. This event is detected when both the gyroscopes and accelerometers are indicating rest. The transition condition becomes
$(\chi_{g,rest}) \wedge (\chi_{a,rest})$.

T5: pre-swing → foot flat

In the case when the subject lifts the heel and then puts it back on the ground a transition is introduced. This event is detected when both the accelerometers and the gyroscopes are indicating rest. Furthermore, to avoid a premature transition back to foot flat phase the sagittal angle has to exceed a certain limit. The transition condition becomes
$(\chi_{a,rest}) \wedge \left(\chi_{g,rest}\right) \wedge \left(\varphi_{foot} > \delta_{\varphi,T5}\right)$.

T6: swing → foot flat

In certain gait patterns the loading response is not detected, as this transition is detected by large peaks in the acceleration. If this is the case, a direct transition from swing to foot flat is useful. This event is detected when both the accelerometers and the gyroscopes are indicating rest. Further requirements are that the rotational velocity around the y^B- axis

and its derivative are approximately zero and that the sagittal angle is larger than a negative threshold:
$(\chi_{a,rest}) \wedge \left(\chi_{g,rest}\right) \wedge \left(|\dot{\omega}^{B}_{meas,y}| < \delta_{\dot{\omega},sw}\right) \wedge \left(|\omega^{B}_{meas,y}| < \delta_{\omega,T6}\right) \wedge \left(\varphi_{foot} > \delta_{\varphi,T6}\right)$.

Table 5.1.: Parameters of the gait phase detection algorithm.

$\delta_{\omega,x}$	$\delta_{\omega,y}$	$\delta_{\omega,z}$	$\delta_{\dot{\omega},x}$	$\delta_{\dot{\omega},y}$	$\delta_{\dot{\omega},z}$
0.2[rad/s]	0.2[rad/s]	0.2[rad/s]	0.05[rad/s^2]	0.05[rad/s^2]	0.05[rad/s^2]
$\delta_{a,x}$	$\delta_{a,y}$	$\delta_{a,z}$	$\delta_{\dot{a},x}$	$\delta_{\dot{a},y}$	$\delta_{\dot{a},z}$
1.5 [m/s^2]	1.5 [m/s^2]	1.5 [m/s^2]	0.15[m/s^3]	0.15 [m/s^3]	0.15 [m/s^2]

$\delta_{\varphi,T1}$	$\delta_{\dot{a},T3}$	$\delta_{\varphi,T3}$	$\delta_{v,T3}$	$\delta_{\varphi,T5}$	$\delta_{\omega,T6}$	$\delta_{\dot{\omega},T6}$	$\delta_{\varphi,T6}$
-2 [°]	1.73 [m/s^2]	-2 [°]	0.45 [m/s]	-2 [°]	0.1 [rad/s]	0.005 [rad/s^2]	-2 [°]

5.5. Experimental Validation

5.5.1. Experimental Procedure

An experimental study was carried out in order to quantify the detection success ratio and its accuracy. A group of five stroke patients with different gait pathologies were recruited. Despite their impairments all patients were all able to walk on a treadmill with a parachute harness independently.

Subject information as hemiplegic side, gender and walking speed is given in Table 5.2. The walking experiments were performed on a motorised treadmill from Woodway[2]. The treadmill speed can be manually adjusted. Before committing the experiments described here, all the subjects had been familiarised with the treadmill and were comfortable walking on it. All patients were for safety reasons walking with a parachute harness. Before each measurement, the patients were standing still on the treadmill. About five seconds after the measurement was started, the treadmill was accelerated up to normal walking speed for the subject and was kept constant throughout the experiment. The subjects were walking continuously with a constant treadmill speed for at least three minutes.

5.5.2. Experimental Setup

The measurement system Parotec from the company Paromed Gmbh[1] was applied for validation of the GPD-IS algorithm. The technical specifications for this system are summarised in Chapter 3. For the

[2] www.woodway.com
[1] Paromed Medizintechnik GmbH, www.paromed.de

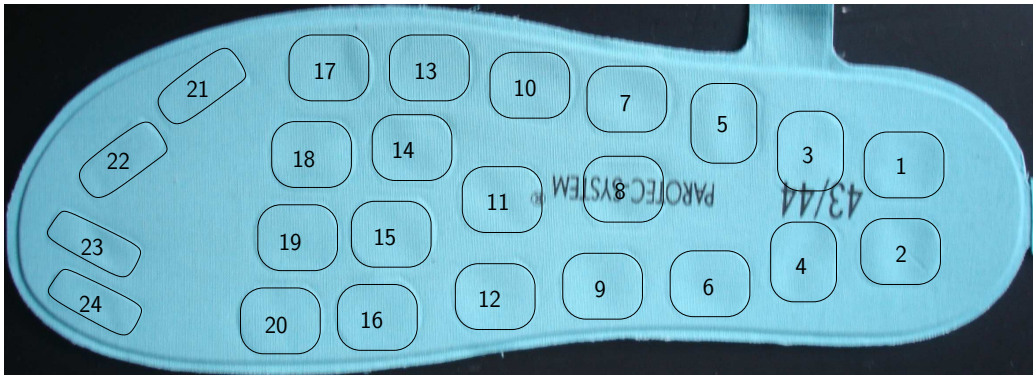

Figure 5.4.: Parotec sole with 24 hydro-cells.

Parotec system a serial data transfer protocol is defined, allowing an online communication between a PC and the Parotec control unit. The protocol allows start and stop of the measurement as well as online reading of the pressure signals. The signals from the Parotec system were sampled at a frequency of 60 Hz whereas the inertial sensor signals were sampled at 500 Hz. On the PC side the signals were collected and synchronised as they were read in through a MATLAB/SIMULINK program. The signals from the different measurement systems were read into a buffer as they were arriving by a separate process/thread and then the MATLAB/SIMULINK program collected the last entries by a fixed sample time. Due to this sampling strategy the Parotec pressure signals are time delayed by a value between 0 and 16.67 ms.

5.5.3. Gait Phase Detection Based on Insole Pressure Measurement

Based on the foot insole pressure measurement an algorithm was developed to detect exactly the same phases as the gait phase detection system with inertial sensors. The gait phases are still represented as states in a state machine, and logical rules are governing the transitions between the states. The idea behind this algorithm is to compare the inertial sensor gait phase detection system with a traditional gait

Table 5.2.: Subject data.

Subject	male/female	walking speed	hemiplegic side
S1	M	1.18 [km/h]	left
S2	M	2.32 [km/h]	right
S3	M	1.18 [km/h]	right
S4	M	1.35 [km/h]	left
S5	M	0.98 [km/h]	right

Table 5.3.: Parameters of the gait detection validation algorithm.

$\delta_{r,1}$ [N/cm^2]	$\delta_{r,2}$ [N/cm^2]	$\delta_{r,3}$[N/cm^2]	$\delta_{r,4}$[N/cm^2]	$\delta_{r,5}$[N/cm^2]
1.25	0.41	0.50	1.66	0.83

phase detection system based on foot switches. From the 24 hydro-cells three meta signals are defined

$$meta\_heel = \frac{1}{4}\sum_{n=1}^{n=4} P(n) \tag{5.5}$$

$$meta\_mid = \frac{1}{6}\sum_{n=7}^{n=12} P(n) \tag{5.6}$$

$$meta\_tot = \frac{1}{24}\sum_{n=1}^{n=24} P(n) \tag{5.7}$$

where $P(n)$ is the pressure from hydro-cell number n defined in Figure 5.4. Four transitions are defined which correspond to the transition $T1..T4$ of the algorithm described in Section 5.4. Since the transitions $T5$ and $T6$ do not correspond to any gait events but are merely introduced to hinder that the gait phase detection is dead locked, they are not used in this detection algorithm.

T1: foot flat → pre-swing

The foot flat phase is lasting until the heel lifts off the ground. The transition is detected as the sum of all sensors measuring pressure underneath the heel sink below a certain threshold: $meta\_heel < \delta_{r,1}$.

T2: pre-swing → swing

The transition from pre-swing to swing is occurring at the moment the toe lift off the ground. For simplicity the transition condition is that the *meta_tot* is below a certain threshold: $meta\_tot < \delta_{r,2}$.

T3: swing → loading response

The swing phase is lasting until the heel is touching the ground. The condition for this transition is that the *meta_heel* is exceeding a certain limit which will occur for a normal heel strike at the point where the heel first hits the ground. For the case when the foot hits the ground flat or the toe hits the ground first, another condition is introduced where the sum of all cells signals are used. The condition becomes:
$meta\_heel > \delta_{r,3} \vee meta\_tot > \delta_{r,4}$.

T4: loading response → foot flat

This transition happens in the moment the foot is flat on the ground, and the condition for this transition is that the signals of the cells underneath the middle of the foot (*meta_mid*)

exceed a limit:
$meta\_mid > \delta_{r,5}$.

5.5.4. Event Validation Procedure

In order to assess the accuracy of the GPD-IS event detection, a comparison with the foot insole reference system was performed. As the measured signals from both the inertial sensor system and from the foot insole system were read into the computer simultaneously. No additional synchronisation of the data was necessary. The gait phase detection considered here is an online procedure but the validation followed afterwards with an offline processing of the recorded data.

Firstly, the errors of the detection were assessed. For the GPD-IS system different errors can occur i.e. complete steps can be missed, transitions can occur to early or single transitions can be completely missed. The following error types can be distinguished:

False heel off (transition T5 occurred): During continuous gait the transition from foot flat to pre-swing and back to foot flat should normally not occur. This transition exist merely for the case where the patients are slightly moving the foot but do not intend to take a step. Consequently, the transition sequence from foot flat to pre-swing and back to foot flat is during walking with a constant speed on a treadmill considered as a detection error. The false detection of heel off was easily found by counting the number of transitions from pre-swing to foot flat.

No loading response (transition T6 occured): Another possible error of the GPD-IS is the direct transition from swing phase to foot flat phase, i.e. the detection of heel strike fails and the transition directly to foot flat is detected. In some types of pathological gait the foot is hitting the floor very softly and consequently no heel strike is detected. For this reason the transition from swing phase to foot flat phase has been introduced. This transition is considered as a fault because a missing heel strike detection would in some cases lead to a prolonged stimulation in an FES-assisted gait system.

Early heel strike: Furthermore, for many patients with pathological gait, the foot on the paretic side can often touch the ground in the swing phase. Depending on the movement of the foot, this often leads to a peak in the accelerometer signals, which in turn are used to detect the heel strike. In order to prevent such a premature transition two rules have been applied as described in Section 5.4. Despite these rules such transition can happen and is defined as an error.

In addition to the error assessment, the accuracy is also validated in terms of the time difference between the detected events from the inertial sensor system and the one from the foot insole based detection. The events detected from the foot insole measurements were used as reference, and the time difference between the reference event and the GPD-IS event was found by searching in a window of ± 300 ms around the time of the reference event. If the event did not occur in this window, it was classified as not

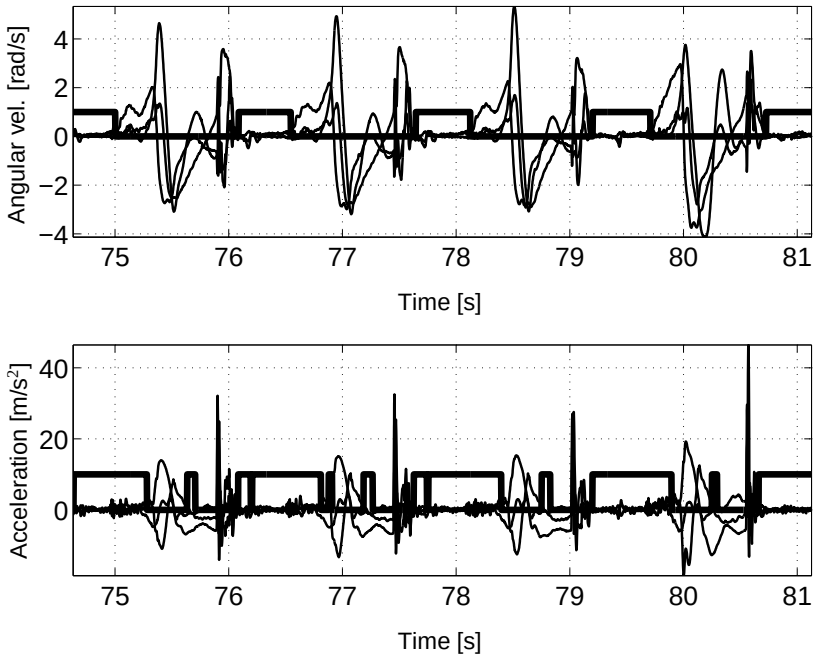

Figure 5.5.: Upper graph shows the angular velocity ω^{B}_{meas} (thin lines) and the detected gyroscope rest χ_g (bold line). The lower graph shows the acceleration $\mathbf{a}^{I}_{foot}$(thin lines) and the detected accelerometer rest χ_a(bold line).

detected. For the events that were successfully detected, the mean difference and the standard deviation of the timing error between the reference events and the GPD-IS events were calculated.

Since the measurements started with zero treadmill velocity, the first three steps were excluded from the analysis.

5.6. Experimental Results

The gait detection system (GPD-IS) was able to detect all gait phases for all five subjects. In Figure 5.5 the measured angular velocity and acceleration are shown for the left side of subject S4. In the same figure, the detection of gyroscope rest χ_g and acceleration rest χ_a are shown. As observed in the figure, the detection of rest by use of the gyroscopes is more reliable than the detection based on the accelerometers. Therefore the former does also play a more important role in the GPD-IS algorithm.

In Figure 5.6 the gait phases detected by the GPD-IS are shown for one subject together with the gait phases detected by the foot insole system.

In Table 5.4 the total number of steps, the number of strides in which the loading response phase were not detected, the number of strides in which early heel strike occurs, the number of false heel off, the number

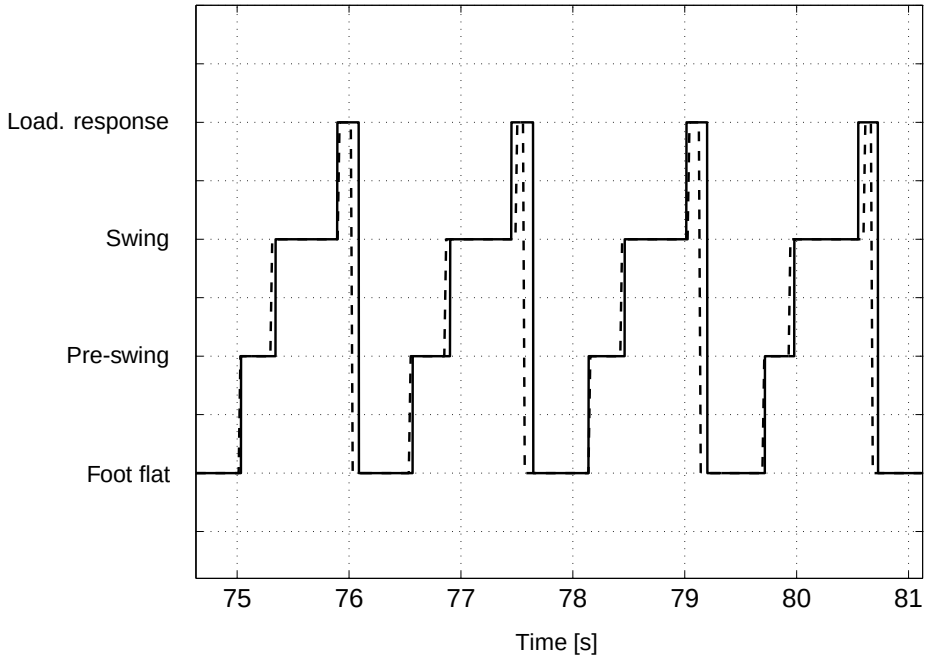

Figure 5.6.: Gait phases detected by the inertial sensor (solid line), and with the Parotec system (dashed line).

of late toe off detection and early foot flat detections are summarised for all patients. It can be observed, that especially for subjects S3 and S5 the loading response detection fails for many steps. The reason for this detection failure was that the peak in the jerk was not evident enough. The heel strike detection is influenced by the magnitude of the threshold. This threshold was tuned with the consideration in mind that if the threshold was to high the heel strike detection could be missed. On the other hand, a too low threshold would lead to a premature detection.

Table 5.4.: Number of steps and detection errors. The table summarises the total number of steps, number of steps with no detection of loading response, early heel strike, false detection of heel off, late toe off detection and early foot flat detection for all patients.

	S1		S2		S3		S4		S5	
	left	right	left	right	left	right	left	right	left	right
Total steps	187	187	127	127	57	57	146	146	141	141
No loading response	0	0	0	0	7	0	0	0	6	20
Early heel strike	0	0	0	0	0	0	0	0	0	2
False heel off	0	0	0	0	0	0	0	0	0	0
Late toe off	0	0	0	0	0	0	0	0	0	1
Early foot flat	0	0	0	0	0	0	0	0	1	0

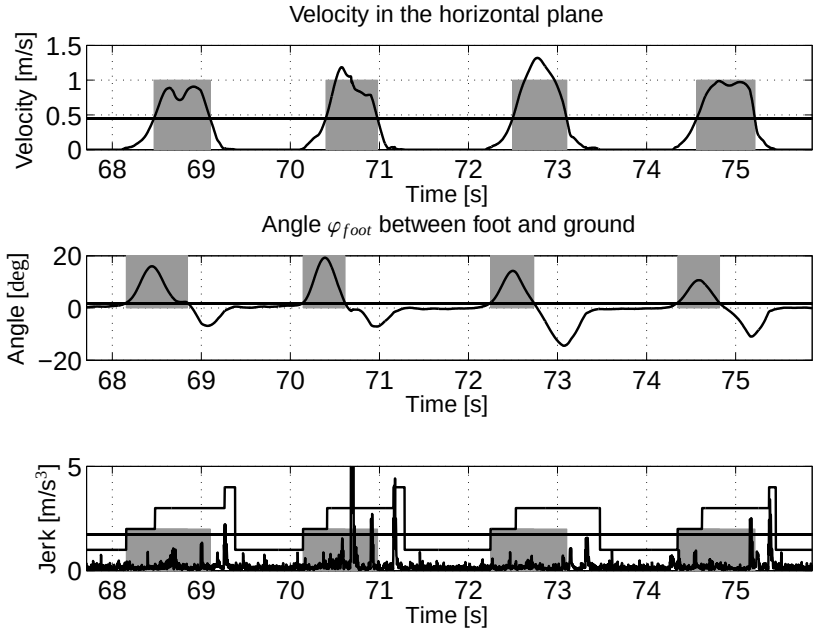

Figure 5.7.: Example of exclusion rules for gait phase detection: The upper graph shows the online estimated velocity in the horizontal plane (solid line) wherein the grey areas indicate that no transitions to loading response can happen. The middle graph shows the angle φ_{foot} between the foot and the ground in the sagittal level. The grey bars indicate the area in which the angle excludes a transition to loading response. The lower graph shows the absolute value of the jerk $\|\dot{a}^I_{foot}\|$, the threshold for detection of loading response as well as the detected gait phases that are equivalent to Figure 5.6. The grey bars in this graph are the union of the grey bars of the two upper graphs.

In Figure 5.7 four steps are shown for the right side of subject S5. In the third stride shown in the figure the loading response is not detected as the peak in the jerk did not exceed the threshold limit. The same

figure illustrates that the rules based on the angle between foot and ground as well as on the velocity do prevent a too early detection of heel strike. This is the case for the second and the forth step shown in the figure.

For subject S5 one instance of a transition from swing to foot flat is detected to early i.e. in the middle of the swing phase. As for the heel strike detection rules could have been implemented to prevent this early swing to foot flat detection. This is not done for the reason that if heel strike is not detected and if simultaneously the velocity calculation is drifting off and hindering the transition from swing to foot flat, no transition to foot flat would happen and the gait detection system would be locked in the swing phase.

For all the subjects there was no false detection of heel off observed. The heel off detection is highly dependent on threshold parameters. Especially the threshold parameter $\delta_{\varphi,T1}$ for the angle φ_{foot} is important in the heel off detection and a small increase of this parameter can lead to a relative large increase in the time of detection. It must be pointed out that this parameter and all other parameters have been kept constant for all experiments described in this chapter as well as those described in Chapter 6.

The detection of toe off appears to be quite robust; only for subject S5 toe off was detected late with GPD-IS comparted with the reference system. In order to make this transition more robust, the maximum in the angular velocity as well as in the angle were used in the rules to detect this transition. When using only one of these criteria this transition would not have been detected in more steps. Unfortunately, as the peak in angle and in angular velocity do not occur at the same moment, the usage of both criteria leads to a larger variation of the detection time for this event.

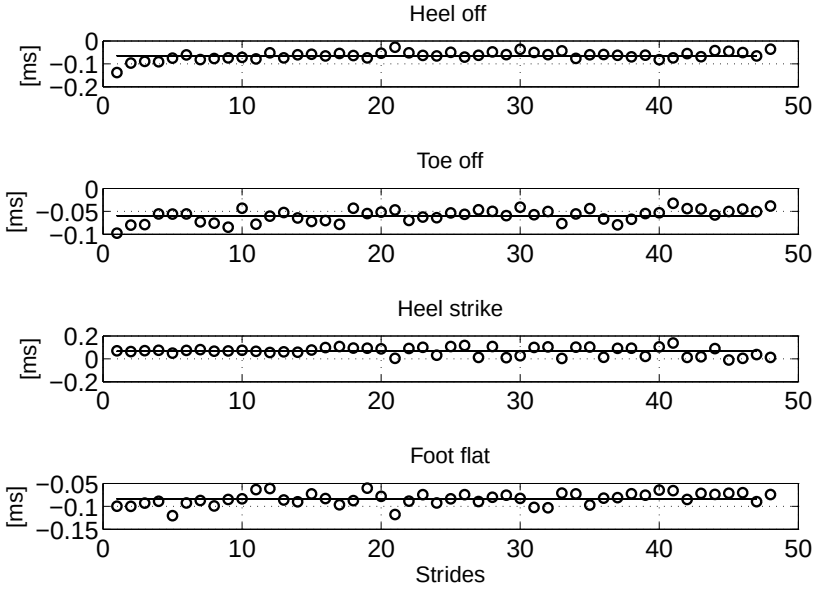

Figure 5.8.: The time differences for the event detection between GPD-IS and reference system are illustrated with circles. The solid lines show the mean differences. The data are taken from the left side of patient S4.

Table 5.5.: Time shift between the detected events of the GDP-IS and the reference system: The table shows the time differences between the events detected by the GPD-IS and the reference system. The number are given in milliseconds and as the percentage of the reference stride duration.

		Heel off	Toe off	Init. contact	Full contact
S1	left	-5.7 ±1.6% -97.4 ± 27.4 ms	-8.1 ± 2.7 % -140.8 ± 49.3 ms	4.4 ± 2.5% 76.8 ± 44.1 ms	-3.2 ± 2.5% -54.7 ± 43.8 ms
	right	-2.2 ±3.4% -39.3 ± 60.8 ms	-2.0 ± 1.6 % -33.8 ± 27.3 ms	10.1 ± 2.6% 173.7 ± 44.3 ms	6.3 ± 5.2% 116.3 ± 95.8 ms
S2	left	-0.7 ±1.3% -9.0 ± 18.7 ms	-3.5 ± 1.9 % -48.5 ± 29.6 ms	2.8 ± 1.3% 37.3 ± 18.8 ms	1.1 ± 3.0% 15.0 ± 40.0 ms
	right	-11.5 ±6.6% -152.0 ± 94.3 ms	-2.2 ± 0.8 % -29.6 ± 11.5 ms	1.1 ± 3.3% 14.3 ± 43.2 ms	-10.6 ± 3.1% -143.7 ± 45.4 ms
S3	left	-6.1 ±2.8% -133.5 ± 58.5 ms	-0.6 ± 0.7 % -12.7 ± 15.4 ms	9.9 ± 4.1% 217.1 ± 82.2 ms	7.3 ± 2.9% 163.2 ± 67.2 ms
	right	3.1 ±1.9% 69.2 ± 41.5 ms	-1.5 ± 1.4 % -32.9 ± 31.8 ms	2.1 ± 1.0% 46.6 ± 22.3 ms	-4.3 ± 1.9% -94.3 ± 40.5 ms
S4	left	-3.6 ±1.2% -55.4 ± 17.9 ms	-3.3 ± 1.1 % -51.2 ± 17.0 ms	4.5 ± 2.5% 70.2 ± 38.6 ms	-4.5 ± 1.6% -70.5 ± 24.2 ms
	right	-5.9 ±2.1% -91.9 ± 32.6 ms	-2.1 ± 2.4 % -32.6 ± 37.3 ms	6.8 ± 1.3% 106.9 ± 22.1 ms	-1.3 ± 1.9% -19.5 ± 29.8 ms
S5	left	-2.9 ±3.9% -61.7 ± 85.1 ms	-2.5 ± 1.9 % -53.9 ± 39.3 ms	8.6 ± 2.1% 184.3 ± 45.9 ms	10.2 ± 4.3% 223.4 ± 104.0 ms
	right	5.4 ±1.7% 117.6 ± 38.0 ms	-3.3 ± 1.5 % -71.3 ± 33.4 ms	0.7 ± 2.6% 14.5 ± 56.0 ms	-5.2 ± 2.8% -117.6 ± 60.2 ms

In Table 5.5, the mean value and the standard deviation of the time difference between the detected events from the GPD-IS and the reference system are summarised for all subjects. The difference are given as the percentage of the gait cycle as well as in milliseconds. In Figure 5.8 the time differences between the GPD-IS and the reference system are plotted as a function of the strides for all four events for the left side of patient S4.

The numbers in Table 5.5 demonstrate that the heel off event takes place later for the GPD-IS than for the reference system. This is the case for the majority of the patients. In average this event is detected 60 ms to late whereas 95 % of the detected heel off events (all patients) happend in the interval [-270 150] ms in relation to the reference system. In percentage of the duration of one complete step, the heel off detection on the right side of subject S2 follows the reference system as the worst case in average with a delay of 11.5 %.

From Table 5.5 it can be seen that the toe off event is detected later for the GPD-IS as for the reference system for all subjects. On average this event follows 62 ms too late and the 95 % confidence interval is [-167 43] ms. Although the inertial sensor based detection of toe off occurred later than the reference

system, the mean difference was relatively low for all subjects, and the largest deviation was found for the right side of subject S1 with a mean shift of 8.1 % with respect to the gait cycle.

The initial contact event was for all subjects detected earlier for the GPD-IS than for the reference system. The event takes on average place 91 ms before the reference system and 95 % of the events happend in the interval [-74 256] ms. The intersubject variation of the mean error was relatively large, for the right side of subject S5 the mean error was 0.7 %, whereas the mean error for subject S1 was 10.1 % on the right side as the worst case.

For the full contact event, intersubject variability of the detection was larger than for the initial contact and toe off events and similar to the heel off event detection.. The 95 % confidence interval for the time shift of the full contact event was [-260 250] ms, thus a large variation of this event is evident but on average the difference was only 6 ms.

The standard deviations of the timing error between the GPD-IS and the reference system for the different subjects were in the range from 1.3 % to 5.2 % in the worst case.

Table 5.6.: The duration of the estimated phases by the GPD-IS and from the reference system. The values are given as percentage of the duration of the complete stride.

		Pre-swing		Swing		Loading resp.		Foot flat	
		GPD-IS	Ref.	GPD-IS	Ref.	GPD-IS	Ref.	GPD-IS	Ref.
S1	left	16.8 %	14.3 %	24.7 %	37.4 %	10.0 %	2.4 %	48.5 %	45.9 %
	right	20.5 %	20.9 %	23.3 %	35.3 %	13.6 %	10.0 %	42.5 %	33.8 %
S2	left	26.1 %	23.2 %	33.4 %	39.7 %	14.1 %	12.6 %	26.3 %	24.5 %
	right	22.9 %	32.3 %	34.8 %	38.0 %	14.8 %	3.2 %	27.4 %	26.5 %
S3	left	22.9 %	28.0 %	26.5 %	38.3 %	9.2 %	5.0 %	41.3 %	28.8 %
	right	13.2 %	8.6 %	29.3 %	33.1 %	8.4 %	2.0 %	49.2 %	56.3 %
S4	left	17.6 %	17.7 %	36.2 %	44.0 %	12.2 %	3.1 %	34.0 %	35.2 %
	right	14.4 %	18.2 %	19.6 %	28.7 %	9.2 %	1.1 %	56.7 %	52.0 %
S5	left	13.8 %	14.1 %	31.1 %	42.2 %	8.4 %	10.5 %	46.7 %	33.2 %
	right	13.8 %	4.8 %	35.1 %	38.4 %	6.5 %	1.7 %	44.7 %	55.1 %

Table 5.7.: The duration of the stance and swing phases estimated by the GPD-IS and by the reference system. The values are given as percentage of the duration of the complete stride.

		Swing		Stance	
		GPD-IS	Ref.	GPD-IS	Ref.
S1	left	24.7 ± 2.8 %	37.4 ± 2.8 %	75.3 ± 2.8 %	62.6 ± 2.8 %
	right	23.3 ± 2.4 %	35.3 ± 3.8 %	76.7 ± 2.4 %	64.7 ± 3.8 %
S2	left	33.4 ± 2.0 %	39.7 ± 1.8 %	66.6 ± 2.0 %	60.3 ± 1.8 %
	right	34.8 ± 2.4 %	38.0 ± 3.2 %	65.2 ± 2.4 %	62.0 ± 3.2 %
S3	left	26.5 ± 6.2 %	38.3 ± 2.8 %	73.5 ± 6.2 %	61.7 ± 2.8 %
	right	29.3 ± 1.8 %	33.1 ± 2.5 %	70.7 ± 1.8 %	66.9 ± 2.5 %
S4	left	36.2 ± 1.5 %	44.0 ± 3.2 %	63.8 ± 1.5 %	56.0 ± 3.2 %
	right	19.6 ± 2.2 %	28.7 ± 1.9 %	80.4 ± 2.2 %	71.3 ± 1.9 %
S5	left	31.1 ± 3.7 %	42.2 ± 3.4 %	68.9 ± 3.7 %	57.8 ± 3.4 %
	right	35.1 ± 5.5 %	38.4 ± 2.7 %	64.9 ± 5.5 %	61.6 ± 2.7 %

After the transition times of the events have been found, also the duration of the phases can be calculated. This information is especially of interest in a gait monitoring system. More specific is the relationship between the duration of the phases on the hemiplegic side compared with the duration on the non affected side of interest. In Table 5.6, the normalised durations of all phases are summarised for the GPD-IS and for the reference detection system. In addition, the durations of swing and stance phases are summarised in Table 5.7. Here, the stance phase is the duration between heel strike and toe off which is equivalent with the sum of the durations of the loading response, foot flat and pre-swing phases.

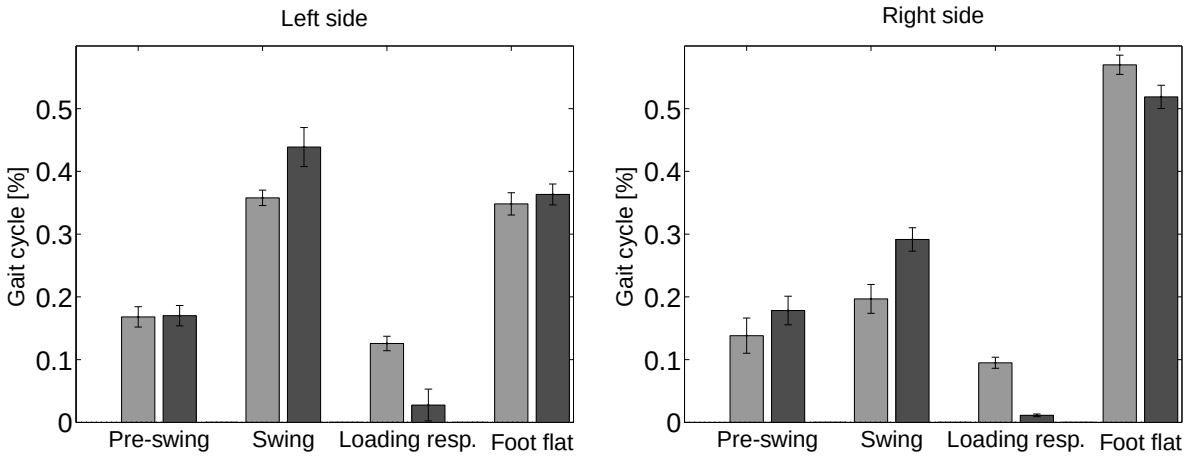

Figure 5.9.: The duration of the phases normalised for one gait cycle for subject S4. The light grey bars are from the GPD-IS and the dark bars are from the reference system.

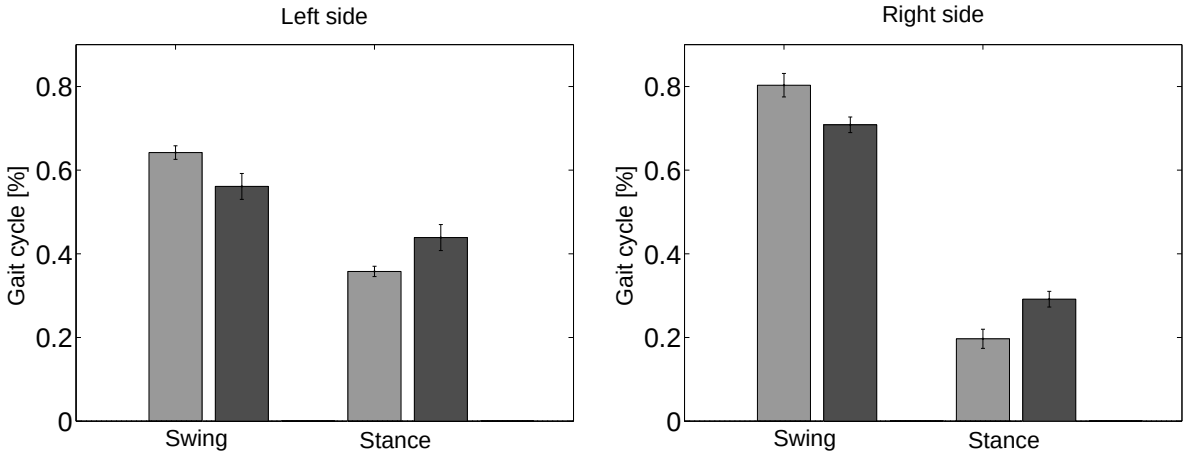

Figure 5.10.: The duration of swing and stance (loading response + foot flat + pre-swing) phases normalised on one gait cycle for subject S4. The light grey bars are from the GPD-IS and the dark bars are from the reference system.

In Figure 5.9 the duration of the gait phases is illustrated for subject S4, and in Figure 5.10 the duration of the swing and stance (loading response +foot flat + pre-swing) phase is illustrated. It can be observed that the duration of the stance phase is longer for the GPD-IS than for the reference measurement and consequently the opposite is the case for the swing phase. Moreover, the coherence for the pre-swing phase is good for all patients.

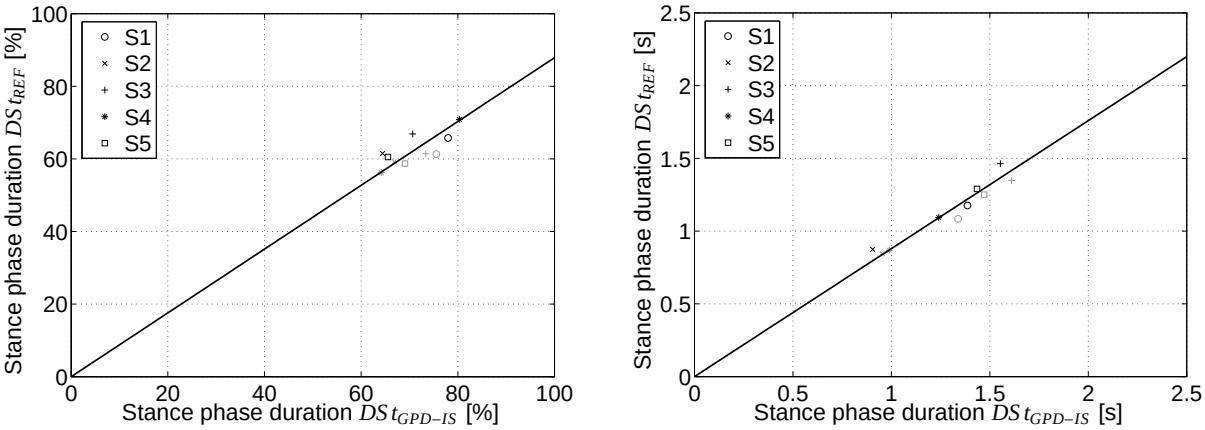

Figure 5.11.: Stance duration as percentage of the gait cycle: Left graph shows the stance duration as percentage of the gait cycle from GPD-IS compared with that obtained from the reference system. Right plot shows the stance duration from GPD-IS compared with that obtained from the reference system in seconds. Grey markers indicate the left side of the patient and black markers indicate the right side of the patient.

The duration of the stance phase DSt_{GPD-IS} measured with the GPD-IS was for all patients longer than the stance duration DSt_{REF} measured with the reference measurement system. An assumption was made that there is a linear relation between the estimated durations of stance and swing phase from GPD-IS and the durations measured with the reference system. A regression analysis was performed where a good coherence between the mean duration of the stance phase measured with the reference system and the one calculated from the GPD-IS was found. Figure 5.12 compares the actual stance duration DSt_{REF} with the measured stance duration DSt_{GPD-IS} for both the normalised and the real value. The linear relation was found to be:

$$DSt_{REF} = 0.87 \cdot DSt_{GPD-IS}. \tag{5.8}$$

The correlation factor was r=0.96 and the RMSE was 57 ms.

Table 5.8.: The symmetry indexes SI_{Stance} and SI_{Swing} calculated from the GPD-IS and from the reference system.

	SI_{stance}		SI_{Swing}	
	GPD-IS	Ref.	GPD-IS	Ref.
S1	-1.0	-1.8	3.0	3.0
S2	1.4	-1.3	-1.8	2.2
S3	1.8	-3.8	-4.7	7.5
S4	-11.5	-12.0	29.7	21.1
S5	2.4	-3.3	-5.8	4.9

From the duration of the phases an index of symmetry can be calculated by the following equation:

$$SI = \frac{X_{left} - X_{right}}{X_{left} + X_{right}} \cdot 100 \tag{5.9}$$

where X_{left} is the temporal variable, i.e the duration of the stance phase of swing phase. The index of symmetry lies in the range from -100% to 100% with perfect symmetry being equivalent to $SI = 0$. In Table 5.8 the symmetry indexes SI_{stance} and SI_{swing} are summarised for all subjects. Only for subject S4 a noticeable asymmetry can be observed and the indexes found by the GPD-IS were in accordance with the indexes found by the reference system. For the other patients only small values of symmetry indexes could be observed.

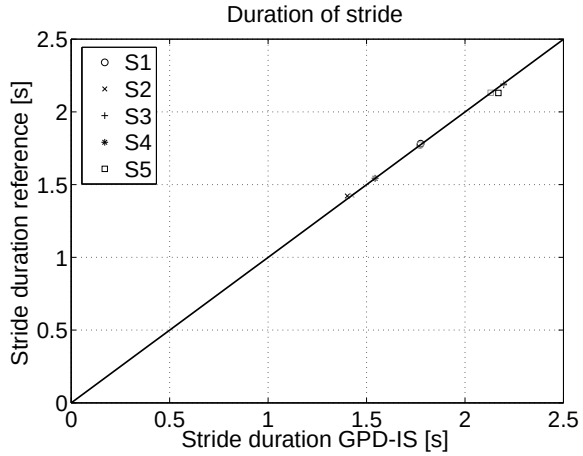

Figure 5.12.: Average stride durations: The figure illustrates the duration of a stride measured with the GPD-IS in relation with that measured with the reference system.

Table 5.9.: Duration of the stride and its standard deviation calculated from heel off in one step to the heel off in the next step measured with the GPD-IS and the reference measurement system.

	RGCT		LGCT	
	GPD-IS	Ref.	GPD-IS	Ref.
S1	1.72 ± 0.11 s	1.73 ± 0.13 s	1.72 ± 0.09 s	1.72 ± 0.09 s
S2	1.35 ± 0.11 s	1.35 ± 0.10 s	1.35 ± 0.12 s	1.36 ± 0.11 s
S3	2.21 ± 0.11 s	2.20 ± 0.12 s	2.21 ± 0.11 s	2.21 ± 0.11 s
S4	1.56 ± 0.04 s	1.56 ± 0.04 s	1.56 ± 0.03 s	1.56 ± 0.03 s
S5	2.18 ± 0.24 s	2.17 ± 0.12 s	2.17 ± 0.15 s	2.17 ± 0.15 s

In Table 5.9 Gait Cycle Time (GCT) (stride durations) from GPD-IS is compared with the gait cycle time obtained from the reference measurement. Also, Figure 5.12 illustrates the good coherence. The RMSE was 12 ms and the correlation coefficient was r=0.99.

5.7. Discussion and Conclusions

The main aim of this work was to develop an algorithm based on the inertial sensor for detection of gait phases in which no extra tuning of parameters has to be applied for individual patients. Several similar algorithms have been developed by other research groups based on accelerometers and gyroscopes. However, to the authors knowledge this system is the first one based on a complete inertial sensor unit (three accelerometers and three gyroscopes). It was shown for five hemiplegic subjects that the detection

system worked robustly and that all gait phases were detected and no critical error occurred that could have been critical if the stimulation had been triggered accordingly to the detected gait phases in an FES-assisted gait training system.

In the literature several gait phase detection systems have been described and compared with reference measurement systems. Due to different methods, measurements and subjects it is hard to compare our results with those. In [101] gait phase detection based on accelerometers by use of machine learning techniques was applied. The correlation with the gait phases based on force sensitive resistors were almost perfect, but these were also used as a training signal for the neural network and for this reason not very suprising.

The finding that toe off detection is biased compared with the insole detection is in accordance with the results of Sabatini et al. [75] who found a bias of 35 ms on average for two healthy subjects. On the contrary, Aminian et al. [2] found no significant difference. In contrast to this detection, offline methods were applied to detect toe off. This difference indicates that the online detection of toe off introduces a time delay. The fact that mean differences vary between 20 and 80 ms depending on the subject must be ascribed to differences in the individual walking patterns of the patients. Furthermore, no systematic correlation of the delay and the walking speed and the hemiplegic side could be seen.

The fact that the inertial sensor (accelerometer) can detect the heel strike event earlier than force sensors is not in concordance with Williamson and Andrews [101] who found no difference making similar comparisons. On the other side, [64] also found a mean delay of 90 ms of the heel strike event based on force sensor compared with a video analysing system. This is not directly comparable but this also indicates a real difference in the detection of heel strike.

Using a complete inertial sensor (3 gyroscopes and 3 accelerometers) for gait phase detection instead of a simplified sensor with for instance only two accelerometers and one gyroscope can be considered by many as not necessary. It must be pointed out that by using the complete inertial sensor several advantages emerged. As an example, in [100] it was demonstrated that using only one accelerometer lead to problems with a too early detection of heel strike for several patients. This has partially been overcome by the algorithm described here by using the knowledge of the rotation, velocity and position of the sensor. The question is whether the added sensors can be defended financially in a commercial product

In the literature many systems for detecting gait phases based on machine learning techniques have been proposed, implemented and successfully tested. The disadvantage of such systems is the time consuming procedure of individually fitting the algorithm to each patient. The overall detection robustness and accuracy might be better than that of a rule based detection systems for one specific patient when the neural network has been trained. But the time consuming procedure cannot be defended in a clinical setting where time is critical.

A gait event detection system is the key component for the automatic control for stimulation in an FES-assisted gait training system. Furthermore, a gait detection system is an important component in an online gait monitoring system, giving information about the symmetry, the relative relation between swing and foot flat, as well as cadence and variance of the gait.

6. Estimation of Movement Parameters

6.1. Summary

Aim: The work presented in this chapter describes methods for obtaining movement parameter estimates based on an inertial sensor. Movement parameters considered here describe the gait on a stride to stride basis. The movement parameters taken into account are the step length and foot clearance. Furthermore, it was a goal to verify the accuracy of the calculated movement parameters with an exact reference measurement system.

Methods: By means of the obtained orientation described in Chapter 4, the acceleration can be transformed into a global coordinate system. The transformed acceleration can be integrated two times in a global coordinate system in order to obtain the position of the sensor/foot. This integration is started at the heel off event and is continued until the full contact event. Based on the 3-dimensional trajectory of the foot, the movement parameters step length and foot clearance are computed. The accuracy of the calculation was improved by introducing start and stop constraints on the movement for the integration. For validation purposes, reference measurements using an optical motion analysis system were performed with five patients.

Results: In the comparison of the estimated movement parameters foot clearance and step length with the reference measurement system it could be shown that the mean errors for both of these values were below 4 % for all subjects walking at least 50 steps on a treadmill. The variance of the estimation error was also shown to be less than 4 % whereas the variance of the foot clearance error was in general higher than the variance of the step length error.

Conclusions: The results have shown that foot movements and gait phases can be reconstructed from an inertial sensor with an accuracy good enough to be used as feedback sensor in an FES-assisted gait rehabilitation system as well as in a gait monitoring system.

Contribution: The author developed the methods, and implemented the experimental software. Furthermore, the author planned and ran the experiments. Parts of this work are published in [56].

6.2. Motivation

Until now the timing of the stimulation in FES-assisted gait training has been synchronised with the gait phases by foot switches, whereas the stimulation intensity has been pre-programmed or changed online manually by the physiotherapist. As already shown in the previous chapter, the inertial sensor can similar to foot switches be applied to robustly detect gait phases. Furthermore, as described in this chapter, more quantitative gait parameters like step length and foot clearance can be estimated. The motivation to estimate these parameters is for gait performance monitoring as well as for online tuning of the stimulation intensity which later will be described in Chapter 7. The algorithms described here are not only expected to be relevant as feedback for automatic tuning but also to assess the quality of gait with quantitative parameters. These can be used to observe the progression of a patient during the rehabilitation. The advantages of the inertial sensors are obvious in contrast to a fully equipped opto-kinetic motion analysis system, which is very expensive and is very time consuming to utilise.

Within this chapter methods for obtaining important movement parameters are described. An accurate algorithm for estimating the movement parameters step length and foot clearance by taking start and stop conditions for the movement into account is explained in Section 6.3. Furthermore, in Section 6.4 another method for obtaining the movement parameters based on a reduced sensor with only two accelerometers and one gyroscope is described. After this, in Section 6.5 an experimental setup and a procedure for making reference measurements with an optical motion analysis system are described. The results from the comparison of the estimated movement parameters from the inertial sensor and from the reduced sensor with the reference measurement system are given in Section 6.6. Finally, a summary is given in Section 6.7.

6.3. Step Length and Foot Clearance

By use of the sensor orientation a three dimensional trajectory of the foot can be estimated through a double integration of the acceleration in a global reference system as shown in Figure 6.1. In Figure 6.2 the structure for calculation of the movement parameters is shown. The first requirement for obtaining a trajectory of the foot/sensor is to know the orientation of the sensor with regard to a global reference system. The Kalman filter to obtain the orientation is described in Chapter 4. The orientation is in this chapter described by the rotation matrix $\mathbf{R}$. Since an endless integration of the acceleration would consequently drift off, a new integration is performed for every step where the position and velocity are reset to zero at the beginning of each step. The integration is started at the beginning of the pre swing phase at the heel off event and is continued until the full contact event occurs as indicated in Figure 6.1. The start time and stop time of integration for the k^{th} step are indicated by $T_{start}(k)$ and $T_{stop}(k)$ respectively, and they were found by the algorithm described in Chapter 5. Due to not foreseeable errors in the integration, the calculated trajectory is error-prone. To increase the accuracy of the estimation, known constraints of

the movement are used to calculate an artificial bias γ for the acceleration measurement. By using the bias γ, the trajectory estimation can be improved.

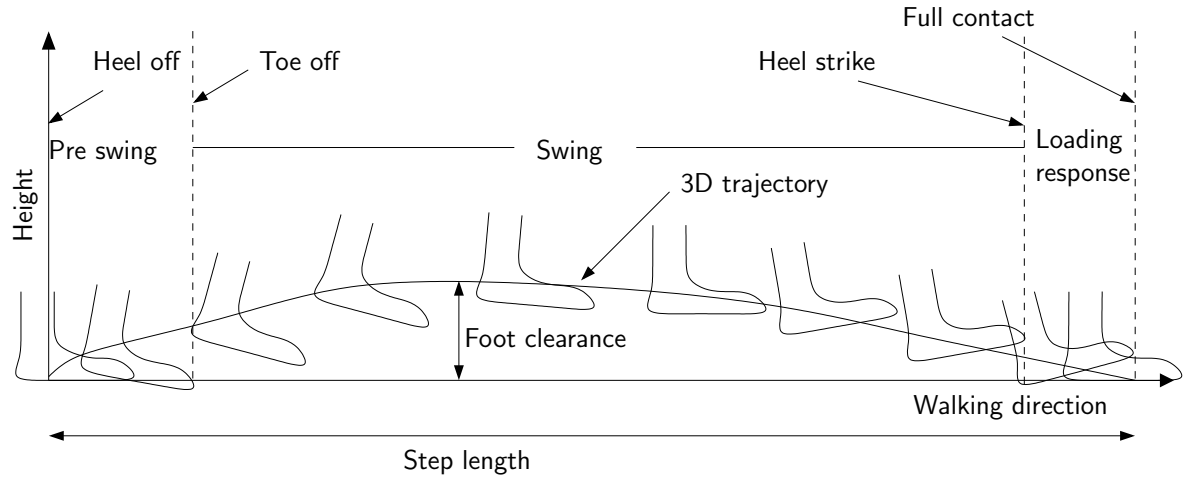

Figure 6.1.: To obtain a three dimensional trajectory of the foot a double integration of the acceleration is started at the heel off event and continued until the full contact event.

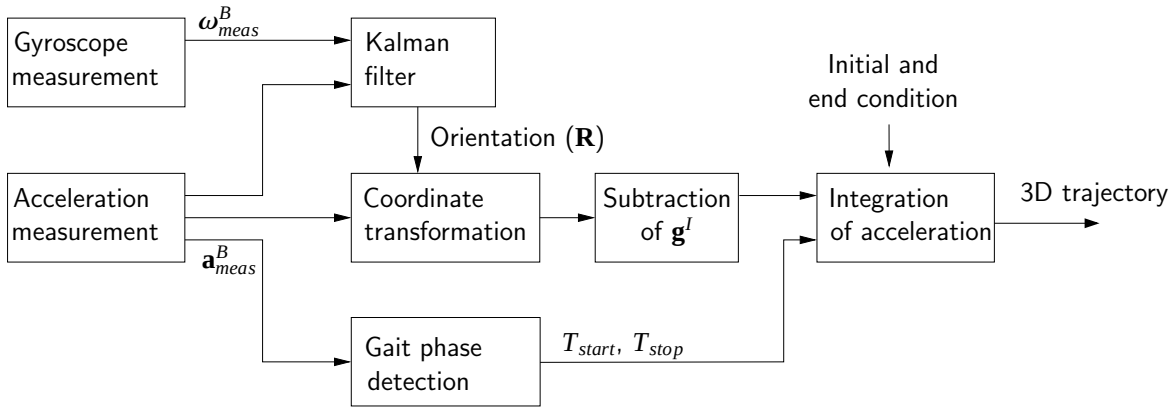

Figure 6.2.: Block diagram of the three dimensional trajectory calculation.

6.3.1. Constraints

In order to improve the accuracy, constraints for the integration have been introduced based on the pre-knowledge of the movement. In the foot flat phase the foot is almost at rest. The velocity of the sensor can then be assumed to be zero relative to the treadmill band before heel off and after the full contact events. These events also coincide with the start and stop of the integration respectively. Furthermore, by the assumption that the patients are walking on horizontal surface, the position in the vertical direction

is also zero at the beginning and at the end of the step. These constraints can be written as:

$$\mathbf{v}(T_{start}) = \mathbf{v}(T_{stop}) = 0 \tag{6.1}$$

$$s_z(T_{start}) = s_z(T_{stop}) = 0 \tag{6.2}$$

where $\mathbf{v}(T_{start})$ is the velocity at the start and $\mathbf{v}(T_{stop})$ is the velocity at end of the step respectively. $s_z(T_{start})$ and $s_z(T_{stop})$ are the vertical positions at the start and end of the step respectively. These constraints would normally not be fulfilled by an integration of the acceleration due to measurements errors, error in the orientation estimation, slowly varying biases and other unknown errors.

6.3.2. Algorithm

In order to fulfil the above given constraints an artificial bias on the acceleration measurement is introduced giving the following measurement equation

$$\mathbf{a}^B_{meas} = \mathbf{a}^B + \mathbf{g}^B + \gamma \tag{6.3}$$

where $\mathbf{a}^B_{meas}$ is the measured acceleration, $\mathbf{a}^B$ is the assumed true acceleration of the sensor, $\mathbf{g}^B$ is the gravity component and γ is the artificially introduced bias which will be calculated by using the constraints. The assumed true acceleration in the sensor coordinate system is transformed into the global coordinate system (as defined in Section 4.4.6) by use of the estimated orientation of the sensor represented by the rotation matrix $\mathbf{R}$:

$$\mathbf{a}^I = \mathbf{R}\mathbf{a}^B_{meas} - \mathbf{R}\gamma - \mathbf{g}^I. \tag{6.4}$$

The gravity component $\mathbf{g}^I = [0\ \ 0\ 9.81]^T$ m/s^2 can easily be subtracted as it is constant in the global coordinate system. The measured acceleration and angular velocity are sampled with the sampling time h. The discrete measurements take place at sampling instants $t = h \cdot i$ and are denoted by $\mathbf{a}^B_{meas}[i]$ and $\boldsymbol{\omega}^B_{meas}[i]$. Furthermore, the integration is replaced with a simple summation

$$\int_0^{t_1} f(t)dt \approx h \sum_{i=1}^{N} f[i] \tag{6.5}$$

where the time $t = h \cdot i$ corresponds to the discrete sample index i and where $N = t_1/h$. Equation (6.3) can be integrated to find the velocity $\hat{\mathbf{v}}[j]$. This is done by the summation

$$\hat{\mathbf{v}}[j] = h \sum_{i=1}^{j} (\mathbf{R}[i]\mathbf{a}^B_{meas}[i] - \mathbf{g}^I) - h \sum_{i=1}^{j} \mathbf{R}[i]\gamma. \tag{6.6}$$

where j is the discrete sample index defined between 1 and N. The index $j = 1$ corresponds to the continuous time instant T_{start} and $N = \frac{T_{stop} - T_{start}}{h}$ corresponds to the continuous time instant T_{stop}. Furthermore,

the position can be found by summation of the velocity

$$\hat{\mathbf{s}}[j] = h \sum_{i=1}^{j} \hat{\mathbf{v}}[i] = h^2 \sum_{i=1}^{j} \left(\sum_{l=1}^{i} (\mathbf{R}[l]\mathbf{a}_{meas}^{B}[l] - \mathbf{g}^{I}) - \sum_{l=1}^{i} \mathbf{R}[l]\gamma \right) \tag{6.7}$$

The velocity and position for which the artificial bias is not compensated ($\gamma = \mathbf{0}$) are denoted as $\mathbf{v}_b[j]$ and $\mathbf{s}_b[j]$ respectively

$$\mathbf{v_b}[j] = h \sum_{i=1}^{j} (\mathbf{R}[i]\mathbf{a}_{meas}^{B}[i] - \mathbf{g}^{I}) \tag{6.8}$$

$$\mathbf{s_b}[j] = h^2 \sum_{i=1}^{j} \left(\sum_{l=1}^{i} (\mathbf{R}[l]\mathbf{a}_{meas}^{B}[l] - \mathbf{g}^{I}) \right). \tag{6.9}$$

From Equations (6.1) and (6.2) there are four constraints, three due to the velocity and one due to the vertical position. The bias which consists of three elements cannot fulfil all constrains simultaneously. The bias estimate $\hat{\gamma}$ can be found by minimising sum of squared residuals

$$\hat{\gamma} = \min_{arg=\gamma} \left((\mathbf{v}[N] - \hat{\mathbf{v}}[N])^T (\mathbf{v}[N] - \hat{\mathbf{v}}[N]) + (s_z[N] - \hat{s}_z[N])^2 \right). \tag{6.10}$$

Using Equation (6.7), the following matrices are defined for $j = N$

$$\mathbf{K} = h^2 \sum_{i=1}^{N} \sum_{l=1}^{i} \mathbf{R}[l] \tag{6.11}$$

$$\mathbf{L} = h \sum_{i=1}^{N} \mathbf{R}[i] \tag{6.12}$$

where the matrix $\mathbf{K}$ can be subdivided in row vectors

$$\mathbf{K} = \begin{bmatrix} \mathbf{k_1} \\ \mathbf{k_2} \\ \mathbf{k_3} \end{bmatrix}. \tag{6.13}$$

Now the condition for the bias can be written as

$$\begin{bmatrix} \mathbf{v}_b[N] \\ s_{b,z}[N] \end{bmatrix} = \mathbf{B}\gamma \tag{6.14}$$

with

$$\mathbf{B} = \begin{bmatrix} \mathbf{L} \\ \mathbf{k_3} \end{bmatrix}. \tag{6.15}$$

The bias estimate is found by applying the standard least square method:

$$\hat{\gamma} = (\mathbf{B}^T\mathbf{B})^{-1}\mathbf{B}^T \begin{bmatrix} \mathbf{v}_b[N] \\ s_{b,z}[N] \end{bmatrix}. \tag{6.16}$$

After the bias estimate is calculated the acceleration can be summed up in order to obtain the velocity and position by Equations (6.6) and (6.7) where γ is replaced by its estimate. As the heading is not known as closer explained in Chapter 4, the step length is calculated from the position at the end of the step by

$$l_{step}\{\hat{\mathbf{s}}\} = \sqrt{\hat{s}_x[N]^2 + \hat{s}_y[N]^2}. \tag{6.17}$$

The foot clearance is defined as the maximum distance in the vertical direction:

$$fc\{\hat{\mathbf{s}}\} = \max(\hat{s}_z[j]), \quad j = 1...N. \tag{6.18}$$

6.4. Movement Parameter Estimation - Sensor Reduction

With the assumption that the movement retains in the sagittal plane the movement parameters can be estimated based on a reduced sensor. In this case only two accelerometers and one gyroscope are applied for the calculation of the movement parameters. In the article by Sabatini et al. [75] algorithms for estimating step length and foot clearance based on a simplified Inertial Motion Unit (IMU) consisting of one gyroscope and two accelerometers are described. In this section similar methods are used.

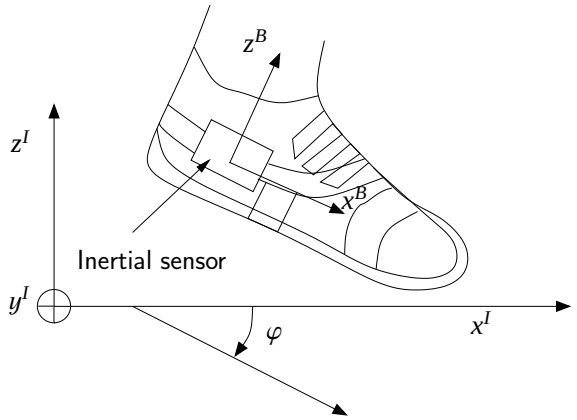

Figure 6.3.: Illustration of the sagittal angle of the foot φ. The angle between the sensor x^B axis and the global coordinate systems x^I and y^I axes is denoted by φ.

In this approach the global coordinate system is defined by the x^I and z^I axes whereas x^I is pointing in the treadmill walking direction and z^I is pointing in the direction opposite the gravity. Movements in the coronal and the frontal plane are ignored and the orientation of the foot is represented by the angle φ (cf.

Figure 6.3). The rotation of the foot can be expressed by the following rotation matrix:

$$\mathbf{R} = \begin{bmatrix} \cos(\varphi) & -\sin(\varphi) \\ \sin(\varphi) & \cos(\varphi) \end{bmatrix}. \tag{6.19}$$

The measured acceleration $\mathbf{a}^B_{meas} = [a^B_{meas,x}\, a^B_{meas,z}]^T$ in the sensor body frame can in similarity to the full sensor configuration be modelled as the sum of the true sensor acceleration $\mathbf{a}^B$, the gravity component $\mathbf{g}^B$ and an artificial bias γ

$$\mathbf{a}^B_{meas} = \mathbf{a}^B + \mathbf{g}^B + \gamma, \tag{6.20}$$

The measured acceleration can be transformed into the global coordinate system in order to obtain the sensor/foot acceleration

$$\mathbf{a}^I_{foot} = \mathbf{R}\mathbf{a}^B_{meas} - \mathbf{g}^I - \mathbf{R}\gamma, \tag{6.21}$$

where $\mathbf{g}^I = [0 \;\; 9.81]^T$. The measured angular velocity around the y^I-axis, $\omega^B_{y,meas}$, is used to estimate the rotation of the foot represented by the angle φ. Assumed that the foot is at rest during the foot flat phase, the accelerometers measure solely the gravity. This means that the initial orientation of the foot before a step can be estimated by calculation of the mean of the last M samples before the heel of event which starts the calculation of the 3D trajectory

$$\varphi_{init} = \frac{1}{M} \sum_{i=T_{start}/h-M}^{T_{start}/h} \tan^{-1}\left(\frac{a^B_{meas,x}[i]}{a^B_{meas,z}[i]}\right). \tag{6.22}$$

Here T_{start} is the start time for the summation of the 3D trajectory. The foot angle can be computed through a summation of the angular velocity from the start of a step till the end of the step

$$\varphi[j] = h \sum_{i=1}^{j} \omega^B_y[i] + \varphi_{init} \tag{6.23}$$

Here it is assumed that the start of the step T_{start} corresponds to the index $j = 1$. It is assumed that the angular velocity measurement is biased, that is

$$\omega^B_{meas,y} = \omega^B_y + \beta, \tag{6.24}$$

where ω^B_y is the real angular velocity, $\omega^B_{meas,y}$ is the measured angular velocity and β is the bias. By the assumption that the angle φ returns to its initial value at the end of a step the following constraint on the angle is defined

$$\varphi(T_{start}) \equiv \varphi(T_{stop}) \equiv \varphi_{init}. \tag{6.25}$$

By summation of Equation (6.23) from the start of a step ($i = 1$) till the stop of a step ($i = N$) with

$N = \frac{T_{stop}-T_{start}}{h}$ it follows that

$$\varphi[N] = h\sum_{i=1}^{N}\omega^{B}_{y,meas}[i] - h\sum_{i=1}^{N}\beta + \varphi_{init} = h\sum_{i=1}^{N}\omega^{B}_{y}[i] + \varphi_{init}. \tag{6.26}$$

From the start and stop condition it is given that

$$h\sum_{i=1}^{N}\omega^{B}_{y}[i] = 0. \tag{6.27}$$

Now, β can be directly computed from (6.26) under the assumption that it is constant during a step

$$\beta = \frac{1}{N}\sum_{i=1}^{N}\omega^{B}_{y.meas}[i]. \tag{6.28}$$

When β is determined, the estimated angle can be found by summation of Equation (6.23) from ($i = 1$) till ($i = N$).

Similar to the previous section, it is possible to use start and stop constraints to improve the accuracy of the velocity and position estimate:

$$\mathbf{v}(T_{start}) \equiv \mathbf{v}(T_{stop}) \equiv 0 \tag{6.29}$$

$$s_z(T_{start}) \equiv s_z(T_{stop}) \equiv 0. \tag{6.30}$$

The two dimensional velocity and position can be found by summation and double summation of the acceleration respectively:

$$\mathbf{v_b}[j] = h\sum_{i=1}^{j}(\mathbf{R}[i]\mathbf{a}^{B}_{meas}[i] - \mathbf{g}^{I}) \tag{6.31}$$

$$\mathbf{s_b}[j] = h^2\sum_{i=1}^{j}\left(\sum_{l=1}^{i}(\mathbf{R}[l]\mathbf{a}^{B}_{meas}[l] - \mathbf{g}^{I})\right). \tag{6.32}$$

The following matrices are defined:

$$\mathbf{K} \equiv h^2\sum_{i=1}^{N}\sum_{l=1}^{i}\mathbf{R}[l] \tag{6.33}$$

$$\mathbf{L} \equiv h\sum_{i=1}^{N}\mathbf{R}[i], \tag{6.34}$$

where the matrices **K** and **L** can be divided in row vectors

$$\mathbf{L} = \begin{bmatrix} \mathbf{l_1} \\ \mathbf{l_2} \end{bmatrix}, \quad \mathbf{K} = \begin{bmatrix} \mathbf{k_1} \\ \mathbf{k_2} \end{bmatrix} \tag{6.35}$$

Now the bias can be found by

$$\gamma = \begin{bmatrix} \mathbf{l_1} \\ \mathbf{k_2} \end{bmatrix}^{-1} \begin{bmatrix} v_{b,x}[N] \\ s_{b,z}[N] \end{bmatrix}, \tag{6.36}$$

where the condition, that the horizontal velocity at the start and end are zero and that the vertical position at the start and end is the zero, has been used. Here, the velocity in the z direction is not used in the constraints as for the full sensor. This could also have been solved similar as for the full sensor, by using the least squares method. The validation showed that the above implementation gave the best results.

In contrast to the full sensor, no Kalman filter is used to estimate the orientation of the sensor. The Kalman filter is also not active during the step for the full sensor. It is only implemented in order to estimate slowly varying biases. In this regard the two methods for estimating movement parameters for full and reduced sensors are comparable.

6.5. Validation of the Estimated Movement Parameters

Five patients with different gait pathologies were recruited for a clinical study. All patients were walking on a treadmill with parachute harness. Two inertial sensors were mounted with brackets on the left and the right foot. One marker of the LUKOtronic AS 202 motion analysis system was placed on the inertial sensor, as seen in Figure 6.6, such that the markers were visible from behind the patients. The patients were walking at their individual normal speed. In Table 6.1 the following subject information are listed: walking speed, gender and lesion/disability. The LUKOtronic measurement system consists of 2 marker

Table 6.1.: Subject data.

Subject	Male/female	Walking speed	Hemiplegic side
S1	F	1.51 [km/h]	left
S2	M	1.95 [km/h]	right
S3	M	1.46 [km/h]	left
S4	M	1.28 [km/h]	right
S5	M	1.40 [km/h]	right

chains, each having 5 markers. The markers were attached to the inertial sensor, the ankle joint, the knee joint, the hip joint and to the pelvis. In this chapter, only the marker attached to the inertial sensor was used in the analysis. The experiment started when the patients were standing at rest on the treadmill. The data acquisition from the inertial sensors and the LUKOtronic measurement system was performed from

two separate computers and the measurements were started separately but simultaneously in order to be able to synchronise the measurements later. During the experiments reported here the optical motion analysis system was sampled with a frequency of 100 Hz and the inertial sensor system was sampled at a frequency of 500 Hz.

Reference measurement

The LUKOtronic camera system was placed 2-4 meters behind the patients and the system was aligned with an inclinometer so that the LUKOtronic x^L axis was pointing in the patients walking direction. The z^L axis was pointing in the direction opposite to the gravity and the y^L axis was orthogonal to the other two axes forming a right handed coordinate system. By this arrangement the z^I axis of the global coordinate and the z^L axis of the LUKOtronic coordinate system coincide. The signals from the two measurement systems were synchronised by manually looking at the peaks of the position in the z direction.

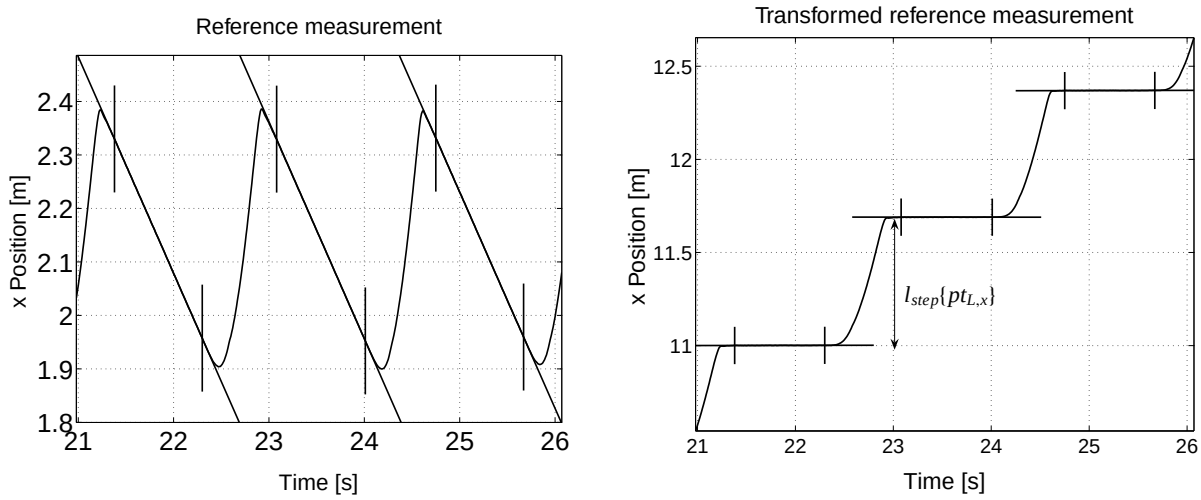

Figure 6.4.: Position measurement by the LUCOtronic motion analysis system. The left graph shows the x position measurement with the optical motion analysis system, the right graph shows the same position time transformed.

The exact speed of the treadmill v_{tm} was calculated from the x position of the reference measurement during the foot flat phase. This was done by using least squares method applied to the following equation

$$p_{L,x} = v_{tm} \cdot t. \tag{6.37}$$

$p_{L,x}$ is the measured x position in the all the foot flat phases. The reference x position was time transformed in order to be able to calculated the step length

$$pt_{L,x} = p_{L,x} + v_{tm} \cdot t \tag{6.38}$$

where $pt_{L,x}$ is the transformed x position of the marker, $p_{L,x}$ is the measured x position, v_{tm} is the treadmill velocity and t is the time.

In the left plot of Figure 6.4 the measured x position $p_{L,x}$ is shown. The vertical bars indicate the start and stop of a step. These are identical to the gait events heel off and full contact detected by the gait phase detection system based on the inertial sensor. The incline of the strait lines between the stop and start of the step indicate the treadmill speed. In the right plot in Figure 6.4 the x position $pt_{L,x}$ after the time transformation is shown. After the time transformation the incline of the line between stop and start is zero. The step length is calculated as the difference in the position at the start of the step and at the stop of the step from the time transformed position:

$$l_{step}^{REF} = pt_{L,x}(T_{stop}) - pt_{L,x}(T_{start}). \tag{6.39}$$

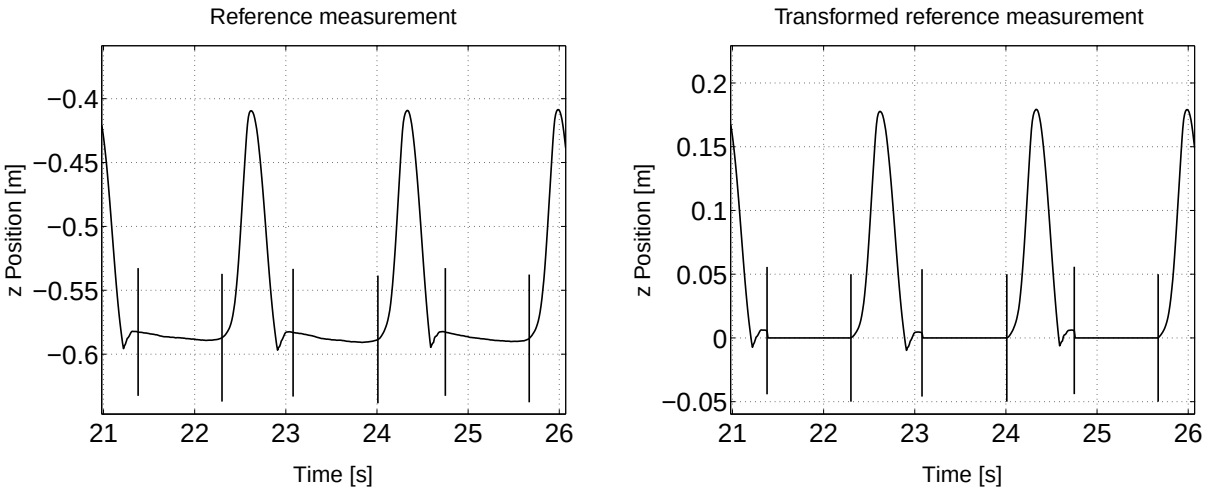

Figure 6.5.: Reference z position measurement.

An example of the reference position measurement in the z direction is shown to the left in Figure 6.5 where the start and stop of steps are indicated by vertical lines. The position at start is used to transform the position to the level of the inertial sensor.

$$pt_{L,z}(t) = p_{L,z}(t) - p_{L,z}(T_{start}). \tag{6.40}$$

The transformed position $pt_{L,z}$ is shown to the right in Figure 6.5 and the maximum value of the transformed signal is used to calculate the reference foot clearance:

$$f_c^{REF} = \max\{pt_{L,z}(t)\}, \quad t \in [T_{start} \;\; T_{stop}]. \tag{6.41}$$

Estimation of the marker position from the inertial sensor

As the motion analysis system marker was placed outside the housing of the inertial sensor, the measured position differs from the estimated position by the inertial sensor which is located inside the sensor housing. In order to compare the estimated position of the sensor with the reference motion analysis system the position of the marker was calculated from the estimated position of the sensor using the assumption that the marker was exactly placed on the sensor's x^B axis as indicated in Figure 6.6.

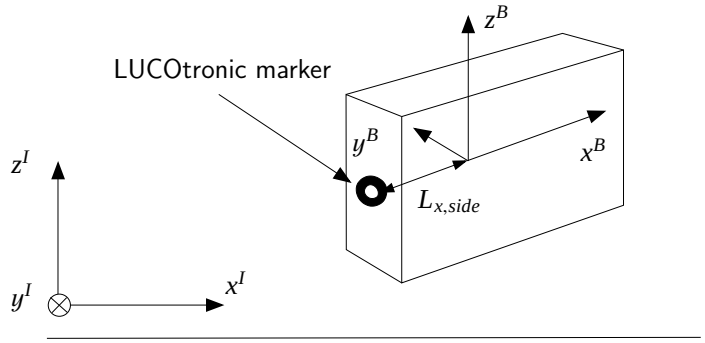

Figure 6.6.: LUKOtronic marker in relation to the inertial sensor. The marker is placed at a distance $L_{x,side}$ from centre of the sensor coordinate system.

The estimated position of the LUKOtronic marker by the full inertial sensor is calculated by the following relation

$$\mathbf{s_m} = \hat{\mathbf{s}} + \mathbf{R} \begin{bmatrix} L_{x,side} \\ 0 \\ 0 \end{bmatrix}, \tag{6.42}$$

where $\hat{\mathbf{s}}$ is the estimated position of the full inertial sensor, $\mathbf{s_m}$ is the estimated position of the marker, $\mathbf{R}$ is the rotation matrix representing the orientation of the full inertial sensor and $L_{x,side}$ is the distance between the centre of the sensor coordinate system and the marker. The lengths $L_{x,left}$ and $L_{x,right}$ were measured with a ruler and their values are given in Table 6.2. The lengths differ because the accelerometers and gyroscopes were not mounted exactly in the centre of the housing. For the reduced sensor, similar estimates for the marker position can be easily obtained.

Table 6.2.: The distance between the centre of the sensor coordinate system and the LUKOtronic marker.

$L_{x,right}$ [cm]	$L_{x,left}$ [cm]
2.5	4.1

6.6. Results

The mean error $\overline{E_{sl}^{INS}}$ between the measured step length and the estimated step length based on the inertial sensors is calculated as follows:

$$\overline{E_{sl}^{INS}} = \frac{1}{N_{steps}} \sum_{k=1}^{N_{step}} \left(l_{step}^{INS}[k] - l_{step}^{REF}[k] \right) \tag{6.43}$$

where N_{steps} is the number of steps. The standard deviation σ_{sl}^{INS} of the same error is computed as follows:

$$\sigma_{sl}^{INS} = \sqrt{\frac{1}{N_{steps}} \sum_{i=1}^{N_{steps}} \left(l_{step}^{INS}[k] - l_{step}^{REF}[k] - \overline{E_{sl}^{INS}} \right)^2} \tag{6.44}$$

The mean error E_{fc}^{INS} and the standard deviation σ_{fc}^{INS} of the error of the foot clearance are defined similar as for the step length.

Table 6.3.: The mean error of the step length $\overline{E_{sl}^{INS}}$ and the foot clearance $\overline{E_{fc}^{INS}}$ with respect to the reference system. The error is given in centimetre and in percentage of the total step length/foot clearance measured with the reference system.

Subject	Steps	Side	Move Par.	Mean V. [cm]	Mean V. Ref. [cm]	Mean Error [cm]	Std. Error [cm]
S1	50	right	l_{step}	54.61	54.70	-0.09 (-0.17 %)	0.48 (0.87 %)
			f_c	15.65	13.55	2.10 (15.48 %)	0.19 (1.23 %)
		left	l_{step}	53.61	54.43	-0.82 (-1.51 %)	0.96 (1.77 %)
			f_c	8.52	7.35	1.16 (15.82 %)	0.31 (4.17 %)
S2	111	right	l_{step}	78.26	77.61	0.65 (0.83 %)	0.46 (0.59 %)
			f_c	14.79	15.03	-0.24 (-1.60 %)	0.29 (1.94 %)
		left	l_{step}	77.77	77.58	0.19 (0.25 %)	0.74 (0.95 %)
			f_c	16.96	17.44	-0.48 (-2.73 %)	0.24 (1.35 %)
S3	100	right	l_{step}	65.29	67.83	-2.54 (-3.75 %)	1.79 (2.74 %)
			f_c	18.48	17.90	0.58 (3.22 %)	0.56 (3.04 %)
		left	l_{step}	67.88	67.72	0.15 (0.23 %)	0.98 (1.45 %)
			f_c	8.11	8.72	-0.61 (-7.00 %)	0.25 (2.92 %)
S4	65	right	l_{step}	72.72	73.64	-0.92 (-1.25 %)	0.65 (0.89 %)
			f_c	9.79	9.54	0.25 (2.67 %)	0.34 (3.50 %)
		left	l_{step}	72.99	73.31	-0.32 (-0.43 %)	0.55 (0.75 %)
			f_c	9.12	9.34	-0.21 (-2.30 %)	0.27 (2.89 %)
S5	54	right	l_{step}	77.05	76.87	0.18 (0.23 %)	1.14 (1.48 %)
			f_c	13.16	13.66	-0.50 (-3.68 %)	0.28 (2.10 %)
		left	l_{step}	78.43	76.78	1.65 (2.14 %)	3.19 (4.15 %)
			f_c	14.44	15.10	-0.67 (-4.40 %)	0.17 (1.14 %)

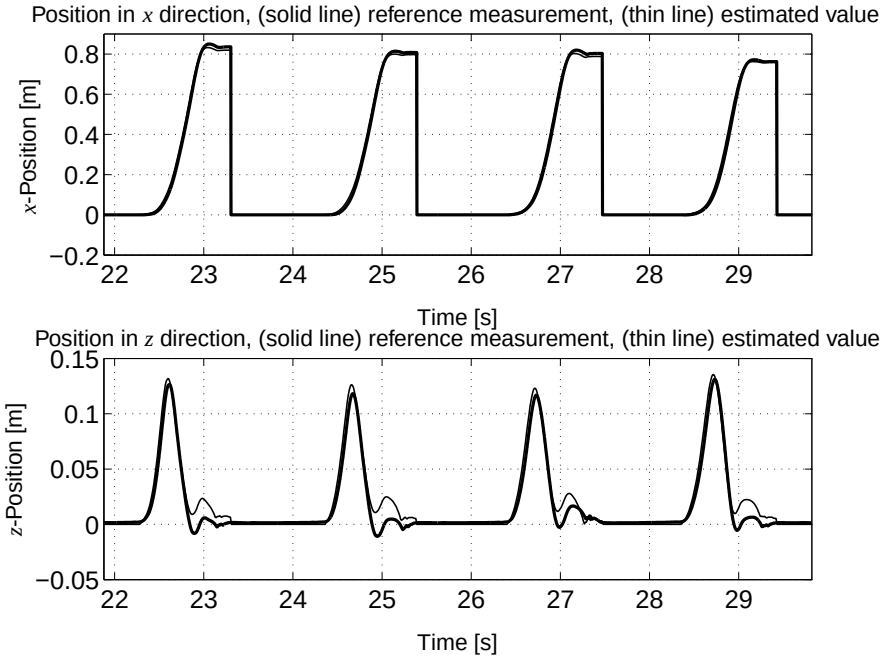

Figure 6.7.: The upper graph shows the estimated and measured position in the walking direction, the lower graph shows the estimated and measured position in vertical direction.

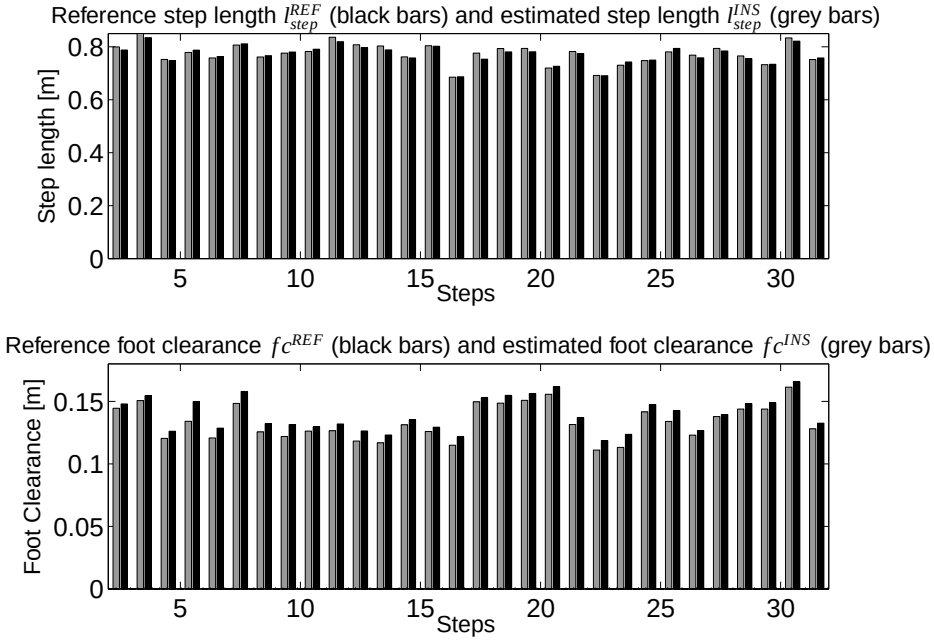

Figure 6.8.: Example of movement parameter estimation for the full inertial sensor with integration constraints taken into account compared to the reference system. The upper graph shows the estimated step length and the lower graph shows the estimated foot clearance.

In Table 6.3 the mean value of the movement parameters measured with the reference system and the mean value of the estimated movement parameters are summarised for five patients. Furthermore, the mean error $\overline{E_{fc}^{INS}}$ of the foot clearance estimate as well as the standard deviation σ_{fc}^{INS} of the error are listed. This table shows the results for the full inertial sensor whereas the bias in the acceleration measurement was estimated via integrations constraints. In Figure 6.7 an example of the estimated position trajectory is shown and in Figure 6.8 the estimated foot clearance and step length are illustrated as bar plots for the subject S4.

The comparison with the reference system shows that the step length can be estimated with a high accuracy when using the artificial bias in the calculation. For all subjects the mean error $\overline{E_{sl}^{INS}}$ was less than 4%. The mean errors of the foot clearance $\overline{E_{fc}^{INS}}$ were generally larger than that of the step length.

Table 6.4.: The mean error in step length $\overline{E_{sl}^{nobias}}$ and foot clearance $\overline{E_{fc}^{nobias}}$ and the standard deviation of the error for the full inertial sensor without the artificial bias calculation with respect to the reference system. The error is given in centimetre and in percentage of the total step length/foot clearance measured with the reference system.

Subjects	Step	Sides	Move Par.	Mean V. [cm]	Mean V. Ref. [cm]	Mean Error [cm]	Std. Error [cm]
S1	50	right	l_{step}	55.11	54.70	0.40 (0.74 %)	0.68 (1.24 %)
			f_c	13.50	13.55	-0.05 (-0.40 %)	0.18 (1.34 %)
		left	l_{step}	55.12	54.43	0.69 (1.27 %)	2.56 (4.70 %)
			f_c	8.17	7.35	0.81 (11.07 %)	0.40 (5.48 %)
S2	111	right	l_{step}	80.43	77.61	2.81 (3.62 %)	1.48 (1.84 %)
			f_c	11.84	15.03	-3.19 (-21.20 %)	0.56 (4.73 %)
		left	l_{step}	78.98	77.58	1.40 (1.81 %)	2.14 (2.76 %)
			f_c	16.01	17.44	-1.43 (-8.18 %)	0.63 (3.59 %)
S3	100	right	l_{step}	70.74	67.83	2.90 (4.28 %)	1.18 (1.67 %)
			f_c	14.78	17.90	-3.12 (-17.43 %)	0.27 (1.84 %)
		left	l_{step}	65.47	67.72	-2.26 (-3.33 %)	3.47 (5.13 %)
			f_c	7.84	8.72	-0.88 (-10.09 %)	0.25 (2.91 %)
S4	65	right	l_{step}	76.48	73.64	2.84 (3.85 %)	3.26 (4.26 %)
			f_c	7.99	9.54	-1.54 (-16.18 %)	0.53 (6.58 %)
		left	l_{step}	68.33	73.31	-4.98 (-6.79 %)	1.80 (2.46 %)
			f_c	9.22	9.34	-0.11 (-1.21 %)	0.22 (2.36 %)
S5	54	right	l_{step}	73.44	76.87	-3.42 (-4.45 %)	3.48 (4.74 %)
			f_c	10.62	13.66	-3.04 (-22.26 %)	0.39 (3.69 %)
		left	l_{step}	77.24	76.78	0.46 (0.60 %)	2.33 (3.03 %)
			f_c	14.14	15.10	-0.97 (-6.41 %)	0.27 (1.79 %)

In Table 6.4 the results from the calculation of the step length and foot clearance without the artificial

bias estimate are summarised. The mean value of movement parameters measured with the reference system and estimated from the inertial sensor are listed. Furthermore, for all patients the mean error of the foot clearance $\overline{E_{fc}^{nobias}}$ and the step length $\overline{E_{sl}^{nobias}}$ are summarised together with the standard deviation of the errors σ_{sl}^{nobias} and σ_{fc}^{nobias}.

Considering the accuracy of the estimated movement parameters omitting the start and stop constraints, the accuracy deteriorate. The intersubject variation of the mean error varies more when the artificial bias calculation is included.

Table 6.5.: The mean error in step length $\overline{E_{sl}^{red}}$ and foot clearance $\overline{E_{fc}^{red}}$ and the standard deviation of the error for the reduced sensor with respect to the reference system. The error is given in centimetre and in percentage of the total step length/foot clearance respectively measured with the reference system.

Subjects	Step	Sides	Move Par.	Mean V. [cm]	Mean V. Ref. [cm]	Mean Error [cm]	Std. Error [cm]
S1	50	right	l_{step}	52.10	54.73	-2.63 (-4.80 %)	0.90 (1.72 %)
			f_c	15.86	13.55	2.31 (17.04 %)	0.29 (1.85 %)
		left	l_{step}	50.65	54.52	-3.87 (-7.09 %)	0.82 (1.51 %)
			f_c	7.90	7.37	0.53 (7.15 %)	0.31 (4.24 %)
S2	111	right	l_{step}	74.55	77.61	-3.07 (-3.95 %)	1.10 (1.48 %)
			f_c	14.69	15.03	-0.34 (-2.27 %)	0.40 (2.73 %)
		left	l_{step}	73.76	77.58	-3.82 (-4.92 %)	1.08 (1.40 %)
			f_c	16.74	17.44	-0.70 (-4.04 %)	0.47 (2.71 %)
S3	100	right	l_{step}	59.59	67.82	-8.23 (-12.13 %)	1.50 (2.52 %)
			f_c	16.21	17.89	-1.69 (-9.43 %)	0.52 (3.23 %)
		left	l_{step}	59.55	67.72	-8.17 (-12.06 %)	1.37 (2.03 %)
			f_c	8.35	8.75	-0.40 (-4.59 %)	0.21 (2.39 %)
S4	65	right	l_{step}	67.22	73.69	-6.46 (-8.77 %)	2.46 (3.67 %)
			f_c	8.95	9.54	-0.59 (-6.20 %)	0.90 (10.09 %)
		left	l_{step}	66.73	73.34	-6.61 (-9.01 %)	1.42 (1.93 %)
			f_c	9.00	9.35	-0.34 (-3.67 %)	0.22 (2.33 %)
S5	54	right	l_{step}	65.55	76.78	-11.23 (-14.63 %)	2.61 (3.98 %)
			f_c	12.94	13.66	-0.72 (-5.24 %)	0.51 (3.92 %)
		left	l_{step}	66.97	76.67	-9.69 (-12.64 %)	3.63 (4.73 %)
			f_c	12.71	15.08	-2.38 (-15.76 %)	0.61 (4.06 %)

Furthermore, in Table 6.5 the mean error of the estimated step length $\overline{E_{sl}^{red}}$ and foot clearance $\overline{E_{fc}^{red}}$ as well as the corresponding standard deviations σ_{sl}^{red} and σ_{fc}^{red} of the error are summarised for the reduced sensor. In the calculation, the movement constraints were taken into account.

The data summarised in the Tables 6.3, 6.4 and 6.5 were obtained from a series of consecutive strides.

The recording started when the patients stood still on the treadmill. After the recording was started, the treadmill was accelerated up to a constant speed. As the transformation of the reference measurement was done under the assumption of a constant treadmill speed, the movement parameters were not correctly measured during the acceleration period. As a consequence, the data from the 3 first steps were excluded from the calculation of the mean error and standard deviation of the error.

Table 6.6.: The mean error and its standard deviation of the foot clearance and step length calculated for all patients.

	l_{step}^{INS}	l_{step}^{nobias}	l_{step}^{red}	f_c^{INS}	f_c^{nobias}	f_c^{red}
Mean error	0.02 [cm]	-0.34 [cm]	5.80 [cm]	0.02 [cm]	1.59 [cm]	0.50 [cm]
St. deviation	2.10 [%]	4.81 [%]	4.55 [%]	6.23 [%]	10.22 [%]	8.81 [%]

In Table 6.6 for all steps over all subjects and steps the mean error and its standard deviation are summarised for all three methods and movement parameters. The estimate based on full inertial sensor is performing at best when taking movement constraints into account. There is basically no bias in the estimate of the movement parameters.

As seen from the previous results, the calculation of the step length with the reduced sensor model yields biased estimates. To investigate the correlation between the measured reference movement parameter and the estimated movement parameters, a regression analysis was performed where the coherence between the mean value of the reference system and the one calculated from the inertial sensor system was found for all three methods. The linear relationship can be expressed as:

$$\overline{l_{step}^{REF}} = a \cdot \overline{l_{step}^{INS}} \tag{6.45}$$

In Table 6.7 the linear factor a, the coefficient of correlation r and the root mean square error are summarised. In the left graph of Figure 6.9 the calculated mean step length $\overline{l_{step}^{INS}}$ is plotted against the measured mean reference step length $\overline{l_{step}^{REF}}$. In the right graph the mean foot clearance $\overline{f_c^{INS}}$ is plotted against the mean reference foot clearance $\overline{f_c^{REF}}$. Furthermore, the same plots for foot clearance and step length calculated without the artificial bias and with the reduced sensor are given in the Figures 6.10 and 6.11.

Table 6.7.: Summary of the linear regression analysis for the movement parameters.

	$\overline{l_{step}^{INS}}$	$\overline{l_{step}^{nobias}}$	$\overline{l_{step}^{red}}$	$\overline{f_c^{INS}}$	$\overline{f_c^{nobias}}$	$\overline{f_c^{red}}$
a	1.00	1.00	1.10	0.99	1.12	1.03
r	0.99	0.95	0.94	0.97	0.94	0.94
RMSE	1.00 [cm]	2.62 [cm]	2.85 [cm]	0.86 [cm]	1.26 [cm]	1.18 [cm]

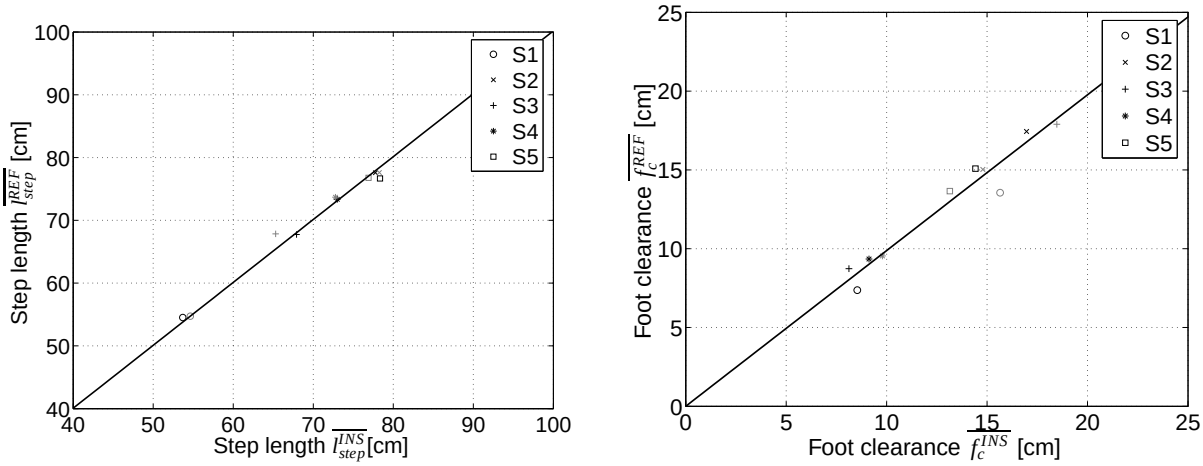

Figure 6.9.: Regression analysis for the full inertial sensor taking movement constraints into account. The left graph shows the correspondence between the reference step length $\overline{l_{step}^{REF}}$ and the calculated step length calculation $\overline{l_{step}^{INS}}$. The right graph shows the correspondence between the reference foot clearance $\overline{f_c^{REF}}$ and the calculated foot clearance $\overline{f_c^{INS}}$. The black markings indicate left side and the grey markings indicate right side.

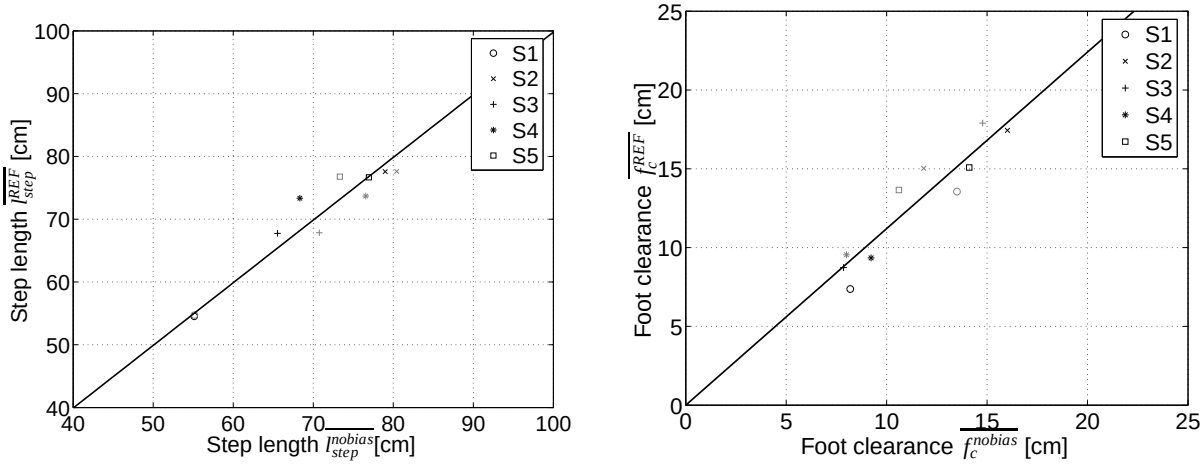

Figure 6.10.: Regression analysis for the full inertial sensor not taking movement constraints into account. The left graph shows the correspondence between the reference step length $\overline{l_{step}^{REF}}$ and the calculated step length calculation $\overline{l_{step}^{nobias}}$. The right graph shows the correspondence between the reference foot clearance $\overline{f_c^{REF}}$ and the calculated foot clearance $\overline{f_c^{nobias}}$. The black markings indicate left side and the grey markings indicate right side.

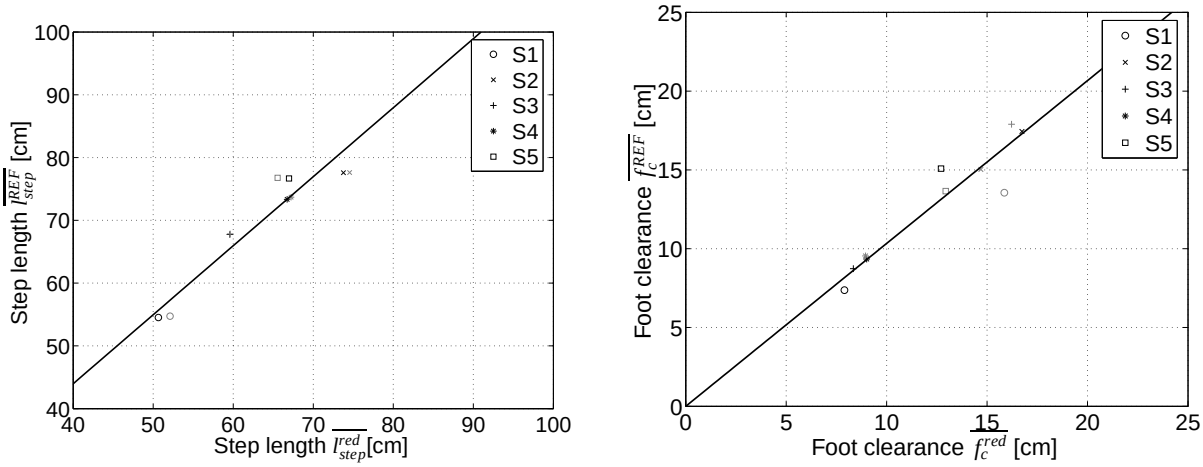

Figure 6.11.: Regression analysis for the reduced inertial sensor taking movement constraints into account. The left graph shows the correspondence between the reference step length $\overline{l_{step}^{REF}}$ and the calculated step length calculation $\overline{l_{step}^{red}}$. The right graph shows the correspondence between the reference foot clearance $\overline{f_c^{REF}}$ and the calculated foot clearance $\overline{f_c^{red}}$. The black markings indicate left side and the grey markings indicate right side.

6.7. Discussion and Conclusions

The feasibility of using an inertial sensor to calculate step length and foot clearance was demonstrated for five subjects with different gait pathologies. All subjects participated in the FES -assisted gait training described in the next chapter. In the calculation of the foot position, there are several sources of errors. It was demonstrated that the use of initial and end conditions of the movement could considerably improve the accuracy of the movement parameter estimates.

The sources of error in the movement parameter calculation are many. An error in the orientation estimation will of course lead to an error in the acceleration by its transformation into the global coordinate system. Furthermore, the foot is in reality never completely at rest during the foot flat phase as the foot is always continuing rolling forward. In addition, as the weight is shifted from one side to the other the shoes are slightly deformed. In Figure 6.5 it can be observed that the inertial sensor is moving as much as 0.5 cm in the vertical direction during the foot flat phase. Due to this movement, the exact moment for the start of integration is impossible to find and the reference movement parameter would also be more sensitive to the start point of integration. As a consequence of this the position estimate in the vertical direction is associated with more error than the position estimate in the horizontal direction.

The correlation analyses showed that the mean value of the movement parameter for the reduced model was lower than the reference value. This can be explained by the fact that the movement is not entirely

in the sagittal plane. Usually the foot is also rotated around the vertical axis. This implies that the acceleration in the sagittal plane in reality is larger than measured with the reduced inertial sensor.

It was shown that a full inertial sensor is superior to a reduced sensor. Furthermore, the known movement constraints can be employed to estimate biases in the acceleration measurement. Taking these biases into account during the double integration of the acceleration significantly improves the accuracy of the position estimate of the inertial sensor.

In conclusion, the current study indicates that foot movements and gait phases can be reconstructed from an inertial sensor with an accuracy good enough to be used as feedback sensor in FES-aided gait rehabilitation system as well as in an analysis tool.

7. FES-Assisted Gait Training by means of Inertial Sensors

7.1. Summary

Aim: The first aim was to develop an experimental laboratory system for FES-assisted gait training based on the gait phases detection algorithm described in Chapter 5. The second goal was to investigate methods for automatic feedback control of certain muscle groups in FES-assisted gait training. Moreover, an aim was to verify the feedback control methods in simulation as well as experimentally.

Methods: A test bed for FES-assisted gait training was developed. The system consists of an inertial sensor system, a standard laptop and an 8 channel stimulator unit. The gait phase detection system described in Chapter 5 was implemented and runs on-line on a laptop using the Linux operating system. The detection of gait phases forms a basis for the stimulation pattern generator i.e. the synchronisation of the stimulation with the gait cycle. Through a MATLAB/SIMULINK interface, a simple adjustment of the stimulation parameters can be performed. In addition, a control strategy for automatic tuning of the stimulation intensity on a stride to stride basis was developed. The feedback control strategy depends upon derived information from the inertial sensor i.e. the maximum sagittal angle before heel strike or the maximum height during the swing phase (foot clearance). A mathematical model was developed in order to validate the proposed controller structure in simulations. The proposed FES-assisted gait training system based on inertial sensors was tested on 12 hemiplegic subjects and the feedback control strategy was validated with one patient.

Results: The stimulation scheme worked robustly for all the possible variation of stimulation channels and stimulation patterns tested on the 12 patients. For two patients who were walking at a low speed, the heel off event were detected too early as a result of fidgety foot during the foot flat phase. This was the only critical problem that occurred. For all the patients the maximum number of stimulation channels used were two. Furthermore, in simulation it was shown that the stimulation of tibialis anterior could influence the maximum sagittal angle of the foot before hitting the floor. The maximum angle was controlled by adjusting the stimulation intensity on a step to step basis. In simulations it was also shown that the stimulation of the hamstrings could influence the maximum foot height during the swing phase

such that it could be controlled on a stride to stride basis. In experiments with one hemiplegic subject, the feasibility of controlling the maximum sagittal angle was demonstrated.

Conclusions: The proposed scheme has also the potential to be applied in a non-clinical setting for patients permanently using foot drop stimulators. It can be concluded that the inertial sensor can be successfully applied as single sensor in an FES-assisted gait training system.

Contribution: The author developed the methods and implemented the experimental software. Furthermore, the author planned and ran the experiments. Parts of this work are published in [58] and in [59].

7.2. Motivation

Upper motor neurone lesion (UMNL) can result from stroke, spinal cord injury, multiple sclerosis, cerebral palsy or head injury. Each patient suffering from stroke has his/her own unique mixture of deficits. Typically, the muscles responsible for extention of the leg, the calf and quadriceps are spastic and the muscles responsible for flexion, the anterior tibialis and hamstrings are weak and in some cases inactive. An important feature of UMNL is that the peripheral nerves are still intact, making it possible to activate the muscles through the use of functional electrical stimulation. For patients with gait deficits FES can be applied to support and enhance the gait.

Liberson et al. [43] was the first, who used electrical stimulation to elicit the withdrawal reflex during the swing phase of the gait in order to initiate the gait and to prevent foot drop. Since then many systems have been commercialised. Most of these systems are using foot switches attached to the heel and/or to the metatarsal head to trigger the stimulation when no force is applied on the sensors. In this chapter we will investigate the possible use of an inertial sensor for control in FES-assisted gait rehabilitation of stroke patients.

In the previous two chapters it was shown how an inertial sensor was applied to obtain gait phases as well as temporal and spatial parameters of the gait. The motivation for obtaining these values is for one reason to directly apply them in the rehabilitation of stroke patients by FES-assisted gait. The gait phases can directly be used to synchronise the stimulation with the walking cadence. More interesting is the exploitation of the additional information the inertial sensor delivers compared to other sensors such as the trajectory of the foot during the swing phase and the from it derived values as foot clearance, step length and maximum sagittal angle during the swing phase. The ultimate goal would be an FES-assisted gait training system which automatically finds the optimal stimulation sequence and for which the stimulation intensity is adapted in such a way that the patients are walking as if they were healthy. On the way there, small steps have to be taken to investigate the feasibility of such system. It was shown in the last chapter, that the gait detection system could successfully applied to detect gait phases for different

patients without the need to tune parameters. Veltink et al. [96] introduced the idea to control the gait on the basis of movement parameters on the level of walking cycle, e.g. the desired dorsiflexion angle before foot landing and foot clearance during mid-swing. The authors proposed a strategy for controlling the sagittal foot orientation just before landing, and proved the concept in simulation. For each new step, stimulation intensity parameters were determined in advance from the measured movement parameters using an inverse model of the relationship between stimulation and movement parameters. In this chapter a similar principle is applied, and a control strategy for the control of the maximum sagittal angle of the foot and the foot clearance is proposed.

In Section 7.3 the laboratory setup is presented and in Section 7.4 the pattern generator is explained. Furthermore, in Section 7.5 an initial clinical study using the FES-assisted gait training system is described. In Section 7.6 a strategy for automatic tuning of the stimulation intensity is proposed. A mathematical model for the free-swinging leg is developed in Section 7.7 and the control concept is demonstrated in simulations in Section 7.8. In Section 7.9 the feasibility of the control concept is experimentally verified on one stroke patient. Finally, a summary is given in Section 7.10.

7.3. Experimental Set-up

A prototype FES-assisted gait training system for treadmill walking has been developed. An inertial sensor system is used as sensory input, namely the RehaWatch system consisting of two miniature Inertial Measurement Units (IMU) and a Digital Signal Processing (DSP) unit which is described closer in Chapter 3. The main computing unit of the laboratory setup is a standard laptop with the Linux operating system. The signals from the inertial sensor system are read into the laptop through an USB interface with a frequency of 500 Hz. The stimulator RehaStim is connected through an USB-interface and is controlled by a special protocol called ScienceMode (see Chapter 3 for a detailed explanation). A galvanic isolation is provided by the stimulator. The stimulator is activated through the external Multi Channel List Mode. This means that the main stimulation frequency is controlled by the PC software. The main frequency of the PC program is 60 Hz, whereas the output stimulation frequency can be chosen to be 20 Hz, 30 Hz or 60 Hz depending if pulse is sent every sampling instance, every second or every third. An illustration of the system is given in Figure 7.1.

For straightforward testing of new stimulation strategies a MATLAB/SIMULINK user interface was developed where new stimulation patterns can be easily realised. The algorithms described in the following sections have been implemented in C++.

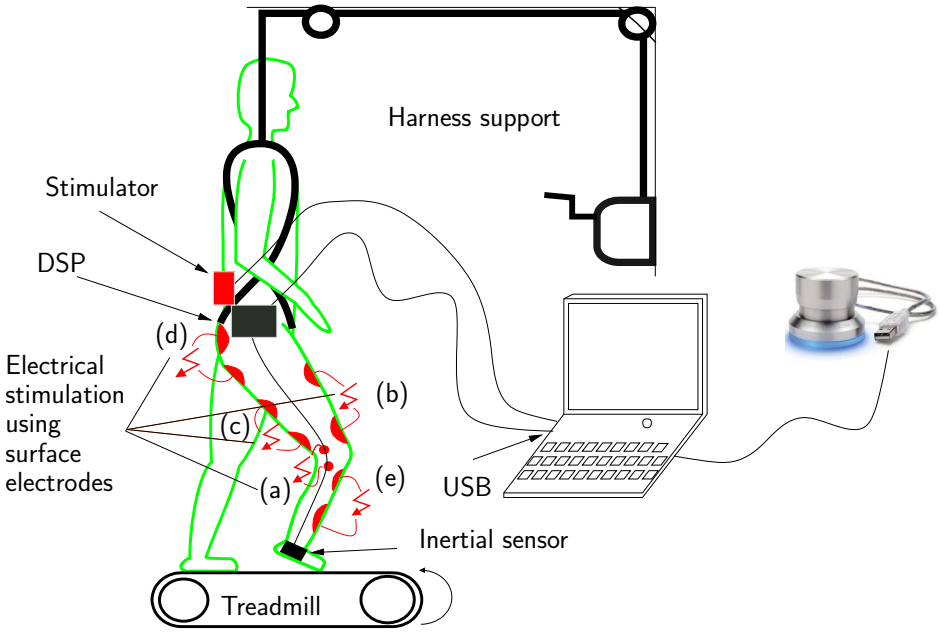

Figure 7.1.: The muscles and nerves stimulated in FES-assisted gait training: (a) peroneal nerve, (b) quadriceps, (c) hamstrings, (d) gluteus maximus and (e) tibialis anterior.

7.4. Stimulation Pattern Generator

An overview of the laboratory data processing software is depicted in Figure 7.2. The gait phase detection runs with the same frequency as the data are read in (typically 500 Hz). All the calculated data such as the orientation and the gait phases for each time instant are buffered. As soon as one complete step is detected i.e. at the full contact event, the algorithm described in Chapter 6 for obtaining the movement parameters is performed. In addition, temporal parameters like the durations of the different phases are determined. The mean value of the durations are calculated over the last three steps.

The main pattern generator is running at a frequency of 60 Hz. This frequency is generated by the real time clock of the PC. The temporal and spatial information as well as the current gait phase from the gait phase detector are re-sampled to 60 Hz and used as inputs to the pattern generator. The stimulation pattern, e.g. start and stop times for the stimulation, is related to one of the gait events and to the cadence. As a finer division of the stimulation timing is advantageous, the stance and swing phases have been divided into four parts and the pre-swing phase is divided into two parts. By this division, the gait cycle is divided into 11 parts. Since the cadence was online estimated, the start and stop times of the stimulation could be set to one of these division. The pulse width is ramped up during three pulses to a decided pulse width value and likewise ramped down in three pulses after the stop time is reached. The decided stimulation intensity i.e. the pulse width can either be manually controlled via a potentiometer[1]

[1]http://www.griffintechnology.com/products/powermate/

or as later explained in Section 7.6 by a step to step discrete-time controller.

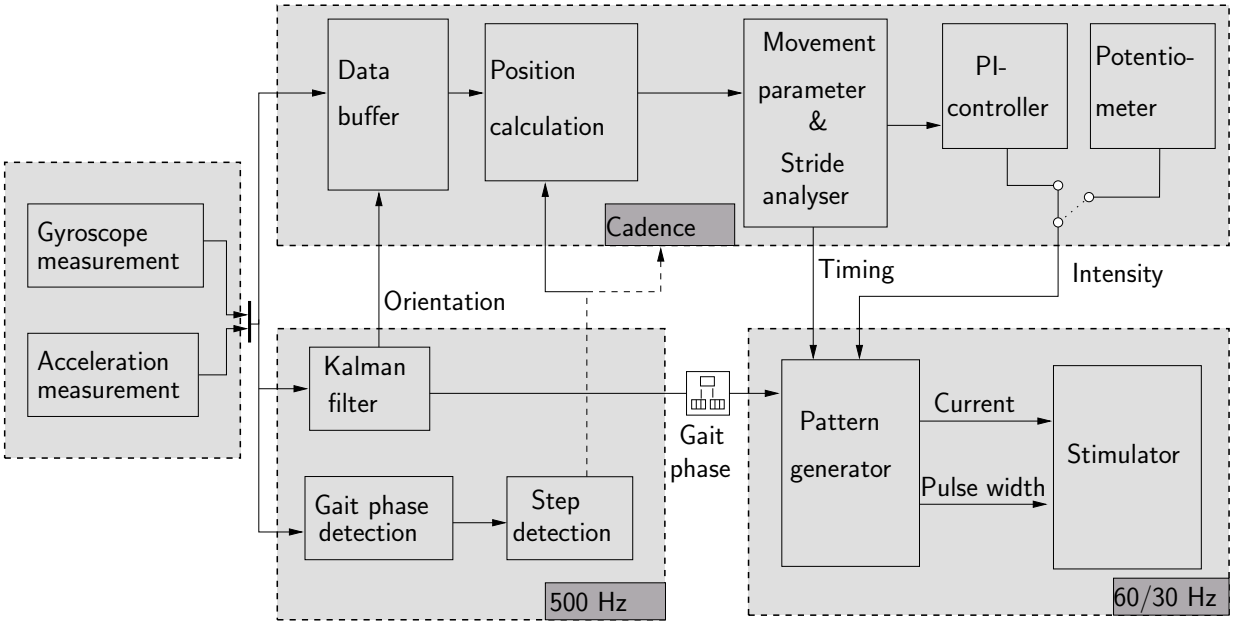

Figure 7.2.: Overview of the gait pattern generator.

In Figure 7.3 a typical complex stimulation pattern is shown. The peroneal nerve stimulation is triggered by the detection of pre-swing and lasts until the loading response. Hamstrings stimulation is also triggered by the detection of pre-swing phase but is turned off earlier as the peroneal nerve stimulation. Furthermore, quadriceps can either be stimulated in the swing phase in order to improve the knee extention or in the stance phase to improve the stability. The gluteus maximus can in some cases be stimulated during the stance phase in order to stabilise the hip.

Another possible stimulation configuration is the stimulation of the peroneal nerve in combination with the tibialis anterior whereas the latter is stimulated up to the end of the swing phases. Peroneal nerve stimulation takes place at a frequency of 60 Hz while muscles are stimulated at 30 Hz.

7.5. Clinical validation of Inertial Sensor Triggered FES-Assisted Gait

The purpose of the experimental clinical pilot study described in this chapter was to measure the instant performance and benefits of FES-assisted gait by means of inertial sensors. Although the performance of the GDP-IS has been extensively validated and analysed in the previous chapter, the application of GDP-IS in FES-assisted gait training is here to be validated. The clinical validation with patients took place at the St. Mauritius Therapieklinik in Meerbush, Germany. Twelve patients with unique pathological gait were recruited to participate in this study. Out of the 12 subjects, 11 were sub-acute stroke patients and

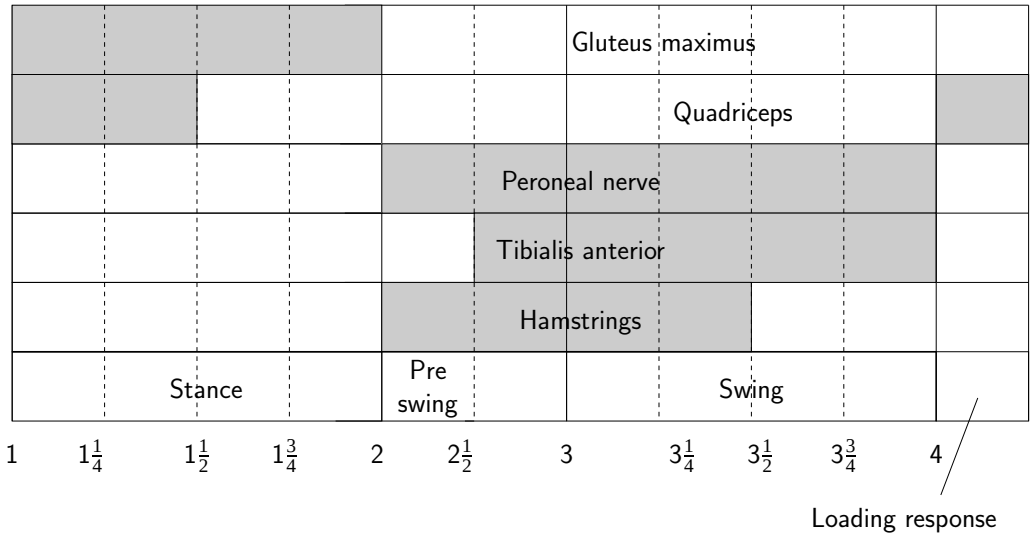

Figure 7.3.: A typical stimulation pattern for FES-assisted gait training. Stimulation periods are indicated by grey areas.

one had Parkinson's disease. The inclusion criteria were that the subjects were able to walk independently on a treadmill with or without parachute harness. The purpose of the FES was to influence the gait pattern instantly in order to improve the quality of the gait. Most of the patients were attending gait training sessions every day in the rehabilitation clinic. Before attending the FES-assisted gait training, the subjects were informed of the purpose of the study and gave their informed consent to participate. The patients were all walking on the treadmill with parachute harness for safety reasons, and the gait was evaluated by physiotherapists who chose appropriate channels for stimulation. In Table 7.1 the gait deficits and the stimulated muscles are summarised. The stimulation sites were determined via stimulation before the therapy. While the patient was sitting on a chair or standing in an upright position, the electrode positions were found by trial and error until the best possible response to the stimulation was found.

Table 7.1.: Stimulation channels and the ranges in which the muscles were stimulated. The phases correspond to the definition in Figure 7.3.

Subject	S1	S2	S3	S4	S5	S6
Channel 1	Hamstrings	Quadriceps	Peroneal nerve	Gastrocnemius	Tibalis ant.	Quadriceps
Range	2 - $3\frac{1}{2}$	4 - $1\frac{1}{2}$	$1\frac{1}{4}$ - $3\frac{1}{4}$	$1\frac{1}{2}$ - 3	$1\frac{1}{2}$ - $3\frac{1}{2}$	1 - 2
Channel 2			Tib. ant.			Quad.
Range			$2\frac{1}{2}$ - 1			$3\frac{1}{2}$ - $1\frac{1}{2}$

Subject	S7	S8	S9	S10	S11	S12
Channel 1	Gluteus max.	Tibialis ant.	Quadriceps	Gastrocnemius	Tibialis ant.	Tibialis ant.
Range	$3.\frac{1}{2}$ - $1\frac{1}{2}$	$2\frac{1}{2}$ -4	3 - 4	$1\frac{1}{2}$ - $3\frac{1}{2}$	2 - 1	2 - $3\frac{3}{4}$
Channel 2	Quadriceps		Tibialis ant.			
Range	$3\frac{1}{2}$ - $1\frac{1}{2}$		2 - $3\frac{3}{4}$			

Table 7.2.: Walking speed of the patients.

Subject	S1	S2	S3	S4	S5	S6
	1.25 [km/h]	0.96 [km/h]	1.26 [km/h]	2.36 [km/h]	0.97 [km/h]	1.40 [km/h]

Subject	S7	S8	S9	S10	S11	S12
	1.18 [km/h]	1.49 [km/h]	0.88 [km/h]	1.63 [km/h]	1.28 [km/h]	1.41 [km/h]

7.5.1. Comments on the Usability of the FES-Assisted Gait Training.

In general the prototype FES-assisted gait training system was working good i.e. the stimulation timing worked as desired. The mounting on and off of the sensor system to the patients took maximum three minutes for a trained person which can be considered as very fast compared to foot insole measurement systems. The only problem regarding the sensor mounting was experienced with patients who walked with the foot pointing outwards such that the inertial sensor was touching the ground and falling of the bracket. Moreover, a few problems with the gait phase detection system occurred with two stroke patients who were walking slowly (subjects S5 and S9 (cf. Table 7.2)). During the foot flat phase the feet were unsettled such that the transition to pre-swing sometimes caused a too early onset of the stimulation (typically for peroneal nerve and tibialis anterior stimulation).

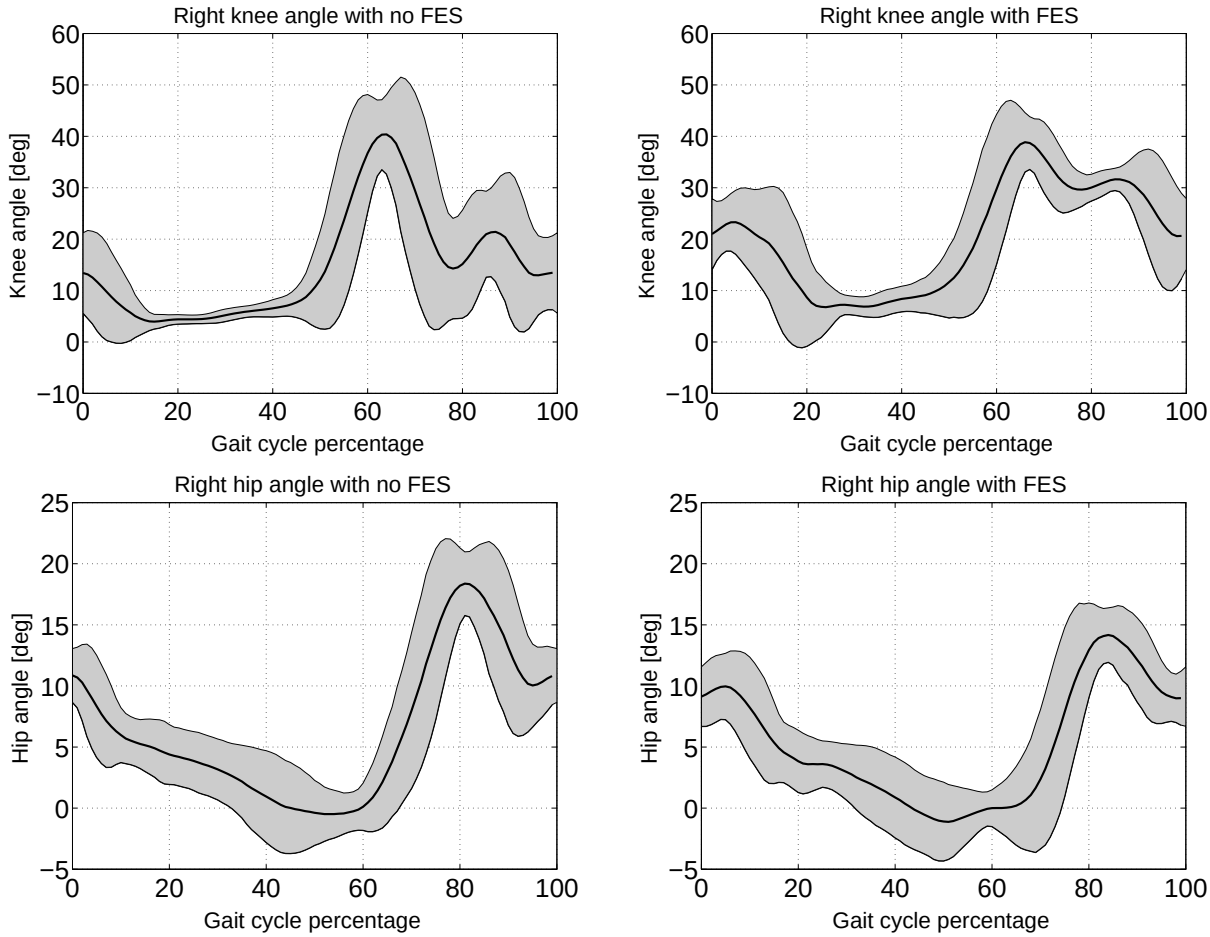

Figure 7.4.: Knee- and hip-joint angle trajectories for Subject S1. In the two upper graphs the mean value of the knee trajectories from 10 consecutive strides recorded with the LUKOtronic motion analysis system are shown (solid line). The grey area indicates the 95 % confidence interval. On the left side the values are shown for trajectories when no FES is applied whereas on the right side the mean value and standard deviation are shown when FES is applied. The two lower graphs show the mean value and standard deviation from hip trajectories for the same strides as for the knee angle.

Generally speaking, positive effects on the gait pattern due to the electrical stimulation were foremost observed when the stimulation was applied in the swing phase. A typical example of such is the stimulation of the peroneal nerve or the muscle tibialis anterior in the swing phase to prevent the drop foot. When stimulation was applied in the stance phase, like stimulation of gluteus maximus in order to improve the stability of the patients, no direct effect of the stimulation could usually be observed from the temporal and spatial parameters calculated from the inertial sensor system. This does not mean that the FES had no impact, but an instant change could not be measured. A reason may be that the patients were always walking on the treadmill with the same constant speed with and without FES. If the patients had walked on a normal floor rather than on a treadmill, an instant improvement would be expected in form of an

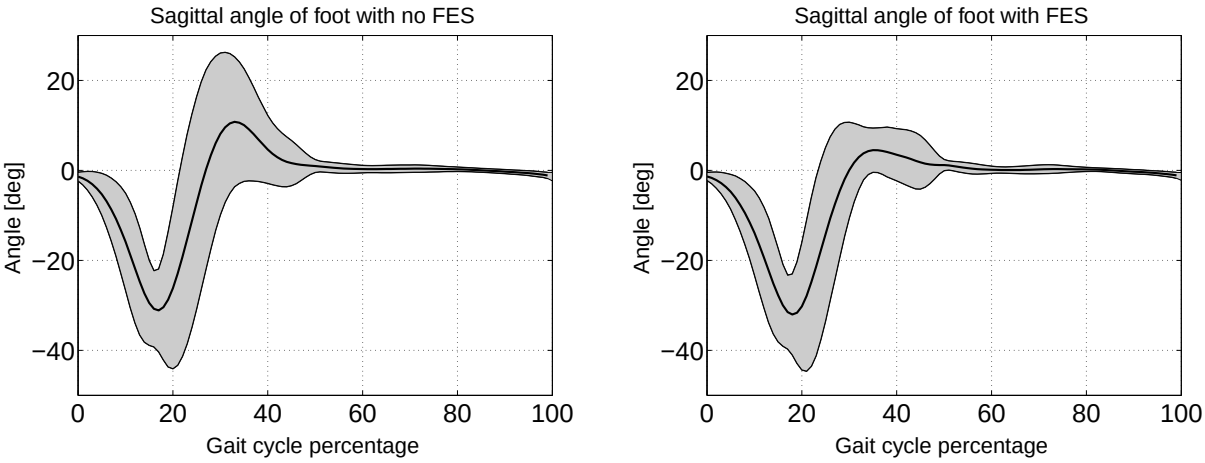

Figure 7.5.: Sagittal angle of foot for Subject S1. In the left graph the mean value (solid line) and the 95 % confidence interval (grey area) of the sagittal angle from 10 consecutive steps are plotted when no stimulation is applied. In the right graph the mean value (solid line) and the 95 % confidence interval (grey area) of the sagittal angle from 10 consecutive steps are plotted for trajectories when stimulation was applied to the hamstring muscle group.

increase in speed. For patient S2 an exception from this rule was found as temporal variables changed when stimulation was applied. This is explained in detail later in this chapter.

As observed from Table 7.1 only one channel and at most two channels were applied in order to improve the walking pattern although eight channels were available alltogether. The reason for not choosing more channels had different reasons. For the patients having a drop foot syndrome, only one channel was chosen. The two patients presented more closely later in this section both had one specific gait deficit related to one muscle (patient S1) or the walking pattern could simply be improved by stimulating one muscle group (patient S2). In a clinical setting where stroke patients are receiving FES to improve the walking pattern, the time is limited. For each channel which is added, time is needed to find appropriate stimulation sites as well as appropriate start and stop times for the stimulation.

From the 12 patients taking part in the FES-assisted gait training, two patients are more closely presented here. In addition to the measurement with the inertial sensor system, knee and hip joint angles were captured by use of the LUKOtronic AS 202 motion analysis system and foot pressure was collected with the Parotec insole measurement system.

Case study subject S1:
Subject S1 was suffering from stroke and was affected on the right side. He could not walk without walking aid or holding on to something. The main problem for the patient was the inability to control the shank at the end of the swing phase. The knee was already in the middle of the swing phase fully extended and was uncontrolled hitting the ground when reaching the initial contact event. The patient was walking with his normal walking speed. In order to improve the gait pattern the hamstring muscle group was stimulated. The onset for the stimulation was at heel-off and offset was set to 50 % of the

swing phase. The subject was participating daily in treadmill training and the session reported here took place instead of regular treadmill training without FES. Markers were fixed at pelvic, hip, knee ankle and at the inertial sensor to measure the position at these points with the LUKOtronic AS 202 motion analysis system.

A comparison of the hip and knee joint trajectories with and without FES is presented in Figure 7.4. The figure shows the mean value and the 95 % confidence interval for hip and ankle trajectories for 10 sequential steps. The upper graphs show the knee angle whereas the lower graphs show the hip angle for the same strides. To the left are the trajectories shown when no FES is applied while the plots to the right have been recorded as FES was applied. From angle recordings the excessive motion of the shank can again be seen as oscillation in the knee joint. During the walking, the knee joint was extended with a high velocity without any damping. After reaching the full extention the shank bounced back leading to unwanted knee flexion at the end of the swing phase. By applying stimulation to the hamstring muscle group the movement of the shank is damped and the oscillations at the knee joint are almost completely vanished.

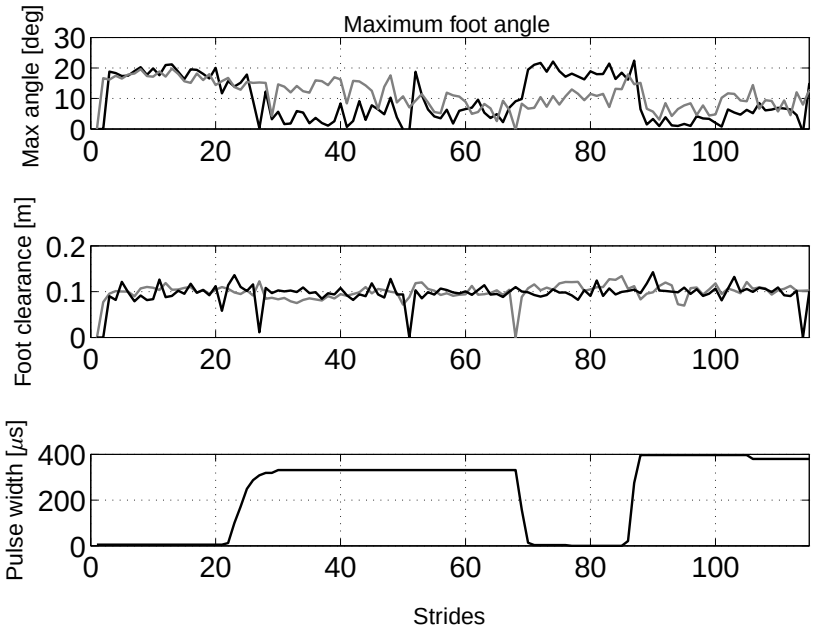

Figure 7.6.: Maximum sagittal angle and foot clearance for Subject S1. The upper graph shows the maximum sagittal foot angles on the affected side (black line) and on the non-affected side (grey line) measured with the inertial sensors. The middle graph shows the foot clearance on the affected side (black line) and on the non-affected side (grey line). The lower graph shows the applied pulse width.

In Figure 7.5 the sagittal angle of the foot with respect to the ground estimated from the inertial sensor is plotted. In the left graph the sagittal angle of the foot is plotted for the case when no stimulation was applied, whereas in the right hand graph the stimulation to the hamstring muscle group was applied. In Figure 7.6 the maximum foot angle for both the affected side as well as for the non-affected side are

shown. It can be observed that the maximum angle was reduced when the stimulation intensity was increased. In addition, on the non-affected side the stimulation has the effect that the maximum sagittal foot angle was reduced. At first glance these figures might indicate that the stimulation degrades the walking pattern as the maximum sagittal angle was reduced. The maximum sagittal angle of the foot was achieved in the moment when the knee was hyperextended. As the stimulation prevented this hyperextension, the maximum foot angle was also reduced. The foot angle at heel strike with and without stimulation was small and more or less identical. This could have been improved by stimulating the tibialis anterior. From the figure it can also be observed that the foot clearance was not affected by the hamstring stimulation. Temporal parameters like the symmetry of the gait were not affected by stimulation. There were no significant difference of the symmetry indexes calculated with stimulation and without stimulation.

Case study subject S2:
Subject S2 was suffering from stroke and was affected on the right side. He could not walk independently without using a walking aid or holding on to something. He could however walk independently using parachute harness on the treadmill. The main problem for the patient occurred in the stance phase as the quadriceps was to weak to bear the body weight. This resulted in knee flexion during the stance phase making it hard for the patient to initiate the next step. In order to improve the gait pattern the quadriceps muscle group was stimulated. The stimulation was switched on by the heel strike event and was turned off as soon as the foot flat phase was finished by the heel off event. The subject was participating in daily treadmill training and the session reported here took place instead of regular treadmill training without FES. The positions of pelvic, hip, knee ankle and inertial sensor were recorded with the LUKOtronic AS 202 motion analysis system in one session and with the Parotec foot insole measurementsystem in another session.

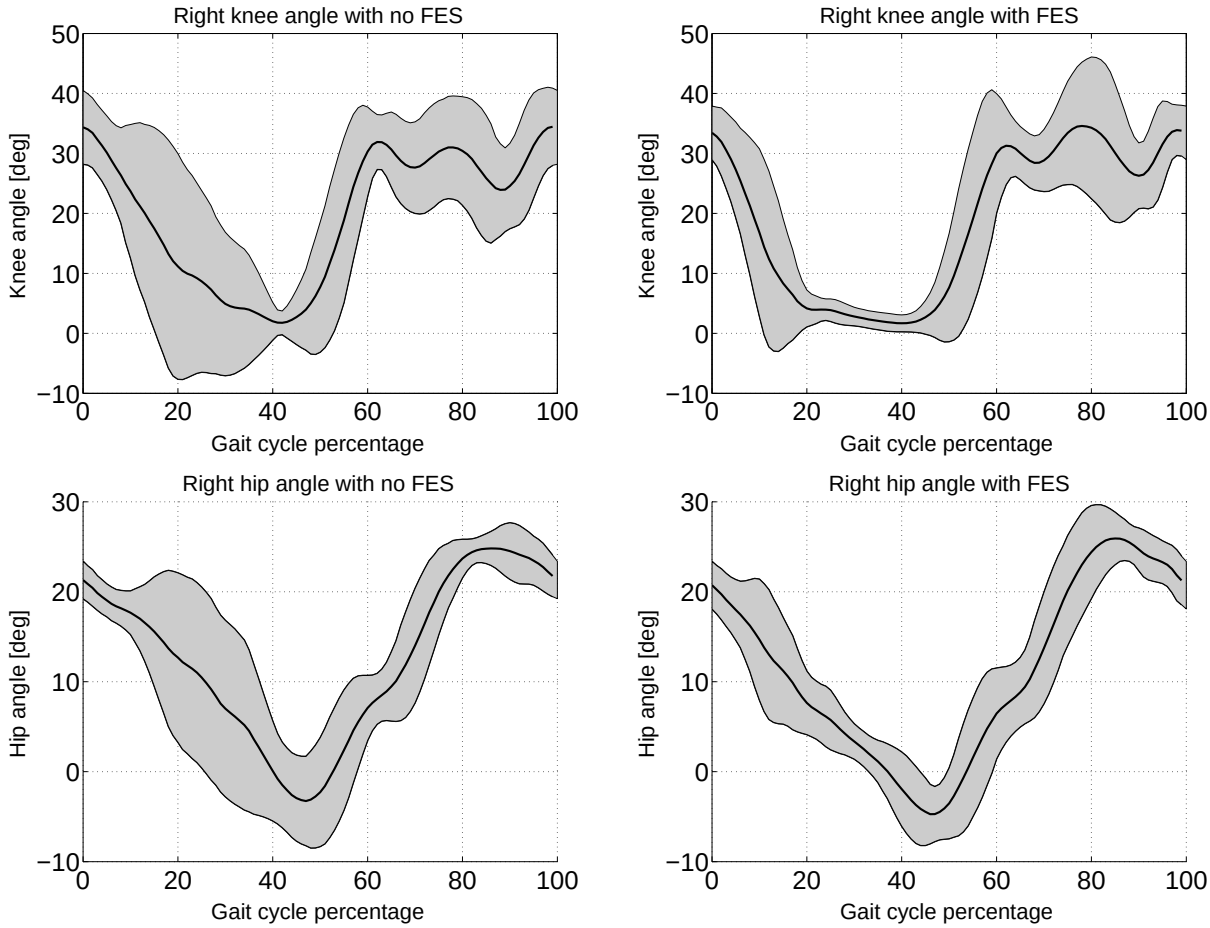

Figure 7.7.: Knee- and hip-joint angle trajectories for Subject S2. In the upper two graphs the mean value (solid line) and the 95 % confidence interval of the knee angle for 10 consecutive strides recorded with the LUKOtronic motion analysis system are shown for subject S2. On the left side the mean value (solid line) and the 95 % confidence interval (grey area) are shown when no FES is applied. On the right side the values are shown for strides when FES is applied. The two lower graphs show the mean value (solid line) of the hip trajectories for the same strides as for the knee angle.

In Figure 7.7 the comparison of angle trajectories with and without FES is shown for subject S2. In the figure the mean value of angle trajectories and the 95 % confidence interval are shown for steps without stimulation and with stimulation applied to the quadriceps muscle group. When the subject is walking on the treadmill and no stimulation is applied it can be observed that the knee joint is flexed during the stance phase. When applying stimulation the improvement is apparent. The knee angle is fully extended during the stance which can be seen from the small confidence interval in upper right graph compared with the upper left graph. The same trend can also be observed on the hip trajectories as the confidence interval becomes smaller indicating that the step to step variation decreases.

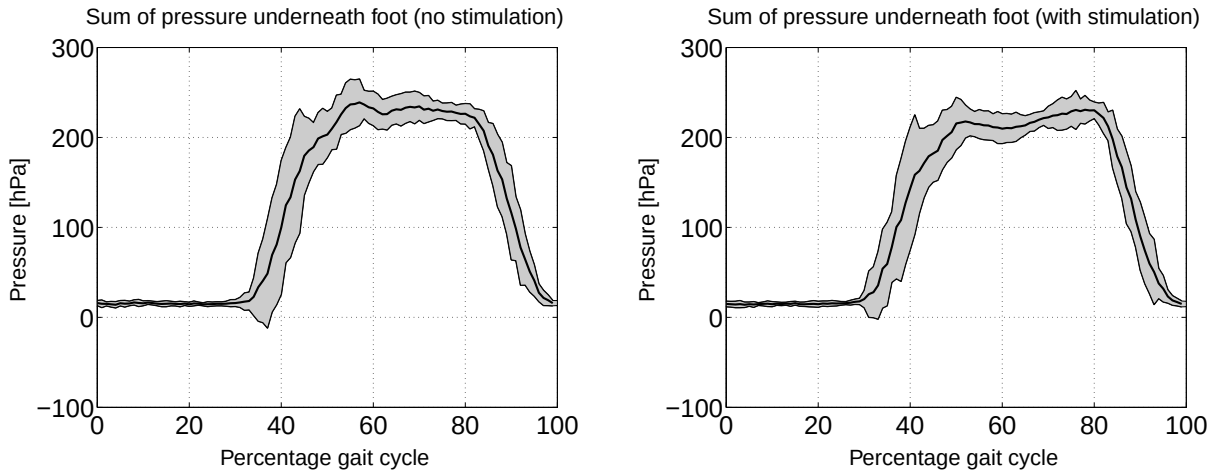

Figure 7.8.: Foot pressure measurements for patient S2. The graphs show the mean pressure underneath the foot (thick solid line) and the 95 % confidence interval for ten consecutive strides. To the left measurement is shown when no stimulation is applied whereas in the right graph stimulation is applied.

Table 7.3.: Temporal information of the gait for subject S2. The table shows the mean values when no FES is applied in the first row and the mean values when FES is applied in the second row.

	Percentage stance [%]	Stride duration [sec.]	SI_{stance}	SI_{swing}
no FES	0.60	2.14	-4.47	9.17
with FES	0.64	2.30	-1.95	3.70

In Figure 7.8 the results from the measurement with the Parotec foot insole measurement system are presented. In the figure the average pressure for the pressure sensors underneat the foot is plotted. To the left the pressure is plotted when no stimulation was applied whereas for the right plot the stimulation was applied to the quadriceps muscle group. From the figure it can be observed that when applying FES the characteristic of the mean pressure becomes more similar to a pattern of a healthy person. A typical peak in the loading response phase as well as in the terminal stance can be seen, whereas without stimulation only one peak in the middle of the stance phase is seen.

Furthermore, it can also be observed that the duration of the stance phase increased when stimulation was applied which indicates that the patient with stimulation trusted his weak side and got a more symmetric gait. In Table 7.3 the mean temporal variables are summarised for subject S2. In the table the percentage of stance, the stride duration and the symmetry indexes SI_{stance} and SI_{swing} are summarised. The values in the table confirm the observation from the pressure measurement. The duration of the stance phase and also the total duration of the strides increased when stimulation was applied. The increased duration of the stance phase does also influence the symmetry indexes which both are improved due to the stimulation. It must be noted that the step to step variation of the values are quite large but the mean values indicate a positive trend.

7.6. Feedback Control of Movement Parameters in FES-Assisted Gait

7.6.1. Motivation

Surface and implantable systems have been developed with some algorithms featuring control which have been tested in laboratory environments for small patient groups. However, the most drop foot systems to date are open loop. These systems require active participation from the user for adjustment of stimulation parameters during initial set-up and in daily use. Furthermore, all previous feedback controlled drop foot orthoses have been using extensive sensory inputs such as goniometers for measuring knee, hip and ankle joints. Application of goniometers is unrealistic outside a laboratory environment as a time consuming procedure for mounting and calibrating the sensors are required before taking the sensors into use. The inertial sensors offer an alternative to other sensors used in drop foot systems and in the application of FES-assisted gait training as inertial sensors are easily mountable and can, as already shown in previous chapter, be used to synchronise the stimulation with the gait cycle. In this section we propose a strategy for feedback control for use in drop foot stimulators and in FES-assisted gait training based on inertial sensors which allow an assessment of certain gait and movement parameters.

7.6.2. Control Concept

As already shown in Chapter 6, inertial sensors deliver after a completed step estimated movement parameters such as maximum height of the foot during the swing phase, length of the step and the maximum sagittal angle between the foot and the ground during swing phase. The idea is that each of these movement parameters can be influenced by stimulation of one muscle group. The stimulation timing of the muscles is still synchronised to the gait phases as already described and the stimulation intensity profile i.e. the pulse width is kept constant during one stride. After a completed step, movement parameters are evaluated and the pulse width is changed for the next step in order to achieve a target value of the movement parameter. This can be done automatically by letting a controller do the task of choosing a new stimulation intensity. Since the update of the stimulation intensity is applied on a step to step basis which of nature is discrete. Such a discrete controller is designed in the next section.

In Figure 7.9 two pairs of a movement parameter and a stimulation channel are illustrated for which the feedback control is closer examined. The first movement parameter evaluated is the foot clearance, which can be influenced by stimulation of the hamstring muscle group. The stimulation is triggered by the heel off event and continues until the middle of the swing phases. The next movement parameter evaluated here is the maximum sagittal angle during the swing phases. The stimulation of the tibialis anterior can influence this movement parameter.

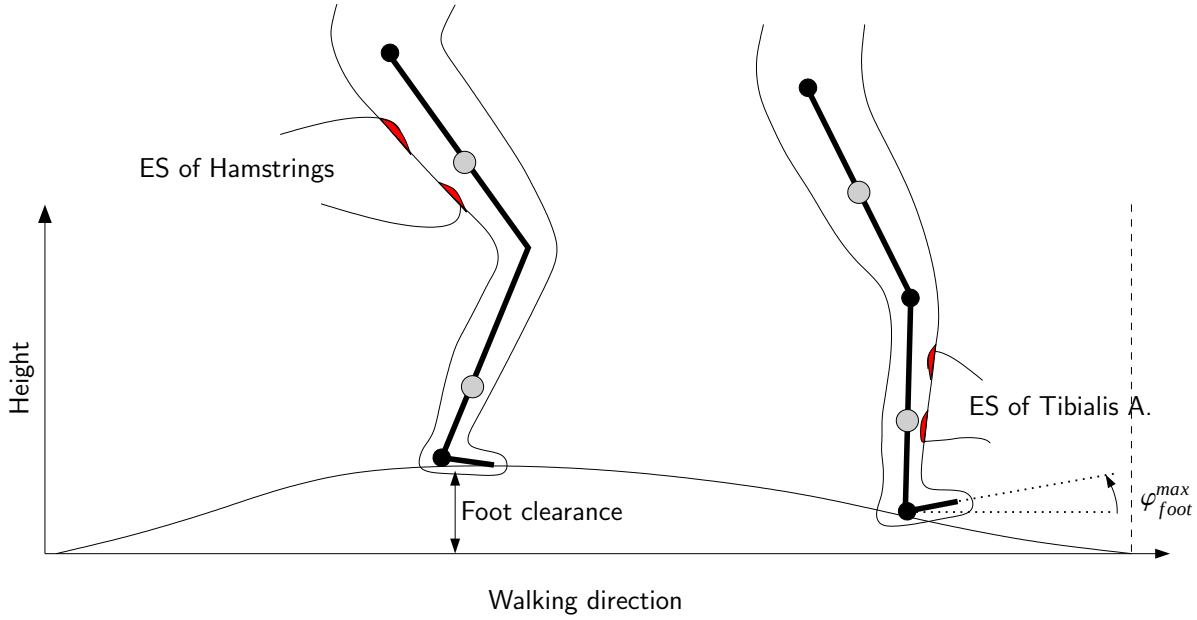

Figure 7.9.: Freely swinging leg with electrical stimulation.

7.6.3. Control Design

Let us assume a discrete-time control system where the sampling instants are the heel strike events of the stimulated leg. The control signals are the amplitudes (intensity) of predefined stimulation profiles and outputs are the movement parameters influenced by the stimulation. At the sampling k the stimulation intensity for the next step must be determined based on the measured value of the movement parameter from the previous step. Note that there is a time delay of one step between stimulation intensity update and the effect on the movement parameter. Under the assumption of independent pairs of stimulation channels and movement parameters the problems simplifies from a MIMO control problem to a set of SISO control problems. The relationship between the applied unsaturated stimulation profile amplitude $u(k)$ of one stimulation channel and the movement parameter $y(k)$ can be assumed to be a linear time-discrete pulse transfer function

$$y(k) = bq^{-1}u(k) + d(k) \tag{7.1}$$

where q^{-1} is the backward operator ($q^{-1}u(k) = u(k-1)$). The plant gain b is dependent upon the electrode placement, the timing of the stimulation and possibly also the speed of the patient. $d(k)$ is an output disturbance comprising all external disturbances as well as voluntarily muscle movements.

Based on the the simple plant model (Eq. 7.1), a pole placement controller may be designed [3]. In Figure 7.10 the block structure of the closed-loop system with movement parameter controller is shown.

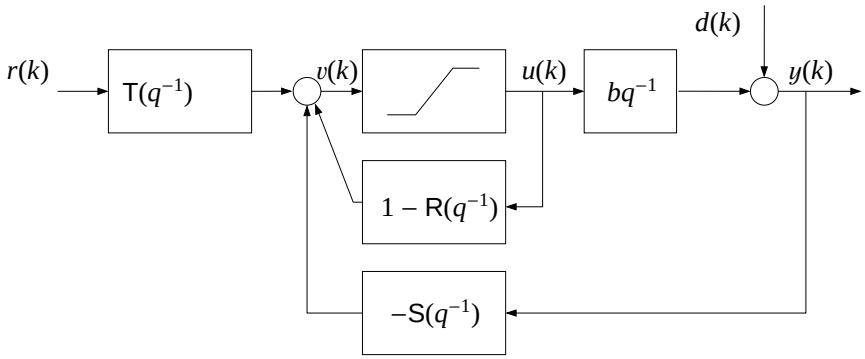

Figure 7.10.: Block structure of the closed-loop system.

The controller is given through

$$u(k) = \text{sat}\left(\mathsf{T}(q^{-1})r(k) - \mathsf{S}(q^{-1})y(k) + (1 - \mathsf{R}(q^{-1}))u(k)\right) \tag{7.2}$$

where $r(k)$ is the desired movement parameter (reference). Here, $\mathsf{R}(q^{-1})$ and $\mathsf{S}(q^{-1})$ are fixed polynomials with the following structure:

$$\mathsf{R}(q^{-1}) = 1 + r_1 q^{-1} + ... + r_{nr} q^{-nr} \tag{7.3}$$

$$\mathsf{S}(q^{-1}) = s_0 + s_1 q^{-1} + ... + s_{ns} q^{-ns}. \tag{7.4}$$

The prefilter $\mathsf{T}(q^{-1})$ is also a polynomial. The controller contains an internal model of the control signal saturation:

$$u(k) = \text{sat}(v(k)) = \begin{cases} \underline{u} & v(k) < \underline{u} \\ v(k) & \underline{u} \leq v(k) \leq \overline{u} \\ \overline{u} & v(k) > \overline{u} \end{cases} \tag{7.5}$$

The lower bound $\underline{u}$ represents the lower pulse width required to produce a measurable influence on the movement parameter. The upper bound $\overline{u}$ is either technically caused by the stimulator device or it is the maximum pulse width the patient can tolerate due to pain. To compensate for constant disturbances and model errors integral action in the controller is required. This is done by choosing the polynominal $\mathsf{R}(q^{-1})$ as follows:

$$\mathsf{R}(q^{-1}) = (1 - q^{-1})\overline{\mathsf{R}}(q^{-1}). \tag{7.6}$$

$$\tag{7.7}$$

With this control design, the closed-loop system becomes

$$y(k) = H_r(q^{-1})r(k) + H_d(q^{-1})d(k) = \frac{bq^{-1}\mathsf{T}(q^{-1})}{\mathsf{A}_{cl}(q^{-1})}r(k) + \frac{(1-q^{-1})\overline{\mathsf{R}}(q^{-1})}{\mathsf{A}_{cl}(q^{-1})}d(k) \tag{7.8}$$

where the closed-loop characteristic polynomial $\mathsf{A}_{cl}(q^{-1})$ is given as

$$\mathsf{A}_{cl} = (1-q^{-1})\bar{\mathsf{R}}(q^{-1}) + \mathsf{S}(q^{-1})bq^{-1} \tag{7.9}$$

The polynomials $\mathsf{R}(q^{-1})$ and $\mathsf{S}(q^{-1})$ are determined by the pole-placement method in which a desired closed-loop characteristic polynomial is specified by this equation

$$\mathsf{A}_{cl}(q^{-1}) = \mathsf{A}_o(q^{-1})\mathsf{A}_c(q^{-1}) \tag{7.10}$$

where $\mathsf{A}_o(q^{-1})$ and $\mathsf{A}_c(q^{-1})$ are polynomials of first order. The reason for splitting the closed-loop polynomial into two parts is to give the controller different properties for reference tracking and for disturbance rejection. A second order closed-loop polynomial was chosen in order to obtain a proper controller of minimal order. By solving the Diophantine Equation (7.9) the following solution is given

$$\overline{\mathsf{R}}(q^{-1}) = 1 \tag{7.11}$$

$$\mathsf{S}(q^{-1}) = \frac{a_{cl1}+1}{b} + \frac{a_{cl2}}{b}q^{-1} \tag{7.12}$$

The second step of the controller design is to choose the polynomial $\mathsf{T}(q^{-1})$. The aim is to obtain a transfer function

$$H_r(q^{-1}) = \frac{bq^{-1}\mathsf{T}(q^{-1})}{\mathsf{A}_c(q^{-1})\mathsf{A}_o(q^{-1})} \equiv \frac{q^{-1}\mathsf{A}_c(1)}{\mathsf{A}_c(q^{-1})} \tag{7.13}$$

from the reference to the movement parameter which is of first order and has unit gain. This is done by cancelling the observer polynomial $\mathsf{A}_o(q^{-1})$ in the transfer function This is done by choosing the following pre-filter $\mathsf{T}(q^{-1})$

$$\mathsf{T}(q^{-1}) = \frac{\mathsf{A}_c(1)\mathsf{A}_o(q^{-1})}{b}. \tag{7.14}$$

The tuning of the controller is specified by the closed-loop poles, i.e. the roots of $\mathsf{A}_o(q^{-1})$ and $\mathsf{A}_c(q^{-1})$ which can be specified through the time constants of equivalent continuous time systems of 1$^{\text{st}}$ order:

$$\mathsf{A}_o(q^{-1}) = 1 - \exp(-1/n_o)q^{-1} \tag{7.15}$$

$$\mathsf{A}_c(q^{-1}) = 1 - \exp(-1/n_c)q^{-1}. \tag{7.16}$$

Here n_o and n_c are the time constants given in strides. Table 7.4 shows the rules for how the closed-loop system can be tuned. The gain b was in this work found through an identification procedure. As the gain remain fairly constant during the experiments, the parameter b was identified offline before the control experiments. Naturally, the parameter b could also be identified on-line in an adaptive control scheme. The controller does comprise an anti-reset windup through the internal input saturation model.

Table 7.4.: Controller tuning.

Rise time	Reference tracking	Disturbance rejection	Noise sensitivity
$n_0 \uparrow$	-	worse	better
$n_0 \downarrow$	-	better	worse
$n_c \uparrow$	slower	worse	better
$n_c \downarrow$	faster	better	worse

7.7. Simplified Model of a Free Swinging Leg

In this section a mathematical model of the free swinging leg is developed in order to verify the proposed control concept in simulations.

The swinging leg is considered as a planar triple pendulum with the hip joint as a fixed hanging point. The pendulum consists of three segments: thigh, shank and foot. Furthermore, it is assumed that the mass of each segment is concentrated in a point mass at its centre of mass. The centre of mass, the moment of inertia about the centre of mass and the length of each segment are assumed to be constant during the movement of the leg. All joints are assumed to be hinge joints. Ground reaction forces do not occur since only the swing phase is considered.

7.7.1. Equation of Motion

The equation of motion can be derived from Lagrangian formulation, which is based on energy relations. The Lagrange's equations in the 2$^{\text{nd}}$ form for a system of n generalised coordinates q_i is defined by

$$\frac{d}{dt}\left(\frac{\partial L}{\partial \dot{q}_i}\right) - \frac{\partial L}{\partial q_i} = Q_i \quad i = 1..n \tag{7.17}$$

where Q_i are externally applied moments e.g. caused by muscle force or passive joint properties, and L is the Lagrangian function which is the difference between the total kinetic energy T and the total potential energy U of the system

$$L = T - U. \tag{7.18}$$

The simplified model of the swinging leg has three generalised coordinates ($n = 3$). These are the hip joint angle $q_1 = \varphi_H$, the knee joint angle $q_2 = \varphi_K$ and the ankle joint angle $q_3 = \varphi_A$ which are defined in Figure 7.11. The total potential energy of the system is the sum of the potential energy of all segments:

$$U = m_T g h_T(\varphi_H) + m_S g h_S(\varphi_K, \varphi_H) + m_A g h_A(\varphi_K, \varphi_H, \varphi_A). \tag{7.19}$$

The first term represents the potential energy of the thigh, the second term represents the potential energy of the shank and the third term represents the potential energy of the foot. In the equation g is the gravitational constant, and the following masses and heights are defined:

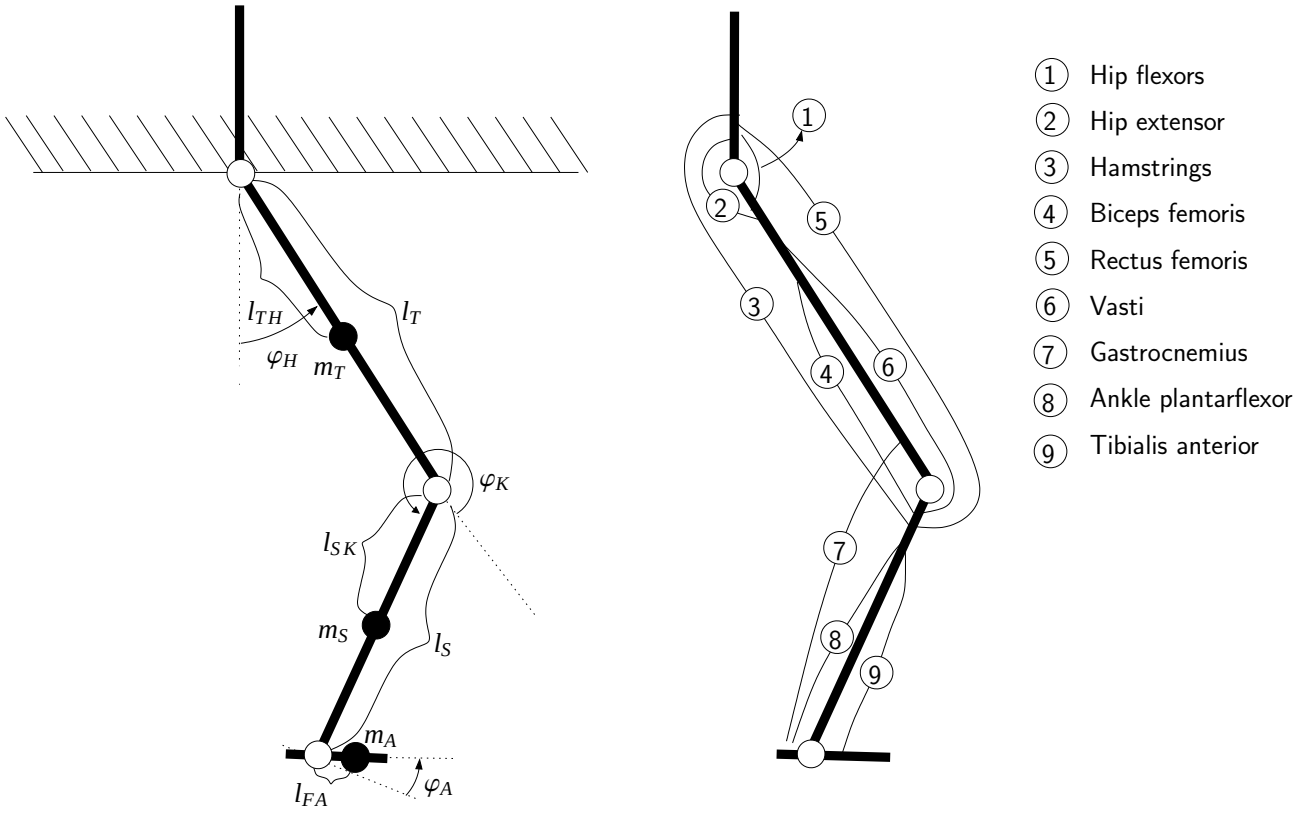

Figure 7.11.: Model of a freely swinging leg.

m_T - mass of thigh
m_S - mass of shank
m_A - mass of foot
h_T - height of the centre of mass of thigh
h_S - height of the centre of mass of shank
h_A - height of the centre of mass of foot

The heights (h_T,h_S,h_A) of the centres of masses are functions of the knee, hip and ankle joint angles and are derived in the the following way:

$$h_T(\varphi_H) = l_{leg} - l_{TH}\cos(\varphi_H) \tag{7.20}$$

$$h_S(\varphi_H, \varphi_S) = l_{leg} - l_T\cos(\varphi_H) - l_{SK}\cos(\varphi_H + \varphi_K) \tag{7.21}$$

$$h_A(\varphi_H, \varphi_S, \varphi_A) = l_{leg} - l_T\cos(\varphi_H) - l_S\cos(\varphi_H + \varphi_K) - l_{FA}\sin(\varphi_H + \varphi_K - \varphi_A) \tag{7.22}$$

The lengths which are used are defined as:

l_{leg} - length of the whole leg
l_{TH} - length from the centre of mass of thigh to the hip joint
l_T - length of thigh
l_{SK} - length from the centre of mass of shank to the knee joint
l_S - length of shank
l_{FA} - length from the centre of mass of foot to the ankle joint

The total kinetic energy of the system is the sum of the kinetic energies of all segments

$$\begin{aligned} T &= \frac{1}{2}(I_1 + m_T l_{TH}^2)\dot{\varphi}_H^2 + \frac{1}{2}I_2(\dot{\varphi}_H + \dot{\varphi}_K)^2 + \\ &\quad \frac{1}{2}(v_{x,S}^2 + v_{y,S}^2)m_S + \frac{1}{2}I_3(\dot{\varphi}_H + \dot{\varphi}_K - \dot{\varphi}_A)^2 + \frac{1}{2}(v_{x,A}^2 + v_{y,A}^2)m_A \end{aligned} \tag{7.23}$$

where the first term is the kinetic energy of the thigh, the second term represents the rotational energy of the shank about its centre of mass. The translational energy of the shank is given in the third term. The fourth and fifth term represent the rotational and translational energy of the foot segment respectively. The terms $v_{x,A}$ and $v_{y,A}$ describe the translational velocity of the foot segment in horizontal and vertical direction. The following moments of inertia and velocities are used:

I_1 - moment of inertia about the centre of mass of thigh
I_2 - moment of inertia about the centre of mass of shank
I_3 - moment of inertia about the centre of mass of foot
$v_{x,S}$ - horizontal velocity of the centre of mass of shank
$v_{y,S}$ - vertical velocity of the centre of mass of shank
$v_{x,A}$ - horizontal velocity of the centre of mass of foot
$v_{y,A}$ - vertical velocity of the centre of mass of foot

By applying the Lagrangian formulation, the general equation of motion for three degrees of freedom can be described as follows:

$$[\mathbf{M}(\mathbf{q})]\,\ddot{\mathbf{q}} = \mathbf{C}(\mathbf{q}, \dot{\mathbf{q}}) + \mathbf{G}(\mathbf{q}) + \mathbf{Q}(\mathbf{q}, \dot{\mathbf{q}}) \tag{7.24}$$

with

$\mathbf{q} = [\varphi_H\ \varphi_K\ \varphi_A]^T$ - vector of angles
$\mathbf{M}(\mathbf{q})$ - 3x3 inertia matrix
$\mathbf{C}(\mathbf{q}, \dot{\mathbf{q}})$ - 3x1 vector of Coriolis and centrifugal terms
$\mathbf{G}(\mathbf{q})$ - 3x1 vector of gravitational terms
$\mathbf{Q}(\mathbf{q}, \dot{\mathbf{q}})$ - 3x1 vector of external applied moments

The components of the matrices and vectors in the model are given in Appendix A.

7.7.2. Passive Moments

The total moment $\mathbf{Q}(\mathbf{q}, \dot{\mathbf{q}})$ at the joints is the sum of active, passive elastic and passive viscous moments. The passive elastic moment is modelled as a double exponential function of the joint angles, whereas the passive viscous joint moment is modelled as a linear damping function. These moments are caused by passive properties of muscles, bones, ligaments etc. and they are assigned to the joint. The viscous joint moment is defined by

$$\mathbf{M}_{vis}(\dot{\mathbf{q}}) = -\mathbf{B}\dot{\mathbf{q}},\ \mathbf{B} = \begin{bmatrix} b_H & 0 & 0 \\ 0 & b_K & 0 \\ 0 & 0 & b_A \end{bmatrix} \tag{7.25}$$

where $\mathbf{B}$ is the positive definite damping matrix. These passive elastic joint moments can be expressed by double exponential functions as described by Riener and Fuhr [69].

$$\mathbf{M}_{ela} = [M_{ela,H}\ M_{ela,K}\ M_{ela,A}]^T \tag{7.26}$$

with

$$M_{ela,H} = \exp(2.108 + 0.9167\varphi_K + 1.117\varphi_H) - \exp(-2.178 - 4.011\varphi_K - 7.729\varphi_H) - 15.24 \tag{7.27}$$

$$\begin{aligned} M_{ela,K} = {} & \exp(1.037 + 0.2292\varphi_A + 2.830\varphi_K + 1.432\varphi_H) - \\ & \exp(-1.156 - 0.1146\varphi_A - 1.455\varphi_K - 0.1719\varphi_H) + \exp(2.500 + 14.32\varphi_K) + 1.0 \end{aligned} \tag{7.28}$$

$$M_{ela,A} = \exp(2.0111 - 4.7727\varphi_A - 0.0090\varphi_K) - \exp(-9.925 + 12.2155\varphi_A) - 2.97. \tag{7.29}$$

7.7.3. Muscle Models

Nine muscles and muscle groups have been taken into account in the model (cf. Figure 7.11). The muscle models used in this paper are based on the models presented by Riener and Fuhr [69]. The muscle models are far too complex for use in control design, but they capture important physiological effects and are suitable to evaluate new control strategies in simulations before carrying out real experiments with subjects. The muscle models can be divided into activation and contraction dynamics. Each muscle or muscle group possesses its own activation and contraction dynamics. Activation dynamics are computed considering the effect of spatial and temporal summation by a nonlinear recruitment curve, a nonlinear activation frequency relationship, and a linear second order calcium dynamics with time delay. Contraction dynamics describe the active moment developed by a single muscle or muscle group, and are calculated from its nonlinear moment arm and the muscle force, which is a function of maximum isometric muscle force, muscle activation, force-length and force-velocity relation. The muscles described in the model are listed in Figure 7.11.

7.7.4. Reflex Model

The electrical stimulation of the mono-articular hip flexors via surface electrodes is hardly realisable as the hip flexor muscles are located deeply within the body. However, the flexion withdrawal reflex can be elicited in order to initiate a step by FES. The withdrawal reflex is causing a flexion in the hip and knee joints as well as an ankle dorsiflexion. The stimulation frequency has to be higher than for surface muscle stimulation and frequencies in the range 50 to 60 Hz are normally used.

Here a new approach of modelling the flexion withdrawal reflex is proposed. Parts of the muscle models from [69] can be used for describing the physiological behaviour of the flexion withdrawal reflex in an adequate way. A number of assumptions regarding the physiological behaviour of the flexion withdrawal reflex and the stimulation conditions are applied:

- Stimulation of the common peroneal nerve results in the contraction of the hip flexors and rectus femoris which causes a hip flexion, and in a contraction of the hamstrings (caput longum), biceps femoris (caput breve) and gastrocnemicus which is causing a knee flexion.
- Contraction dynamics, calcium dynamics and muscle fatigue are equal to normal muscle stimulation.
- The time delay of reflex activation is higher than the one of direct muscle activation because the afferent neural signal is transmitted first to the spinal cord and then the motor signal is transmitted from the spinal cord to the muscles which is a longer distance than at direct muscle activation.
- The activation caused by reflex stimulation is different for each muscle. Therefore, the reflex activation of each muscle is weighted by a constant.
- Mono-articular muscles like biceps femoris (short head) and hip flexors have larger weighting constants than biarticular muscles.
- Reflex activation reduces the activation potential of direct muscle stimulation via surface electrodes.

The activation dynamics are extended by a pulse width-reflex activation relation, an additional time delay, a constant c and a term specifying the superposition of reflex activation and direct muscle stimulation. The relationship of the reflex activation a_{reflex} to the applied pulse width pw can be expressed by an exponential function (cf. Figure 7.12), as in [78]:

$$a_{reflex} = 1 - \exp(-0.0125 pw). \tag{7.30}$$

The time delay is taken from [94] and [70]. Both references define a time delay of 200ms between stimulation input and reflex activation. Taking the activation dynamics into consideration a slightly

smaller time delay of 175ms has been chosen. A constant c, ranging between 0 and 1 is introduced weighting the reflex activation of each muscle. The constants which are implemented in the model are a rough estimate based on trial and error. For muscles which can be simultaneously activated by peroneal nerve stimulation and direct stimulation the reflex activation and the direct activation have to be superposed in an adequate way. The superposition of direct muscle stimulation activation a_{muscle} and reflex activation a_{reflex} to the total activation a is represented by the following equation:

$$a = a_{muscle}(1 - a_{reflex}) + a_{reflex}. \tag{7.31}$$

This equation is a simple approximation to a nonlinear and complicated relation. Direct surface muscle stimulation via surface electrodes activates motor neurons which are located near the surface. Peroneal nerve stimulation activates motor neurons in the whole muscle. Equation (7.31) assumes that direct stimulation and reflex stimulation activate partially the same motor units. For instance, a reflex activation a_{reflex} of 0.5 superposed to a surface muscle activation a_{muscle} of 0.5 will result in a total activation of 0.75. Furthermore, a total activation higher than 1 is not possible. This is an improvement in comparison with other existing models.

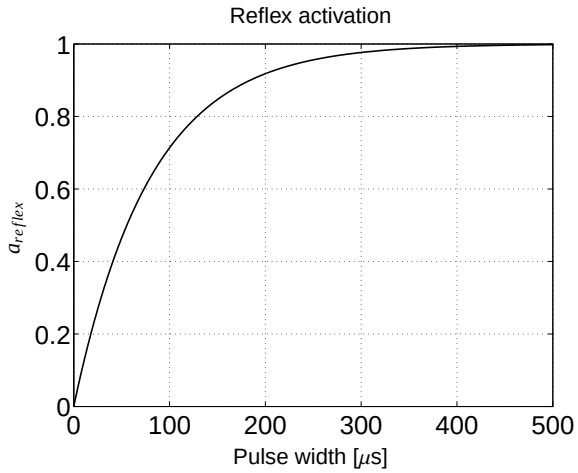

Figure 7.12.: Pulse width dependency of reflex activation.

7.8. Feedback Controlled FES-Assisted Gait - Simulation Study

7.8.1. Stimulation Pattern

The model described in the previous section was used to verify the proposed control scheme. As there are no contact forces described in the model, it is only valid in the swing phase of the gait. Consequently, the simulation is repeatedly started after a finished swing phase, with the same initial states. Before validation of the control scheme, appropriate stimulation intervals for the four different channels were

Table 7.5.: Stimulation pattern used in the simulation.

	Start[s]	Stop [s]	Pulse width [μs]	Frequency[Hz]
Peroneal Nerve	0	0.5	400	60
Quadriceps	0.3	0.6	270	20
Hamstrings	0	0.3	variable	20
Tibialis anterior	0.7	1.0	variable	20

found, which provide a natural gait movement. During the simulation, the parameters current amplitude, pulse width, frequency and range of stimulation were kept constant, while the pulse width profile of the channel influencing the movement parameter i.e. hamstrings or tibialis anterior have been modulated in the amplitude by the controller.

Movement parameters used within this section are the foot clearance and the maximal angle of the foot in the sagittal plane. The foot clearance fc in the model is computed as the distance between the foot and an imaginary ground. This is defined as a perfect circle with the hip joint as origin with radius equal to the complete length of the extended leg l_{leg}. The foot clearance is then

$$fc = l_{leg} - \sqrt{l_T^2 + l_S^2 - 2 l_T l_S \cos(\varphi_K - \pi)}. \tag{7.32}$$

Note that the hip angle φ_H does not influence the foot clearance as the imaginary ground is used. Furthermore, the maximum sagittal angle between the foot and the ground can from the model be found by this equation

$$\varphi_{foot}^{max} = \max(-(\varphi_H + \varphi_K + \varphi_A)). \tag{7.33}$$

Equation (7.33) assumes that the ground is flat.

In the simulation, the quadriceps, the hamstring, the tibialis anterior and the peroneal nerve were stimulated. Quadriceps comprises the vastii and rectus femoris muscles. In Table 7.5 the stimulation timing, the pulse width and frequency of the respective channels are summarised. The pulse width for tibialis anterior and quadriceps were as below described variable.

7.8.2. Test Procedure

Simulations were performed to investigate the performance of the feedback controller. For both the foot clearance and the maximum sagittal angle of the foot the control scheme was tested. As shown in Chapter 6 the foot clearance estimate based on inertial sensor is associated with a certain noise. To make the simulations more realistic, the estimated movement parameters were superposed by white noise with a standard deviation of 5% of the mean value to simulate the measurements with the inertial sensor. Separately, for both the hamstring as stimulation channel and foot clearance as movement parameter and the tibialis anterior as stimulation channel and maximum sagittal angle before heel strike as movement parameter the following tests were performed for finding the control parameters and to validate the

controller:

- *Open loop test:* The stimulation intensity of one target muscle was changed between two stimulation levels in a predefined manner, while the parameters for the other stimulation channels were kept constant.
- *Parameter identification*: After the open loop test was performed, the plant gain b was found for stimulation channel/movement parameter relation. After the plant gain b was determined, the controller was tuned using the rules defined in Table 7.4. Furthermore, the range in which the movement parameters were lying was found in order to define appropriate reference values for the closed-loop tests.
- *SISO Closed-loop test:* During this test only one controller was active and the reference was changing between two values lying in the range found in the open loop test. The reference movement parameter was kept constant for 20 steps and then changed to the other value. Stimulation parameters of the other stimulation channels were kept constant.

Two additional test have been performed in which both movement parameter controllers were active:

- *MIMO test 1:* The reference value for the foot clearance was constant. The reference value for the maximum sagittal angle was a square wave signal.
- *MIMO test 2:* The reference value for the maximum sagittal angle was a square wave signal. The reference value for the foot clearance was a square wave signal.

7.8.3. Results

In Figure 7.13 the results from the *open loop tests* are shown. In the left graph the *open loop test* for the foot clearance is depicted. The hamstrings stimulation was changed after 30 step from 200 μs to 300 μs. The plant gain was calculated to be $b_{ham} = 0.085$ cm/μs. The foot clearance was in the range 8 cm for no stimulation to 16 cm for maximum stimulation of the hamstrings.

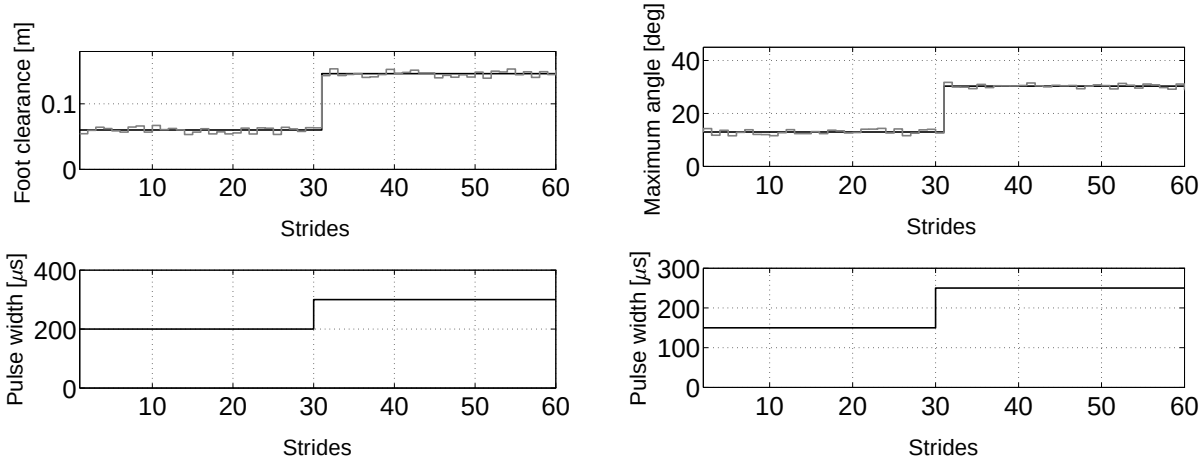

Figure 7.13.: Results from the *open loop tests*: The upper graph to the left shows the measured foot clearance (grey line) and the real foot clearance (solid line), whereas the lower graph to the left shows the corresponding pulse width applied to the hamstrings. In the upper graph to the right are the measured maximum sagittal angle (grey line) and the real maximun sagittal angle (solid line) shown, whereas in the lower right graph is the corresponding pulse width applied to the tibialis anterior depicted.

In the right graph the results from the *open loop test* for the tibialis anterior stimulation and the related maximum sagittal angle are shown. The pulse width of the tibialis anterior stimulation was changed after 30 steps from 150 μs to 250 μs. The gain between the pulse width of the tibialis anterior stimulation and the maximum sagital angle was found to be $b_{tib} = 0.15$ deg/μs. It was also observed that the maximum sagittal foot angle was lying between 12 and 31 degrees.

In Figure 7.14 the results from the *SISO closed-loop test* for the foot clearance regulation are shown. The reference was between 11 cm and 14 cm. In the upper graph the reference (dotted line), the measured (grey line) and the real foot clearance (solid line) are shown. In the lower graph the corresponding pulse width is shown. As seen from the plot, the controller has no problem to follow the reference value. The new reference value was achieved after 5-7 steps.

In Figure 7.15 the results from the *SISO closed-loop test* for the maximum sagittal angle regulation are shown. The reference (dotted line) was changing between 18 and 23 degrees and is shown in the upper graph with the measured angle (grey line) as well as the real angle (solid line). The lower graph depicts the corresponding pulse width applied to the tibialis anterior. As seen from the plot, the controller has no problem to follow the reference value. The new reference value was achieved after 5-7 steps.

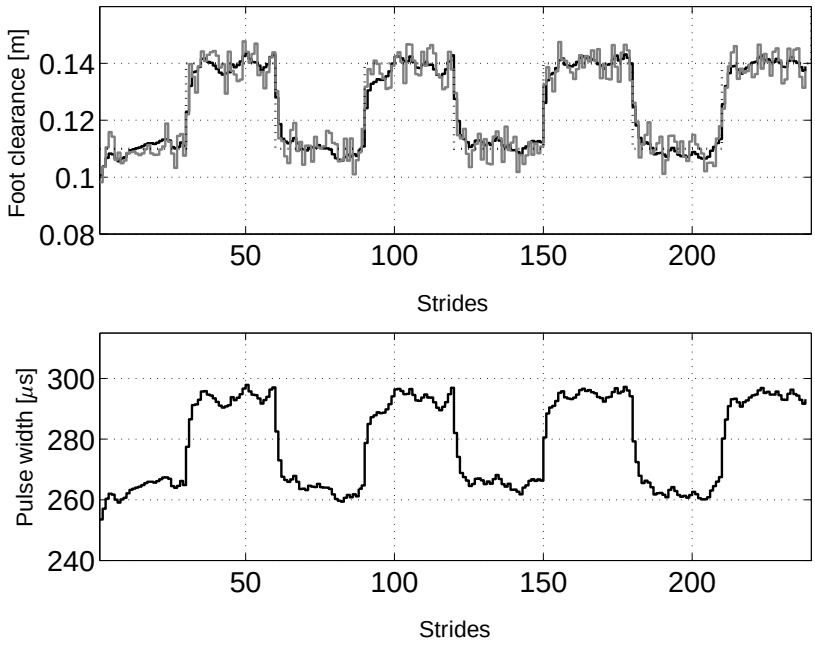

Figure 7.14.: The results of the *SISO closed-loop test* for the foot clearance. The upper graph shows the reference foot clearance (dotted line), the real foot clearance (solid line) and the measured foot clearance (dashed line). The lower graph shows the stimulation pulse width applied to the hamstrings.

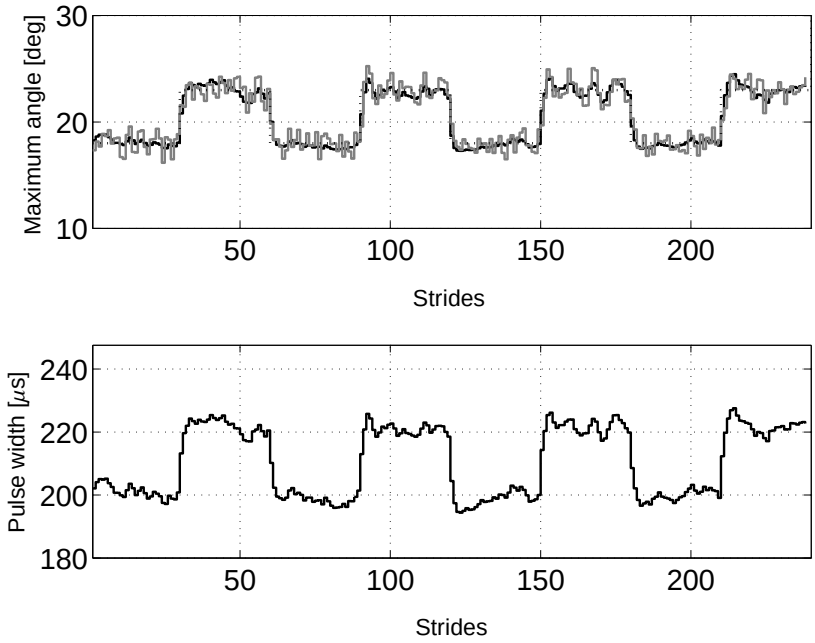

Figure 7.15.: Results from the *SISO closed-loop test* for the maximum sagittal angle. The upper graph shows the reference value (dotted line), the real maximum sagittal angle (solid line) and the measured maximum sagittal angle (grey line). The lower graph shows the stimulation pulse width applied to the tibialis anterior.

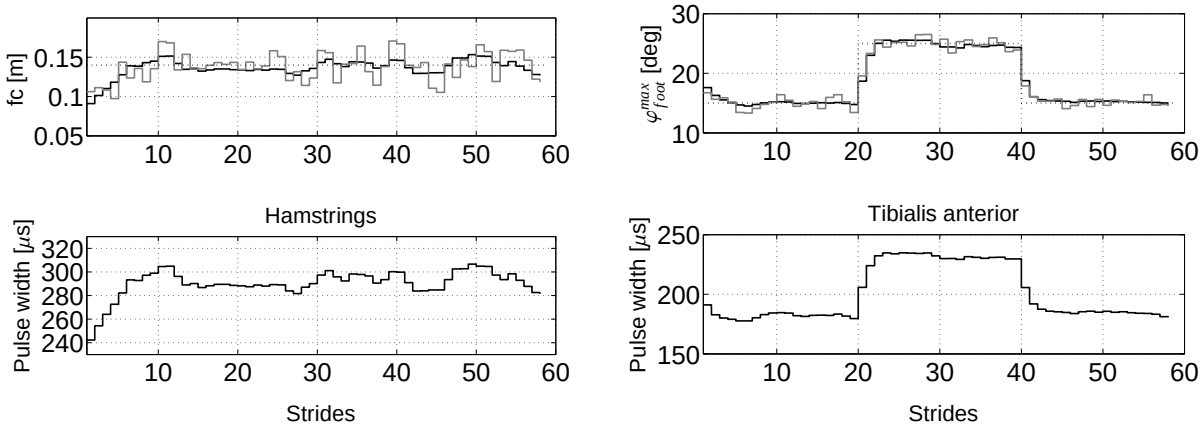

Figure 7.16.: Results from the *MIMO test 1*: In the upper left graph are the reference foot clearance (dotted line), the measured foot clearance (grey line) and the real foot clearance (solid line) shown. In the lower left graph is the corresponding pulse width applied to the hamstrings depicted. In the upper right graph are the maximum sagittal angle reference (dotted line), the measured maximum sagittal angle (grey line) and the real maximum sagittal angle (solid line) shown. In the lower right graph is the corresponding pulse width applied to the tibialis anterior depicted.

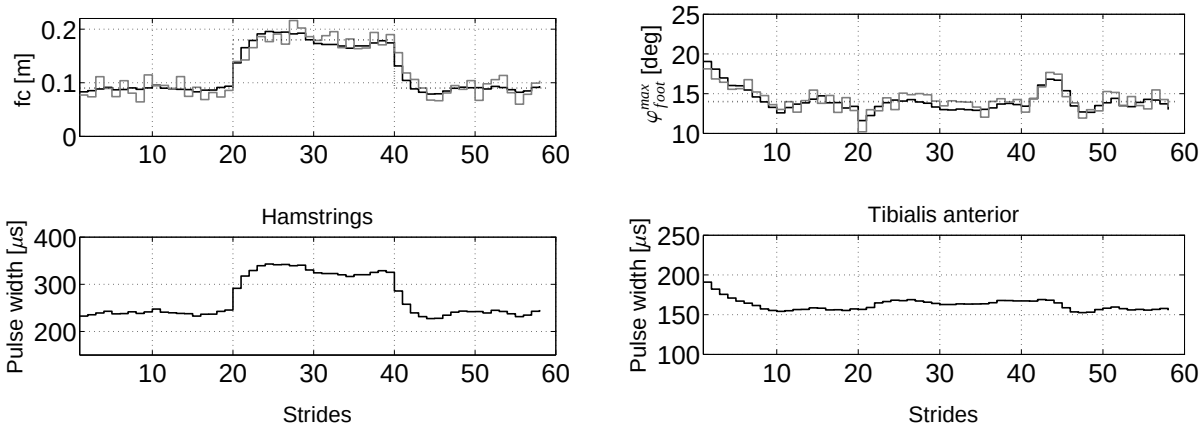

Figure 7.17.: Results from the *MIMO test 2*: In the upper left graph are the reference foot clearance (dotted line), the measured foot clearance (grey line) and the real foot clearance (solid line) shown. The corresponding pulse width applied to the hamstrings is depicted in the lower left graph. In the upper right graph are the maximum sagittal angle (dotted line), the measured maximum sagittal angle (grey line) and the real maximum sagittal angle (solid line) shown. In the lower right graph is the corresponding pulse width applied to the tibialis anterior depicted.

In Figure 7.16 the results from the *MIMO test 1* are shown. In the upper graph the measured foot clearance (grey line), the real foot clearance (solid line) and the reference foot clearance (dotted line) are shown. After 20 steps the reference maximum sagittal angle was changed from 15 degrees to 25 degrees and the new desired value was achieved after 5-7 steps as in the previous tests. After the 40th step the reference value of the maximum sagittal foot angle was reduced from 25 to 15 degrees again. Both steps had no influence on the regulated foot clearance as seen from the figure.

In Figure 7.17 the results from the *MIMO test 2* are shown. The reference foot clearance was after 20 steps changed from 9 cm to 18 cm and the new reference value was achieved after 5-7 steps as in the *SISO closed-loop test*. After the 20th step the maximum sagittal angle is falling slightly as it is influenced by the increased hamstrings stimulation. The maximum sagittal foot angle controller reacts to this disturbance and the reference values is after a few steps back to the reference value. After the 40th step the reference value of the foot clearance was reduced from 18 cm to 9 cm again. After 7-8 steps the reference value was achieved again. The maximum sagittal angle was increased as a consequence of the reduced hamstring stimulation. The maximum sagittal angle controller reacted to the situation and decreased the stimulation to the tibialis anterior. After 7-8 steps the reference was reachieved.

7.9. Feedback Controlled FES-Assisted Gait - Patient Study

7.9.1. Subject

One hemiplegic stroke patient affected on the left side had a good response to the tibialis anterior stimulation and was found suited to be used in the control scheme. Except for having drop foot, he had problems to stabilise the affected leg during the stance phase. The patient was compensating this by moving the non affected side faster through the swing phase making the gait asymmetrical. Nevertheless, the main purpose here was to show that the maximum sagittal angle of the foot could be controlled on a step to step basis.

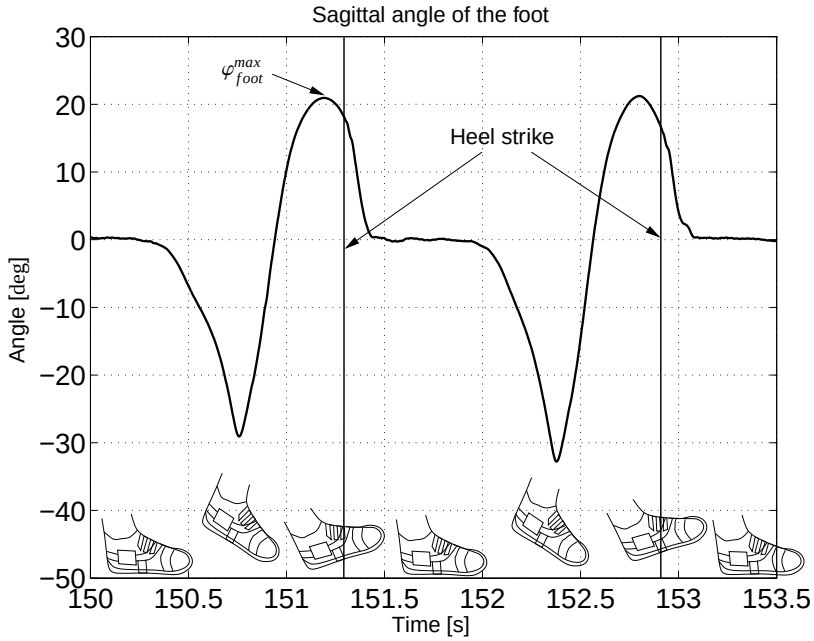

Figure 7.18.: Example trajectory of the sagittal foot angle φ_{foot}.

In this section the movement parameter φ_{foot}^{max} is used as movement parameter (see Figure 7.18). The maximum sagittal angle of the foot was calculated after a completed swing phase by searching the maximum of the buffered angle during the swing phase.

7.9.2. Experimental Procedure

For the subject who had an appropriate response to stimulation of the tibialis anterior, the following procedure was carried out to find control parameters and to validate the control scheme experimentally.

- *Open loop test:* The stimulation intensity of the tibialis anterior was manually changed via the potentiometer.
- *Parameter identification*: After the open loop test was performed, the static plant gain b was found as well as the range in which the maximum sagittal angle was lying.
- *Closed-loop test 1:* Closed-loop test of the designed feedback controller. During this test the reference angle was set to constant 20 degrees.
- *Closed-loop test 2:* During this test the square wave reference angle was changing between 18 and 23 degrees. The reference angle was kept constant for 45 seconds before it was changed to a new value.

The current was set to 45 mA and the frequency was set to 30 Hz. For all tests the stimulation was triggered by the heel off event and continued until 3/4 of the swing phase.

7.9.3. Results

In Figure 7.19 the result from the *Open loop test* is shown. In the lower graph the applied stimulation intensity is plotted (pulse width). In the upper graph the estimated maximum foot angle φ_{foot}^{max} is given. Without stimulation the achieved maximum angle was lying in the range 13 to 15 degrees. When stimulation was applied, the maximum angle φ_{foot}^{max} measured was lying in the range 14 - 26 degrees depending on the stimulation level. The plant gain was somewhat difficult to estimate as the response changed from one test to another. But from the tests the constant was conservatively estimated to be $b = 0.025$ deg/μs. The controller was tuned by setting the time constants $n_o = 2$ and $n_c = 2$.

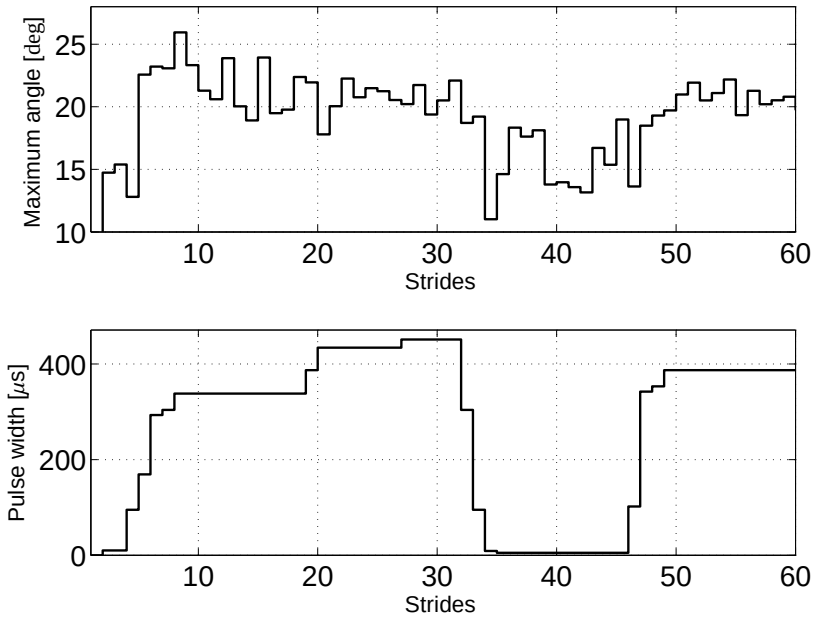

Figure 7.19.: Results from the *Open loop test*: The upper plot shows the achieved maximum sagittal foot angle φ_{foot}^{max}. The corresponding pulse width is shown in the lower graph.

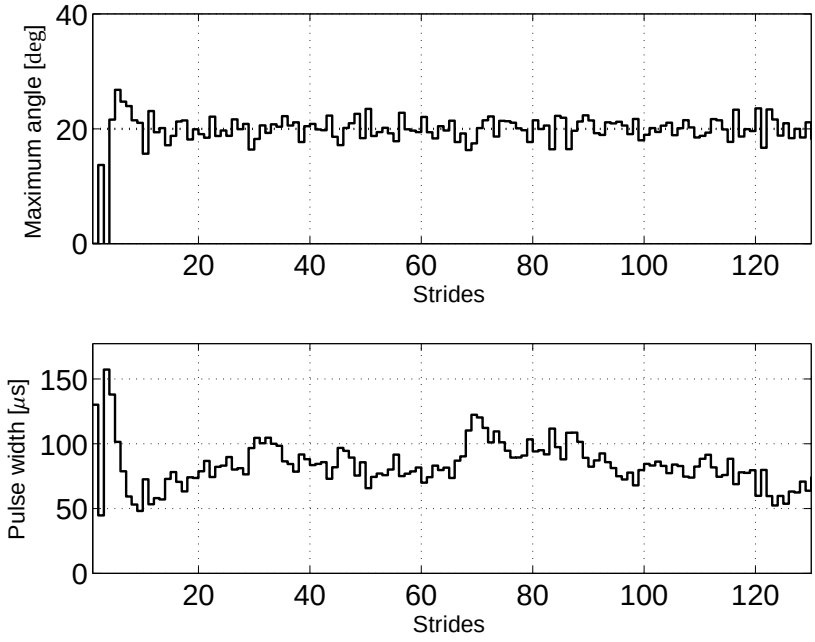

Figure 7.20.: Results from the *Closed-loop test 1*: In the upper graph the reference angle (dashed line) and the measured maximum sagittal foot angle (solid line) are given. The applied pulse width is given in the lower graph.

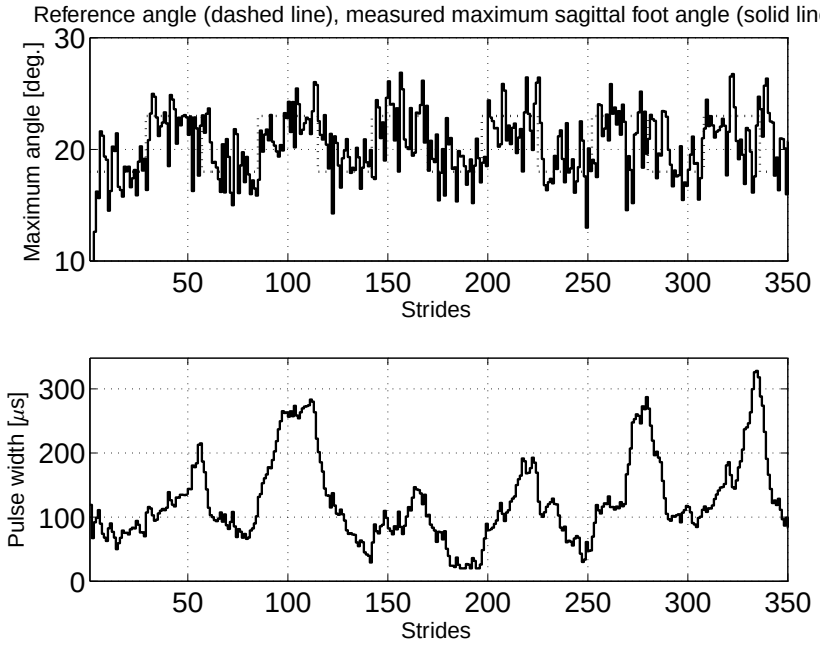

Figure 7.21.: Results from *Closed-loop test 2*: In the upper graph the reference angle of 20 deg (dashed line) and the measured maximum sagittal foot angle (solid line) are shown. The reference angle changes between 18 deg and 23 deg. The applied pulse width is given in the lower graph.

In Figure 7.20 the results from *Closed-loop test 1* are shown. The achieved maximum sagittal angle φ_{foot}^{max} is shown in the upper graph, whereas the applied stimulation intensity (pulse width) is shown in the lower graph. As seen from the figure, the controller was able to keep the maximum angle constant during the whole test (ca. 4 min/120 steps). Even though the averaged maximum angle was held constant, there was a considerable step to step variation which was either caused by variation of gait or by measurement noise. The standard deviation of the maximum angle was calculated to be 1.5 degrees during this test.

In Figure 7.21 the results from the *Closed-loop test 2* are shown. In the upper graph the achieved maximum sagittal angle φ_{foot}^{max} (dashed line) is shown together with the reference angle. The corresponding pulse width is shown in the lower graph. The new reference value was normally achieved after 5 to 7 steps.

7.10. Discussion and Conclusions

The positive results from the GPD-IS triggered FES gait training indicate that an inertial sensor is a appropriate sensor for such purpose. The general testing of the FES-assisted gait training showed that the triggering based on the GPD-IS worked robustly for nearly all of the 12 hemiplegic patients participating in the study. Only for two patients who were walking at a low speed, the heel off events were detected

too early as a result of a fidgety foot during the foot flat phase. This was the only critical problem that occurred.

The experiments showed that by applying electrical stimulation the joint trajectories of hip, knee, and ankle could be changed such that the gait patterns were qualitatively improved. The same experiments showed that the improvements caused by electrical stimulation could not be revealed from the inertial sensors derived temporal values for subject S1. For subject S2, an improvement in symmetry could be seen from the temporal values derived from the inertial sensors.

The number of stimulated muscle groups was normally limited. In experiments, only one or two muscle group were stimulated because of the elaborate procedure to find appropriate muscles, and because of the time consuming task to find the right stimulation pattern.

In experiments with a stroke patient, it has been shown that the maximum sagittal angle estimated from an inertial sensor can be used as feedback signal in a closed-loop FES control scheme on a step to step basis. Even though the experiments were performed in a clinical setting, the control scheme has a potential to be used for drop foot patients who are using a stimulator at home. The feedback controller used is simple to tune and no advanced modeling was needed for the control design. An obvious extension of the controller is to make it adaptive by identifying the plant gain online.

The control scheme was successfully demonstrated with two movement parameters in simulation and with one movement parameter in experiments. It was not possible to show that hamstrings stimulation could influence the foot clearance in experiments with a patient due to the limited number of patients available. In the simulation, the MIMO controller tests showed that the influence of the foot clearance from the stimulation of tibialis anterior was minimal. In simulations it was shown that the maximum sagittal angle was influenced by hamstrings stimulation. The same effect was also seen in experiments with one patient. Although this was not a problem for this patient, a MIMO controller could have been used to stabilise the maximum sagittal angle when stimulating the hamstrings.

Further investigation should in the future consider more movement parameters derived from the inertial sensor in simulation as well as in experiments. The model developed in this work is a good basis for further investigation of the proposed control scheme.

8. Conclusions and Recommendations for Future Work

In this thesis the use of inertial sensors in FES-assisted gait training was investigated. As a first step an algorithm for gait phase detection was developed, for which it was assumed that the one inertial sensor unit is mounted to the foot. Several similar detection systems have been developed by other research groups based on accelerometers and gyroscopes. To the authors best knowledge the system presented in this work is the first one based on a complete inertial sensor unit (three accelerometers and three gyroscopes). Compared to other systems the developed algorithm has the advantage that no individual tuning of the parameters for each patient is necessary. Even though a full sensor do imply an advantage compared to a reduced sensor (one gyroscope and two accelerometers) measuring acceleration and angular velocity in the sagittal plane, no direct comparison was done in this thesis regarding gait phase detection, and this should be investigated in future work.

The feasibility of using an inertial sensor to calculate accurate estimates of step length and foot clearance was demonstrated for five subjects with different gait pathologies walking on a treadmill with partial body weight support. It could be demonstrated that the consideration of initial and end conditions of the movement could considerably improve the accuracy of the step length and foot clearance estimation. In conclusion, the current study indicates that foot movements and gait phases can be reconstructed from inertial sensor data with an accuracy good enough to be used as feedback sensor in an FES-assisted gait rehabilitation system.

Experiments with 12 hemiplegic patients showed that FES-assisted gait training based on the gait phase detection system described in Chapter 5 worked robustly for all patients except for two subjects who were walking at a low speed. For these two patients, the heel off events were detected too early as a result of a fidgety foot during the foot flat phase. When applying electrical stimulation, it could be shown that the joint trajectories could be altered such that the gait patterns were qualitatively improved. The improvements in gait can be online monitored by temporal and spatial parameters estimation as well as indirect derived values from an inertial sensor system such as symmetry indices's. Although inertial sensors attached to the shoes do not directly measure joint- angle trajectories, they do represent an alternative to optical motion analysis systems because they can easily be applied in a clinical setting and monitor the progress of the rehabilitation. The number of stimulated muscle groups is normally

limited. Usually only one or two muscle groups were stimulated because this was in most cases sufficient to improve the gait pattern. In the cases where more than two channels were needed, the disability was so severe that other rehabilitation methods like an electromechanical gait trainer should be considered.

It has been experimentally demonstrated that the maximum sagittal angle of the foot with respect to the ground estimated from the inertial sensor can be used as feedback signal in a closed-loop FES control scheme. The estimated movement parameter e.g. maximum sagittal angle was after a completed step used as feedback in the controller in order to adjust the stimulation intensity for the next step. Even though the experiments were performed in a clinical setting, the control scheme has potential to be used for drop foot patients who are using a drop foot stimulator at home. The feedback controller used was simple to tune and no advanced model was needed for the controller design. An obvious extention of the controller is to make it adaptive by on-line identification of the plant gain. Further research should consider more movement parameters derived from the inertial sensor in simulation as well as in experiments. The biomechanical model of the freely swinging lower limb developed in this work is a good basis for further investigations of the proposed control scheme.

A. Model Equations

In Chapter 7 a dynamic model of the free swinging leg is described as:

$$[\mathbf{M}(\mathbf{q})]\,\ddot{\mathbf{q}} = \mathbf{C}(\mathbf{q},\dot{\mathbf{q}}) + \mathbf{G}(\mathbf{q}) + \mathbf{Q}(\mathbf{q},\dot{\mathbf{q}}) \tag{A.1}$$

The components of the inertia matrix are:

$$M(\mathbf{q}) = \begin{bmatrix} m_{11} & m_{12} & m_{13} \\ m_{21} & m_{22} & m_{23} \\ m_{31} & m_{32} & m_{33} \end{bmatrix} \tag{A.2}$$

$$\begin{aligned} m_{11} =& m_S l_{SK}^2 + m_T l_{TH}^2 + I_1 + I_2 + m_S l_T^2 + m_A l_S^2 + m_A l_{FA}^2 + I_3 + 2m_A l_T l_{FA} \sin(2\varphi_H + \varphi_K - \varphi_A) \\ & + 2m_A l_S l_{FA} \sin(2 * \varphi_H + 2 * \varphi_K - \varphi_A) + 2m_A l_T l_S \cos(\varphi_K) + 2m_S l_T l_{SK} \cos(\varphi_K) + m_A l_T^2 \end{aligned} \tag{A.3}$$

$$\begin{aligned} m_{12} =& m_A l_S^2 + m_A l_{FA}^2 + 2m_A l_S l_{FA} \sin(2\varphi_H + 2 * \varphi_K - \varphi_A) + I_2 + m_S l_{SK}^2 + \\ & m_A l_T l_{FA} \sin(2\varphi_H + \varphi_K - \varphi_A) + m_A l_T l_S \cos(\varphi_K) + m_S l_T l_{SK} \cos(\varphi_K) + I_3 \end{aligned} \tag{A.4}$$

$$m_{13} = -m_A l_{FA}^2 - m_A l_T l_{FA} \sin(2\varphi_H + \varphi_K - \varphi_A) - m_A l_S l_{FA} \sin(2\varphi_H + 2\varphi_K - \varphi_A) - I_3 \tag{A.5}$$

$$m_{21} = m_{12} \tag{A.6}$$

$$m_{22} = m_A * l_S^2 + m_A l_{FA}^2 + I_2 + m_S l_{SK}^2 + I_3 + 2m_A l_S l_{FA} \sin(2\varphi_H + 2\varphi_K - \varphi_A) \tag{A.7}$$

$$m_{23} = -m_A l_{FA}^2 - I_3 - m_A l_S l_{FA} \sin(2\varphi_H + 2\varphi_K - \varphi_A) \tag{A.8}$$

$$m_{31} = m_{13} \tag{A.9}$$

$$m_{32} = m_{23} \tag{A.10}$$

$$m_{33} = I_3 + m_A l_{FA}^2 \tag{A.11}$$

The components of the vector of gravitational terms are:

$$G(\mathbf{q}) = \begin{bmatrix} g_1 \\ g_2 \\ g_3 \end{bmatrix} \tag{A.12}$$

$$g_1 = -gm_T l_{TH} \sin(\varphi_H) - m_S g(l_T \sin(\varphi_H) + l_{SK} \sin(\varphi_H + \varphi_K)) - m_A g(l_T \sin(\varphi_H) + l_S \sin(\varphi_H + \varphi_K) - l_{FA} \cos(\varphi_H + \varphi_K - \varphi_A)) \quad \text{(A.13)}$$

$$g_2 = -gm_S l_{SK} \sin(\varphi_H + \varphi_K) - m_A g(l_S \sin(\varphi_H + \varphi_K) - l_{FA} \cos(\varphi_H + \varphi_K - \varphi_A)) \quad \text{(A.14)}$$

$$g_3 = -gm_A l_{FA} \cos(\varphi_H + \varphi_K - \varphi_A) \quad \text{(A.15)}$$

The components of the vector of Coriolis and centrifugal terms are:

$$C(\mathbf{q}, \dot{\mathbf{q}}) = \begin{bmatrix} c_{11} & c_{12} & c_{13} \\ c_{21} & c_{22} & c_{23} \\ c_{31} & c_{32} & c_{33} \end{bmatrix} \quad \text{(A.16)}$$

$$C_{11} = (2m_A l_T l_{FA} \cos(2\varphi_H + \varphi_K - \varphi_A) + 2m_A l_S l_{FA} \cos(2\varphi_H + 2\varphi_K - \varphi_A))\dot{\varphi}_H + (m_A l_T l_{FA} \cos(2\varphi_H + \varphi_K - \varphi_A) + 2m_A l_S l_{FA} \cos(2\varphi_H + 2\varphi_K - \varphi_A) - m_A l_T l_S \sin(\varphi_K) - m_S l_T l_{SK} \sin(\varphi_K))\dot{\varphi}_K + (-m_A l_T l_{FA} \cos(2\varphi_H + \varphi_K - \varphi_A) - m_A l_S l_{FA} \cos(2\varphi_H + 2\varphi_K - \varphi_A))\dot{\varphi}_A \quad \text{(A.17)}$$

$$C_{12} = (m_A l_T l_{FA} \cos(2\varphi_H + \varphi_K - \varphi_A) + 2m_A l_S l_{FA} \cos(2\varphi_H + 2\varphi_K - \varphi_A) - m_A l_T l_S \sin(\varphi_K) - m_S l_T l_{SK} \sin(\varphi_K))\dot{\varphi}_H + (m_A l_T l_{FA} \cos(2\varphi_H + \varphi_K - \varphi_A) + 2m_A l_S l_{FA} \cos(2\varphi_H + 2\varphi_K - \varphi_A) - m_A l_T l_S \sin(\varphi_K) - m_S l_T l_{SK} \sin(\varphi_K))\dot{\varphi}_K + (-m_A l_T l_{FA} \cos(2\varphi_H + \varphi_K - \varphi_A) - m_A l_S l_{FA} \cos(2\varphi_H + 2\varphi_K - \varphi_A))\dot{\varphi}_A \quad \text{(A.18)}$$

$$C_{13} = -m_A l_{FA}(l_S \cos(2\varphi_H + 2\varphi_K - \varphi_A) + l_T \cos(2\varphi_H + \varphi_K - \varphi_A))(\dot{\varphi}_H + \dot{\varphi}_K - \dot{\varphi}_A) \quad \text{(A.19)}$$

$$C_{21} = (2m_A l_S l_{FA} \cos(2\varphi_H + 2\varphi_K - \varphi_A) + m_A l_T l_{FA} \cos(2\varphi_H + \varphi_K - \varphi_A) + m_A l_T l_S \sin(\varphi_K) + m_S l_T l_{SK} \sin(\varphi_K))\dot{\varphi}_H + 2m_A l_S l_{FA} \cos(2\varphi_H + 2\varphi_K - \varphi_A)\dot{\varphi}_K - m_A l_S l_{FA} \cos(2\varphi_H + 2\varphi_K - \varphi_A)\dot{\varphi}_A \quad \text{(A.20)}$$

$$C_{22} = m_A l_S l_{FA} \cos(2\varphi_H + 2\varphi_K - \varphi_A)(2\dot{\varphi}_H + 2\dot{\varphi}_K - \dot{\varphi}_A) \quad \text{(A.21)}$$

$$C_{23} = -m_A l_S l_{FA} \cos(2\varphi_H + 2\varphi_K - \varphi_A)(\dot{\varphi}_H + \dot{\varphi}_K - \dot{\varphi}_A) \quad \text{(A.22)}$$

$$C_{31} = -m_A l_{FA}(\dot{\varphi}_H l_S \cos(2\varphi_H + 2\varphi_K - \varphi_A) + \dot{\varphi}_H l_T \cos(2\varphi_H + \varphi_K - \varphi_A) + \dot{\varphi}_K l_S \cos(2\varphi_H + 2\varphi_K - \varphi_A)) \quad \text{(A.23)}$$

$$C_{32} = -m_A l_S l_{FA} \cos(2\varphi_H + 2\varphi_K - \varphi_A)\dot{\varphi}_H - m_A l_S l_{FA} \cos(2\varphi_H + 2\varphi_K - \varphi_A)\dot{\varphi}_K \quad \text{(A.24)}$$

$$C_{33} = 0 \quad \text{(A.25)}$$

Bibliography

[1] J.J. Abbas and R.J. Triolo. Experimental Evaluation of an Adaptive Feedforward Controller for Use in Functional Neuromuscular Stimulation Systems. *IEEE Trans. Rehab. Eng.*, 5(1):12–22, Mar. 1997.

[2] K. Aminian, B. Najafi, C. Büla, P.-F. Leyvraz, and Ph. Robert. Spatio-temporal parameters of gait measured by an ambulatory system using miniature gyroscopes. *J. Biomechanics*, 35:689–699, 2002.

[3] K.J. Åström and B. Wittenmark. *Computer-Controlled Systems: Theory and Design*. Prentice-Hall, Inc., Upper Saddle River, N.J., 3rd edition, 1997.

[4] G. Baselli, G. Legnani, P. Franco, F. Brognoli, A. Marras, F. Quaranta, and B. Zappa. Assessment of inertial and gravitational inputs to the vestibular system. *J. Biomechanics*, 34(6):821–826, 2001.

[5] A.L. Behrman and S.J. Harkema. Locomotor Training After Human Spinal Cord Injury: A Series of Case Studies. *Physical Therapy*, 80(7):688–700, Jul. 2000.

[6] U. Bogataj, N. Gros, M. Kljajic, and R. Acimovic-Janeuziuc. Enhanced Rehabilitation of Gait After Stroke: A Case Report of a Therapeutic Approach Using Multichannel Functional Electrical Stimulation. *IEEE Trans. Rehab. Eng.*, 5(2):221–232, 1997.

[7] U. Bogataj, M. Kljajic, U. Stanic, R. Acimovic, and N. Gros. Gait pattern behavior of hemiplegic patients under the influence of a six-channel microprocessor stimulator in a real environment. In *in Proc. 2nd Int. Conf. Rehabil. Eng.*, pages 529–530, 1984.

[8] J.E. Bortz. A New Mathematical Formualtion for Strapdown Inertial Navigation. *IEEE Trans. on Aerospace and Electronic Systems*, AES-7(1):61–66, 1971.

[9] J.H. Burridge. Does the Drop-Foot Stimulator Improve Walking in Hemiplegia. *Intern. Neuromod. Society*, 4(2):77–83, 2001.

[10] J. Chae, Z.-P. Fang, M. Walker, S. Pourmehdi, and J. Knutson. Intramuscular Electromyographically Controlled Neuromuscular Electrial Stimulation for Ankle Dorsiflexion Recovery in Chronic Hemiplegia. *American Journal of Physical Medicine & Rehabilitation*, 80(11):842–847, nov 2001.

[11] Y.-L. Chen, Y.-C. Li, T.-S. Kuo, and J.-S. Lai. The Development of a Closed-loop Controlled Functional Electrical Stimulation (FES) in Gait Training. *Journal of Medical Engineering & Technology*, 25(2):41–48, Mar./Apr. 2001.

[12] Y.-L. Chen, S.-C.Chen, W.-L. Chen, C.-C. Hsiao, T.-S. Kuo, and J.-S. Lai. Neural network and fuzzy control in FES-assisted locomotion for the hemipleigc. *Journal of Medical Engineering & Technology*, 28(1):32–38, Jan./Feb. 2004.

[13] G. Colombo, M. Jörg, and V. Dietz. Driven Gait Orthosis to do Locomotor Training of Paraplegic Patients. In *Proceedings of the 22nd Annual EMBS International Conference*, pages 3159–3163, Chicago,IL,USA, Jul. 2000.

[14] R. Dai, R.B. Stein, B.J. Andrews, K.B. James, and M. Wickler. Application of Tilt Sensors in Functional Electrical Stimulation. *IEEE Trans. Rehab. Eng.*, 4(4):62–72, 1996.

[15] R. Davoodi, B.J. Andrews, G.D. Wheeler, and R. Lederer. Development of an indoor rowing machine with manual FES controller for total body exercise in paraplegia. *IEEE Trans. Neural Syst. Rehabil. Eng.*, 10(3):197–203, 2002.

[16] J.P. Dewald, J.D. Given, and W.Z. Rymer. Long-lasting reductions of spasticity induced by skin electrical stimulation. *IEEE Trans. Rehab. Eng.*, 4(4):231–42, 1996.

[17] P.C. Eser, N. de N. Donaldson, H. Knecht, and E. Stussi. Influence of different stimulation frequencies on power output and fatigue during FES-cycling in recently injured SCI people. *IEEE Trans. Neural Syst. Rehabil. Eng.*, 11(3):236–240, 2003.

[18] F. Ferraris, U. Grimaldi, and M. Parvis. Procedure for Efforless In-Field Calibration of Three-Axis Rate Gyros and Acclerometers. *Sensors and Materials*, 7(5):311–330, 1995.

[19] E.C Field-Fote. Combined Use of Body Weight Support, Functional Electric Stimulation, and Treadmill Training to Improve Walking Ability in Individuals With Chronic Incomplete Spinal Cord Injury. *Arch. Phys. Med. Rehabil.*, 82:818–824, Jun. 2001.

[20] N. Fiskekovic and D.B. Popovic. New controller for functional electrical stimulation systems. *Med. Eng & Phys.*, 23:391–399, 2001.

[21] H.M. Franken, P.H. Veltink, G. Baardman, R.A. Redmeyer, and H.B.K. Boom. Cycle-to-cycle control of swing phase of paraplegic gait induced by surface electrical stimulation. *Med. & Bio. Eng. & Comp.*, 33(3):440–51, May. 1995.

[22] T. Fuhr, J. Quintern, and G. Schmidt. Stair ascending and descending with the cooperative neuroprothesis WALK! *Neuromodulation*, 6(1):57–67, 2003.

[23] T. Fuhr and G. Schmidt. Neue Ansätze zur Steuerung und Regelung einer kooperativen Gang-Neuroprothese. *at - Automatisierungstechnik*, 50(7), Jul. 2002.

[24] P.H. Gorman and J.T. Mortimer. The effect of stimulus parameters on the recruitment characteristics of direct nerve stimulation. *IEEE Trans. Biom. Eng.*, 30:301–308, 1983.

[25] M.H. Granat, D.J. Maxwell, A.C. Ferguson, K.R. Lees, and J.C. Barbenel. Peroneal stimulator; evaluation for the correction of spastic drop foot in hemiplegia. *Arch. Phys. Med. Rehabil.*, 77(1): 19–24, 1996.

[26] M.S. Grewal and A.P. Andrews. *Kalman Filtering*. Wiley-Interscience, 2001.

[27] W. Hacke, M. Kaste, J. Bogousslavsky, M. Brainin, A. Chamorro, K. Lees, and D. Leys. European Stroke Initiative Recommendations for Stroke Management-update 2003. *Cerebrovasc Dis.*, 16: 311–337, 2003.

[28] M. Hansen, M. Haugland, A. Kostov, and T. Sinkjær. Machine Learning for Real Time Control of Foot-Drop Correction using Natural Sensors. In *Proc. of the 5th Annual Conference of the International Functional Electrical Stimulation Society (IFESS 2000)*, Aalborg, Denmark, jul 2000.

[29] M. Hansen, M.K. Haugland, and F. Sepulveda. Feasibility of Using Peroneal Nerve Recordings for Deriving Stimulation Timing in a Foot Drop Correction System. *Neuromodulation*, 6(1):68–77, 2003.

[30] E. Henneman. Recruitment of motoneurones: the size principle. In J. E. Desmedt, editor, *Motor Unit Types, Recruitment and Plasticity in Health and Disease. Progress in Clinical Neurophysiology*, pages 26–90. Karger, Basel, 9 edition, 1981.

[31] S. Hesse, C. Bertelt, M.T. Jahnke, A. Schaffrin, P. Baake, M Malezic, and K.H. Mauritz. Treadmill Training with Partial Body Weight Support Compared with Physiotherapy in Nonambulatory Hemiparetic Patients . *Stroke*, 26(6):976–81, Jun. 1995.

[32] S. Hesse, M. Konrad, and D. Uhlenbrock. Treadmill Walking With Partial Body Weight Support Versus Floor Walking in Hemiparetic Subjects . *Arch. Phys. Med. Rehabil.*, 80(4):421–7, 1999.

[33] S. Hesse, M. Malezic, A. Schaffrin, and K.H. Mauritz. Restoration of Gait by Combined Treadmill Training and Multichannel Electrical Stimulation in Non-ambulatory Hemiparetic Patients. *Scand. J. Rehab. Med.*, 27(4):199–204, Dec. 1995.

[34] S. Hesse, C. Werner, D. Uhlenbrock, S.v. Frankenberg, A. Bardeleben, and B. Brandl-Hesse. An Electromechanical Gait Trainer for Restoration of Gait in Hemiparetic Stroke Patients: Preliminary Results. *Neurorehabilitation and Neural Repair*, 15:39–50, 2001.

[35] D.M. Hettinga, B.J. Andrews, G.D. Wheeler, J.Y. Jeon, J. Verellen, J.J. Laskin, L.M. Olenik, R. Lederer, R. Burnham, and R.D. Steadward. FES-rowing for persons with spinal cord injury. In I. Swain and P. Taylor, editors, *Proc. of the 9th Annual Conference of the International Functional Electrical Stimulation Society (IFESS 2004)*. Bournemouth, UK, Sep. 2004.

[36] H. Hugenholtz, P. Humphreys, W.M.J. McIntyre, R.A. Spasoff, and K. Steel. Cervical Spinal Cord Stimulation for Spasticity in Cerebral Palsy. *Neurosurgery*, 22:707–714, 1988.

[37] R.P. Jaime. *On the control of paraplegic standing using functional electrical stimulation*. PhD thesis, University of Glasgow, 2002.

[38] J.M. Jasiewicz, J.H.J. Allum, J.W. Middleton, A. Barriskill, P. Condie, B. Purcell, and R.C.T. Li. Gait event detection using linear accelerometers or angular velocity transducers in able-bodied and spinal-cord injured individuals. *Gait & Posture*, 2006.

[39] H.S. Jørgensen, H. Nakayama, H.O. Raaschou, and T.S. Olson. Recovery of walking function in stroke patients: the copenhagen stroke study. *Arch. Phys. Med. Rehabil.*, 76(1):27–32, 1996.

[40] D. Kotiadis, H. Hermens, P.Veltink, and P. Slyke. Inertial gait phase detection system: Design. In *Proceedings of the 9th Ann. IFESS Conference*, Bournemouth, UK, 2004.

[41] A. Kralj, T. Bajd, R. Turk, J. Kranjnik, and H. Benko. Gait restoration in paraplegic patients: A feasibility demonstration using multichannel surface electrode fes. *Journal of Rehabilitation R and D*, 20(1):3–20, 1983.

[42] M. Ladouceur. The therapeutic effect of functional electrical stimulation assited walking in incomplete spinal cord injured participants. In *6th Internet World Congress for Biomedical Sciences*, 2000.

[43] W.T. Liberson, H.J. Holmquest, D. Scot, and M. Dow. Functional Electrotherapy: Stimulation of the Peroneal Nerve Synchronized with the Swing Phase of the Gait of Hemiplegic Patients. *Archives of Physical Medicine and Rehabilitation*, 21:101–105, 1961.

[44] H.J. Luinge. *Inertial Sensing of Human Movement*. PhD thesis, University of Twente, 2002.

[45] H.J. Luinge and P.H. Veltink. Inclination Measurement of Human Movement Using a 3-D Accelerometer With Autocalibration. *IEEE Trans. Neural Syst. Rehabil. Eng.*, 12(1):112–121, Mar. 2004.

[46] G.M. Lyons, T. Sinkjær, J.H. Burridge, and D.J. Wilcox. A Review of Portable FES-Based Neural Orthoses for the Correction of Drop Foot. *IEEE Trans. Neural Syst. Rehabil. Eng.*, 10(4):260–279, Dec. 2002.

[47] G.M. Lyons, D.J. Wilcox, D.J. Lyons, and D. Hilton. Evaluation of a drop foot stimulator fes intensity envelope matched to tibialis anterior muscle activity during walking. In *Proceedings of IFESS 2000*, pages 421–424, Jun. 2000.

[48] M. Malezic, U. Bogataj, N. Gros, I. Decman, P. Vrtacnik, and M. Kljajic. Application of a programmable dual-channel adaptive electrical stimulation system for the control and analysis of gait. *J. Rehabil. Res. Dev.*, 29(4):41–53, 1992.

[49] M. Malezic and S. Hesse. Restoration of gait by functional electrical stimulation in paraplegic patients: a modified programme of treatment. *Paraplegia*, 33(3):126–132, 1995.

[50] A. Mansfield and G.M. Lyons. The use of accelerometry to detect heel contact events for use as a sensor in fes assisted walking. *Med. Eng & Phys.*, 25:879–866, 2003.

[51] J. L. Marins, X. Yun, E. R. Bachmann, R. B. McGhee, and M. J. Zyda. An Extended Kalman Filter for Quaternion-Based Orientation Estimation Using MARG Sensors. In *Proceedings of the 2001 IEEE/RSJ International Conference on Intelligent Robots and Systems*, pages 2003–2011, Mani, HI, Nov. 2001.

[52] R.E. Mayagoitia, A.V. Nene, and P.H. Veltink. Accelerometer and rate gyroscope measurement of kinematics: an inexpensive alternative to optical motion analysis systems. *J. Biomechanics*, 35: 537–542, 2002.

[53] S. Miyazaki. Long-Term Unrestrained Measurement of Stride Length and Walking Velocity Utilizing a Piezoelectric Gyroscope. *IEEE Trans. Biom. Eng.*, 44(8):753–759, 1997.

[54] J.C. Moreno, E.R. de Lima, A.F. Ruíz, F.J. Brunetti, and J.L. Pons. Design and implementation of an inertial measurement unit for control of artificial limbs: Application on leg orthoses. *Sensors and Actuators*, 118:333–337, 2006.

[55] N. Mourselas and M.H. Granat. Correction of drop foot using a fuzzy logic controlled miniature stimulator. In *Proceedings of IFESS 2000*, Jun. 2000.

[56] N.-O. Negård, R. Kauert, S. Andres, T. Schauer, and J. Raisch. Gait phase detection and step length estimation of gait by means of inertial sensors. In *Proc. of the 3rd European Medical & Biological Engineering Conference*, Prag, Czech Republic, November 2005.

[57] N.-O. Negård, T. Schauer, J.de Gersigny, S. Hesse, and J. Raisch. Application Programming Interface and PC control for the 8 channel stimulator MOTIONSTIM8. In *Proc. of the 10th Annual Conference of the International Functional Electrical Stimulation Society (IFESS 2005)*, Montreal, Canada, July 2005. IFESS.

[58] N.-O. Negård, T. Schauer, R. Kauert, and J. Raisch. An FES-assisted gait training system for hemiplegic stroke patients based on inertial sensors. In *6th IFAC Symposium on Modelling and Control in Biomedical Systems, Reims, France*, Sep. 2006.

[59] N.-O. Negård, T. Schauer, J. Raisch, S. Schumacher, and V. Hömberg. Control of FES-assisted Gait Training After Stroke Using Inertial Sensors. In *Proc. of the 11th Annual Conference of the International Functional Electrical Stimulation Society (IFESS 2006)*, Zao, Japan, September 2006. IFESS.

[60] S.K. Ng and H.J. Chizeck. Fuzzy Model Identification For Classification of Gait Events in Paraplegics. *IEEE Trans. Fuzzy and Systems*, 5(4):536–544, Nov 1997.

[61] D.T. O'Keeffe, A.E. Donnelly, and G.M. Lyons. The Development of a Potential Optimized Stimulation Intensity Envelope for Drop Foot Applicationsi. *IEEE Trans. Neural Syst. Rehabil. Eng.*, 11(3):249–256, Sep. 2003.

[62] D.T. O'Keeffe and G.M. Lyons. A versatile drop foot stimulator for research applicationst. *Med. Eng & Phys.*, 24:237–242, 2002.

[63] J. Ou, J. Riess, and J.J. Abbas. Adaptive Control of Cyclic Movements in a Multi-Segment System. In *Proc. of the 6th Annual Conference of the International Functional Electrical Stimulation Society*, Cleveland, Jun. 2001.

[64] I.P.I. Papas, M.R. Popovic, T. Keller, V. Dietz, and M. Morari. A Reliable Gait Phase Detection System. *IEEE Trans. Neural Syst. Rehabil. Eng.*, 9(2):113–125, June 2001.

[65] J. Perry. *Gait Analysis: Normal and Pathological Function*. SLACK Incorporated, 1992.

[66] M. Pohl, C. Werner, M. Holzgraefe, G. Kroczek, J. Mehrholz, I. Wingendorf, G. Hölig, R. Koch, and S. Hesse. Repetitive locomotor training and physiotherapy improve walking and basic activities of daily living after stroke: a single-blind, randomized multicentre trial (deutche gangtrainer-studie, degas). *Clinical Rehabilitation*, 21:17–27, 2007.

[67] J. Quintern, C. Krewer, G. Bisle, B. Husemann, and S. Heller. Enhancement of Gait Retraining by Electrical Stimulation of Flexor Reflex Afferents in Acute Stroke Patients: A Randomized, Controlled Clinical Study. In I. Swain and P. Taylor, editors, *Proc. of the 9th Annual Conference of the International Functional Electrical Stimulation Society (IFESS 2004)*, pages 454–456, Bournemouth, UK, Sep. 2004. IFESS.

[68] R. Riener, M. Ferrarin, E.E. Pavan, and C.A. Frigo. Patient-driven control of FES-supported standing up and sitting down: Experimental results. *IEEE Trans. Rehab. Eng.*, 8(4):523–529, Dec. 2000.

[69] R. Riener and T. Fuhr. Patient-driven control of FES-supported standing up: A simulation study. *IEEE Trans. Rehab. Eng.*, 6(2):113–124, June 1998.

[70] R. Riener, T. Fuhr, D. Antico, and J. Quintern. Modelling and Control of the Flexion withdrawal Reflex for Gait Neuroprotheses. In *Proceedings of IFESS 2000*, pages 421–424, Jun. 2000.

[71] J.A. Riess and J.J. Abbas. Adaptive Neural Network Control of Cyclic Movements Using Functional Neuromuscular Stimulation. *IEEE Trans. Rehab. Eng.*, 8(1):42–52, Mar. 2000.

[72] S.M. Robbins, P.E. Houghton, and M.G. Woodbury. The Therapeutic Effect of Functional and Transcutaneous Electric Stimulation on Improving Gait Speed in Stroke Patients: A Meta-Analysis. *Arch. Phys. Med. Rehabil.*, 87:853–859, 2006.

[73] D.N. Rushton. Functional electrical stimulation. *Physiol. Meas.*, 18:241–275, 1997.

[74] A. M. Sabatini. Quaternion-Based Extended Kalman Filter for Determining Orientation by Inertial and Magnetic Sensing. *IEEE Trans. Biom. Eng.*, 53(7):1346–1356, Jul. 2006.

[75] A.M. Sabatini, C. Martelloni, S. Scapellato, and F. Cavallo. Assessment of Walking features From Foot Inertial Sensing. *IEEE Trans. Biom. Eng.*, 52(3):486–494, Mar. 2005.

[76] T. Schauer. *Feedback Control of Cycling in Spinal Cord Injury using Functional Electrical Stimulation*. PhD thesis, University of Glasgow, 2005.

[77] M.R. Schindl, C. Forstner, H. Kern, and S. Hesse. Treadmill Training With Partial Body Weight Support in Nonambulatory Patients With Cerebral Palsy. *Arch. Phys. Med. Rehabil.*, 81, 2000.

[78] J. Schneider and T. Fuhr. Virtual Patient: Software library, 2000-20002. Institute of Automatic Control Engineering, TU Munich.

[79] L. Sciavicco and B. Siciliano. *Modeling and control of robot manipulators*. The McGraw-Hill Companies, Inc., 1996.

[80] F. Sepulveda, M.H. Granat, and A. Cliquet. Two artificial neural systems for generation of gait swing by means of neuromuscular electrical stimulation. *Medical Engineering & Physics*, 19(1): 21–28, Jan. 1997.

[81] R. Shinton and G. Beevers. Meta-analysis of relation between cigarette smoking and stroke. *Bmj.*, 298:789–794, 1989.

[82] S. Simcox, S. Parker, G. M. Davis, R. W. Smith, and J. W. Middleton. Performance of orientation sensors for use with a functional electrical stimulation mobility system. *Journal of Biomechanics*, 38:1185–1190, 2005.

[83] M.M. Skelly and H.J. Chizeck. Real-Time Gait Event Detection for Paraplegic FES Walking. *IEEE Trans. Neural Syst. Rehabil. Eng.*, 9(1):58–68, Mar. 2001.

[84] B. Stegmayr, K. Asplund, K. Kuulasmaa, A.M. Rajakangas, P. Thorvaldsen, and J. Tuomilehto. Stroke incidence and mortality correlated to stroke risk factors in the WHO MONICA Project. An ecological study of 18 populations. *Stroke*, 29(4):1367–1374, 1998.

[85] R. B. Stein, P. H. Peckham, and D. P. Popovic. *Neural Protheses: Replacing Motor Function After Disease or Disability*. Oxford University Press, Oxford, 1992.

[86] B. Stöne. *Control Strategies for Functional Electrical Stimulation Includes Cycling*. PhD thesis, University of Glasgow, 2005.

[87] K.D. Strange and J.A. Hoffer. Gait phase information provided by sensory nerve activity during walking: applicability as state controller feedback for fes. *IEEE Trans. Biomed. Eng.*, 46(7): 797–809, 1999.

[88] P.N. Taylor, J. Burridge, A.L. Dunkerley, A. Lamb, D.E. Wood, J.A. Norton, and I.D. Swain. Patients' perceptions of the Odstock Dropped Foot Stimulator (ODFS). *Clinical Rehabilitation*, 13:439–446, 1999.

[89] P.N. Taylor, J. Burridge, A.L. Dunkerley, D.E. Wood, J.A. Norton, C. Sinleton, and I.D. Swain. Clinical Use of the Odsctock Dropped Foot Stimulator: Its Effects on the Speed and Effort of Walking. *Arch. Phys. Med. Rehabil.*, 80:1577–1583, 1999.

[90] R.K.Y. Tong, M.F.W. Ng, L.S.W. Li, and E.F.M. So. Gait Training of Patients After Stroke Using an Electromechanical Gait Trainer Combined With Simultaneous Functional Electrical Stimulation. *Physical Therapy*, 86(9):1282–1294, 2006.

[91] J.H. van der Spek, W.J.R. Velthuis, P.H. Veltink, and T.J.A. de Vries. Neuro fuzzy control of the FES assisted freely swinging leg of paraplegic subjects. In *Proc. 18th Annual Int. Conf. of the IEEE Eng. in Med. and Bio. Soc.*, volume 5, pages 2234–2235, Amsterdam, 1996.

[92] R.P.S. van Peppen, G. Kwakkel, S. Wood-Dauphinee, H.J.M. Hendriks, Ph.J van der Wees, and J. Dekker. The Impact of Physical Therapy on Functional outcomes after Stroke: What's the Evidence? *Clinical Rehabilitation*, 18:833–862, 2004.

[93] P.H. Veltink. Control of FES-induced cyclical movements of the lower leg . *Med. & Bio. Eng. & Comp.*, 29:8–12, 1991.

[94] P.H. Veltink and H.M. Franken. Detectionof knee unlock during stance by accelerometry. *IEEE Trans. Rehab. Eng.*, 4(4):395–402, 1996.

[95] P.H. Veltink, H.M. Franken, J.A. van Alste, and H.B. Boom. Modelling the optimal control of cyclical leg movements induced by functional electrical stimulation. *International Journal of Artificial Organs*, 15(12):746–55, Dec. 1992.

[96] P.H. Veltink, J.H. Hemssems, R. Ekkelenkamp, P. Slycke, S. Stramigioli, and H.J. Hermens. A Strategy for Adaptive Tuning of a Two-Channel Peroneal Nerve Stimulator for Dropfoot . In *Proc. of the 7th IFESS Conference*, Ljubljana, Slovenia, June 2002.

[97] P.H. Veltink, P. Slycke, J. Hemssems, R. Buschman, G. Bultstra, and H. Hermens. Three dimensional inertial sensing of foot movements for automatic tuning of a two-channel implantable drop-foot stimulator. *Med. Eng & Phys.*, 25(1):21–28, Jan 2003.

[98] M. Visintin, H. Barbeau, N. Korner-Bitensky, and N.E. Mayo. A New Approach to Retrain Gait in Stroke Patients Through Body Weight Support and Treadmill Stimulation. *Stroke*, 29(6):1122–1128, Jun. 1998.

[99] L. Vodovnik, A. Kralj, U. Stanic, R. Acimovic, and N. Gros. Recent Application of Functional Electrical Stimulation to Stroke Patients in Ljubliana. *Clinical Orthopaedics and Related Research*, 131:64–70, 1978.

[100] A.Th.M. Willemsen, F. Bloemhog, and H.B.K. Boom. Automatic stance-swing phase detection from accelerometer data for peroneal nerve stimulation. *IEEE Trans. Biom. Eng.*, 37(12):1201–1208, Dec. 1990.

[101] R. Williamson and B. Andrews. Gait Event Detection for FES Using Accelerometers and Supervised Machine Learning. *IEEE Trans. Rehab. Eng.*, 8(3):312–319, Sep. 2000.